



University
of Glasgow

Halliday, Crawford Alasdair (2015) *The role of microRNA 21 in the development of in-stent restenosis*. PhD thesis.

<http://theses.gla.ac.uk/7062/>

Copyright and moral rights for this thesis are retained by the author

A copy can be downloaded for personal non-commercial research or study

This thesis cannot be reproduced or quoted extensively from without first obtaining permission in writing from the Author

The content must not be changed in any way or sold commercially in any format or medium without the formal permission of the Author

When referring to this work, full bibliographic details including the author, title, awarding institution and date of the thesis must be given

The role of microRNA 21 in the development of in-stent restenosis

Crawford Alasdair Halliday
BSc(Med Sci)(Hons), MB ChB(Hons), MRCP (UK)

Submitted in fulfilment of the requirements for the Degree
of Doctor of Philosophy

Institute of Cardiovascular and Medical Sciences
College of Medicine, Veterinary & Life Sciences
University of Glasgow

July 2015

© Crawford Alasdair Halliday 2015



University
of Glasgow

Authors's Declaration

I declare that this thesis has been written entirely by myself and is a record of work performed by myself with the exception of in situ hybridisation presented in Figure 4-5 which was performed by Dr Robert A McDonald. This thesis has not been submitted previously for a higher degree. The research was conducted at the Institute of Cardiovascular and Medical Sciences, University of Glasgow and the Golden Jubilee National Hospital, Clydebank under the supervision of Professor Andrew H Baker, Professor Keith G Oldroyd and Dr Simon Kennedy.

Crawford Halliday

July 2015

Acknowledgements

I would like to start by thanking my supervisors, Professor Andrew H Baker, Professor Keith G Oldroyd and Dr Simon Kennedy for their guidance throughout this project. I would also like to thank the British Heart Foundation for funding this project.

Many thanks to all those at the University of Glasgow who have been extremely helpful over the course of this project. In particular, the staff in the GCRC should be given a special mention for their patience and support, especially Robert, Nic, Gregor, Ashley and Iona who taught me many of the laboratory techniques used within this thesis. Without the assistance of both Nosrat and Alastair, from the bioelectronics unit, the building of the electrolysis equipment would not have been possible. Thank you both very much for the random wire, power packs and cables which you happily lent me.

Thank you to Hollie and Gillian who showed me the micro surgical procedure and provided me with encouragement even when it seemed impossible to master. In addition, I would like to thank the staff at the CRF who provided excellent anaesthetic support and banter.

This project was driven not only by enthusiasm but also caffeine. Thank you to all those in our office, with whom I shared in numerous cups of tea, coffee and cake. In particular, thank you to Keith, Stacy, Ange, Margaret, Emily, Karine and Mounia. Your encouragement and advice has been invaluable. Merci.

Throughout this PhD my family have been my greatest supporters. I would like to thank my parents for their never ending support. However, I would like to say my biggest thank you to my amazing wife Claire, whose relentless support and encouragement has kept me going through some very challenging periods. Words cannot express my gratitude. Your patience and love knows no bounds and I could not have done this without you. The birth of our beautiful daughter Isabella Iona has been the most wonderful experience to happen to us and I would like to dedicate this thesis to you both.

Crawford
July 2015

For Claire and Isabella,

Table of Contents

Authors's Declaration.....	2
Acknowledgements.....	3
List of Publications.....	7
*Joint first authors.....	7
Appendix.....	8
Abbreviations.....	9
Abstract.....	19
1 Introduction.....	21
1.1 Global burden of Cardiovascular Disease.....	22
1.2 Risk Factors for Coronary Disease.....	23
1.3 Arterial wall structure.....	24
1.4 Atherosclerosis.....	24
1.5 Clinical Manifestations of Coronary Heart Disease.....	29
1.6 Management of Coronary Heart Disease.....	29
1.7 Coronary Angiography and Intervention.....	32
1.8 In-stent Restenosis.....	33
1.9 Animal Models of In-stent Restenosis.....	38
1.10 Vascular Smooth Muscle Phenotype.....	40
1.11 MicroRNAs.....	42
1.12 Expression of microRNAs are essential for development.....	48
1.13 MicroRNA expression and cardiovascular development.....	49
1.14 Role of MicroRNAs following Vascular Injury.....	51
1.15 The role of microRNAs in macrophage function following vascular injury 66	
1.16 Aims.....	72
1.17 Hypotheses.....	73
2 Methods.....	74
2.1 Animals.....	75
2.2 Genotyping.....	75
2.3 RNA and miRNA Extraction from Cells and Tissues.....	80
2.4 Quantification of RNA.....	81
2.5 Complementary Deoxyribonucleic Acid (cDNA) Synthesis.....	82
2.6 TaqMan [®] quantitative real-time polymerase chain reaction (qRT-PCR) ...	83
2.7 Cell Culture.....	86
2.8 Murine Monocyte and Macrophages.....	92
2.9 Luminex Assay.....	95

2.10	Conditioned Media Experiments.....	97
2.11	Arterial Stenting and Grafting Operation	98
2.12	Tissue Processing	101
2.13	Histochemical Staining	105
2.14	Immunohistochemistry.....	107
2.15	<i>In situ</i> Hybridisation	110
2.16	Image Analysis	112
2.17	Statistical analysis	115
3	Refinement of the Mouse Model of ISR and Stent Electrolysis.....	116
3.1	Introduction.....	117
3.2	Aims.....	120
3.3	Results.....	121
3.4	Discussion	141
4	Investigation of Multiple Strategies to Manipulate MicroRNA-21 Expression and the Impact on the Development of In-stent Restenosis.....	146
4.1	Introduction.....	147
4.2	Aims.....	149
4.3	Results.....	150
4.4	Discussion	185
5	Effects of microRNA-21 on macrophage polarisation and function in the development of in-stent restenosis	195
5.1	Introduction.....	196
5.2	Aims.....	198
5.3	Methods.....	199
5.4	Results.....	201
5.5	Discussion	223
6	General Discussion.....	228
	References	236
	Appendix.....	259

List of Publications

Papers

Halliday CA*, McDonald RA*, Miller AM, Diver LA, Dakin RS, Montgomery J, McBride MW, Kennedy S, McClure JD, Robertson KE, Douglas G, Channon KM, Oldroyd KG, Baker AH (2015). Reducing In-Stent Restenosis: Therapeutic Manipulation of miRNA in Vascular Remodeling and Inflammation. *J Am Coll Cardiol*; 65(21): 2314-2327.

McDonald RA, White KM, Wu J, Cooley BC, Robertson KE, Halliday CA, McClure JD, Francis S, Lu R, Kennedy S, George SJ, Wan S, van Rooij E, Baker AH (2013). miRNA-21 is dysregulated in response to vein grafting in multiple models and genetic ablation in mice attenuates neointima formation. *Eur Heart J*; 34(22):1636-43.

Abstracts

Halliday CA, Robertson KE, McDonald RA, Kennedy S, Oldroyd KG, Douglas G, Channon KM, Baker AH (2013). MicroRNA 21 is Upregulated Following Coronary Artery Stenting and Genetic Deletion Limits Neointima Formation. *Eur Heart J* 34 (suppl1):806. Oral presentation at European Society of Cardiology Congress 2013 Amsterdam.

Halliday CA, Robertson KE, McDonald RA, Kennedy S, Oldroyd KG, Douglas G, Channon KM, Baker AH (2013). The Role of MicroRNA 21 in Porcine and Murine Models of In-Stent Restenosis. Oral presentation at Scottish Cardiovascular Forum 2013

*Joint first authors

Appendix

Halliday CA, et al. (2015). Reducing In-Stent Restenosis: Therapeutic Manipulation of miRNA in Vascular Remodeling and Inflammation. *J Am Coll Cardiol*; 65(21): 2314-2327.

Abbreviations

AAA	Abdominal Aortic Aneurysm
ABCA1	ATP Binding Cassette A1
ACh	Acetylcholine
AHA	American Heart Association
AngII	Angiotensin II
ANOVA	Analysis of Variance
AP-1	Activator Protein - 1
ApoE	Apolipoprotein E
Arg1	Arginase 1
Bcl-2	B-cell lymphoma 2
Bcl-6	B-cell lymphoma 6
BH ₄	5,6,7,8-tetrahydrobiopterin
BMDM	Bone Marrow Derived Macrophages
BMP	Bone Morphogenetic Protein
BMPR	Bone Morphogenetic Protein Receptor
BMS	Bare Metal Stent
BrdU	5-Bromo-2'-deoxyuridine
BSA	Bovine Serum Albumin

C. elegans	Caenorhabditis elegans
CABG	Coronary Artery Bypass Grafting
CCL	Chemokine (CC motif) ligand
CCR	Chemokine (CC motif) Receptor
CD	Cluster Differentiation
CDC25A	Cell Division Cycle 25A
Cdc42	Cell division control protein 42
CDK	Cyclin dependent kinase
cDNA	complementary DNA
CHD	Coronary heart disease
Chi3l3	Chitinase 3-like 3
Ct	Cycle threshold
CVD	Cardiovascular Disease
DAB	3,3 diaminobenzidine
DEPC	Diethylpyrocarbonate
DES	Drug Eluting Stent
DGCR8	DiGeorge Critical Region 8
dH ₂ O	deionised water
DMEM	Dulbecco's Modified Eagle's Medium

DNA	Deoxyribose Nucleic Acid
dNTP	Deoxynucleotide Triphosphates
E	Embryonic Day
EC	Endothelial Cell
ECG	Electrocardiogram
ECM	Extracellular Matrix
EDTA	Ethylenediaminetetraacetic Acid
EEL	External Elastic Lamina
EGFP	Enhanced Green Fluorescence Protein
eIF 4E	eukaryotic initiation Factor 4E
eNOS	endothelial Nitric Oxide Synthase
ERK 1 / 2	Extracellular signalling kinase 1 / 2
EVG	Elastic-Van Gieson
FACS	Flow Assisted Cell Sorting
FCS	Fetal Calf Serum
FFR	Fractional Flow Reserve
FGF-basic	Fibroblast Growth Factor - basic
GAGs	Glycosaminoglycans
GAPDH	Glyceraldehyde 3-Phosphate Dehydrogenase

GM-CSF	Granulocyte macrophage colony-stimulating factor
h	hour
H&E	Haematoxylin and Eosin
HASMCs	Human Aortic Smooth Muscle Cells
HCl	Hydrochloric Acid
HET	Heterozygote
HIF α	Hypoxia Inducible Factor alpha
ICAM-1	Intercellular Adhesion Molecule 1
IEL	Internal Elastic Lamina
IFN γ	Interferon gamma
IgG	Immunoglobulin G
IHC	Immunohistochemistry
IL	Interleukin
IP-10	IFN-gamma-inducible protein 10
IRES	Internal Ribosome Entry Site
IRF5	Interferon Regulatory Factor 5
ISH	<i>In situ</i> Hybridisation
ISR	In-Stent Restenosis
IST	In-Stent Thrombosis

IU	International Unit
KC	Keratinocyte Chemoattractant
KCl	Potassium Chloride
KLF	Kruppel-Like Factor
KO	Knockout
LAD	Left Anterior Descending
LCx	Left Circumflex
LDL	Low Density Lipoprotein
LDLR	Low Density Lipoprotein Receptor
LPS	Lipopolysaccharide
LST	Late Stent Thrombosis
MAC-1	Macrophage Antigen - 1
MAPK	Mitogen Activated Protein Kinase
MCP-1	Monocyte Chemoattractant Protein - 1
M-CSF	Macrophage - Colony Stimulating Factor
MFI	Mean Fluorescent Intensity
MgCl ₂	Magnesium Chloride
MHC II	Major Histocompatibility Complex II
MI	Myocardial Infarction

MIG	Monokine induced by gamma interferon
min	minute
MIP-1 α	Macrophage Inhibitory Protein - 1alpha
MIP-2	Macrophage Inhibitory Protein - 2
miR	MicroRNA
miRISC	miRNA Induced Silencing Complex
mL	millilitre
mmLDL	minimally modified Low Density Lipoprotein
MMP	Matrix Metalloprotease
mRNA	messenger Ribose Nucleic Acid
MRTF-A	Myocardin Related Transcription Factor -A
MRTF-B	Myocardin Related Transcription Factor -A
mTOR	mammalian Target of Rapamycin
MYH	Myosin Heavy Chain
MYH11	Myosin Heavy Chain 11
NFIB	Nuclear factor 1 B-type
NF κ B	Nuclear Factor kappa B
ng	nanogram
NIH	Neointimal Hyperplasia

NO	Nitric Oxide
NOR1	Neuron-derived Orphan Receptor 1
NOS	Nitric Oxide Synthase
NR4A	Nicotinic Receptor 4 Associated
ORP9	Oxysterol binding protein-related Protein 9
oxLDL	Oxidised Low Density Lipoprotein
PASMCs	Pulmonary Artery Smooth Muscle Cells
PAZ	PIWI-Argonaute-Zwillie
PBS	Phosphate Buffered Saline
PBS-T	Phosphate Buffered Saline - Tween
PCI	Percutaneous Coronary Intervention
PCNA	Proliferating Cell Nuclear Antigen
PCR	Polymearase Chain Reaction
PDA	Posterior Descending Artery
PDCD4	Programmed Cell Death 4
PDGF	Platelet Derived Growth Factor
PDGFR α	Platelet Derived Growth Factor Receptor alpha
PFA	Paraformaldehyde
PGI ₂	Prostacyclin

PI3K	Phosphoinositide -3-kinase
PIWI	P-element induced wimpy testes
PKC ϵ	Protein Kinase C epsilon
POBA	Plain Old Balloon Angioplasty
PPAR γ	Peroxisome Proliferator-Activated Receptor gamma
PPE	Porcine Pancreatic Elastase
Pre-miRNA	Preliminary microRNA
Pri-miRNA	Primary microRNA
PTEN	Phosphatase and tensin homolog
RT-qPCR	Reverse Transcriptase - quantitative Polymerase Chain Reaction
RCA	Right Coronary Artery
Retnla	Resistin-like α
RhoB	Ras homolog gene family member B
RNA	Ribose Nucleic Acid
ROS	Reactive Oxygen Species
RPE	R-Phycoerythrin
rpm	revolutions per minute
RPMI	Roswell Park Memorial Institute
s	second

SEM	Standard Error of Mean
shRNA	short hairpin RNA
siRNA	short inhibitory ribose nucleic acid
SM MHC	Smooth Muscle Myosin Heavy Chain
SM α -actin	Smooth Muscle alpha actin
SM22 α	Smooth Muscle 22 alpha
SOCS	Supressor of Cytokine Signalling
SP-1	Specificity Protein-1
SRF	Serum Response Factor
SSC	Standard Saline Citrate
STAT	Signal and Transduction and Transcription Factor
TBE	Tris/Borate/EDTA
Tbp	TATA box binding protein
Tg	Transgenic
TGF β	Transforming Growth Factor beta
TIMP	Tissue Inhibitor of Metalloprotease
TLR	Toll-like Receptor
TMB	3,3',5,5'-Tetramethylbenzidine
TMEM49	Transmembrane Protein 49

TNF α	Tumour Necrosis Factor - alpha
TPM1	Tropomyosin 1
TRBP	TAR RNA-binding protein
UTR	Untranslated Region
VCAM-1	Vascular Adhesion Molecule - 1
VEGF	Vascular Endothelial Growth Factor
VMP1	Vacuole Membrane Protein 1
VSMC	Vascular Smooth Muscle Cell
w/v	weight / volume
WT	Wild type
μg	microgram
μL	microlitre
μm	micrometre

Abstract

Coronary heart disease is a major cause of morbidity and mortality worldwide. Percutaneous coronary intervention (PCI) has become the most widely used method of coronary artery revascularisation. The use of stents to hold open atherosclerosis induced arterial narrowing has significantly reduced elastic recoil and acute vessel occlusion following balloon angioplasty. However, bare metal stents have been associated with in-stent restenosis attributed to vascular smooth muscle cell (VSMC) hyperplasia and excessive neointimal formation. The resultant luminal renarrowing may manifest clinically with the return of symptoms such as chest pain or shortness of breath. The development of drug eluting stents has significantly reduced the incidence of in-stent restenosis (ISR). Unfortunately the antiproliferative medications used not only inhibit VSMC proliferation but also re-endothelialisation of the stented vessel. In addition, the drug impregnated polymer coating has been associated with a chronic inflammatory response within the vessel wall predisposing patients to stent thrombosis. Thus the identification of novel therapies which promote vessel healing without excessive proliferative or inflammatory response may improve long term outcome and reduce the need for repeated revascularisation.

MicroRNAs (miRs) are short (18-25 nucleotide) non-coding RNAs acting to regulate gene expression. By binding to the 3'untranslated region of mRNA they act to fine tune gene expression either by mRNA degradation or translational repression. Originally identified in coordinating tissue development microRNAs have also been shown to play important roles coordinating the inflammatory response and in numerous cardiovascular diseases. MiR-21 has been identified in human atherosclerotic plaques, arteriosclerosis obliterans and abdominal aortic aneurysms. In addition, its up regulation has been documented in preclinical models of vascular injury.

This study sought to identify the role of miR-21 in the development of ISR. Utilising a small animal model of stenting and *in vitro* techniques, we sought to investigate its influence upon VSMC and immune cell response following stenting.

The refinement of a murine stenting model within the Baker laboratory and the electrochemical dissolution of the metal stent from within harvested vascular tissues significantly improved the ability to perform detailed histological analysis. In addition, identification of miRNAs using *in situ* hybridisation was achieved for the first time within stented tissue.

Neointimal formation and ISR was significantly reduced in mice in which miR-21 had been genetically deleted. In addition, neointimal composition was found to be altered in miR-21 KO mice with reductions in VSMC and elastin content demonstrated. Importantly, no difference in re-endothelialisation was observed. *In vitro* analysis demonstrated that VSMCs from miR-21 KO mice had both reduced proliferative and migratory capacity following platelet derived growth factor stimulation. Molecular analysis revealed that these differences may, at least in part, be due to de-repression of programmed cell death 4 (PDCD4). PDCD4 is a known miR-21 target within VSMCs implicated in the suppression of proliferation and promotion of apoptosis. Unfortunately, initial attempts at antimiR mediated knockdown of miR-21 *in vivo*, failed to produce a similar change in the suppression of ISR.

Furthermore, a significant alteration in macrophage polarisation state within the neointima of miR-21 WT and KO mice was noted. Immunohistochemical staining revealed a preponderance of anti-inflammatory M2 macrophages in KO mice. Analysis of bone marrow derived macrophages from miR-21 KO mice demonstrated an increased level of the peroxisome proliferation activating receptor- γ (PPAR γ) which facilitates M2 polarisation. Importantly, significant alterations in numerous pro-inflammatory cytokines, which also have mitogenic effects, were also found following genetic deletion of miR-21.

In Summary, this is the first study to look at miRs in the development of ISR. MiR-21 plays an important role in the development of ISR by influencing the proliferative response of VSMCs and modulating the immune response following stent deployment. Further attempts to modulate miR-21 expression following PCI may reduce ISR and the need for repeat revascularisation while also reducing the risk of stent thrombosis.

1 Introduction.

1.1 Global burden of Cardiovascular Disease

1.1.1 Epidemiology

Cardiovascular disease (CVD) is leading cause of death worldwide, responsible for the deaths of over 17 million people per year. It is expected that by 2030 over 23 million deaths per year will be attributable to cardiovascular disease, an increase of over one third (Wong, 2014). In addition, over the last decade a global shift in total burden of coronary heart disease away from high-income western societies towards middle- and low-income countries has been observed (Wong, 2014)

Coronary heart disease (CHD) and cerebrovascular disease account for the majority of deaths due to CVD; approximately 45% and 35% respectively (Wong, 2014). Other diseases contributing to total cardiovascular mortality figures include valvular heart disease, non-ischaemic cardiomyopathy, endocarditis, myocarditis, channelopathies, congenital heart disease, peripheral vascular disease, aortic aneurysms, subarachnoid and intracerebral haemorrhage.

Throughout the UK, deaths due to cardiovascular disease fell by over 40% between 2000 and 2010, for both men and women (Nichols et al., 2014). Two common clinical presentations of coronary heart disease are acute myocardial infarction and angina. The most recent available CHD data for Scotland show that across all ages the reported incidence of acute myocardial infarction was 154 and 66 per 100,000 population, for men and women respectively (BHF, 2014). Additionally the incidence of angina was 48.6 and 37.7 per 100,000 population, for men and women respectively (BHF, 2014).

Despite improvements in morbidity and mortality, CHD continues to place a major burden on health at both an individual and societal level. The cost to the NHS of CHD alone is estimated to be £1.8 billion per year with an equal split in spending between primary and secondary care (BHF, 2014). Coronary heart disease is also thought to cost the UK economy a further £3 billion per year in loss of productivity and on top of that a further £1.7 billion is lost in informal care of those with coronary heart disease (BHF, 2014).

1.2 Risk Factors for Coronary Disease

Current understanding of the causes of coronary heart disease is derived from large epidemiological studies commenced over 50 years ago. Seen by many as the first important epidemiological study into cardiovascular disease the Framingham Heart Study was initiated in the middle of the 20th century by Dr Thomas R Dawber (Wong and Levy, 2013). Funded by the National Heart Institute its goal was to understand the growing burden of cardiovascular disease observed in the USA within the early 20th century (Wong and Levy, 2013). Recruiting over 5200 participants from the Framingham District in Massachusetts, these participants aged between 30 and 62 year old were followed on a biannual basis with data collected by history, examination and laboratory analysis (Kannel et al., 1961). After 6 years follow up Kannel et al described several “Factors of Risk” associated with the development of coronary heart disease including male gender, increasing age, elevated cholesterol and hypertension (Kannel et al., 1961). Later observations from the Framingham study also documented that those with diabetes had a two to three fold increased risk of developing ischaemic heart disease (Kannel and McGee, 1979). Interestingly, determining an association with smoking proved more difficult, requiring the pooling of data with that of the Albany Cardiovascular Health Centre (Doyle et al., 1962). Other large epidemiological data sets have confirmed the above findings from the Framingham study (Stamler et al., 1986).

The INTERHEART study was undertaken to determine whether the traditional risk factors previously identified in western Caucasian populations were applicable to other ethnic populations across the world at the beginning of the 21st century (Yusuf et al., 2004). This case-control study involving almost 30,000 people across 52 countries identified 9 modifiable risk factors associated with myocardial infarction including: smoking, an abnormal lipid profile, diabetes mellitus, abdominal obesity, psychological stress, low fruit and vegetable consumption, regular alcohol intake and low levels of physical exercise (Yusuf et al., 2004). Taken together these risk factors were found to account for around 90% of the risk of developing an acute myocardial infarction (Yusuf et al., 2004).

1.3 Arterial wall structure

Arteries are composed of three major components: endothelial cells (EC), VSMCs and extracellular matrix (ECM). ECM is composed of collagen, elastin and glycosaminoglycans (GAGs) (Stevens, 1999). These components are arranged in three distinct layers forming concentric circles. The layer adjacent to the vessel lumen is the intima (tunica intima) comprised of a single layer of endothelial cells resting upon a basement membrane. Immediately underlying this basement membrane is a fenestrated layer of ECM called the internal elastic lamina (IEL). This represents the inner most layer of the vessel media (tunica media). The media is comprised of layers of VSMCs and elastic fibres. A further layer of connective tissue called the external elastic lamina (EEL) demarcates the outer edge of the media (Stevens, 1999). The adventitial layer (tunica adventitia) surrounds the media and is comprised of connective tissue within which nerve fibres and network of small blood vessels called the vaso vasorum are located. The vaso vasorum supplies oxygen and other nutrients to the adventitia and outer portion of the media while the inner portion of the media and intima receive nutrients from the luminal blood by the process of diffusion (Stevens, 1999).

1.4 Atherosclerosis

Atherosclerosis is a chronic inflammatory condition characterised by the deposition of lipids and inflammatory mediators within the wall of affected large and medium sized arteries (Ross, 1999). Over time these deposits undergo dynamic changes resulting in vessel fibrosis and calcification. Atherosclerotic lesions occur at multiple sites along the arterial tree being particularly common in the coronary arteries as well as the aorta, carotid, renal and iliac arteries. They demonstrate preponderance for sites exposed to non-laminar blood flow and low shear stress such as the inner curves of arterial bends, branch points and bifurcations (Ross, 1999).

Several large histological studies have systematically characterised different atherosclerotic lesions leading the American Heart Association (AHA) to produce a histological classification system. Last updated in 2000 this classification system is significantly simplified from earlier versions, (Figure 1-1 ;(Stary, 2000).

In particular it was noted that the morphological changes do not necessarily follow a well defined sequence as suggested in previous versions. The AHA classification acknowledges the heterogeneity of lesions, the non-linear progression of lesions through different histological sequences and the dynamic remodelling processes that occur within individual lesions after they become atheromatous plaques (type IV lesions). The caps of type IV lesions may thicken with layers of VSMCs and ECM overlying the lipid pools within the necrotic core (type V lesions) or become thinned and erode. Alternatively, the necrotic cores may undergo calcification or fibrosis giving rise to type VII and VIII lesions, respectively.

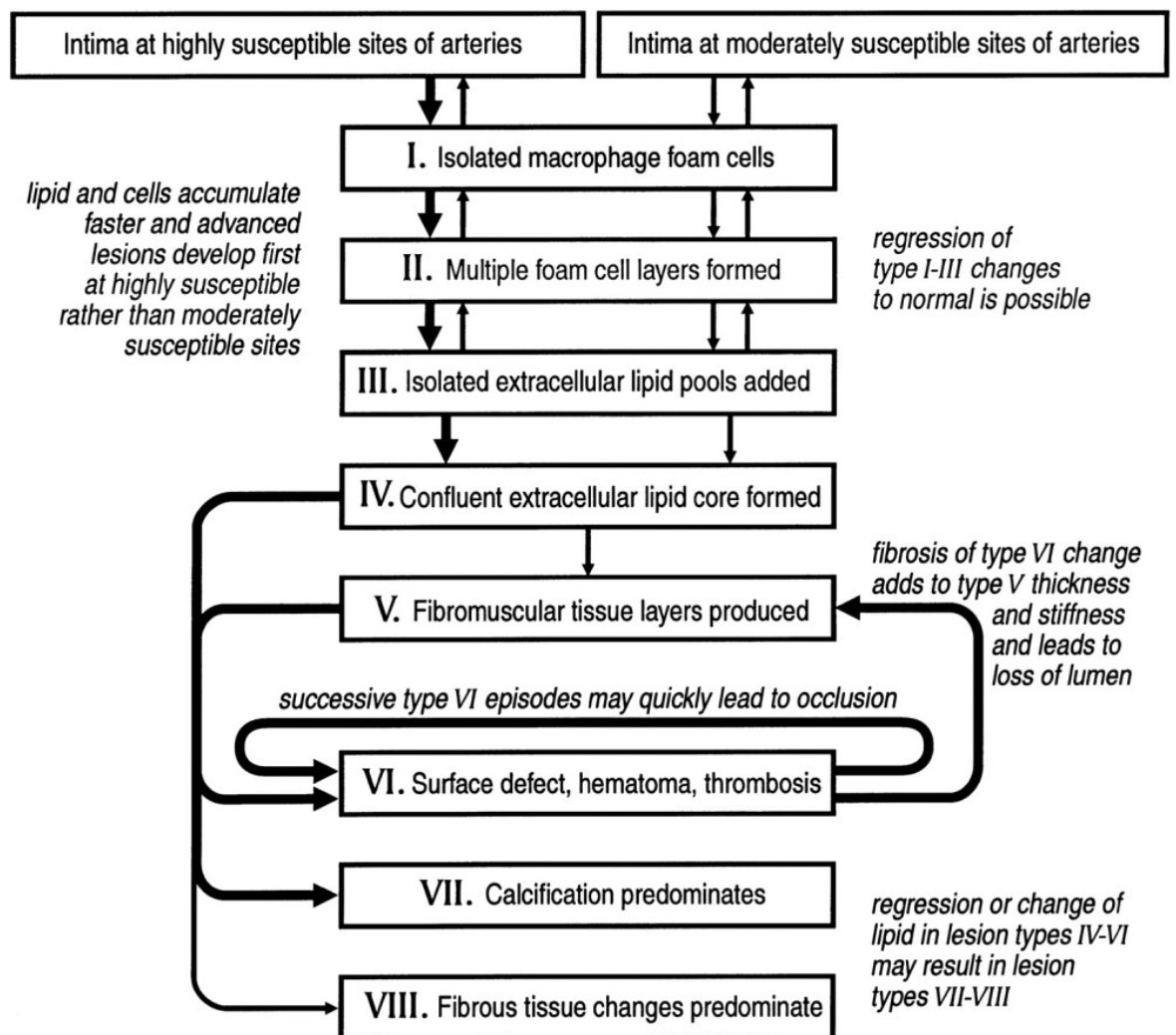


Figure 1-1. American Heart Association Classification of Atherosclerotic Lesion Development and Evolution. Reproduced with permission from Herbert C. Stary *Arterioscler Thromb Vasc Biol.* 2000;20:1177-1178. Copyright American Heart Association.

1.4.1 Lesion Development

Endothelial dysfunction, as determined by loss of endothelial-dependent vasodilation, due to the relative reduction in nitric oxide (NO) and an abundance of reactive oxygen species (ROS) such as superoxide anion, predates atherosclerosis development in healthy individuals in the presence of traditional risk factors such as smoking, hypertension and hypercholesterolaemia (Pagano et al., 1995, Forstermann et al., 1994, Celermajer et al., 1994). In addition to, and as a result of endothelial dysfunction low density lipoprotein (LDL) cholesterol is deposited within the sub-endothelial layer of the vessel wall, forming fatty streaks also known as intimal xanthoma. The resultant imbalance of NO : ROS and oxidation of LDL induces endothelial activation, nuclear factor kappa B (NF κ B) signalling and the expression of adhesion molecules, cytokines, chemoattractants and growth factors (Smith et al., 1995, Quinn et al., 1987). These chemical mediators facilitate the transmigration of inflammatory cells including monocytes, T and B cells into the forming plaque (Pritchard et al., 1995).

Once recruited into the fatty streaks, monocytes proliferate and differentiate becoming macrophages. Within the forming plaques macrophages become polarised by responding to various environmental triggers in order to alter their gene expression and hence functional capability. A multitude of polarisation states have been identified in different subpopulations of macrophages, some peculiar to atherosclerosis (Wolfs et al., 2011). The most common fate of infiltrating macrophages, in response to macrophage colony stimulating factor (M-CSF), is to become foam cells (Irvine et al., 2009). Through the expression of both scavenger receptors and cluster differentiation 36 (CD36), macrophages take up oxidised LDL (oxLDL) (van Tits et al., 2011). These lipid laden foam cells further potentiate the release of pro-inflammatory cytokines (Kunjathoor et al., 2002). Eventually foam cells undergo apoptosis and necrosis with the resultant release of their lipid stores into the vessel wall (Crisby et al., 1997). Together with cell debris these lipid pools coalesce forming a necrotic core of thrombogenic material (Stary, 2000).

Cytokines and growth factors liberated from inflammatory cells promote the dedifferentiation of VSMCs into a synthetic phenotype, before migrating and

proliferating within the forming plaque, Figure 1-2 (Sasu and Beasley, 2000, Sundaresan et al., 1995, Pidkovka et al., 2007). VSMCs are the cell type primarily responsible for the formation of the fibromuscular cap (Ross, 1999). During lesion development they migrate towards the luminal surface of the plaque secreting ECM, Figure 1-2. Transforming growth factor beta (TGF β) secreted by numerous cell types including T cells is thought to be important in stimulating cap development (Lutgens et al., 2002).

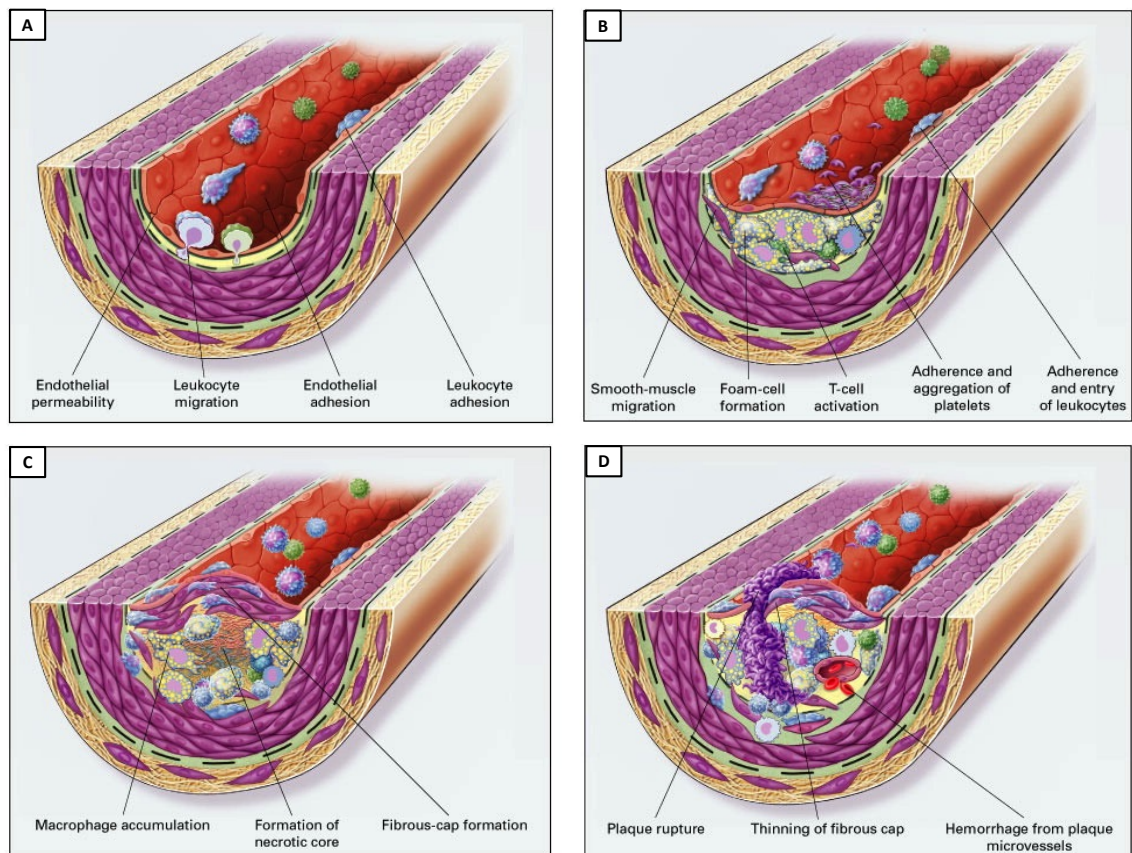


Figure 1-2. Development of an atherosclerotic lesion. A, Endothelial dysfunction and activation with expression of adhesion molecules allowing immune cell attachment. B, Fatty streaks initially consisting of lipid-laden foam cells, T cells and VSMCs. C, Development of a necrotic core with overlying fibromuscular cap. D, Plaque thinning and rupture resulting in intraplaque haemorrhage and superimposed thrombosis. Reproduced with permission from Ross, N Engl J Med 1999; 340:115-126, Copyright Massachusetts Medical Society.

1.4.2 Plaque Instability and Intraplaque Haemorrhage

Dynamic remodelling of the fibrous cap as a result of increased inflammatory cell infiltrate and liberation of enzymes such as matrix metalloproteases results in cap thinning (Gough et al., 2006). This process leaves the cap vulnerable to fissuring and erosion of the endothelial surface (Galis et al., 1994). Cap rupture with exposure of thrombogenic material to luminal blood results in thrombus formation both within the plaque and on its surface, Figure 1-3 (van der Wal et al., 1994). This process may result in rapid plaque expansion and clinically the development of an acute coronary syndrome.

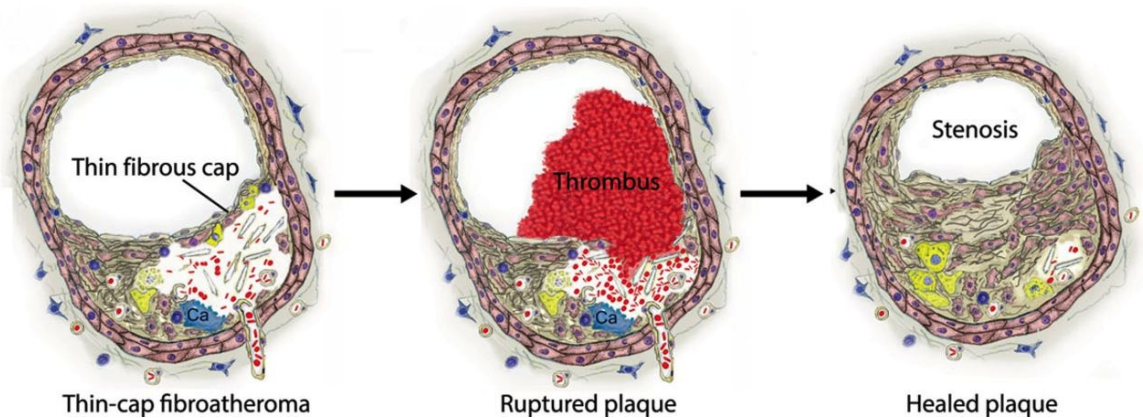


Figure 1-3. Rupture of thin-cap atheroma with thrombus. Healing with resultant constrictive remodelling and luminal stenosis. Reproduced with permission from Jacob Fog Bentzon et al. *Circulation Research*. 2014;114:1852-1866. Copyright American Heart Association.

1.5 Clinical Manifestations of Coronary Heart Disease

The two major clinical manifestations of coronary heart disease are angina pectoris and myocardial infarction. Both may result in chest pain classically described as a tightness or heaviness across the chest, which may radiate to the left arm and or jaw.

1.6 Management of Coronary Heart Disease

1.6.1 Management of Angina

Angina is caused by a fixed stenosis of one or more coronary arteries which limits blood flow and hence oxygen supply to the myocardium. Usually self-limiting, angina is commonly relieved with rest. Following diagnosis made usually on the basis of history and non-invasive testing, initial management of stable angina should focus on risk factor reduction through health related behaviours such as weight loss, physical exercise and smoking cessation. Pharmacological management can be divided into 3 categories:

1. Drugs used to prevent or treat angina attacks by reducing myocardial oxygen demand such as short and long acting nitrates, beta-blockers, calcium channel antagonists (Montalescot et al., 2013).
2. Antiplatelet drugs used to prevent acute coronary syndromes (myocardial infarction and unstable angina) such as aspirin or clopidogrel (Yusuf et al., 2001)
3. Drugs used to modify risk factors and reduce disease progression including HMG CoA reductase inhibitors (Statins) and medication used to treat hypertension (Montalescot et al., 2013).

Failure to adequately control anginal symptoms with medications commonly necessitates further investigation by angiography and possibly revascularisation. Indications for revascularisation published by the European Society of Cardiology are presented in

Table 1. Revascularisation methods available include percutaneous coronary intervention with the use of balloon angioplasty with or without the use of stents (see section 1.7) and coronary artery bypass grafting (CABG). Coronary artery bypass grafting involves either mobilisation of one or both internal mammary arteries from the internal surface of the thoracic cavity and creating an anastomosis with it to the diseased coronary artery beyond the stenosis. Alternatively, the long saphenous veins from the leg or radial arteries can be harvested and used as bypass conduits.

The decision to undertake one revascularisation strategy over another is determined by several factors including risk stratification to predict surgical mortality, location and complexity of disease, presence of diabetes and existence of adequate surgical targets (Head et al., 2012).

Extent of CAD (anatomical and/or functional)	
For prognosis	Left main disease with stenosis >50% ^a
	Any proximal LAD stenosis >50% ^a
	Two-vessel or three-vessel disease with stenosis > 50% ^a with impaired LV function (LVEF<40%) ^a
	Large area of ischaemia (>10% LV)
	Single remaining patent coronary artery with stenosis >50% ^a
For symptoms	Any coronary stenosis >50% ^a in the presence of limiting angina or angina equivalent, unresponsive to medical therapy

Table 1-1. Indications for revascularisation in patients with stable angina. CAD = coronary artery disease; LAD = left anterior descending coronary artery; LV = left ventricular. ^a With documented ischaemia. Reproduced from Windecker et al European Heart Journal (2014) 35, 2541–2619. Copyright European Society of Cardiology.

1.6.2 Management of Myocardial Infarction

Myocardial infarction occurs following superficial erosion and rupture of the fibrous cap as discussed in section 1.4.2. Exposure of the circulating blood to the prothrombotic ECM and lipid-filled necrotic core quickly results in thrombus formation, myocardial cell death and the release of cardiac troponin into the blood. In addition to chest pain, patients commonly complain of shortness of breath and may have features of autonomic disturbance such as sweating, tachycardia, bradycardia, hypo or hypertension, nausea and vomiting. Initial management of myocardial infarction includes the administration of opiate analgesia, nitrates, dual antiplatelet agents such as aspirin and ticagrelor or clopidogrel (Wallentin et al., 2009, Yusuf et al., 2001). In addition, patients should be anticoagulated with low molecular weight heparin or fondaparinux (Yusuf et al., 2006, Cohen et al., 1997).

Myocardial infarctions are commonly divided according to whether ST segment elevation is observed or not on the electrocardiogram (ECG). It should be noted that ST elevation represents the presence of an occlusive thrombus and mandates urgent referral to a percutaneous coronary intervention (PCI) centre for emergency PCI (Authors/Task Force et al., 2014). Primary PCI involves reopening of the vessel using an over the wire balloon catheter and subsequent stent deployment. The use of thrombolytic therapy is largely historical as it has been shown to be inferior to primary PCI therapy (Andersen et al., 2003). Thrombolysis is now only considered in those greater than 2 hours from a PCI centre (Widimsky et al., 2000).

For patients presenting with a Non ST elevation MI urgent angiography is only indicated in the presence of cardiogenic shock or following resuscitation in the event of cardiac arrest (Authors/Task Force et al., 2014). Early risk stratification should be conducted to identify high-risk patients who would benefit from invasive management in addition to optimal medical therapy (Authors/Task Force et al., 2014).

1.7 Coronary Angiography and Intervention

The first cardiac catheterisation in human was carried out in 1929 when Werner Forssmann catheterised the right side of his own heart using a urinary catheter introduced via his antecubital fossa (King, 1998). However, it was almost 30 years before Mason Sones performed the first selective coronary angiogram, accidentally during an elective aortogram (Ryan, 2002). Despite the increasing use of coronary angiography to guide surgical revascularisation it took until 1977 before Andreas Gruntzig conducted the first percutaneous transluminal balloon angioplasty (Gruntzig, 1978).

The initial success of balloon angioplasty was moderated by the immediate complications of acute vessel occlusion, elastic recoil, dissection and thrombosis. In addition, over time negative remodelling resulted in return of clinical symptoms and need for either repeat procedures or CABG. The introduction of metallic stents in the 1980s resulted in the reduction in acute vessel closure following balloon angioplasty (Sigwart et al., 1987). The initial self-expandable stents were soon superseded by balloon expandable stents, found to produce superior long term angiographic results (Serruys et al., 1994, Fischman et al., 1994).

Despite preventing acute vessel occlusion due to elastic recoil and dissection, the placement of stents mandated the use of dual antiplatelet therapy to prevent stent thrombosis. In addition, over a longer time course renarrowing within the stented segment caused by overactive tissue healing was noted in 20 - 30% of cases (Carrozza et al., 1992). In the early 2000's the development of drug eluting stents (DES), metallic stents coated in a polymer impregnated with antiproliferative drugs, resulted in a significant reduction in ISR development (Morice et al., 2002). Despite improvements in stent technology, polymers and antiproliferative drugs, real world occurrence of ISR with DES use may be as high as 10% (Kastrati et al., 2006). Given that in the UK last year over 90,000 PCI procedures were performed ISR represents a significant clinical problem (BHF, 2014).

1.8 In-stent Restenosis

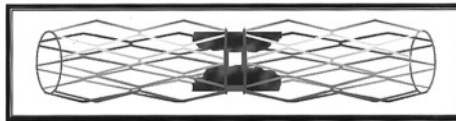
1.8.1 Definition

Angiographically ISR has been defined as the loss of $\geq 50\%$ of the vessel lumen within the stent or up to 5 mm beyond either stent edge (Mehran et al., 1999). Clinically significant ISR requires both the presence of the angiographic finding of $\geq 50\%$ luminal stenosis and either,

1. A history of recurrent angina,
2. Objective evidence of ischaemia either at rest or during non-invasive functional testing, or
3. Objective evidence of impaired blood flow during invasive investigation (eg. Fractional flow reserve (FFR) <0.80)

One early study of 288 ISR lesions in almost 250 patients proposed a classification system based on angiographic pattern observed, Figure 1-4. Investigators were able to demonstrate that target vessel revascularisation was more common with increasing grades of ISR. In addition they demonstrated that previously documented ISR and the presence of diabetes were also associated with higher grades of ISR (Mehran et al., 1999).

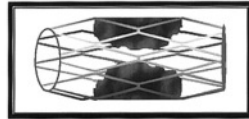
ISR Pattern I: Focal



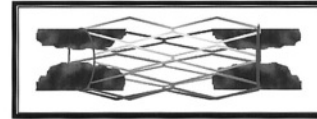
Type IA: Articulation or Gap



Type IB: Margin

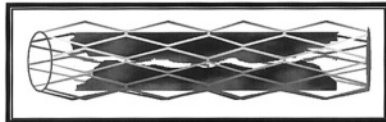


Type IC: Focal Body

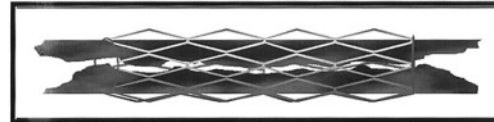


Type ID: Multifocal

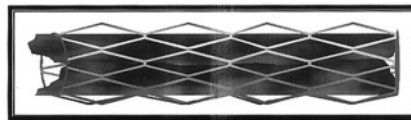
ISR Patterns II, III, IV: Diffuse



ISR Pattern II: Intra-stent



ISR Pattern III: Proliferative



ISR Pattern IV: Total Occlusion

Figure 1-4. Classification of in-stent restenosis. Focal ISR ≤ 10 mm divided into 4 subtypes. Diffuse ISR > 10 mm. Reproduced from (Mehran et al., *Circulation* 1999; 100; 1872-1878). Copyright American Heart Association.

1.8.2 Contributing factors in the development of ISR

Numerous reports have been published documenting factors associated with ISR development and can broadly be divided into three categories: patient, lesional and procedural factors. One of the most commonly reported patient related factors is the presence of diabetes mellitus, in particular if treated with insulin (Kornowski et al., 1998, Abizaid et al., 1998). The fact that insulin is a potent mitogen known to stimulate VSMC growth may account for this observation (Stout et al., 1975). Hypertension and peripheral vascular disease have also been associated with increased incidence of ISR (Agema et al., 2004). However, current smoking, hyperlipidaemia and gender have not (Agema et al., 2004). Lesion characteristics, which predispose to ISR development include long or complex lesions or those present in small calibre vessels (Kastrati et al., 2006). Procedural risk factors include the use of BMS, multiple stents and under expansion of the stent resulting in malapposition against the vessel wall (Kastrati et al., 2006). Interestingly the use of intravascular ultrasound which would detect malapposition has been associated with reduction in ISR development (Kasaoka et al., 1998). The use of high pressure inflation has itself not been associated with increased ISR unless the stent is oversized resulting in deep vessel injury (Gunn et al., 2002). Indeed the severity of vessel injury has been directly correlated with size of neointima and degree of stenosis (Schwartz et al., 1992). In addition, stent geometry has been found to significantly impact on the development of ISR with increasing stenosis directly related to several factors including degree of strut protrusion, inter-strut distance, medial bowing, strut depth, angular burden and strut thickness (Kastrati et al., 2001, Garasic et al., 2000). Concordantly, increasing the number of struts per cross sectional area produces a polygon with a greater number of sides, alleviating many of these stent geometry related factors and reducing ISR (Dean et al., 2005).

1.8.3 Pathophysiology of in-stent restenosis

Following stent placement normal tissue healing results in the coverage of stent struts with a thin layer of neointima composed of VSMCs, ECM and a single layer of endothelial cells lining the vessel lumen (Virmani and Farb, 1999, Costa and Simon, 2005). It should be noted that the healing process and extent of luminal

renarrowing represents a continuum from incomplete strut coverage to total vessel occlusion due to neointimal hyperplasia (Joner et al., 2006).

The process of ISR development involves a complex series of events over time often referred to as a “cellular and molecular cascade”, delineated by an early inflammatory response followed by a late proliferative phase (Chaabane et al., 2013). The iatrogenic endothelial disruption, denudation and medial rupture which occur as a result of stenting exposes blood to the underlying thrombogenic vessel components. Deposition of inflammatory aggregates composed of platelets, fibrin and leucocytes occurs around stent struts and overlying areas of vessel damage have been identified from human pathological samples (Mickelson et al., 1996). In various porcine and canine, balloon injury and stenting models up regulation of adhesion molecules on the surface of activated platelets (P-selectin and integrin glycoprotein IIb/IIIa), ECs, VSMCs (vascular cell adhesion molecule-1 (VCAM-1), Intercellular adhesion molecule-1 (ICAM-1), E selectin), neutrophils and macrophages (macrophage1 antigen-1 (MAC-1)) increases inflammatory cell binding (Neumann et al., 1996, Kornowski et al., 1998, Kim et al., 2001). This process is also aided by the release of cytokines from EC and VSMCs including monocyte chemoattractant protein-1 (MCP-1) and interleukin-8 (IL-8) (Roque et al., 2002). Early canine and porcine balloon injury studies suggested a direct correlation between degree of vessel inflammation and neointimal size (Schwartz et al., 1992). Additionally, significant differences in the inflammatory response were identified between balloon injury and stenting in rabbits and pigs (Rogers et al., 1996, Welt et al., 2000). Balloon injury results in a short lived increase in MCP-1 and IL-8 peaking at between 4 and 8 hours and returning to baseline shortly after (Welt et al., 2000). Elevation of MCP-1 and IL-8 were found to be more pronounced and still increased at 14 days after stenting (Welt et al., 2003). In addition, cellular composition of the forming neointimal also varied between the two rabbit injury models (Welt et al., 2003). Balloon injury induced a neutrophil predominant infiltrate, which peaked at day 3 and returned to baseline by day 6. In addition to an early neutrophil response, stenting produced a profound increase in monocyte / macrophage infiltration, which continued to rise by day 14 (Welt et al., 2003). Interestingly, blockade of the MCP-1 receptor c-c chemokine receptor type 2 (CCR2) in primates reduced ISR following stenting while blockade of cluster differentiation 18 (CD18)

reduced neointimal hyperplasia (NIH) in balloon injury (Horvath et al., 2002). This confirmed not only the importance of inflammation in neointima development but also the relative importance of neutrophils and macrophages with respect to different injury modalities. In addition, use of liposomal alendronate to produce a systemic but transient depletion of monocytes / macrophages in a hypercholesterolaemic rabbit model also reduced ISR (Danenberg et al., 2003).

In conjunction with the loss of anti proliferative factors including nitric oxide (NO) and heparin sulphate proteoglycans, growth factors such as platelet derived growth factor (PDGF) and fibroblast derived growth factor (FGF) are released from a variety of cells including neutrophils, macrophage and VSMCs during this early inflammatory period (Chaabane et al., 2013, Daemen et al., 1991). During ISR development these potent mitogens act on VSMCs to dedifferentiate and begin migrating into the neointima (Ferns et al., 1991). Through receptor tyrosine kinases they activate several signalling cascades including the ras / raf / mitogen activated protein kinase (MAPK) pathway (Graf et al., 1997, Eguchi et al., 1996). The net effect of these signalling cascades is the down regulation of cyclin dependent kinase inhibitor p27^{Kip1} which in turn drives the VSMC through the G1/S phase check point inducing VSMC proliferation and migration (Polyak et al., 1994, Sun et al., 2001). In addition, growth factors, cytokines and vasoactive compounds including angiotensin II (AngII) and endothelin 1 induce these dedifferentiated VSMCs to secrete ECM (Daemen et al., 1991). VSMCs also play a significant role in the remodelling of this ECM scaffold over time by secreting proteolytic enzymes including matrix metalloproteases (MMPs) (Johnson et al., 2011, Cho and Reidy, 2002). Re-endothelialisation is the final step in the healing process, through release of NO and Prostacyclin (PGI₂) endothelial cells inhibit further VSMC, proliferation, migration and ECM synthesis (Jeremy et al., 1999, Peiro et al., 1995). Complete re-endothelialisation may take 12 months or longer in humans (Joner et al., 2006).

1.9 Animal Models of In-stent Restenosis

Much of our understanding of the molecular mechanisms underlying ISR development has been extrapolated from numerous small animal non-stenting vascular injury models including air desiccation, wire, filament, ligation and balloon injury (Kumar and Lindner, 1997, Lindner et al., 1993, Fishman et al., 1975). However, it has become clear that different injury methods, not least stenting, produce different and distinct molecular and cellular responses. Thus researchers have endeavoured to design more complex models, which more accurately replicate the vascular response to stenting. Initial stenting models utilised large animals including dog, pigs and primates (Geary et al., 1996, Roubin et al., 1987, Steele et al., 1985). Importantly the size of these animals allowed the use of human stents, wires and balloons. However, several problems including cost and difficulty in handling has limited their use. In addition to the considerations mentioned above, the ability to manipulate the mouse genome has driven researchers to develop several murine stenting models.

The first published murine stenting model was based on previously developed vein grafting and aortic allograft models (Dietrich et al., 2000, Zou et al., 1998). Using an over the balloon method a stainless steel stent was deployed in the thoracic aorta of a euthanised mouse (Ali et al., 2007). The stented vessel was subsequently interposition grafted into the carotid artery of a recipient mouse. Plastic cuffs were used to facilitate the construction of vascular anastomosis at each end of the graft (Ali et al., 2007). This model demonstrated stenting produces a significantly greater injury response than balloon injury alone. In addition, greater ISR was found in apolipoprotein E (ApoE) $-/-$ mice compared to wild-type (WT) controls (Ali et al., 2007). Despite the success of this model it is not without its criticisms. The use of two mice per procedure increases the number of animals needed and a high degree of surgical skill is required. In addition, disruption of the vaso vasorum around the stented aorta may increase vessel wall anoxia, altering the response to injury.

In response to criticism noted above, the three subsequently developed murine stenting models have all utilised a single animal per procedure. Chamberlain et al developed a self expanding nitinol stent, which was deployed in the infra renal aorta (Chamberlain et al., 2010). Noted complications included

haemorrhage and hind limb paralysis, which occurred in over half of the animals used following femoral artery vascular access (Chamberlain et al., 2010). In addition, nitinol stents are not currently used in clinical practice.

Rodriguez-Menocal et al also developed an infra renal aortic stenting model (Rodriguez-Menocal et al., 2010). This model appears more clinically relevant due to the use of an over the balloon stent. However, vascular access was obtained via a direct incision to the infra renal aorta and likely contributed to the very high fatal haemorrhage rate described (Rodriguez-Menocal et al., 2010).

More recently a carotid artery direct stenting model has been published. This model used a self expanding nitinol stent. Following tissue harvesting, such profound vessel damage was observed that interpretation of the resultant histology was almost impossible (Simsekyilmaz et al., 2013). In addition, to the use of a non-clinically relevant stent the carotid artery of a mouse does not contain a vaso vasorum which has been shown to play an important role in vascular remodelling following injury (Gabeler et al., 2002).

While none of these models is without criticism, they are important in assisting our understanding of the molecular mechanisms involved in ISR. Of note the only model to be repeatedly utilised is that described by the Channon laboratory, (Ali et al., 2007, Douglas et al., 2012, Douglas et al., 2013).

1.10 Vascular Smooth Muscle Phenotype

Vascular smooth muscle cells present within the tunica media of the vessel wall are highly differentiated cells, which primarily function to maintain vessel wall integrity and regulate vessel tone (Owens et al., 2004). In addition, in response to numerous environmental stimuli they display considerable plasticity, being able to change their phenotype between a contractile or quiescent state to that of a synthetic phenotype also known as a proliferative phenotype (Owens et al., 2004).

Healthy, mature, differentiated VSMCs within the vessel wall display a predominantly contractile phenotype possessing an elongated spindle shape. They have also been shown to express elevated levels of contractile proteins including smooth muscle α -actin, smooth muscle myosin heavy chain (SM MHC), smooth muscle 22 alpha (SM22 α) and calponin among others (Li et al., 1996, Miano et al., 1994). Another key feature of contractile VSMC is their low proliferation rate. In contrast de-differentiated VSMCs display a synthetic phenotype exhibit an epithelioid shape as well as demonstrating increased proliferative and migratory capacity, Figure 1-5 (Miano, 2010). As suggested by their name, synthetic VSMCs contain copious amounts of rough endoplasmic reticulum and are the main cell type responsible for ECM generation (Miano, 2010). It is interesting to note that proliferation of VSMC need not necessarily involve complete phenotypic switch to an extreme de-differentiated phenotype.

Environmental stimuli directing VSMC phenotype are known to include growth factors, cytokines, ECM interactions and mechanical stretch (Davis-Dusenbery et al., 2011b). Interestingly, both chemical and mechanical injury influences VSMCs, inducing a de-differentiated phenotype, which plays a role in atherosclerosis, vein graft failure and ISR as, discussed in section 1.8.3.

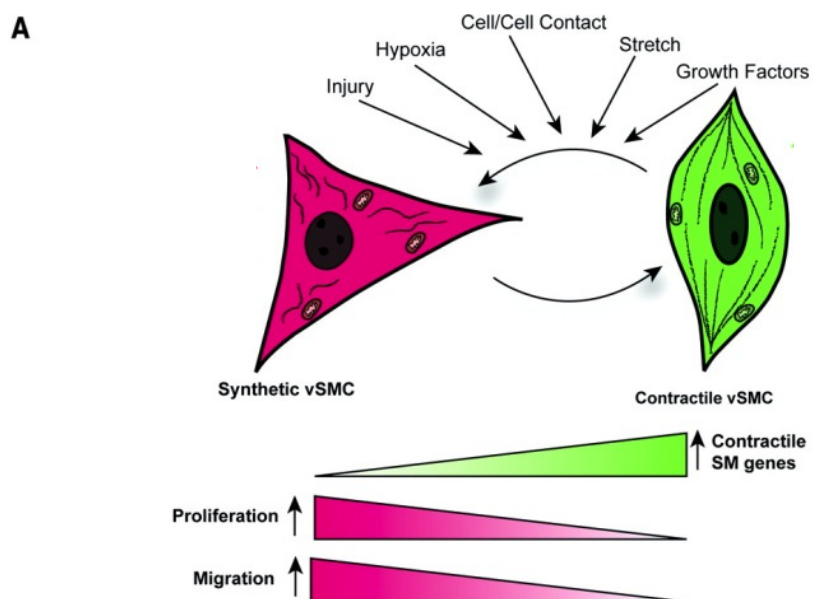


Figure 1-5. Vascular smooth muscle cell phenotype regulation. A, Multiple stimuli capable of modulating VSMC phenotype. Contractile phenotype demonstrates elongated shape with elevated expression of contractile genes and low proliferation rate. Synthetic phenotype characterised by increased migratory and proliferative capacity. Adapted from Davis-Dusenbery et al. *Arterioscler Thromb Vasc Biol.* 2011;31:2370-2377. Reproduced with permission.

1.11 MicroRNAs

In 1993 two groups studying the temporal control of *Caenorhabditis elegans* (*C. elegans*) development published their findings that *lin-4* was a non protein coding gene producing a 22 nucleotide long single stranded ribose nucleic acid (RNA) molecule (Lee et al., 1993, Wightman et al., 1993). They demonstrated that through complimentary binding in an antisense manner to the 3' untranslated region (3'UTR) of *lin-14* messenger RNA (mRNA), translation and hence protein levels were temporarily suppressed (Wightman et al., 1993, Lee et al., 1993). Initially thought to be peculiar to *C. elegans* it took a further 7 years before a second example (*let 7*) was identified again in *C. elegans* (Reinhart et al., 2000). However, shortly afterwards *let-7* was identified in *Drosophila* and various mammals including humans (Pasquinelli et al., 2000).

Many more regulatory RNA molecules have since been discovered with the same mechanisms of generation and action. These short RNAs have been termed microRNAs (miRNAs) in order to distinguish them from other classes of regulatory RNAs such as short inhibitory RNAs (siRNAs), and PIWI interacting RNAs (piRNAs) (Bartel, 2004). MiRNAs are short 19 - 25 nucleotide non-coding RNA molecules found in plants, insects and animals, which function to post-transcriptionally regulate the translation of messenger RNA (Bartel, 2004). Over 1000 miRNAs have been identified in the human genome and are thought regulate around 30% of all protein coding genes (Friedman et al., 2009). Interestingly, significant homology in miRNAs is observed across animal species. MiRNAs can have numerous targets often repressing multiple genes at different points in the same biological pathway. Conversely multiple miRNAs may be able to target the same mRNA. Across numerous biological processes including development miRNA - mRNA networks exist to fine tune protein expression (van Rooij et al., 2012). In addition, miRNAs have been identified to play important roles in almost every disease including cancer and cardiovascular disease (van Rooij and Olson, 2012).

1.11.1 Biogenesis

1.11.1.1 Transcription

MiRNAs have been described in various genomic locations, including the introns of previously identified protein coding genes where they may be positioned on either the sense or antisense strand. In addition, depending on splice variations of the protein coding gene, miRNAs may be located within an exon (Rodriguez et al., 2004). If running in the sense orientation to the protein coding gene, miRNAs may be transcribed as part of the protein coding mRNA transcript under the control of the host promoter (Baskerville and Bartel, 2005). Alternatively, it has been demonstrated that intronic miRNAs may be transcribed under the control of their own distinct promoter (Cai et al., 2004). MiRNA-21 being an example which can be transcribed under the control of both its own promoter and that of the protein coding gene in which it resides (Ribas et al., 2012, Cai et al., 2004, Fujita et al., 2008, Loffler et al., 2007). Many miRNAs are located within intergenic regions far from known protein coding genes and may be transcribed singly or as clusters (Bartel, 2004). Clustered miRNAs are commonly transcribed under the control of one promoter (Bartel, 2004). In addition clustered miRNAs are often family members possessing significant homology and regulating the same genes or pathways (Friedman et al., 2009). MiRNA promoters have been shown to possess the same transcription response elements as protein coding genes (Loffler et al., 2007).

The majority of miRNAs are believed to be transcribed by RNA polymerase II (Lee et al., 2002). Primary miRNAs (Pri-miRNAs) can be 1kb or longer and most are noted to be methyl G capped at their 5' end and contain polyadenylation signals at their 3' terminus, Figure 1-6 (Cai et al., 2004).

1.11.1.2 Nuclear Processing

Following transcription the pri-miRNA containing the stem loop hairpins are processed within the nucleus by the RNaseIII endonuclease Drosha which is part of a larger microprocessor complex also containing a DiGeorge Critical Region 8 (DGCR8) and the DEAD box RNA helicases p68 and p72, Figure 1-6 (Lee et al., 2003). This Drosha / DGCR8 microprocessor cleaves the stem loop from its primary transcript to form a pre-miRNA molecule 65 to 100 nucleotides in length

which importantly has a 2 nucleotide overhang on its 3' end (Lee et al., 2003). Enhanced Drosha/DGRC8 processing of pri-miRNA transcripts has been documented in response to both TGF β and bone morphogenic protein 4 (BMP4) stimulation. The induction of receptor specific SMAD interaction with the p68 component of the microprocessor complex has been shown to promote stabilisation of the Drosha / DGCR8 interaction, increasing pri-miR-21 processing (Kang et al., 2012, Davis-Dusenbery and Hata, 2011). Additionally, the tumour suppressor p53 has been shown to increase the processing of anti-proliferative miRNAs including miR-143 and miR-145 (Suzuki et al., 2009). It should be noted that for miRNAs transcribed as part of a longer protein coding mRNA, splicing does not need to occur before the miRNA is processed by Drosha/DGCR8. In addition, pri-miRNA processing does not negatively impact on the preliminary mRNA (pre-mRNA) to undergo splicing into mature mRNA (Kim and Kim, 2007).

1.11.1.3 *Transportation across the Nuclear Membrane*

The resulting preliminary miR (pre-miR) hairpin product is exported from the nucleus into the cytoplasm by an active process involving Exportin-5 and Ran-GTP. The importance of the 3'overhang for Exportin-5 recognition has previously been demonstrated. Interestingly, having the pre-miR base ends of equal length reduced export from the nucleus (Zeng and Cullen, 2005). Additionally, binding to Exportin-5 has been shown to protect the pre-miR from nuclear degradation, Figure 1-6 (Zeng and Cullen, 2004).

1.11.1.4 *Cytoplasmic Processing and Maturation*

Once in the cytoplasm the pre-miRNA is then recognised by Dicer, a second RNaseIII endonuclease. Dicer, which contains helicase activity and two RNase binding domains, cleaves the loop from the pre-miRNA creating a second 3' overhang (Lee et al., 2002). This imperfect RNA duplex 19-25 nucleotides long was initially denoted miRNA:miRNA* referring to the active or guide miRNA stand involved in mRNA regulation and the star (or passenger) strand of RNA which was thought to have no function and to be degraded by the cellular apparatus. However, recent studies have shown that both strands may be biologically active (Bang et al., 2014). Thus, newer nomenclature commonly uses the suffixes -5p or -3p dependent on which side of the stem loop they are generated from.

Once cleaved by Dicer the mature duplex is unwound and the appropriate guide strand selected for loading into the Argonaute (Ago) protein (Bartel, 2009). Along with other co-factors such as TAR RNA-binding protein (TRBP), this Argonaute protein and mature miRNA form the microRNA induced silencing complex (miRISC) (Bartel, 2009). In humans four different Argonaute proteins present in humans each containing a PIWI-Argonaute-Zwillie (PAZ) domain which binds the 3' end of the miRNA, a MID domain binding the 5' end and an central P-element induced wimpy testes (PIWI) domain (Song et al., 2004). Argonaute proteins are responsible for facilitating mRNA translational repression (Pillai et al., 2005). Ago2 is the only Argonaute protein containing endonuclease activity within its PIWI domain (Lima et al., 2009).

1.11.1.5 *MiRNA mechanisms of action*

Nucleotide residues 2 - 8 at the 5' end of the miRNA, known as the "seed sequence" are primarily responsible for the binding of the guide miRNA to the 3'UTR of target mRNA, inhibiting translation (Bartel, 2009). Perfect complementarity of the miRNA seed and 3'UTR in the presence of Ago2 is likely to induce cleavage of the mRNA and thus prevent translation. However, imperfect seed sequence complementarity, in conjunction with the binding of other residues outwith the seed sequence to the 3'UTR is more commonly observed. This results in translation repression, possibly by interfering with the initiation of translation through blockade of the eukaryotic initiation factor (eIF) 4E - mRNA interaction (Humphreys et al., 2005). Despite direct cleavage of mRNA by Ago2 being an uncommon event a reduction in target mRNA levels are commonly observed (Guo et al., 2010). This has been attributed to the miRISC directing the mRNA target towards intracellular p-bodies where they are deadenylated, uncapped and degraded, Figure 1-6 (Wu et al., 2006, Eulalio et al., 2009).

Although the majority of miRNA - mRNA interactions occur at the 3'UTR of the mRNA notable exceptions have been discovered. Several miRNAs including miR-134, miR-296 and miR-470 have been shown to suppress the translation of key regulatory genes involved in stem cell differentiation through binding to target sequences within their coding sequence rather than 3'UTR (Tay et al., 2008). Additionally, miR-10a has been demonstrated to upregulate cellular protein

synthesis by binding to the 5'UTR of several ribosomal proteins increasing their translation (Orom et al., 2008).

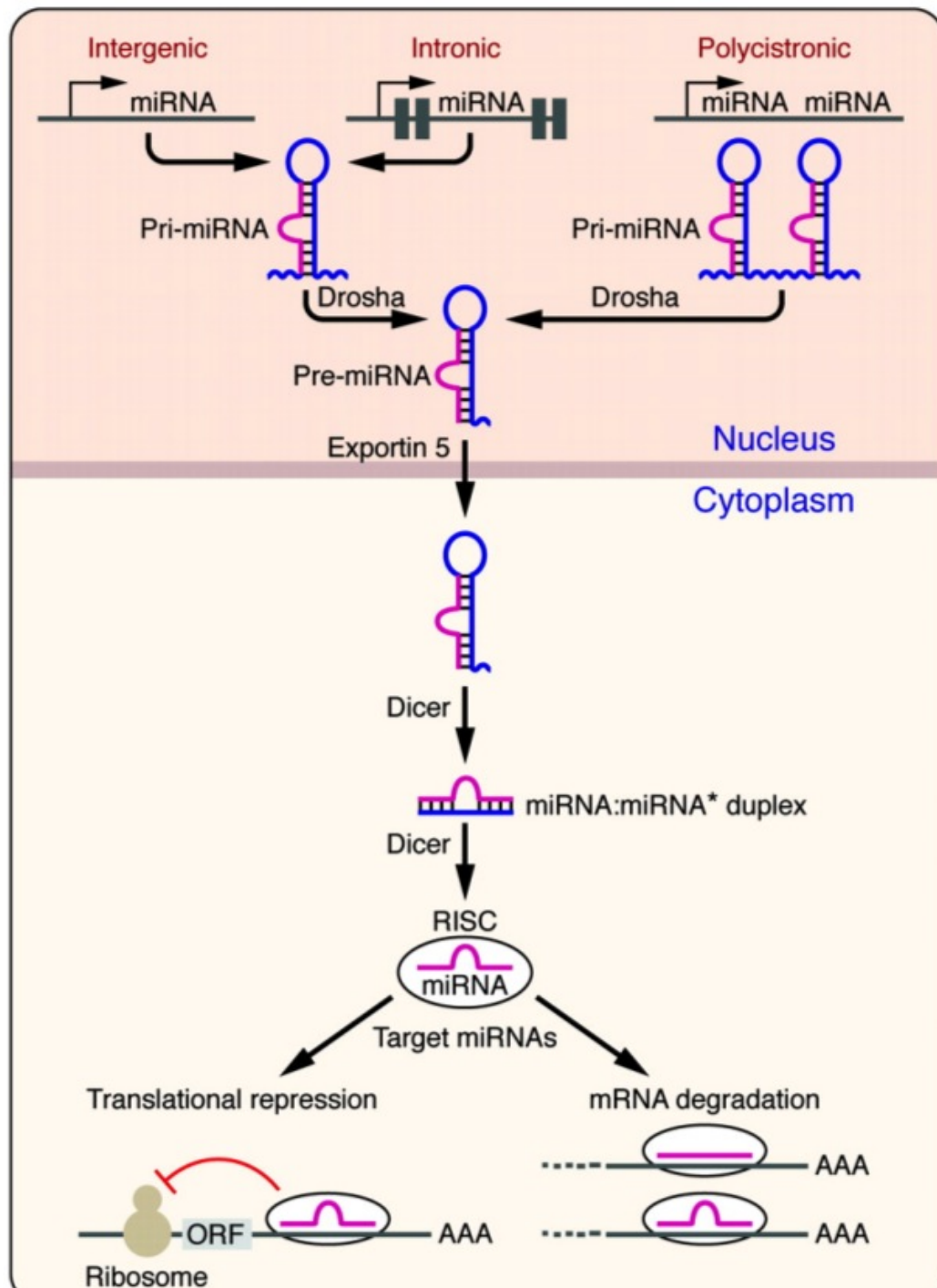


Figure 1-6. miRNA Biogenesis Pathway. The primary transcripts of miRNAs, pri-miRNAs, are transcribed from individual miRNA genes, introns host genes, or polycistronic clusters. The RNaseIII Drosha cleaves the pri-miRNA into a pre-miRNA. Pre-miRNAs are exported from the nucleus by exportin 5. Within cytoplasm, another RNaseIII, Dicer cleaves the pre-miRNA forming a miRNA:miRNA* (miRNA-5p:mRNA-3p) duplex. Mature miR is loaded in to RISC complex containing Argonaute protein and henceforth negatively regulates gene expression by either translational repression or mRNA degradation. RISC – RNA induced silencing complex. ORF - open reading frame. Reproduced with permission, Van Rooij *Circ Res.* 2011;108:219-234. Copyright American Heart Association.

1.12 Expression of microRNAs are essential for development

Lin-4 and let-7, the first two identified miRNAs initially were shown to play an important role in *C. elegans* development. By suppressing translation of their respective mRNA targets lin-14 and lin-41 they facilitated normal progression through the larval phase of development (Lee et al., 1993). The necessary role of miRNAs in the development of vertebrates has since been documented. In Zebra fish embryos, genetic deletion of Dicer demonstrated that normal development appeared to occur during the first week post fertilisation, while on day 8 growth arrest was noted and most were dead by the end of the second week (Wienholds et al., 2003). A notably elevated level of pre-miR26a was demonstrated and mature let-7 found to be absent, implying that alternative processing pathways were not facilitating miR maturation within the embryos (Wienholds et al., 2003). Interestingly, knockdown of Dicer produced an earlier phenotype than that of genetic deletion attributed to the concomitant suppression of maternal Dicer (Wienholds et al., 2003). Importantly, post mortem examination revealed general growth arrest rather than a single organ defect suggesting a global role of miRNAs in development (Wienholds et al., 2003). Another group independently identified that in mice complete absence of Dicer was lethal at embryonic day 7.5 (E7.5) immediately prior to gastrulation (Bernstein et al., 2003). They attributed their findings to the depletion of stem cells from the blastocyst as a consequence of their premature terminal differentiation (Bernstein et al., 2003).

1.13 MicroRNA expression and cardiovascular development

Several studies have looked at the importance of miRNAs in the development of different vascular tissues. Within the heart, genetic deletion of Dicer in mice, while not being embryonically lethal did result in death within 4 days of birth (Chen et al., 2008). Hearts from these mice demonstrated the virtual absence of mature miRNAs, dilated cardiomegaly, left ventricular mural thrombi and myofibril disarray (Chen et al., 2008). However, Dicer deletion did not affect cardiomyocyte proliferation but did affect expression of contractile proteins including myosin heavy chain and α -tropomyosin (Chen et al., 2008). Interestingly, analysis of human hearts with dilated cardiomyopathy revealed a significant reduction in Dicer at the time of left ventricular assist device implantation, a finding which was reversed upon functional recovery (Chen et al., 2008). Another study of targeted postnatal Dicer deletion in cardiomyocytes using a tamoxifen-inducible Cre recombinase approach demonstrated similar findings with structural and electrical remodelling in juvenile and adult mice (da Costa Martins et al., 2008).

Within vascular endothelial cells, both Drosha and Dicer knockdown using siRNA have demonstrated the importance of miRNAs in cardiovascular development. *In vitro* analysis demonstrated that endothelial sprout formation was reduced when either RNaseIII was knocked down (Kuehbach et al., 2007). However, only Dicer knockdown impaired human umbilical vascular endothelial cell (HUVEC) migration (Kuehbach et al., 2007). Using nude mice, researchers subcutaneously implanted matrigel plugs containing siRNA transfected HUVECs. As with the *in vitro* migration experiment this demonstrated only Dicer inhibition reduced angiogenesis (Kuehbach et al., 2007). These findings confirmed previously published work, which had used similar Dicer knockdown strategies to demonstrate alterations in the expression of several key regulators of angiogenesis (Suarez et al., 2007). Further work using a postnatal inducible EC Dicer deletion approach demonstrated Dicer to be essential for post natal angiogenesis and that the effects on EC proliferation, migration and angiogenesis was likely as a result of miR-17-92 cluster inhibition (Suarez et al., 2008).

An essential role for miRNAs in VSMC development has also been elucidated. Conditional Dicer deletion in VSMC was noted to be embryonically lethal between E15.5 and E16.5 as a result of subcutaneous and intracerebral haemorrhage (Albinsson et al., 2010, Pan et al., 2011). Detailed analysis revealed Dicer deletion resulted in blood vessels which were thin walled, dilated and lacking VSMCs. Myography of umbilical arteries revealed impaired contractile response to both potassium chloride (KCl) and calcium stimulation (Albinsson et al., 2010). Histological analysis of the elastic lamellae also revealed profound fragmentation (Albinsson et al., 2010). In addition, VSMCs from the KO mice revealed reduced proliferative capacity and a reduction in VSMC specific gene expression including, smooth muscle α -actin, calponin and myosin heavy chain 22 (MYH22) (Pan et al., 2011). These findings show that, not only are miRNAs essential for VSMC proliferation but that they are also involved in VSMC differentiation. Postnatal deletion of Dicer in VSMC has subsequently been shown to result in vascular remodelling, reduced blood pressure and contractile function in resistance vessels (Albinsson et al., 2011).

1.14 Role of MicroRNAs following Vascular Injury

While microRNAs are essential for normal development and maintenance of homeostasis they have also been implicated in numerous disease states. From infectious and autoimmune diseases to cancer and notably cardiovascular disease their aberrant expression often results in the induction of maladaptive molecular and cellular responses (Small and Olson, 2011, Schee et al., 2012, Zhu et al., 2012). MicroRNAs have been shown to be dysregulated in numerous cardiovascular diseases including myocardial infarction, hypertension, dilated cardiomyopathy, atherosclerosis, cardiac allograft vasculopathy, aneurysm formation, vein graft failure and in the development of in-stent restenosis following percutaneous coronary intervention (Small and Olson, 2011, van Rooij and Olson, 2012, O'Sullivan et al., 2011).

Different MiRNAs have been shown to promote either a contractile or synthetic VSMC phenotype. In addition, following vascular injury their dysregulation facilitates the transitioning towards a synthetic phenotype. Several microRNAs, which are known to influence VSMC phenotype, are discussed below, Table 1-2.

Table 1-2. Summary of VSMC miRNA Expression Following Vascular Injury.

miRNA	Expression after Injury	Biological Effect	mRNA target	Reference
miR-21	Increased	Pro-synthetic / pro-contractile	PTEN PDCD4 TPM1 c-Ski	Ji et al 2007, Maegdefessel et al 2012, McDonald et al 2013, Lin et al 2009, Song et al 2012, Wang et al 2012, Wang et al 2011, Li et al 2014
miR-221 / 222	Increased	Pro-synthetic	p27, p57	Liu et al 2009, Davis et al 2009
miR-143 / 145	Decreased	Pro-contractile	KLF4, KLF5, Elk-1, PKC ϵ , PDGF-R α , Fascin	Cheng et al 2009, Cordes et al 2009, Quintavalle et al 2010.
miR-133a	Decreased	Pro-contractile	Sp-1, Moesin	Torella et al 2011
miR-195	Decreased	Pro-contractile / anti-inflammatory	Cdc42	Wang et al 2012b
miR-663	Decreased	Pro-contractile	JunB	Li et al 2013c
miR-638	Decreased	Pro-contractile	NOR1	Li et al 2013b

Legend. PTEN, phosphatase and tensin homologue. PDCD4, programmed cell death 4. TPM1, tropomyosin-1, KLF, Kruppel-like factor. PKC ϵ , protein kinase C epsilon. PDGF-R α , platelet derived growth factor receptor alpha. Sp-1, specificity protein-1. Cdc42, cyclin dependent kinase 42. NOR1, neuron derived orphan receptor 1.

1.14.1 miR-21 (Pro-synthetic and Pro-contractile)

MicroRNA-21 is located on human chromosome 17q23.1. An intronic miRNA, its stem loop is located within the 11th intron of the transmembrane protein 49 (TMEM49) gene also known as vacuole membrane protein 1 (VMP1) (Cai et al., 2004). This transmembrane spanning protein localised to the endoplasmic reticulum has been implicated in the initiation and regulation of autophagy: the process of cell organelle degradation, which serves to maintain cell survival during periods of cellular stress or starvation (Calvo-Garrido et al., 2008). In addition, it has also been implicated in the resistance of some cancers including pancreatic cancer to chemotherapeutic agents (Gilabert et al., 2013). Several groups have demonstrated that miR-21 can be transcribed independently from the protein coding host gene through a distinct promoter. Three overlapping promoter regions have been proposed and while it is acknowledged to span much of the 10th intron of the protein coding host gene no conclusive agreement upon its size has yet been reached (Cai et al., 2004, Fujita et al., 2008, Loffler et al., 2007). The primary transcript of miR-21 has been shown, like messenger RNA molecules, to be both 5' capped and 3' polyadenylated (Cai et al., 2004). MiRNA-21 is processed as described in section 1.11.1 with pre-miR-21 containing 72 nucleotides its mature form being 22 nucleotides in length with the sequence 5'-UAGCUUAUCAGACUGAUGUUGA-3'. Mature miR-21 is derived from the 5' end of the pre-miR hairpin giving it the suffix -5p (miR-21-5p) (Asangani et al., 2008). Throughout the remainder of this thesis it shall be denoted as miR-21 unless there is a specific need to distinguish it from the passenger (star) strand where the terms miR-21-5p and miR-21-3p will be used, respectively.

Initially described as an “oncomir” due to its ubiquitous over-expression and deleterious function in many cancers, two studies have highlighted its importance in patients with vascular disease. MiRNA-21 has been shown to be up regulated in both the intima and serum of patients with Arteriosclerosis Obliterans as well as within atherosclerotic plaques (Li et al., 2011, Raitoharju et al., 2011).

Conflicting reports as to whether miR-21 promotes either a contractile or synthetic VSMC phenotype following vascular injury have been published. De-differentiated synthetic VSMCs demonstrate greatest miR-21 expression while

others have demonstrated up regulation of miR-21 is necessary for TGF β to induce a contractile phenotype (Ji et al., 2007, Davis et al., 2008). More recently, the miR-21 targeting of tropomyosin-1 (TPM1), a contractile protein regulating the calcium-dependent interaction of actin and myosin, induced cell elongation (a contractile feature) while concurrently inducing an increase in proliferation and migration; two classic features of synthetic VSMCs (Wang et al., 2011). Thus it would appear that the effect of miR-21 in VSMCs phenotype are complex and may depend on their origin, the disease process and mRNA target.

Regardless of which VSMC phenotype miR-21 induces, its up regulation has been demonstrated consistently in multiple injury models. The following sections discuss the effects of miR-21 up regulation in relation to mRNA targets.

1.14.1.1 Phosphatase and tensin homolog

One of the earliest published studies investigating miR-21 in vascular injury utilised a rat carotid artery balloon injury model (Ji et al., 2007). Investigators demonstrated that 7 days following injury miR-21 was up regulated over 6 fold. This elevation persisted at day 14, before returning to baseline by day 28 (Ji et al., 2007). Investigators found a significant reduction in neointimal formation by applying a miR-21 antagomiR containing poloxamer gel to the adventitial surface of the carotid vessel at the time of balloon injury. Two reasons given for this finding are a reduction in cellular proliferation as evidenced by significantly fewer 5-Bromo-2'-deoxyuridine (BrdU) positive cells within both the vessel neointimal and media. Secondly a significant increase in apoptosis was observed within the developing neointima upon miR-21 knockdown (Ji et al., 2007). *In vitro* analysis demonstrated elevated miR-21 expression within de-differentiated VSMCs cultured in 10% serum. In addition, the *in vitro* effects of knockdown on proliferation and apoptosis were in keeping with those found *in vivo* (Ji et al., 2007).

Further analysis revealed that *in vitro* over expression of miR-21 using an adenovirus vector in VSMCs, resulted in reduced phosphatase and tensin homolog (PTEN) protein expression and an increase in the anti apoptotic protein B-cell lymphoma-2 (Bcl-2) (Ji et al., 2007). The increase in Bcl-2 is likely an indirect

downstream signalling effect. Concordant with the observed reduction in PTEN, an increase in phosphorylated Akt was also demonstrated. PTEN is a previously validated target of miR-21, which acts to block the growth factor-mediated activation of Akt by phosphoinositide-3-kinase (PI3K) (Meng et al., 2007). As a result of PTEN inhibition, Akt-mediated activation of mammalian target of rapamycin (mTOR) increases with consequent increases in proliferation and reduced apoptosis (Meng et al., 2007).

Further evidence of the importance of PTEN inhibition by miR-21 was documented in two mouse models of abdominal aortic aneurysm (AAA) development. As aneurysms developed following porcine pancreatic elastase (PPE) or AngII infusion a parallel increase in miR-21 expression was observed (Maegdefessel et al., 2012). Systemic over expression of miR-21 using a lentiviral vector induced PTEN down regulation at both mRNA and protein levels (Maegdefessel et al., 2012). In addition, miR-21 over expression was associated with a reduction in aneurysm expansion attributed to increased VSMC proliferation and a decrease in apoptosis within the aortic wall (Maegdefessel et al., 2012). Interestingly, a single tail vein injection of anti-miR-21 at 10 mg/kg appeared sufficient to block miR-21 for up to 14 days, increase PTEN expression and produce aneurysm expansion. In human samples of AAA, miR-21 and PTEN levels were found to be dysregulated in the same manner as occurred in the experimental mouse models (Maegdefessel et al., 2012).

Using these murine aneurysm animal models, researchers also assessed the effect on inflammatory cytokine production as a consequence of miR-21 and PTEN modulation. They demonstrated MCP-1 and IL-6 were elevated upon miR-21 over expression (Maegdefessel et al., 2012). This is in keeping with previous reports that PTEN deficiency in the setting of a murine carotid artery ligation results in increased inflammatory cytokine and NIH production (Furgeson et al., 2010).

Another key study confirming the conservation of miR-21 / PTEN axis across species assessed multiple vein-grafting models in mice, pigs and humans (McDonald et al., 2013). Vein grafts in all three species demonstrated an increase in miR-21. This was confirmed to be present in all three layers of the vein graft with co-localisation identifying up regulation in VSMCs, macrophages

and myofibroblasts. Genetic deletion of miR-21 in a mouse model of interposition grafting demonstrated an 81% reduction in NIH development (McDonald et al., 2013). Grafting between miR-21 KO and WT mice demonstrated that the graft genotype was key to reduction of NIH rather than that of the recipient. In addition, *ex vivo* antimiR-21 treatment of human saphenous vein grafts demonstrated a de-repression of several previously validated targets including PTEN (McDonald et al., 2013).

1.14.1.2 Programmed cell death 4

Programmed cell death 4 (PDCD4) is a tumour suppressor protein known to inhibit the initiation of mRNA transcription by binding eIF4A (Yang et al., 2003). In addition, it is also known to inhibit the activity of AP-1 and initiate apoptosis (Liu et al., 2010).

In vitro investigation by two independent groups using different injury methods have demonstrated PDCD4 is an important target of miR-21 in rodent VSMCs. Firstly, chemical injury with hydrogen peroxide was shown to increase miR-21 expression, concomitantly repressing PDCD4 expression and reducing apoptosis. Using luciferase reporter assays they confirmed PDCD4 to be a miR-21 target. In addition, they demonstrated miR-21 modulation using pre-miR and antimiR strategies repressed and de-repressed PDCD4 expression which resulted in a reduction and increase in apoptosis, respectively (Lin et al., 2009).

Interestingly mechanical stretch has been shown to induce a biphasic response in miR-21 expression within murine VSMCs (Song et al., 2012). Researchers demonstrated that while moderate stretch reduced miR-21 expression, excessive stretch produced the opposite effect. A reduction in PDCD4 was observed with excessive stretch while miR-21 inhibition restored PDCD4 levels. At a cellular level apoptosis was observed following excessive stretch and this was exacerbated further by miR-21 inhibition (Song et al., 2012). This implies miR-21 up regulation is a protective mechanism inhibiting apoptosis following mechanical injury.

Confirmation that miR-21 targets PDCD4 *in vivo* was demonstrated in a rat iliac balloon injury model (Wang et al., 2012a). This study implicated miR-21 induced

PDCD4 inhibition in both reducing apoptosis and increasing proliferation. Using antagomiR applied to the adventitial surface of the ballooned iliac artery a reduction in NIH was observed. *In vitro* PDCD4 knockdown using siRNA ameliorated the reduction in cell proliferation observed with miR-21 inhibition (Wang et al., 2012a).

Taken together these studies involving the miR-21 / PDCD4 axis show its importance in regulating apoptosis and proliferation following vascular injury.

1.14.1.3 Tropomyosin 1

Arteriosclerosis obliterans is progressive vascular disorder characterised by progressive vascular occlusion due to uncontrolled VSMC hyperplasia. MicroRNA dysregulation was observed in human samples of patients with arteriosclerosis obliterans. In particular an almost eight fold increase in miR-21 was identified within VSMCs (Wang et al., 2011). This increase in miR-21 was associated with a reduction in tropomyosin (TPM1), a contractile protein found in VSMCs, which regulates the calcium-dependent interaction of actin and myosin (Wang et al., 2011). TPM1 was confirmed as a target of miR-21 by luciferase reporter assay. Careful *in vitro* analysis using siRNA and antagomiR strategies revealed PDGF-induced VSMC stimulation of proliferation and migration was mediated by an increase in hypoxia inducible factor alpha (HIF- α), which in turn stimulated the expression of miR-21 (Wang et al., 2011). Researchers were unable to identify a HIF α response element within the miR-21 promoter and it remains unclear as to the exact mechanism of this interaction (Wang et al., 2011).

Down regulation of TPM1 by miR-21 was associated with VSMC elongation (Wang et al., 2011). The VSMCs elongation implies the presence of a contractile phenotype despite the increase in proliferation and migration which are two key features of a synthetic phenotype (Wang et al., 2011).

1.14.1.4 c-Ski

c-Ski is a protein found within VSMC which primarily acts to increase cell cycle inhibitor p27 and p21 (Li et al., 2013a). Following balloon injury in a rat model miR-21 increase was accompanied by c-Ski reduction and increased proliferation (Li et al., 2014). Confirmation that c-Ski is a miR-21 target was conducted by

luciferase reporter assay. Utilising a miR-21 mimic strategy c-Ski was down regulated in A10 cells a rat derived cell line of VSMCs. Over expression of c-Ski in the presence of miR-21 mimic inhibited proliferation. Researches demonstrated the miR-21 mimic reduced both p21 and p27, the effects of which were reversed by c-Ski over expression (Li et al., 2014). These data show c-Ski is a miR-21 target in the setting of vascular injury.

Taken together the above studies demonstrate the up regulation of miR-21 in response to a variety of different types of vascular injury. Through careful miR-21 and target manipulation they demonstrate that miR-21 actively participates in the healing response promoting proliferation, migration and preventing apoptosis.

1.14.2 miR-221/222 (Pro-synthetic)

Encoded as a miRNA cluster on the X chromosome, miR-221 and miR-222 have the same seed sequence (Davis et al., 2009). Their expression has been demonstrated in human blood vessels, in particular VSMCs although expression in the endothelium has been documented (Nicoli et al., 2012). Both miR-221 and miR-222 appear co-expressed within the systemic circulation while in pulmonary artery smooth muscle cells (PASMCs) their differential expression has also been noted (Davis et al., 2009). They primarily function to promote a synthetic VSMC phenotype with the up regulation of miR-221 in particular shown to coincide with a reduction in contractile VSMC markers including calponin and SM22 (Davis et al., 2009).

In cultured VSMCs stimulation with PDGF induced miR-221 and miR-222 expression in a dose-dependent manner (Davis et al., 2009). Both were also up regulated within the carotid artery following balloon injury. *In situ* hybridisation and co-localisation with smooth muscle α -actin demonstrated this increase occurred in VSMCs (Liu et al., 2009).

Knockdown strategies using antimiRs successfully inhibited both miRs *in vitro* and *in vivo*, when administered systemically. The resulting decrease in

proliferation indicates miR-221 and miR-222 exert a positive effect on VSMC proliferation (Liu et al., 2009).

Not only did PDGF stimulation of VSMCs induce miR-221 and miR-222 but a reduction in p27 and p57 was also found. Both of these cell cycle inhibitors are predicted targets of miR-221 and miR-222 (Liu et al., 2009). 3'UTR luciferase reporters confirmed miR-221 and miR-222 binding. In culture, loss of function experiments demonstrated that inhibition of both miRs increased p27 and p57. De-repression of p27 and p57 was confirmed *in vivo* by locally applying anti-miR-222 to the vessel wall at time of angioplasty. In addition to de-repression of these targets a reduction in proliferating cells was also observed within the vessel wall (Liu et al., 2009).

1.14.3 miR-143/145 (Pro-contractile)

MiR-143 and miR-145 are both markers and promoters of the contractile VSMC phenotype (Boettger et al., 2009). Located on human chromosome 5 (mouse chromosome 18), miR-143 and miR-145 together compose a bicistronic cluster, co-transcribed as part of the same pri-miR (Rangrez et al., 2011). During embryonic development they are first expressed in the developing heart at E7.5 before peaking at E9.5 and can no longer be detected in ventricular myocardium by E16.5. In addition, at E11.5 miR-143 and miR-145 are both highly expressed within the developing great vessels before becoming evident in blood vessels of all developing organs (Cordes et al., 2009). Postnatally miR-143 and miR-145 have been shown to be expressed within the media of blood vessels in particular within VSMCs (Cheng et al., 2009).

1.14.3.1 miR-143 and miR-145 as markers and modulators of a contractile phenotype

Evidence confirming, *in vitro* and *in vivo*, that miR-143 and miR-145 are markers of a pro-contractile phenotype has been published by several groups (Boettger et al., 2009, Cheng et al., 2009, Davis-Dusenbery et al., 2011a, Hutcheson et al., 2013, Xin et al., 2009). Culture of primary VSMCs demonstrated high initial levels of miR-145 expression, which was noted to fall over time as cells de-

differentiated into a synthetic state (Boettger et al., 2009, Cheng et al., 2009). The addition of PDGF, a known inducer of a synthetic phenotype, to freshly isolated VSMCs accelerated the reduction in miR-145 expression and fall in markers of contractile phenotype (Cheng et al., 2009). *In vivo*, balloon injury of the carotid artery in rats is known to induce VSMCs towards a synthetic state prior to proliferation and migration (Clowes and Clowes, 1986). A concomitant reduction in miR-143 and miR-145 following balloon injury has also been demonstrated (Cheng et al., 2009). Interestingly, other models of vascular injury including carotid ligation, transverse aortic constriction and atherosclerosis in ApoE *-/-* mice, have also demonstrated reduction in miR-143 and miR-145 (Elia et al., 2009, Cordes et al., 2009). Concordant with these findings, human samples taken from patients with AAA demonstrated a reduction in both miRs compared to aortic samples from healthy controls has been demonstrated (Elia et al., 2009).

Loss and gain of function studies using siRNAs and premiRs were subsequently utilised to determine whether miR-143 and miR-145 plays a role in VSMC phenotype modulation *in vitro*. miR-145 knockdown augmented PDGF mediated de-differentiation *in vitro* with a resultant decrease in smooth muscle markers α -actin and calponin (Cheng et al., 2009). The addition of premiR-145 to VSMCs cultured in the presence of PDGF inhibited their de-differentiation and maintained the expression of VSMC markers smooth muscle α -actin and calponin (Cheng et al., 2009).

In vivo, locally administered adenovirus mediated up regulation of miR-143 and miR-145 demonstrated a reduction in NIH and an increase in smooth muscle cell markers within the vessel wall 7 days after balloon injury (Cheng et al., 2009). Lenti-miR-145 has also been demonstrated in a carotid artery ligation model to increase VSMC differentiation markers including calponin and smooth muscle α -actin (Cordes et al., 2009).

1.14.3.2 miR-143 and miR145 knockout studies

Several groups have independently generated miR-143 KO, miR-145 KO or miR-143/145 combined KO mice. Analysis of their phenotype demonstrated structural changes within the vascular tree including thinning of the aorta and femoral

arteries. However, changes in ECM have been conflicting in miR-143/145 KO mice, with some reporting extended areas of ECM degradation while others have found VSMCs encased in thick layers of ECM (Elia et al., 2009, Xin et al., 2009). Additionally, these mice demonstrated no change in cell number but an increase in the presence of de-differentiated VSMCs as evidenced by an increase in rough endoplasmic reticulum suggesting the presence of a synthetic state (Elia et al., 2009, Xin et al., 2009). VSMCs from KO mice have also been noted to have disorganised actin fibres and no cytoskeletal stress fibres (Xin et al., 2009).

The effect of miR-143 and miR-145 KO on NIH formation is complex and not fully understood. Two groups have reported spontaneous neointimal lesions in aged mice, which initially comprised of VSMCs but over time the accumulation of macrophage and amorphous type I collagen was also observed (Boettger et al., 2009, Elia et al., 2009). These lesions occurred in the presence of a normal lipid profile and exhibited a predilection for the femoral arteries rather than the aorta (Boettger et al., 2009). Given that miR-143 and miR-145 over expression in the setting of vascular balloon injury has been shown to reduce NIH it would be expected that genetic deletion may result in increased lesion size. However, it has been reported that carotid ligation in WT mice produced a thick neointima, while in miR-143 KO, miR-145 KO and miR-143/145 combined KO mice a significant reduction in NIH was observed (Xin et al., 2009). In particular, almost no neointima was formed in either the miR-145 KO or the double knockout mice. Interestingly, a 50% mortality rate was observed following carotid ligation in miR-145 KO mice which was attributed to stroke secondary to systemic hypotension and likely failure of cerebral blood flow auto-regulation (Xin et al., 2009). The reasons underlying the counterintuitive results observed in KO mice remain unclear but could be due to a combination of factors. Firstly, genetic deletion may induce compensatory responses in other miRs or cell signalling pathways, which are not present following temporary knockdown or over expression. Thus, the blood vessels are already abnormal at the time of injury. Additionally, as hypertension is known to promote NIH and ISR the profound hypotension observed in KO mice may limit lesion development (Meguro et al., 2000). Interestingly, only one of the three groups, which used different methods to independently generate miR-143 KO and or miR-145 KO mice, actually conducted vascular injury experiments in these mice. Comparing lesion

formation across all three colonies as well as the effect of *in vivo* knockdown may help explain the reduction in NIH with absence of this bicistronic cluster.

In summary, miR-143 and miR-145 are highly expressed in VSMCs where they act to maintain a contractile phenotype. Further work is required to understand the complex and seemingly contradictory findings between *in vitro* and *in vivo* manipulation of these miRs.

1.14.4 miR-133a (Pro-contractile)

miR-133a is another miRNA shown to promote a contractile phenotype in VSMCs. While two copies of miR-133a are present, each clustered with a copy of miR-1, only miR133a is found in VSMCs. miR-133a is found abundantly in quiescent VSMCs but is reduced when they are stimulated to proliferate by either growth factor stimulation or mechanical injury (Torella et al., 2011). ERK1/2 activation by the ras / MAPKinase pathway has been attributed to this down regulation of miR-133a (Torella et al., 2011).

The over expression of miR-133a, using a premiR, in VSMCs stimulated with 10% FCS reduced proliferation significantly implying this miRNA plays an active role in maintaining quiescence.

In VSMCs two predicted miR-133a targets, specificity protein 1 (SP-1) and moesin have been validated using 3'UTR luciferase reporter assays as well as by gain and loss of function experiments. SP-1 is a transcription factor shown previously to be up regulated following vascular injury, while moesin is known to play a role in VSMC migration (Torella et al., 2011).

In vivo, adenovirus mediated over expression of miR-133a was accomplished at time of balloon injury by local administration to the vessel wall. This resulted in SP-1 and moesin down regulation as well as reduction in NIH development (Torella et al., 2011). This suggests miR-133a acts to inhibit VSMC proliferation and migration maintaining a contractile phenotype.

1.14.5 miR-195 (Pro-contractile)

Oxidised LDL is known to stimulate proliferation and migration of VSMCs (Zettler et al., 2003). Researchers investigating the mechanisms underlying this effect in HASMCs identified numerous miRNAs dysregulated upon oxLDL exposure (Wang et al., 2012b). MiR-195, highly expressed in human arterial smooth muscle cells (HASMCs) compared to ECs and macrophages was significantly down regulated by oxLDL treatment. *In vitro*, augmentation of miR-195 expression using premiR-195 was shown to reduce oxLDL-induced proliferation and migration. Conversely, knockdown of miR-195 increased the migratory effects of oxLDL on HASMCs (Wang et al., 2012b).

By comparing protein coding gene microarray data following stable miR-195 over expression with bioinformatic target prediction programmes several putative targets were identified. Of these, cell division cycle 42 (Cdc42), a RhoB GTPase implicated in cell growth, proliferation and migration was confirmed as a target using 3'UTR luciferase reporter constructs (Wang et al., 2012b). Importantly, knockdown of Cdc42 using shRNA had the same negative effect on oxLDL treated HASMC proliferation as miR-195 overexpression (Wang et al., 2012b).

In vivo, a reduction in miR-195 expression within the vessel wall was confirmed following balloon injury. Over expression of miR-195 by intra-arterial infusion of an adenovirus expressing miR-195 reduced not only Cdc42 but also NIH (Wang et al., 2012b).

Interestingly, miR-195 also had an inhibitory effect on IL-1 β , IL-6 and IL-8 pro-cytokine expression from HASMCs stimulated with oxLDL (Wang et al., 2012b). These pro-inflammatory cytokines have been shown to stimulate VSMC proliferation (Chamberlain et al., 2006, Ikeda et al., 1991).

Taken together these data implicate miR-195 in promoting a quiescent anti-inflammatory phenotype within VSMCs. Consequently, manipulation of miR-195 may not only have a role in treatment of atherosclerosis but also in preventing NIH and ISR following balloon angioplasty and stent placement, respectively.

1.14.6 miR-663 (Pro-contractile)

MiR-663, first noted to be up regulated within ECs following oscillatory shear stress also plays a role in regulating the inflammatory process within these cells (Ni et al., 2011). In addition, its increased expression in head and neck cancers promotes tumour growth and invasion (Yi et al., 2012). More recently miR-663 has been identified as a novel phenotypic marker in VSMCs, with an increase in expression upon the induction of a contractile phenotype by either exposure to differentiation medium or trans-retinoic acid (Li et al., 2013c). Conversely upon stimulation with PDGF, miR-663 expression was significantly reduced.

MiR-663 over expression using an adenovirus vector was sufficient to increase VSMC differentiation markers, including SM22 α , calponin and myosin heavy chain 11 (MYH11), in both quiescent and pro-synthetic states. Furthermore, a gain of function approach also reduced VSMC proliferation and migration while knockdown with anti-miR-663 had the opposite effect (Li et al., 2013c).

The transcription factor JunB, comprising one half of the heterodimer activator protein 1 (AP-1) (Jun/Fos), has been validated as a miR-663 target. AP-1 is an important regulator of VSMC proliferation and migration, the down regulation of which is key to the suppressive effect of miR-663 on both proliferation and migration. *In vivo*, miR-663 over expression in a mouse carotid artery ligation model reduced NIH development by over 60%. This effect was attributed to a reduction in proliferating cells as evidenced by lower proliferating cell nuclear antigen (PCNA) positive stained cells and suppression of JunB (Li et al., 2013c).

Thus not only is miR-663 a marker of VSMC differentiation but it actively modulates their phenotype. In addition, its over expression following vascular injury may be of therapeutic benefit in reducing NIH development.

1.14.7 miR-638 (Pro-contractile)

The pro-contractile miR-638 is abundantly expressed in VSMCs contributing to the expression of differentiation markers including smooth muscle α -actin and calponin (Li et al., 2013b). Stimuli known to induce a dedifferentiated phenotype significantly reduce the expression of miR-638 in both human aortic and pulmonary artery SMCs. Selective blockade of individual PDGF-induced

signalling cascades have shown that the MAPK / ERK1/2 pathway is responsible for this down regulation. Conversely, miR-638 expression is increased within VSMCs when cultured in media promoting a contractile phenotype (Li et al., 2013b).

In order to determine that miR-638 plays an active role in VSMC biology, gain and loss of function approaches have shown that the augmentation and inhibition of miR-638, by *in vitro* administration of premiR-638 and siRNA, reduced and increased proliferation, respectively. Using a scratch assay it has also been demonstrated that miR-638 inhibits migration of HASMCs. In addition, its inhibition by anti-miR promoted migration, *in vitro* (Li et al., 2013b).

Researchers confirmed neuron-derived orphan receptor 1 (NOR1), a component of the orphan nuclear receptor NR4A, which stimulates the expression of cyclin D1, as a target of miR-638 in HASMCs. MiR-638 over expression reduced NOR1 and cyclin D1 expression, inhibiting cell cycle progression from G1 into S phase. Interestingly NOR1 over expression could partially reverse the inhibitor effect of miR-638 on VSMC proliferation and migration (Li et al., 2013b).

While the data strongly suggests miR-638 promotes a contractile phenotype, limiting VSMC proliferation and migration, its effect on the development of NIH and ISR *in vivo* remains to be evaluated.

1.15 The role of microRNAs in macrophage function following vascular injury

Macrophages are pivotal cellular components of the innate immune system. Not only do they play an important role in immunity, combating invading pathogens through phagocytosis and antigen presentation, but they have also been shown to have an important role initiating inflammation and organ development, including haematopoiesis (Sica and Mantovani, 2012). They also play an important role in the resolution of inflammation and tissue repair (Mantovani et al., 2013). In addition, their activity has been associated with various disease states including autoimmunity, neoplasia, neurodegenerative and cardiovascular disease (Leitinger and Schulman, 2013, Lucas et al., 2010, Mantovani and Locati, 2013).

In order to perform the diverse number of roles required of them, macrophages alter their phenotype in response to environmental cues (Davis et al., 2013). Such cues include but are not limited to colony stimulating factors, growth factors, lipids and cytokines (Mosser and Edwards, 2008). The resultant phenotypic transformation induced by altered gene expression is referred to as polarisation, the two extremes of which are commonly referred to as classically (M1) polarised macrophages or alternatively (M2) polarised macrophages (Mosser and Edwards, 2008). Classical polarising stimuli include lipopolysaccharide (LPS) and interferon gamma (IFN γ), which upon toll-like receptor (TLR) stimulation results in an increased expression of pro-inflammatory cytokines, major histocompatibility complex (MHC) class II and nitric oxide synthase 2 (NOS2) via a combination of signal transduction and transcription factor 1 (STAT1), IRF5 and NF κ B signalling (Tugal et al., 2013). M1 macrophages play an important role in combating bacterial and viral infection as well as in the development of atherosclerosis (Robbins et al., 2013, Leitinger and Schulman, 2013).

Alternative polarisation is commonly induced by IL-4, IL-10 and IL-13 stimulation, which via STAT3 and STAT6 pathways promote the expression of arginase 1 (Arg1), peroxisome proliferator activator receptor gamma (PPAR γ), CD206, resistin-like α (Retnla) and chitinase 3-like 3 (Chi3l3) also known as YM-1 (Tugal et al., 2013, Szanto et al., 2010, Raes et al., 2002, Odegaard et al., 2007). M2 macrophages can be further divided into a variety of subclasses (Ho

and Sly, 2009). They are known to play a role in combating helminth infection, wound healing, tissue remodelling, various cancers and the development of atopy (Mantovani and Locati, 2013, Lucas et al., 2010, Guiducci et al., 2005).

Macrophage polarisation represents a phenotypic continuum, which has been demonstrated to be reversible both *in vitro* and *in vivo* (Guiducci et al., 2005, Davis et al., 2013). The recognition that microRNAs, including let-7c and miR-125a-5p, can dynamically influence polarisation has added further complexity to the determination of macrophage phenotype (Banerjee et al., 2013b, Banerjee et al., 2013a).

Macrophages have been implicated in the development of several cardiovascular diseases including atherosclerosis, aneurysm formation and cardiac allograft vasculopathy (Moore et al., 2013, Blomkalns et al., 2013, Kitchens et al., 2007). Importantly, macrophages rather than neutrophils have also been shown to play a pivotal role in arterial remodelling and the development of NIH following stenting (Welt et al., 2000, Rogers et al., 1996). Despite recognition that microRNAs are up regulated within various forms of vascular disease, there is a relative paucity of data regarding their role within macrophages following vascular injury. However, it is likely that there are common processes observed across the spectrum of cardiovascular disease, which can be extrapolated to this particular setting. Several microRNAs implicated in macrophage function have been shown to be up regulated within atherosclerotic plaques and macrophages following oxLDL exposure (Wolfs et al., 2011, Leitinger and Schulman, 2013). Of these miRNAs miR-21, miR-155, miR-146a and miR-125a-5p have been more closely examined as discussed below.

1.15.1 miR-21

Several studies have already demonstrated the complex role played by miR-21 in regulating the immune response. Within endothelial cells oscillatory shear stress has been shown to upregulate miR-21 expression, which via NF κ B activation increased endothelial activation and adhesion molecule expression (Zhou et al., 2011). Following vascular injury it is likely that this contributes significantly to the recruitment of immune cells including T-cells and macrophages.

A pro-inflammatory role within T-cells has been described by independent groups showing miR-21 enhances pro-inflammatory cytokine release including IL-12, TNF α , IFN γ and MIP-2 (Ando et al., 2013, Shi et al., 2013). In addition, the genetic deletion of miR-21 and resultant immunosuppressive effect, demonstrated improved survival in a mouse model of colitis (Shi et al., 2013).

Conflicting reports of the action of miR-21 within macrophages have been published. Using an immortalised macrophage cell line investigators have found that miR-21 suppresses LPS / TLR4 induced inflammation, reducing IL-6 and enhancing IL-10 production through the targeting of PDCD4 a pro-inflammatory protein also known to promote apoptosis (Sheedy et al., 2010). Conversely, miR-21 itself has been demonstrated to activate intracellular TLR7 and TLR8 due to its GU-rich motif, resulting in an increase in pro-inflammatory cytokines including TNF α and IL-6 (Fabbri et al., 2012). The later finding suggests miR-21 may induce an M1 polarisation state, which is known to promote NIH development following vascular injury (Lavin et al., 2014). Furthermore, miR-21 has been shown to inhibit M2 polarisation by targeting of STAT3 (Wang et al., 2015).

The contradictory findings presented above suggest the exact role played by miR-21 in immune regulation is complex and may be determined by the timing and context in which it is expressed. Whether the expression and action of miR-21 within macrophages is important in the development of NIH and ISR remains to be investigated.

1.15.2 miR-155

Located on human chromosome 21 within the B-cell integration cluster gene, miR-155 is highly expressed within haemopoietic cells. Not only has this miRNA been demonstrated to play a role in haemopoiesis and immune function its dysregulation has been documented in viral infections, cancer, and cardiovascular disease (Wei et al., 2013, Sethupathy et al., 2007, Cai et al., 2012).

In vitro characterisation of miR-155 within bone marrow-derived macrophages revealed it to be up regulated 120-fold following M1 polarisation (Cai et al., 2012). In addition, by blocking its action, M1 macrophages could be repolarised towards an M2 phenotype. The converse was found upon over expression within M2 macrophages. Interestingly within tumour associated macrophages which exhibit an M2-like phenotype, low levels of miR-155 were also found (Cai et al., 2012).

Conflicting reports exist as to whether miR-155 is pro- or anti-inflammatory (Donners et al., 2012, Cai et al., 2012). However, the most consistent and compelling evidence is for a pro-inflammatory and pro-atherogenic action. Observational data has shown miR-155 along with tumour necrosis factor alpha (TNF α) to be highly expressed within atherosclerotic lesions taken not only from ApoE $-/-$ and LDLR $-/-$ mice but also human plaques. Minimally modified LDL, LPS and IFN γ have been shown via TLR4 stimulation to induce the expression of miR-155 (Nazari-Jahantigh et al., 2012, Du et al., 2014). A positive correlation between miR-155, TNF α and IL-6 has also been demonstrated. In addition, lentiviral mediated over expression of miR-155 was associated with an increase in TNF α release (Du et al., 2014).

Furthermore, by knocking out miR-155, a reduction in pro-inflammatory cytokine release as well as an increase in cholesterol efflux from macrophages was demonstrated (Du et al., 2014). Further support of a pro-inflammatory, pro-atherogenic role for miR-155 was derived from experiments in ApoE $-/-$ miR-155 $-/-$ double knockout mice (Nazari-Jahantigh et al., 2012, Du et al., 2014). These mice were found to have smaller atherosclerotic lesions with a reduction in lipid and macrophage accumulation. Investigators demonstrated that miR-155 targets B-cell lymphocyte 6 (Bcl-6) and suppressor of cytokine signalling-1 (SOCS-1), two known repressors of cytokine release (Nazari-Jahantigh et al., 2012, Du et al., 2014). They elegantly demonstrated that the absence of miR-155 results in Bcl-6 target de-repression, which in turn suppresses pro-inflammatory cytokine release including MCP-1 expression (Nazari-Jahantigh et al., 2012, Du et al., 2014). Genetic deletion of miR-155 has also been demonstrated to reduce CD11 $^+$ /Ly6C $^{\text{hi}}$ cells, thought to be precursors of M1 macrophages important in developing atherosclerotic lesions and possibly in ISR (Du et al., 2014).

With respect to vascular injury, miR-155 $-/-$ mice have been demonstrated to produce less NIH following carotid artery ligation (Zhang et al., 2014). Notably, this study did not demonstrate that the reduction in vascular injury response was mediated by the absence of miR-155 specifically from macrophages. However, bone marrow transplantation from miR-155 $-/-$ mice into ApoE $-/-$ mice demonstrated a reduction in both atherosclerotic lesion size and in NIH development following partial carotid artery ligation (Nazari-Jahantigh et al., 2012). Given the methodology used in the later study it can be inferred that within leukocytes miR-155 is important in promoting the development of NIH. Indeed it is likely that this effect is, at least in part, mediated by its expression in macrophages.

Taken together these findings suggest by influencing macrophage biology including polarisation, cholesterol handling and release of mitogenic cytokines miR-155 may play an important role in the development of NIH and ISR.

1.15.3 miR-146a

MiR-146a has been found within human atherosclerotic plaques and has been shown to be up regulated following vascular injury (Ji et al., 2007, Raitoharju et al., 2011). While recent reports have suggested a role for miR-146a in modulating VSMC phenotype by targeting KLF4, initial studies of this miR focused on its influence upon the innate immune system (Sun et al., 2011). Within monocytes and macrophages the expression of miR-146a is induced by TLR activation and has been found to be NF κ B transcription factor dependent (Yang et al., 2011). MiR-146a is up regulated within these cells following exposure to oxLDL (Chen et al., 2009). Interestingly, miR-146a acts to reduce oxLDL accumulation and the release of several cytokines, which have been implicated in neointimal development, including IL-6, IL-8 and CCL2 (Chen et al., 2009).

Further work would be required to determine whether the inhibition of foam cell formation and release of pro-migratory and pro-proliferative cytokines by miR-146a play an important role in limiting the development of neoatherosclerosis and ISR following stenting.

1.15.4 miR-125a-5p

Not only has miR-125a-5p been implicated in the regulation of macrophage polarisation, it has also been shown to be up regulated following oxLDL exposure (Chen et al., 2009). Similar to miR-146a, miR125a-5p inhibition has been shown to increase lipid uptake by macrophages. De-repression of oxysterol binding protein-related protein 9 (ORP9), a protein that plays an important role in lipid metabolism and transport, has been implicated in the action of miR-125a-5p (Chen et al., 2009).

In addition, miR-125a-5p appears to have an anti inflammatory role in suppressing the release of IL-2, IL-6, TNF α and TGF β (Chen et al., 2009). Given the influence of miR125a-5p on macrophage polarisation, lipid metabolism and cytokine expression it would appear reasonable to suggest this miRNA may play a role in NIH and ISR development. However, direct evidence is lacking and further work would be required to confirm this hypothesis.

Taken together it is clear that numerous miRNAs are important in regulating macrophage function within cardiovascular disease. However, it is also clear that further investigation is required to fully elucidate their role within macrophages following vascular injury.

1.16 Aims

In-stent restenosis remains a significant clinical burden to patients, resulting in the return of clinical symptoms. Despite significant advances in stent design, polymers and anti-mitogenic medications, ISR still occurs in up to 5% of deployed stents. In addition, the need for prolonged use of dual antiplatelet agents to prevent in-stent thrombosis puts patients at risk of major haemorrhage. Thus, there is a need to develop novel therapies to prevent ISR, reducing the need for repeat revascularisation and to lower the bleeding risk associated with long-term dual antiplatelet use. Numerous microRNAs have been found to influence either VSMC proliferation or inflammation, two key pathologies associated with ISR. MicroRNA 21 has been implicated in regulating both. Thus, this thesis shall investigate the role of miR-21 in the development of ISR by;

1. Reproducing a small animal model of stenting
2. Investigating the potential role played by miR-21 within VSMCs during the development of ISR, using a variety of gain and loss of function approaches.
3. Investigating the potential role of miR-21 in macrophage phenotype and function in the development of ISR.

1.17 Hypotheses

1. MiR-21 is likely to play an important role in facilitating the development of ISR.
2. The deleterious actions of miR-21 on ISR development is likely to be multifactorial;
 - a. Through the promotion of VSMC proliferation and migration.
 - b. Through alteration of the inflammatory response in particularly within macrophages the dominant cell type involved in ISR.
3. Blocking the actions of miR-21 through genetic deletion and or pharmacological knockdown may reduce the development of ISR.
4. Genetic overexpression of miR-21 may increase the development of ISR.

2 Methods

2.1 Animals

Four groups of mice were used. C57BL6 mice (Charles River, Maidstone, UK), miR-21 wild type (WT) mice miR-21 Knock-out (KO) mice and miR-21 Transgenic (Tg) over expressing mice (Gift from Eric Olsen, University of Texas Southwestern, USA)(Hatley et al., 2010). Mice gifted from Professor Olsen's Laboratory were created on a C57BL6 parent strain, which had been crossed with SJLB6 mice. The pre-miR-21 sequence was deleted in mice to create MiR-21 KO mice using homologous recombination using standard loxP and CAG-Cre methods as described previously (Patrick et al., 2010). Deletion of pre-miR-21 was not associated with disruption of TMEM49 gene expression as evidenced by reverse transcriptase quantitative polymerase chain reaction (RT-qPCR) (Patrick et al., 2010). All mice were fed a diet of standard chow and had free access to water. Male mice aged 18-22 weeks, weighing between 25 and 30 g were used for *in vivo* experiments. Cells isolated from male mice aged between 8 and 12 weeks were used for *in vitro* experiments. All animal work was conducted under Home Office licence and in accordance with the Animals Scientific Procedures Act (1986).

2.2 Genotyping

The genotype of all miR-21 WT, KO and Tg miR-21 over expressing mice was confirmed prior to inclusion in all studies as outlined below.

2.2.1 DNA Extraction

Ear notches from mice were obtained by staff from biological services when numbering animals as per institutional protocol. Samples were stored at -20°C until deoxyribose nucleic acid (DNA) was ready to be extracted using QIAamp DNA mini kit (250) (cat. 51306) (Qiagen, Manchester, UK) as per manufacturer's protocol. Briefly, mechanical and biological tissue lysis was conducted by adding 180 µL of ATL buffer, 20 µL of Proteinase K and one 3 mm tungsten carbide bead (cat. 69997) (Qiagen, Manchester, UK) to each sample. Samples were then shaken vigorously in a TissueLyser (Qiagen, Manchester, UK) for 2 min at 25 Hz and repeated once. Samples were then left overnight in a water bath at 55°C. The following day 400 µL of AL buffer : ethanol (1:1) mixture was added to

samples containing tissue lysates and vortexed for 15 s. Buffered lysates were then added to a QIAamp mini spin column containing a silica membrane and centrifuged at 8000 revolutions per minute (rpm) for 1 min. During centrifugation DNA present within the lysates binds to the silica membrane while proteins and any other contaminants including divalent ions which interfere with PCR are passed through and were discarded. Samples were washed with two further buffers AW1 and AW2 to remove any residual contaminants by centrifugation for 1 min at 8000 rpm and 13200 rpm respectively. The QIAamp spin column was then placed in a clean 1.5 mL Eppendorf and 50 μ L of nuclease free water added. The column and Eppendorf were spun at 8000 rpm for 1 min to elute the DNA bound to the silica membrane. This was repeated by placing the sample back into the column which was spun again to ensure maximal DNA elution. Samples were stored at -20°C prior to PCR amplification.

2.2.2 Polymerase Chain Reaction for microRNA-21 WT and KO Mice

DNA isolated from ear notches of miR-21 WT and miR-21 KO mice were amplified by PCR using a Promega Green GoTaq-Flexi polymerase kit (Promega, Southampton, UK). Each 25 μ L reaction was prepared using: 5xGoTaq Flexi Buffer (5 μ L), magnesium chloride (MgCl_2) 25 mM (3 μ L), dNTPs 10 mM (0.5 μ L), miR-21 forward primer 10 μ M 5'-GGGCGTCGACCCGGCTTTAACAGGTG-3' (1 μ L), miR-21 reverse primer 10 μ M 5'-GGGCGTCGACGATACTGCTGCTGTTACCAAG -3' (1 μ L) (Exiqon, Vedbaek, Denmark), nuclease free dH_2O (12.875 μ L), Taq 5 U/ μ L (0.125 μ L) and genomic DNA 1 in 5 dilution (1.5 μ L). The cycling conditions used were as follows: 95°C for 2 min (enzyme activation) followed by 35 cycles of 95°C for 15 s (DNA denaturation), 62.5°C for 35 s (primer binding) and then 72°C for 30 s (primer extension). The PCR products were separated by gel electrophoresis within 2% Agarose/ Tris/Borate/EDTA (TBE) gel. The amplicons (miR-21 WT 469 base pairs (bp), miR-21 KO 330 bp) were identified by size in comparison against a 100 bp ladder run simultaneously, Figure 2-7.

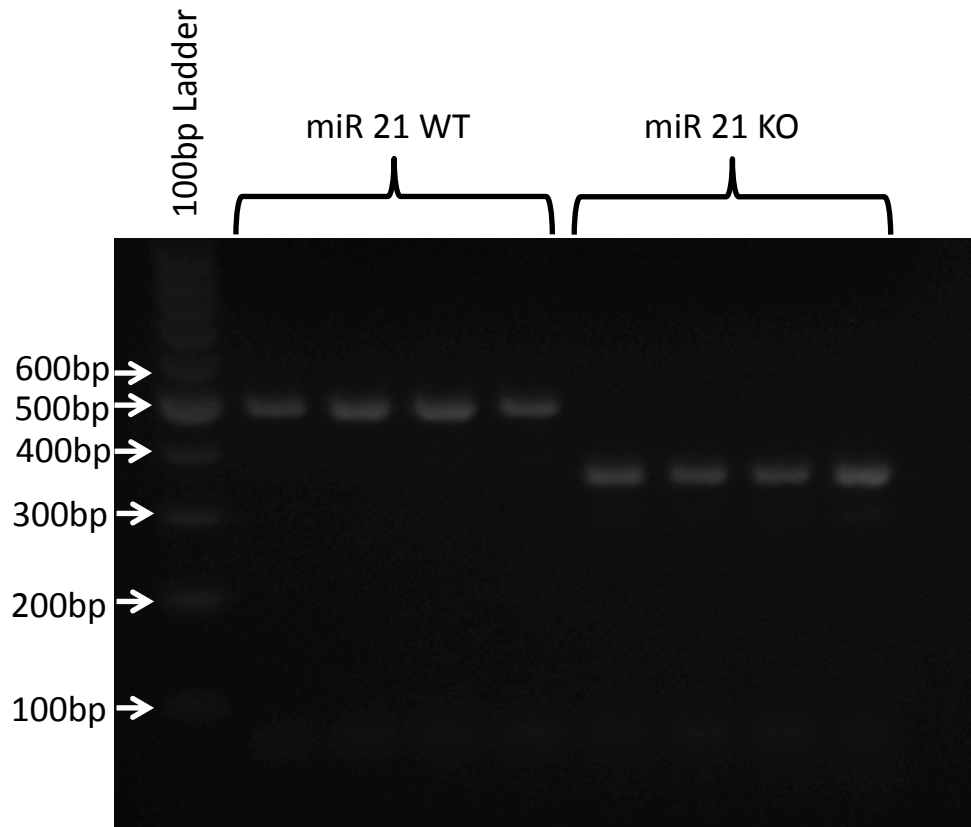


Figure 2-7. MiR-21 colony genotyping. Gel electrophoresis following PCR of ear samples taken from mice of miR-21 KO colony. From left, Lane 1 100 bp ladder. Lanes 2-5, samples from four miR-21 WT mice (469bp amplicon). Lanes 6-9, samples from four miR-21 KO mice (330bp amplicon).

2.2.3 Genotyping of microRNA-21 Transgenic Overexpressing Mice

Genotyping of miR-21 overexpressing mice was conducted by PCR and identification of the reporter enhanced green fluorescent protein (EGFP) gene present within the transgene construct, Figure 2-8(Hatley et al., 2010). PCR was conducted using the same kit as described in section 2.2.2. However 1 μ L rather than 1.5 μ L of genomic DNA was added to each reaction. The addition of extra nuclease free dH₂O was used to maintain a total reaction volume of 25 μ L. Primer sequences used were as follows EGFP forward 5'-TCTTCTTCAAGGACGACGGCAACT-3' and EGFP reverse 5'-TGTGGCGGATATTGAAGTTCACCT-3' (Exiqon, Vedbaek, Denmark). The cycling conditions used were: 95°C for 2 min (enzyme activation) followed by 32 cycles of 95°C for 30 s (DNA denaturation), 60°C for 30 s (primer binding) and then 72°C for 60 s (primer extension). The PCR product was 216 bp long and its presence identified by gel electrophoresis within 2% Agarose/TBE gel, Figure 2-9.

MicroRNA 21 Overexpression Construct

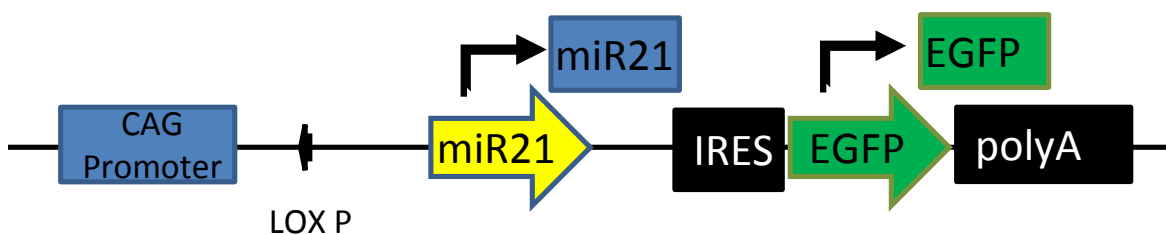


Figure 2-8. Schematic of Transgenic microRNA 21 Overexpression Construct. PCR conducted to determine presence or absence of reporter EGFP. Presence of EGFP signifies presence of miR-21 overexpressing construct. (IRES - Internal Ribosome Entry Site, EGFP - Enhanced Green Fluorescence Protein). Adapted from Hatley et al *Cancer Cell* 2010;18; 282 - 293. Supplemental Figure 1. Reproduced with permission.

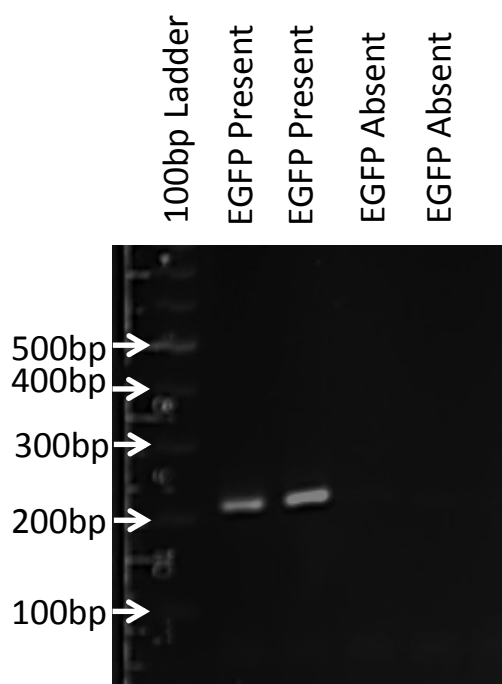


Figure 2-9. MiR-21 Transgenic colony genotyping. Gel electrophoresis following PCR of ear samples taken from miR-21 transgenic mouse colony. The identification of EGFP (216 bp amplicon) present within the miR-21 overexpression construct, was used to identify Tg miR-21 $+/+$ mice. From Left, Lane 1 100 bp ladder. Lanes 2 and 3 EGFP present, Tg miR-21 $+/+$ mice. Lanes 4 and 5 EGFP absent, WT miR-21 $+/+$ mice.

2.3 RNA and miRNA Extraction from Cells and Tissues

Total and miRNA was extracted using the miRNeasy mini kit (Qiagen, Manchester, UK), including on-column DNase (Qiagen, Manchester, UK) treatment to remove any DNA contamination, as per manufacturer's instructions. Cells were washed in PBS to remove any residual media and lysed by the addition of 700 μ L QIAzol lysis reagent. Lysates were vortexed to homogenize prior to the addition of 140 μ L of chloroform. For tissues 1400 μ L of QIAzol was added to an Eppendorf containing the tissue of interest along with two 3 mm tungsten carbide beads. Samples were then shaken vigorously in a TissueLyser (Qiagen, Manchester, UK) for 2 min at 25 Hz and repeated once. Tissue lysates were then divided equally between two Eppendorfs and 280 μ L of Chloroform added to each. Chloroform facilitates separation of the sample. Protein remains in the lower organic phase and DNA partitions to the interphase while the RNA partitions to the upper aqueous phase. The sample was partitioned fully by centrifugation at 12,000 rpm for 15 min at 4°C. The RNA containing aqueous phase was transferred to a fresh RNase free Eppendorf and 1.5 x volume of 100 % ethanol was added to facilitate binding to the RNeasy mini spin column. Samples were immediately added to the spin column and centrifuged at 8000 rpm for 15 s to bind the RNA to the spin column. Columns were washed with 350 μ L of buffer RWT for 15 s and 8000 rpm and the flow through discarded. Digestion of residual DNA was performed by incubating the spin columns with DNase for 15 min at room temperature. The column was again washed with 350 μ L RWT buffer, followed by two washes of 500 μ L RPE buffer by centrifugation at 8000 rpm for 15 s to remove any traces of salts from the sample. To dry, spin columns were placed in clean collection tubes and centrifuged at 13,200 rpm for 1 min. RNeasy spin columns were transferred to RNase free Eppendorfs and RNA was eluted using 50 μ L of RNase free water and centrifugation at 8000 rpm for 1 min. This was repeated by placing the sample back into the column which was spun again to ensure maximal RNA elution. RNA samples were stored at -80°C until use.

2.4 Quantification of RNA

Total RNA was quantified using a NanoDrop 1000 Spectrophotometer (ThermoScientific, Loughborough, UK). The NanoDrop measures the concentration of nucleic acid in solution by exposing the sample to a pulse of light at 260 nm and then measuring the amount of light absorbed. The relationship between the absorbance and the concentration of the sample is based on the Beer-Lambert law:

$$c=A/(\Theta \times l)$$

Where:

c = nucleic acid concentration (ng/ μ l)

A = absorbance

Θ = molar absorptivity (constant for given solution)

l = path length of light passing through (constant for given instrument)

The purity of the sample was assessed by calculating the ratio of absorbance at 260 and 280 nm. A 260 / 280 ratio of <2.0 was accepted as pure.

2.5 Complementary Deoxyribonucleic Acid (cDNA) Synthesis

mRNA extracted from cells was reverse transcribed to cDNA to allow for analysis of gene or miRNA expression via RT-qPCR. For both gene expression and miRNA cDNA synthesis two negative control reactions were prepared: one containing water instead of mRNA and the other containing no reverse transcriptase, the enzyme responsible for cDNA synthesis.

2.5.1 Gene Expression

mRNA extracted from cells was reverse transcribed to cDNA for gene expression analysis using the Taqman Reverse Transcription Reagents (Applied Biosystems, Warrington, UK) as per manufacturer's instruction. Reverse transcription of RNA was conducted in 40 μL reactions containing: 10 x RT buffer (4 μL) 25 mM MgCl_2 (8.8 μL), 10 mM dNTPs (8 μL), 50 μM random hexamers (2 μL), 0.5 U/ μL RNase inhibitor (0.8 μL), 50 U/ μL multiscribe reverse transcriptase (1 μL), 100 ng/mL RNA (10 μL) and dH_2O (5.4 μL). Cycling conditions used were as follows: 25°C for 10 min (annealing), 48°C for 30 min (reverse transcription), 95°C for 5 min (inactivate reverse transcriptase). cDNA was stored at -20°C.

2.5.2 microRNA Expression

miRNA was reverse transcribed to cDNA for the detection of miRNA using specific stem-loop reverse transcription primers as per the Taqman miRNA Reverse Transcription kit (Applied Biosystems, Paisley, UK). Reverse transcription of microRNA was conducted in 7.5 μL reactions containing: 100 mM dNTPs (0.075 μL), 10 x RT buffer (0.75 μL), 5 x RT primer (1.5 μL), 0.25 U/ μL RNase inhibitor (0.095 μL), 6.6 U/ μL multiscribe reverse transcriptase (0.5 μL), dH_2O (2.08 μL) and 2.5 μL of total RNA diluted to 2 ng/ μL . The cycling conditions used were as follows: 16°C for 30 min (anneal), 42°C for 30 min (reverse transcription), 95°C for 5 min (inactivate reverse transcriptase). cDNA was stored at -20°C.

2.6 TaqMan[®] quantitative real-time polymerase chain reaction (qRT-PCR)

TaqMan[®] qRT-PCR was used to quantify relative expression levels of genes or miRNAs of interest. TaqMan[®] assays contain forward and reverse primers specific to the target DNA sequence between which a probe can anneal. The probe is labelled with a reporter fluorophore at the 5' end and a non-fluorescent quencher at the 3' end, when intact the quencher suppresses fluorescent emission by the reporter. In the presence of target sequence the probe anneals and is then cleaved upon amplification of the target sequence by the forward and reverse primers. This produces separation of the quencher from the reporter and a fluorescent signal can be detected. Further reporter dye molecules are cleaved from their respective probes with each cycle, resulting in an increase in fluorescence intensity directly proportional to the concentration of the target product produced. Data is acquired whilst PCR is in the exponential phase and is measured when the reporter dye emission reaches a threshold, known as the cycle threshold (Ct). Results were normalised to a housekeeping gene, whose expression remains stable, to correct for any errors in RNA content. Results are shown relative to the experimental control using the $-2^{\Delta\Delta Ct}$ method described by Livak. (Livak and Schmittgen, 2001)

2.6.1 Gene Expression

For gene expression, qRT-PCR was performed using TaqMan[®] gene expression assays. Ten microlitre reactions were prepared for each sample containing: 2 x TaqMan[®] Universal MasterMix II (5 μ L), probe (0.5 μ L), RNase free H₂O (3 μ L) and 1.5 μ L cDNA. Samples were run in technical duplicate on a 384 well plate. For each probe tested the negative reverse transcription control was run in addition to a water only control. qRT-PCR was performed in simplex using the 7900HT sequence detection system (Applied Biosystems) using the following cycling conditions: 50°C for 20 s, 95°C for 10 min (enzyme activation), 40 cycles of 95°C for 15 s (denaturing of cDNA) then 60°C for 60 s (primer and probe annealing, primer extension). Three genes: Glyceraldehyde 3-Phosphate Dehydrogenase (GAPDH), 18S and TATA box binding protein (Tbp) were used as housekeepers for gene expression depending on which tissue RNA was initially extracted from. Table 2-3 lists the gene expression assays used.

Table 2-3. List of TaqMan Gene Expression Assays

Gene	Assay ID	RefSeq Gene ID
GAPDH	Hs02758991_g1	NM_001256799.1
18s	Hs03003631_g1	
Tbp	Mm00446971_m1	NM_013684.3
Arginase1	Mm00475988_m1	NM_007482.3
YM-1	Mm00657889_mH	NM_009892.2
PPAR γ	Mm01184322_m1	NM_011146.3
Retnla	Mm00445109_m1	NM_020509.3
NOS2	Mm01309897_m1	NM_010927.3
STAT3	Mm01219775_m1	NM_213660.2
PTEN	Mm00477208_m1	NM_008960.2
TIMP3	Rn00441826_m1	NM_012886.2
BMPR2	Mm00432134_m1	NM_007561.4
PDCD4	Mm01266062_m1	NM_011050.4
IL-12p35	Mm00434165_m1	NM_008351.2
PPAR α	Mm00440939_m1	NM_011144.6
CCL3	Mm00441259_g1	NM_011337.2

2.6.2 miRNA Expression

Quantitative RT-PCR for miRNA expression was performed using miR probes complementary to the mature miRNA sequence. Expression of each miRNA was normalised to the housekeeper U6. For each sample a 10 μ L reaction was prepared for each sample containing: 2x TaqMan[®] Universal MasterMix II (5 μ L), probe (0.5 μ L), RNase free water (3.8 μ L) and miRNA RT product (0.7 μ L). Each sample was run in a 384 well plate in technical duplicate. Controls were performed as above and the experiment performed using the 79000HT sequence detection system as in section 2.6.1. Table 2-4 lists the TaqMan[®] assays used.

Table 2-4. List of TaqMan miRNA Expression Assays

miRNA	Assay ID	MIRBASE ID
hsa-miR-21-5p	000397	hsa-miR-21-5p
mmu-miR-21-3p	002493	mmu-miR-21-3p
U6	Hs00984809_m1	NM_024598.3 (NCBI accession)

2.7 Cell Culture

2.7.1 Isolation and Culture of Murine Aortic Vascular Smooth Muscle Cells

Male mice 8 - 12 weeks old were euthanized by rising CO₂ concentration within a sealed chamber. Following confirmation of death the mice were placed supine on a sterile drape and perfused with sterile saline by ventricular puncture. The thoracic and abdominal aorta was harvested and all adipose and connective tissue carefully dissected off. The vessel was cut longitudinally and stored temporarily in serum-free media containing 1% penicillin/streptomycin and L-Glutamine prior to transfer into aseptic conditions. Further vessel preparation was undertaken within a sterile tissue culture hood under laminar airflow. The vessel was removed from serum-free media, placed on a sterile petri dish and endothelial cells removed by gently rubbing the luminal surface with the plunger from a 1ml syringe. The aorta was dissected horizontally and longitudinally using a sterile scalpel blade before being resuspended in 400 µL of Amniomax C100 basal cell media containing 15% Amniomax C100 growth supplement (Life Technologies, Paisley, UK). The explants were placed in a T25 tissue culture flask and incubated at 37°C with 5% CO₂. Following adherence of aortic tissue to the flask surface, 2 mL of supplemented Amniomax media was added. Media was changed every 3 days for 1 week until VSMC outgrowth was observed, Figure 2-10. Tissue explants were removed and cells washed twice with 3 ml of sterile phosphate buffered saline (PBS) and incubated at 37°C in 0.5 mL trypsin-ethylenediamine tetra-acetic acid (0.05% trypsin, 0.02% EDTA) for approximately 5 min or until the majority of the cells had detached from the flask and re-plated into the same T25 flask (Passage 1, P1). Supplemented Amniomax media was added to neutralise the enzymatic activity of trypsin-EDTA Cells were grown to near confluence prior to changing media to Dulbecco's Modified Eagle Media (DMEM) containing 20% (volume/volume [v/v]) fetal calf serum (FCS), 100 international units (I/U)/mL penicillin, 100 µg/mL streptomycin and 2 mM L-glutamine (Life Technologies, Paisley, UK). VSMCs were then trypsinised and plated into a T75 flask (P2) and after 24 h media was changed to final growth media of DMEM containing 10% FCS, 100 IU/mL penicillin, 100 µg/mL streptomycin and 2 mM L-glutamine. VSMCs were further passaged when 80 - 90 % confluent and were used for experiments between P4 and P6.

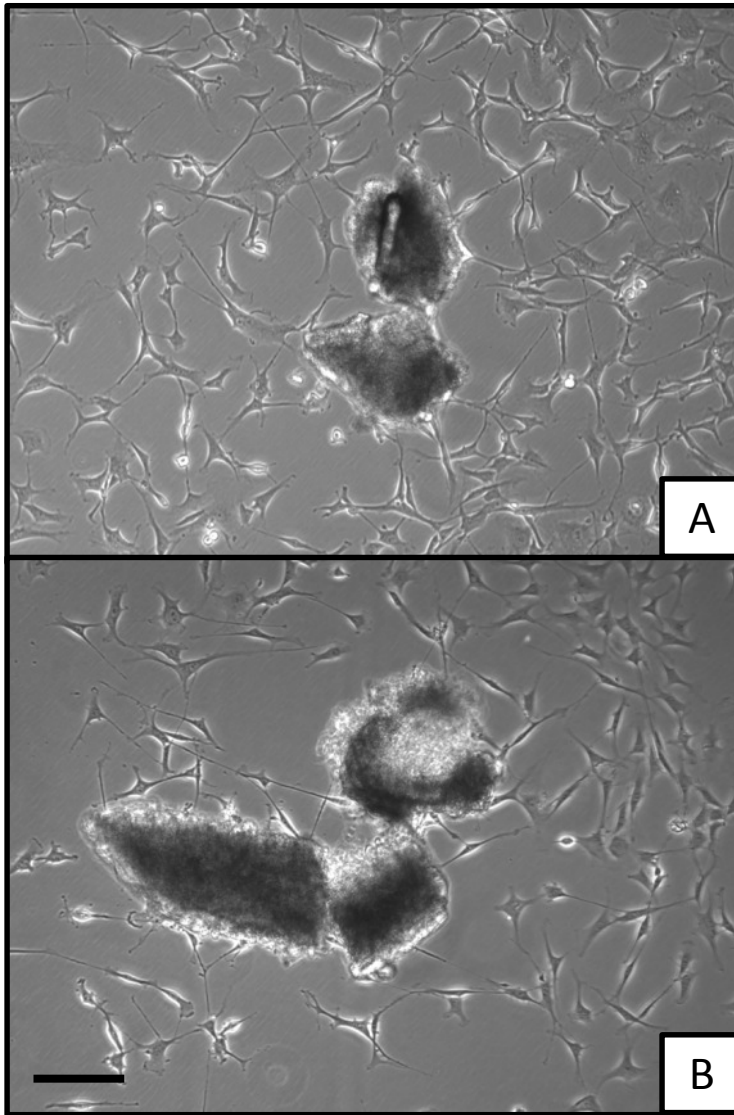


Figure 2-10 Aortic Vascular Smooth Muscle Cells growing out from aortic explants of mice at 7 days following harvest. A, WT mice. B, KO mice. Scale bar = 100 μ m.

2.7.2 Cell Counting

Cells were suspended in either Trypsin-Ethylenediaminetetraacetic Acid (EDTA) or Cell Dissociation Solution (Sigma Aldrich, Poole UK), centrifuged at 1500 rpm for 5 min and then resuspended in 1 mL of appropriate culture media. A cover slip was placed on a Bright Line Haemocytometer (Sigma Aldrich, Poole, UK) and 20 μ L of cell suspension placed across the chamber by capillary action. A light microscope was used to count the number of cells in each of four corner squares and the mean calculated. Each corner square represents a total volume of 0.1 mm^3 or $1 \times 10^{-4} \text{ cm}^3$. As 1 cm^3 equals 1 mL the concentration of cells per ml can be calculated using the following equation:

$$\text{Cells/mL} = \text{average cell count per square} \times 10^4$$

The calculated cell concentration was then used to plate out cell at the required density.

2.7.3 Proliferation Assay

Murine VSMCs isolated and grown until passage 4 to 6 were trypsinised and counted as described in sections 2.7.1 and 2.7.2, respectively. Cells from miR-21 WT and KO mice were seeded into 96 well plates at a density of 7×10^3 cells/well in DMEM with 10 % FCS and incubated overnight at 37°C in the presence of 5% CO_2 . VSMCs were quiesced for 24 h by changing media to DMEM with 0.2% FCS, 100 international units (I/U)/mL penicillin, 100 μ g/mL streptomycin and 2 mM L-glutamine. Following quiescence cell proliferation was stimulated by the replacement of media with media containing one of four experimental conditions: 10% FCS, PDGF-BB (R&D Systems, Abingdon, UK) 10 ng/mL, PDGF-BB 20 ng/mL or PDGF-BB 50 ng/mL. 0.2 % FCS was used as control. All experimental conditions were conducted in biological triplicate and technical duplicate. Experiments were terminated at 48 h.

Proliferation of VSMCs was assessed using a commercially available 5-Bromo-2'-deoxyuridine (BrdU) assay (Millipore, Livingstone, UK). BrdU, a thymidine analogue is incorporated into newly synthesized DNA strands of actively proliferating cells. The incorporation of BrdU can be detected immunologically thus allowing the assessment of cells using a colourimetric method for

determining the quantity of BrdU incorporation. The manufacturer's protocol was followed as outlined. Five hours following the stimulation of quiesced cells under experimental conditions BrdU was added at a final concentration of 1:500 from supplied stock. This allowed DNA repair to occur following changing of cell media without BrdU incorporation. After 48 h cell media was removed and cells washed twice with sterile PBS, followed by the addition of the supplied fixing solution to fix and partially denature DNA thus allowing immunological detection of BrdU. After 30 min the fixing solution was removed and cells washed with supplied wash buffer. The 96 well plate was then blotted dry and samples incubated with mouse anti-BrdU antibody for one hour at room temperature followed by further washing to remove unbound primary antibody. Samples were then incubated with goat anti-mouse IgG peroxidase conjugated antibody for 30 min before unbound antibody was removed by washing. The plate was blotted dry prior to incubation with 3,3',5,5'-Tetramethylbenzidine (TMB) substrate for 30 min in the dark. The absorbance of the blue product is directly proportional to the quantity of BrdU incorporated and was measured using a spectrophotometer microplate reader set at a dual wavelength of 450 / 550 nm. Absorbance readings from wells which did not have BrdU added were subtracted from experimental readings prior to further analysis.

2.7.4 Migration Assay

Scratch assay was utilised to assess cell migration (Liang et al., 2007). VSMCs isolated from miR-21 WT and KO mice as described in section 2.7.1 were seeded into 12 well plates at a density of 1×10^5 cells per well and grown in DMEM with 10% FCS and incubated overnight at 37°C in the presence of 5% CO₂ until fully confluent. The cells were quiesced as described in section 2.7.3. Horizontal lines were drawn on the under surface of each well to act as a reference for measurements. Three straight, scratches perpendicular to the reference lines were incised in the cell monolayer of each well using a sterile 200 µl pipette tip. Cellular debris was removed by gently washing cells once with 1 mL of sterile PBS. Cells were incubated with DMEM containing either 0.2% FCS, 10% FCS or PDGF-BB 20 ng/mL. All experiments were run in biological triplicate and technical duplicate. Images of the scratch were taken at the same position in relation to the reference line in each well using a Nikon Eclipse TS1000 microscope and imaged on QICAM Fast1394 camera (QImaging, Maidenhead, UK)

at 0, 6, 12 and 24 h. Image analysis was performed using Image pro software. The distance between wound edges were measured in 10 places and an average taken, Figure 2-11. Distance migrated between each time point was analysed.

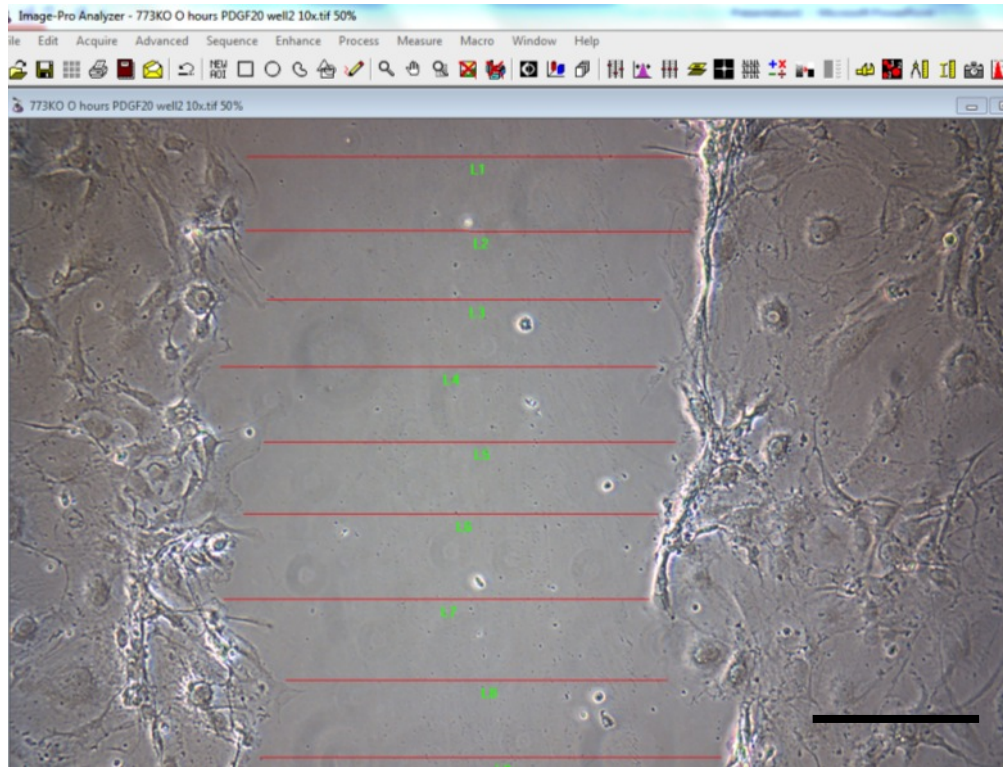


Figure 2-11. . Migration Assay. Incised scratch and measurements between wound edges. Scale bar = 100 μ m.

2.8 Murine Monocyte and Macrophages

2.8.1 Isolation and Culture of Murine Bone Marrow Cells

Male mice were euthanized as per section 2.7.1. Both hind legs from the acetabulum to foot were amputated, covering pelt removed and placed in serum free wash media (RPMI containing, 100 IU/mL penicillin, 100 µg/mL streptomycin and 2 mM L-glutamine) on ice prior to transfer into a tissue culture hood with laminar airflow. The intact tibia and femur from each leg were carefully isolated by removal of all muscle tissue. The epiphyses were removed to expose the bone marrow cavity and bone marrow flushed out into a petri dish using a 25 G needle. The wash media containing the bone marrow was then filtered through a 70 µm cell strainer (BD biosciences, Oxford, UK). Cells were then spun at 1500 rpm, 4°C for 5 min and the supernatant discarded. Red cells were removed by adding 2 mL of Red Blood Cell Lysing Buffer Hybri-Max™ (Sigma-Aldrich, Dorset, UK) for 2 min. The reaction was arrested by adding 12 mL of wash media and centrifuging cells as above. The supernatant was discarded and cells resuspended in macrophage growth media (RPMI containing 10% FCS, 100 IU/mL penicillin, 100 µg/mL streptomycin and 2 mM L-glutamine). Cells were counted as described in section 2.7.2 and 2 million cells were plated into 10 cm petri dishes. Eight 10 cm petri dishes were obtained from each animal. In order to ensure the differentiation of bone marrow derived monocytes into macrophages Macrophage-Colony Stimulating Factor (M-CSF) (Peprotech) was added to each petri dish to ensure a final concentration of 50 ng/mL. Complete RPMI media containing 50 ng/mL M-CSF was changed every second day

2.8.2 Polarisation of Bone Marrow Derived Macrophages

Following 6 days of culture and differentiation from murine monocytes into macrophages (section 2.8.1), cell media was removed and cells washed with sterile PBS. Two mL of cell dissociation solution was added to each petri dish and cells gently scrapped off the bottom of the dish. Cell dissociation solution was removed by centrifuging cells at 1500 rpm at 4°C for 5 min then discarding supernatant and resuspending them in complete RPMI media without M-CSF. Macrophages were counted and plated into 6 well plates at 1 million cells per well and left overnight to adhere to culture plates. On day 7 macrophages were

polarised by changing media for complete RPMI on its own (unstimulated control) or complete RPMI either containing LPS (from *E.coli* 0111:B4), 100 ng/mL, (Enzo Life Sciences, Exeter, UK) or IL-4, 2 ng/mL, (Peprotech, London, UK) to drive macrophages towards an M1 phenotype or M2 phenotype, respectively.

Following 24 h of exposure to LPS or IL-4 the conditioned media from cells was harvested and stored at -80°C. In addition Macrophages were harvested for either flow cytometry immediately or cells lysed by the addition of QIAzol and stored at -80°C prior to RNA extraction as per section 2.3.

2.8.3 Flow Cytometry

Polarised murine Macrophages (described in section 2.8.2) were harvested by adding 500µL of cell dissociation solution to each well, gently scraping each well and transferring cells into an Eppendorf. Eight hundred microliters of Flow Assisted Cell Sorting (FACS) buffer, composed of standard PBS (pH 7.4) containing 2 % FCS and 2 mM EDTA, was added to each cell suspension before centrifugation at 12000 rpm for 5 min. Supernatant containing cell dissociation solution and FACS buffer was discarded. Cells were resuspended in 50 µL of FACS buffer containing Fc receptor block (CD16/CD32) at a final concentration of 0.005 mg/mL (BD Pharmingen, Oxford, UK). Following incubation with Fc receptor block at 4°C for 15 min, 1 µL of fluorescent labelled antibodies were added to each tube depending on desired antigen staining. Three staining panels were used for all samples.

Panel 1: F4/80

Panel 2: F4/80, MHC II, TLR2, CD206, CD86

Panel 3: F4/80, CD69, CD11c

Table 2-5 contains the antibodies used and their fluorescent label. Following incubation of samples with appropriate antibodies for 30 min on ice and in darkness, 1 mL of FACS buffer was added and cells centrifuged at 12000 rpm for 5 min. The supernatant was discarded and cells resuspended in 300 µL of FACS buffer prior to analysis using a BD FACS Canto™ II. (BD biosciences, Oxford, UK).

An unstained sample, samples stained with each individual antibody, and samples stained with all but one antibody were used as controls to facilitate calibration of the FACS machine.

Table 2-5. FACS Antibodies.

Supplier	Antibody	Clone
eBiosciences	CD86-FITC	GL1
	F4/80 antigen APC-efluor 780	BM8
	MHC Class II-PE-CY7	M5/114.15.2
	TLR2(CD282)-PE	6C2
Biolegend	CD206-APC	C068C2
BD biosciences	CD11c-FITC	HL3
	CD69 PerCP-Cy 5.5	H1.2FE

2.9 Luminex Assay

Quantitative analysis of cytokines present within the conditioned media from miR-21 WT and KO polarised murine macrophages was conducted using a murine 20-plex Luminex™ kit (Invitrogen, Paisley, UK, catalogue number LMC0006)(Goritzka et al., 2014). Cytokines measured simultaneously were FGF-basic, GM-CSF, IFN- γ , IL-1 α , IL-1 β , IL-2, IL-4, IL-5, IL-6, IL-10, IL-12, IL-13, IL-17, IP-10, KC, MCP-1, MIG, MIP-1 α , TNF- α and VEGF.

The assay was conducted in accordance with manufacturer's protocol. The principle of the assay is as follows. Polystyrene beads of 5.6 μm diameter conjugated with antibodies specific to one of the above cytokines are internally stained with a fluorophore of defined spectral property. The beads were added to samples of interest (in addition to controls and known standards of each cytokine) which had been placed in a 96 well filter bottom plate. Any cytokines of interest bound to the antibody covered beads immobilised on the floor of the plate.

Following incubation the beads were then washed and cytokine specific biotinylated detector antibodies added which bound the immobilised protein. Excess unbound biotinylated antibodies were removed by washing.

Streptavidin-R-Phycoerythrin conjugate was then added and allowed to incubate for 30 min following which excess reagent was removed by washing. The Streptavidin bound to the biotinylated detector antibodies associated with the immune complexes on the beads thus completed a four-layer sandwich, Figure 2-12.

The Luminex™ 100 plate reader was used to detect the spectral properties of the beads and the amount of associated R-Phycoerythrin (RPE) fluorescence, thus allowing the concentration of each cytokine to be determined.

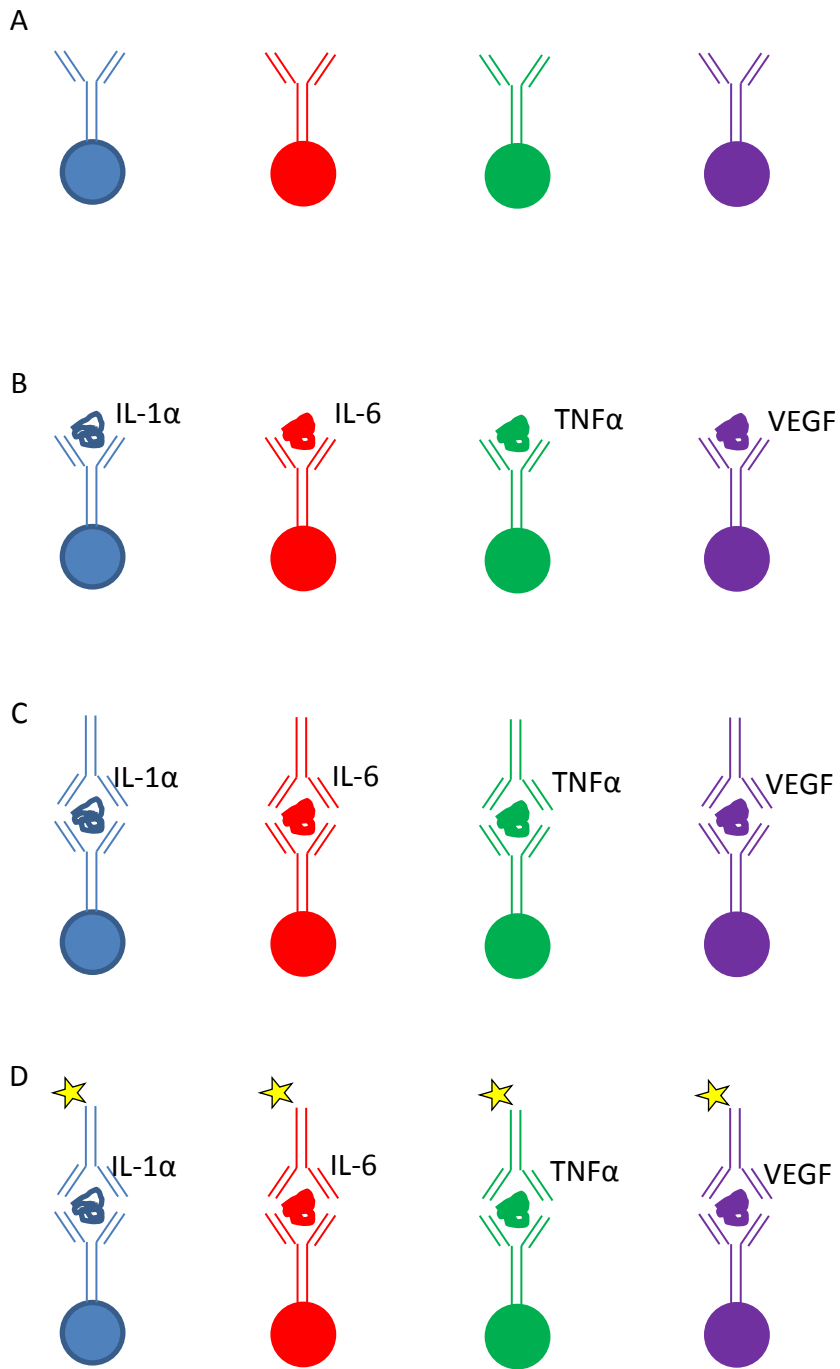


Figure 2-12. Pictorial Representation of Luminex Assay. A, Antibody conjugated beads stained with fluorophore unique to each cytokine. B, Analyte bound to antibody. C Biotinylated secondary antibody. D. Streptavidin-R-Phycoerythrin.

2.10 Conditioned Media Experiments

VSMCs isolated from WT and KO mice as described in section 2.7.1 were plated out into 96 well plates at a seeding density of 7×10^3 cells per well, $n=3$ for each. The effect on VSMC proliferation was assessed by incubating quiesced VSMCs with 150 μL conditioned media from polarised WT and KO macrophages for 48 h. A proliferation assay using BrdU was conducted as described in section 2.7.3. 0.2 % FCS and 10 % FCS were used as negative and positive controls, respectively.

2.11 Arterial Stenting and Grafting Operation

The mouse stenting model described below is taken from Ali et al (Ali et al., 2007). To reduce the risk of in stent thrombosis (IST) one week prior to surgery procedure each mouse had their drinking water supplemented with Aspirin (Boots, Byres Road) at a concentration of 300mg/L. Each procedure was carried out under sterile conditions and under direct microscopy. A donor mouse was selected and by intraperitoneal (IP) injection given an overdose of pentobarbitone (200mg/mL). The abdomen and thorax exposed anteriorly and thoracic cage was reflected superiorly to expose the heart. The right atrium was opened and the left ventricle perfused with 10ml of heparinised saline (10units/ml). The aorta was then exposed and the layer of adipose tissue dissected from its anterior surface. A small v-shaped incision was made in the aorta at the level of the diaphragm and a deflated 1.2 mm x 8 mm minitrek (Abbott Vascular, Paisley UK) coronary balloon catheter onto which a 1.25 mm long stainless steel stent had been hand crimped was passed retrogradely into the thoracic aorta. Using an Encore 26 Advantage Kit (Boston Scientific, Massachusetts USA) inflation device the coronary balloon was inflated and stent deployed at 10 atmospheres of pressure. After 30 s the balloon was deflated and removed leaving the stent in situ. The thoracic aorta from diaphragm to arch including stent was harvested using diathermy to cauterise and seal all intercostal vessels. The harvested stented aorta was stored in heparinised saline prior to interposition grafting into a recipient mouse of similar genotype.

The recipient mouse was anaesthetised with a 1:1 mixture of midazolam and buprenorphine according to weight at a dose of 0.3 mg/kg, for each drug. The recipient mouse was placed supine on a heated mat and given supplemental oxygen via a nose cone for the duration of the procedure. Lack of a withdrawal reflex to pain was used to determine that an appropriate depth of anaesthesia was achieved. The ventral surface of its neck was shaved and cleaned with chlorhexidine before a 1 - 1.5 cm midline incision was made from the suprasternal notch extending superiorly. The right salivary gland was reflected laterally and wrapped in a saline soaked swab. The right sternocleidomastoid muscle was isolated, ligated with 6-0 silk suture, transected cranial to the suture and reflected infero-laterally in order to expose the right neurovascular bundle containing the right carotid artery. The common carotid was isolated and

separated from all surrounding fascia between the level of the thoracic cage and point of bifurcation into its internal and external branches. The common carotid was ligated and transected between two 7-0 silk sutures. Polyurethane cuffs 0.8 mm diameter were threaded onto each side of the carotid and held in place with micro-haemostatic clips (Braun, UK) in order to maintain haemostasis while the 7-0 sutures placed previously were removed. Each cut end of carotid was reflected over the corresponding cuff and held in place using 8-0 silk sutures. The stented graft was then flushed with saline to remove heparin and sleeved onto either end, before being secured in place using 7-0 silk sutures. The micro-haemostatic clips were carefully removed, both anastomoses checked for haemostasis and vigorous pulsation seen within graft. Figure 2-13 summarises the key steps involved in the stenting operation. The graft was covered by replacement of the sternocleidomastoid muscle and salivary gland prior to closure of the skin with 5-0 vicryl suture. Animals were recovered following a subcutaneous injection of 1 ml of saline in a heated cage with close observation. If their recovery was prolonged or they showed signs of distress they were euthanized using a schedule one method. Animals were maintained on aspirin supplemented water until harvesting of the graft at day 28 post-operatively, although some animals were sacrificed immediately after grafting. At harvesting animals were euthanized using a schedule one method, the heart was then perfused with saline and the graft, aorta, contralateral carotid artery and heart were removed. Tissues were fixed for 12 h in 4% Paraformaldehyde (PFA).

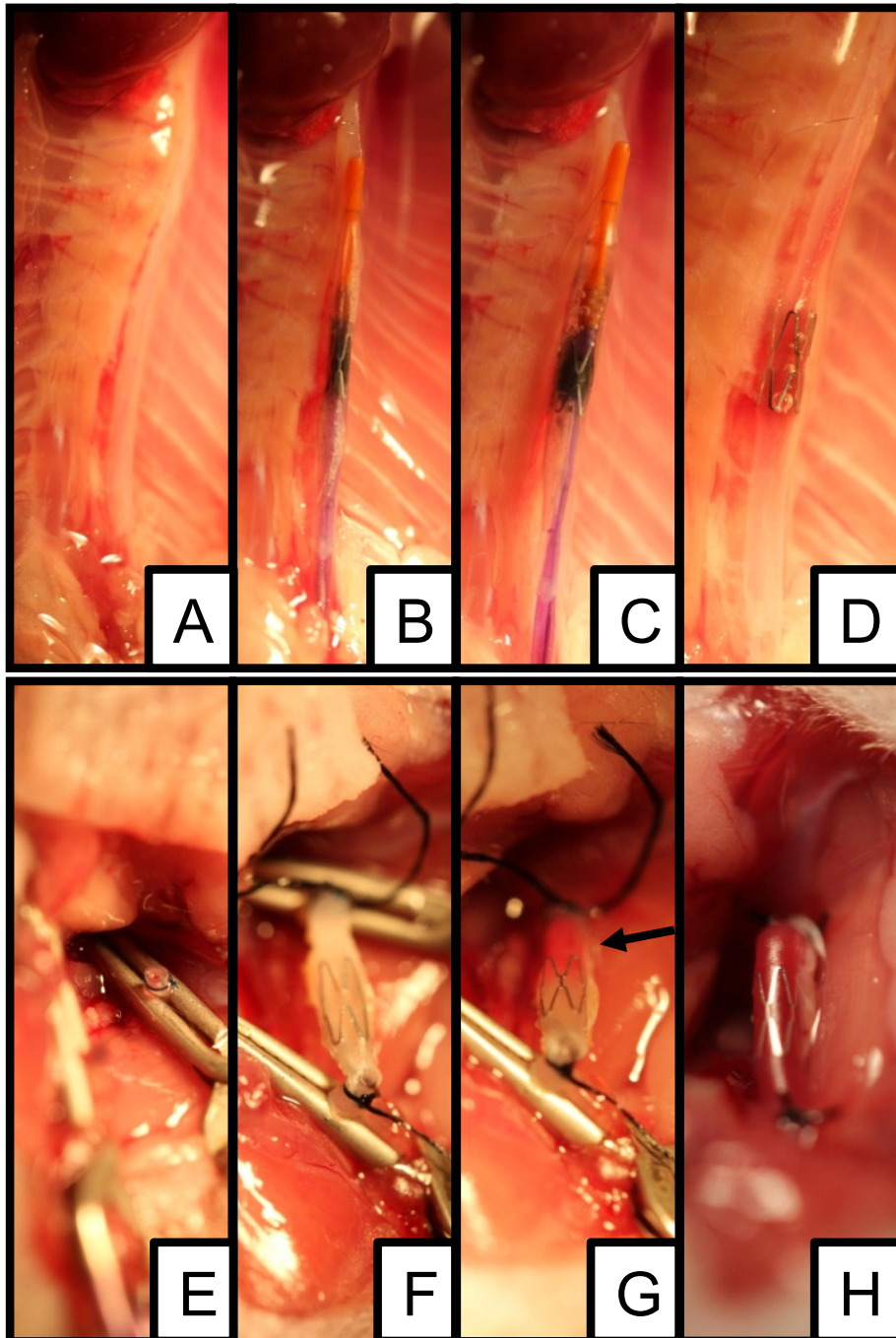


Figure 2-13. : Stenting Procedure. A, Donor Aorta. B & C, Balloon catheter with stent in aorta deflated and inflated respectively. D, Deployed stent. E, Carotid of recipient everted and secured over plastic cuff. F Graft secured in situ. G, Distal clip released demonstrating retrograde filling of graft (arrow). H, Successful stented graft with pulsatile flow.

2.12 Tissue Processing

Following fixation in 4% PFA the graft was stored in either PBS or 70% ethanol for at least 24 h prior to further processing.

2.12.1 Electrolysis

The graft was sectioned into three parts, proximal, stented and distal, Figure 2-14. The stented section was immersed in PBS and a v-shaped incision made in the distal end of the tissue overlying a stent strut. The exposed stent loop was then mounted onto either a stainless steel spring from a ball point pen (Bic, Ryman Stationers Byres Road), copper or solid silver wire (gift from Nosrat Mirzai, Bioelectronics, University of Glasgow). The other end of the tissue was partially submerged in a 5% citric acid solution with 5% (w/v) sodium chloride. The stainless steel spring was suspended on the stainless steel stylet from a minitrek balloon catheter and threaded through a truncated 18 G needle, The 18 G needle was used as a guide to maintain a central position of the stented tissue within the chamber, preventing its direct contact with the copper cathode. The stent and wire / spring were connected to the anode from a DC power source and the cathode submerged in the citric saline solution. Three to 12 Volts and 0.1 mA were run across the circuit containing the stent ensuring that bubbles of gas were being released from the cathode. After between 5 and 30 min the stent had partially dissolved. Undissolved stent was either reconnected to the spring and the process repeated or carefully removed by manual dissection under microscopy. Figure 2-15 shows apparatus used for electrolysis of stented mouse tissue.

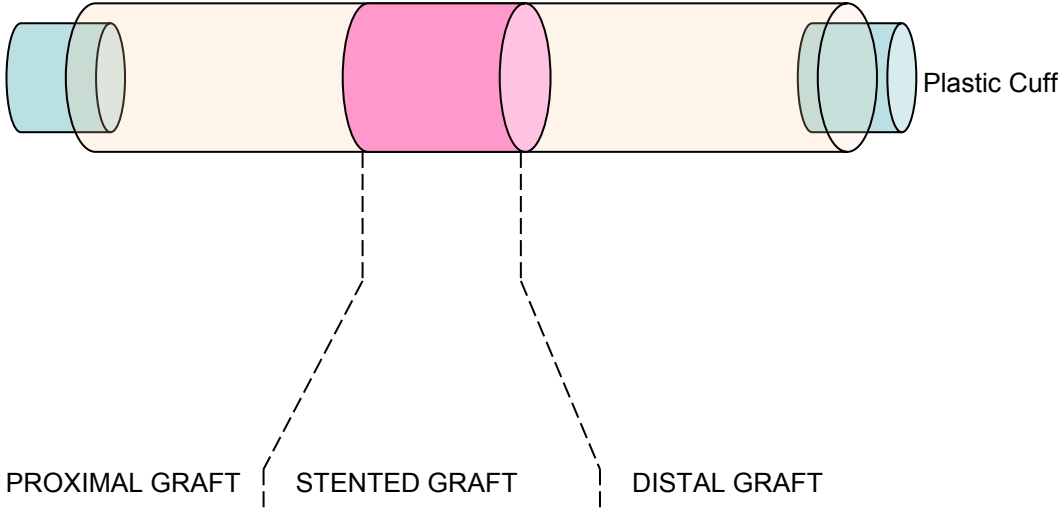


Figure 2-14. Schematic of Graft. Demonstrating gross dissection of graft to remove stented section for electrolysis. Plastic cuffs (blue), Stented graft (pink). Proximal and distal graft (yellow).

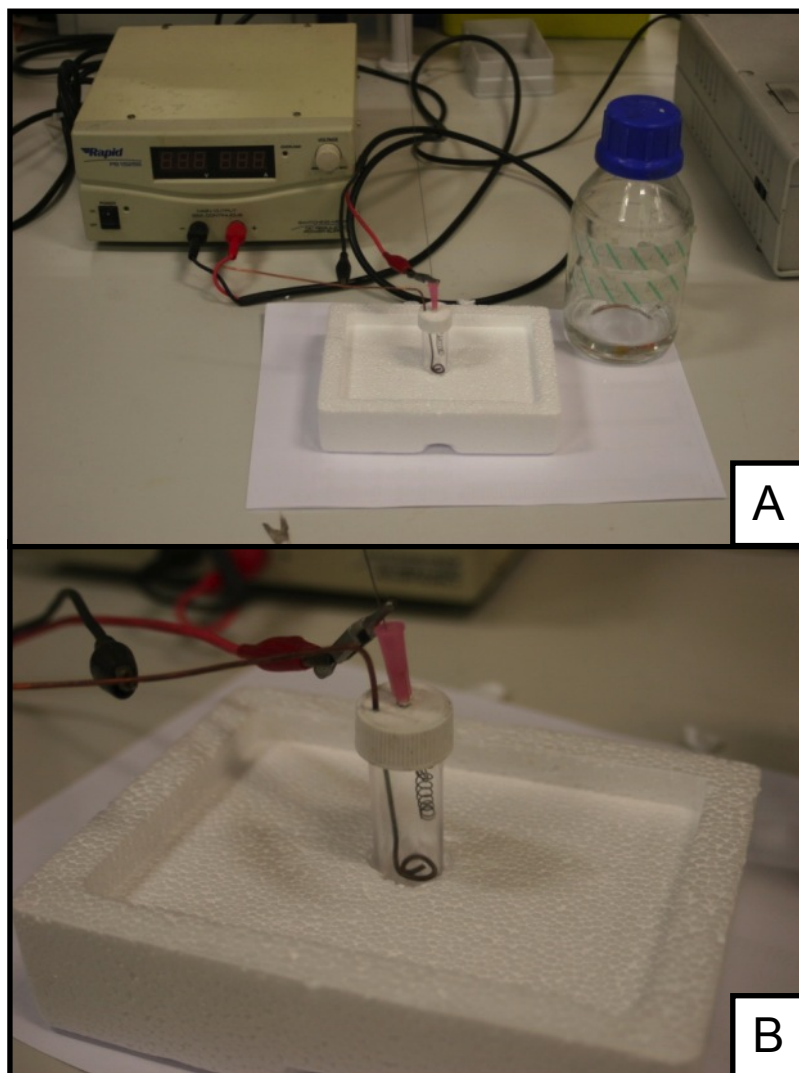


Figure 2-15. Electrolysis Apparatus. A. DC power pack top left, bijou, connector leads and bottle containing electrolysis solution. B. Electrolysis chamber consisting of bijou, copper cathode and stainless steel spring.

2.12.2 Tissue Embedding

All tissues, including those from which the stent had been dissolved, were stored in 70% ethanol prior to processing overnight in an automated Shandon Excelsior Tissue processor. Tissues were automatically submerged in increasing alcohol gradients followed by xylene then finally in molten wax. The exact processing series of gradients were as follows, 70% ethanol 30 min, 95% ethanol 30 min, absolute ethanol 30 min, absolute ethanol 30 min, absolute ethanol 45 min, absolute ethanol 45 min, absolute ethanol 1 hour, absolute ethanol/xylene 30 min, xylene 30 min, xylene 30 min, wax 30 min, wax 30 min, wax 45 min and wax 45 min. Following processing tissues were embedded in paraffin wax blocks using a Shandon Histocentre 3.

2.12.3 Tissue Sectioning

Paraffin embedded tissue blocks were cooled to 4°C and cut into sections between 3 and 7 microns thick using a bench top microtome, Leica RM2235 (Leica, Milton Keynes, UK). Tissue sections were floated on a Leica HI1210 water bath (Leica, Milton Keynes, UK) at 40°C containing 0.01% Tween20 prior to mounting on silanized glass slides (Thermo Scientific, Germany). Tissues were baked onto slides overnight at 60°C.

2.13 Histochemical Staining

2.13.1 Deparaffinisation and Rehydration

Prior to all staining protocols tissues were deparaffinised and rehydrated by immersion in 2 x 5 min washes of HistoClear (ThermoScientific, UK) followed by graded concentrations of ethanol: 100%, 90%, 70% for 5 min each and maintained under running tap water for 5 min.

2.13.2 Haematoxylin and Eosin

Tissue sections were deparaffinised as above and slides placed in Harris Haematoxylin for 2 min, then rinsed in running tap water for 2 min prior to immersion in eosin for a further 2 min. Excess eosin was removed by tapping slides and tissue sections were then dehydrated in 90% ethanol 2 x 5 min washes, 100% ethanol 2 x 5 min washes and finally HistoClear 2 x 5 min washes. Coverslips were mounted onto slides with DPX mount.

2.13.3 Elastic Van Geison

Following deparaffinisation using protocols documented above, tissue sections were placed in potassium permanganate (0.5% w/v) for 10 min then rinsed in running tap water for 5 min prior to immersion in oxalic acid (1% w/v) for a further 5 min. Slides were again rinsed in running tap water for 5 min, dipped in 70% ethanol then immersed in Miller's Stain (catalogue number 3511545) (VWR International Ltd, Lutterworth, UK) for 3 h. Slides were then removed, excess Miller's stain tapped off and rinsed by immersing 5 times in 70% ethanol. The slides were then washed in distilled water for 5 min prior to counter staining in Van Geison's solution for 10 min.

2.13.4 Picro-sirius Red

Deparaffinised and rehydrated tissues were immersed in Weigert's Haematoxylin for 8 min to counterstain nuclei. Weigert's haematoxylin was purchased as two separate solutions. Weigert's Solution A (cat HS375) and Weigert's Solution B (cat HS 380) (TCS Biosciences Ltd, Buckingham, UK) and mixed in equal quantities immediately prior to use. Slides were then washed for 10 min in

running tap water. A saturated aqueous solution of picric acid was made by adding 0.5 g Sirius Red (cat 365548) (Sigma-Aldrich, Dorset, UK) to deionised water until saturated. The slides were immersed in the picric acid solution. After 90 min the slides were given 2 x 5 min washes in acidified water. Acidified water was made by adding 0.86 ml of glacial hydrochloric acid (HCl) to 1 litre of water giving a final concentration of 0.01 M. Slides were then tapped and blotted with tissue to remove as much excess water as possible before 2 x 5 min washes in absolute ethanol followed by 2 x 5 min in HistoClear. Coverslips were mounted as previously described.

2.14 Immunohistochemistry

The following general protocol for immunohistochemical staining was followed for each antibody unless otherwise stated.

2.14.1 Antigen Retrieval

After deparaffinisation and rehydration, described previously, antigen retrieval was achieved by boiling the slides in a prewarmed citrate buffer (10 mM, pH 6) using a microwave. For cytoplasmic and nuclear staining 10 min and 20 min of microwaving were required respectively. Antigen retrieval was not required for MAC-2. Care was taken to top up citrate buffer at regular intervals to avoid tissues drying out. Tissue slides were allowed to cool slowly over 20 - 30 min at room temperature in order to minimise epitope refolding then placed under running tap water for 10 min.

2.14.2 Quenching of Endogenous Peroxidases

Slides were immersed in distilled water containing 3% H₂O₂ for 10 min at room temperature to block endogenous peroxidase activity and then rinsed for 10 min in running tap water.

2.14.3 Blocking

Tissue sections were encircled using a wax pen and non-specific staining was reduced by incubating tissue sections with blocking buffer for one hour. Blocking buffer was composed of phosphate buffered saline (PBS) containing 0.05% Tween20 plus 20% normal serum from the species in which the secondary antibody was raised. For YM-1 staining the blocking buffer also contained 5% bovine serum albumin (BSA).

2.14.4 Primary and Secondary Antibody Incubation

Blocking buffer was removed by tapping slides and the appropriate primary antibody or isotype matched IgG control applied. All primary antibodies were diluted in PBS containing 2% serum from the species in which the secondary antibody was raised. Following incubation overnight at 4°C in a humidified chamber excess primary antibody was removed with 2 x 15 min washes in PBS-T.

After washing sections with TBS they were then incubated with appropriate biotinylated secondary antibody diluted in PBS-T with 2% serum for 1 hour at room temperature.. Table 2-6 contains the different antibodies and the dilutions used.

2.14.5 Antibody detection

Excess unbound secondary antibody was removed by 2 x 15 min washes in PBS-T. Sections were then incubated with Extravidin-Peroxidase (cat E-2886 Sigma) diluted 1 : 200 in PBS-T. Staining was visualized using 3,3 diaminobenzidine (Vector Labs SK-4100) and nuclei were counterstained with Mayer's haematoxylin for 30 s.

. Table 2-6. Immunohistochemistry Antibodies.

Primary Antibody	Supplier	Species and Clonality	Dilution	IgG control	Secondary Antibody	Dilution	Blocking Serum
Anti-Alpha Smooth Muscle Actin	Abcam (ab5694)	Rabbit Polyclonal IgG	1 in 200	Normal Rabbit IgG control Invitrogen (10500C)	Goat anti-rabbit Vector Labs (BA-1000)	1 in 200	Normal Goat Serum Vector Labs (S-1000)
PCNA	Abcam (ab2426)	Rabbit Polyclonal IgG	1 in 200	Normal Rabbit IgG control Invitrogen (10500C)	Goat anti-rabbit Vector Labs (BA-1000)	1 in 250	Normal Goat Serum Vector Labs (S-1000)
CD31 (PECAM)	Histonova (SZ31)	Rat Monoclonal IgG	1 in 20	Rat IgG2a BD Pharmingen (559073)	Rabbit anti-rat Vector Labs (BA-4000)	1 in 200	Normal Rabbit Serum Vector Labs (S-5000)
MAC-2	Cedarlane (CL8942AP)	Rat Monoclonal IgG	1 in 5000	Rat IgG2a BD Pharmingen (559073)	Rabbit anti-rat Vector Labs (BA-4000)	1 in 200	Normal Rabbit Serum Vector Labs (S-5000)
YM-1 (Anti-Chitinase-3 like Protein 3)	Abcam (ab93034)	Rabbit Polyclonal IgG	1 in 500	Normal Rabbit IgG control Invitrogen (10500C)	Goat anti-rabbit Vector Labs (BA-1000)	1 in 200	Normal Goat Serum Vector Labs (S-1000)

2.15 *In situ* Hybridisation

Tissue section cut to 7 μM and baked onto silanized slides at 60 °C overnight were deparaffinised and rehydrated as described previously.

2.15.1 Unmasking and Deproteinizing Sections

Sections were placed in freshly prepared 0.1% DEPC for 1hr then transferred them into DEPC-treated 10 mM sodium citrate buffer, pH 6, and heated in a microwave for 10 min. The samples were then allowed to cool for 15 min at room temperature prior to washing in PBS for 1 min. Slides were immersed in 0.2 M HCl for 20mins then washed in DEPC-treated PBS 2 x 5 min and further immersed in 0.3% Triton-X in DEPC treated PBS for 10 min. Slides were then washed again with DEPC-treated PBS 3 x 5 min and then prewarmed (37°C) proteinase K (10ug/mL in DEPC-treated PBS) applied to each section in a humidified chamber at 37°C. After 20 min, sections were rinsed with DEPC-treated PBS 2 x 5 min and fixed in 4% PFA in DEPC treated PBS for 10 min at room temperature.

2.15.2 Hybridisation

Fifty to 100 μL of hybridisation buffer (50 % deionised formamide, 4 x standard saline citrate (SSC), 2.5 % Denhardt's solution, 0.245 $\mu\text{g}/\text{mL}$ salmon sperm DNA, 0.2 mg/mL yeast transfer RNA, 0.025 % SDS and 0.1 % DIG-blocking reagent (Roche) was placed on each section and a cover slip added. Slides were placed in a sealed, humidified, RNase free box at hybridisation temperature for 1 hour (miR-21 52°C, scramble 58°C). Probe was then diluted in hybridisation buffer (1.6 μL probe per 1mL hybridisation buffer, final conc. 40 nM) and heated to 95°C to linearise and then chilled on ice. Twenty-five to 50 μL of probe was added per slide and covered with a coverslip and incubated overnight at hybridisation temperature in the humidified RNase free box wrapped in saran wrap.

2.15.3 Stringency washing

Coverslips were gently removed with 5 x SSC before being washed in 1 x SSC at hybridisation temperature for 20 min then in 0.2 x SSC at hybridisation

temperature for 20 min. Slides were then further washed at room temperature in 0.2 x SSC for 5 min while being gently agitated on a shaker and finally washed in 1 x DEPC-treated PBS at room temp for 5 min on a shaker.

2.15.4 Immunological detection

Sections were incubated with blocking buffer (0.5% blocking reagent (Roche), 10% heat inactivated goat serum, 0.1% Tween, 1 x PBS) for one hour prior to overnight antibody incubation (1 : 500) anti-Dig-AP Fab (Roche) in blocking buffer + 10 % heat inactivated goat serum in humidified chamber at 4°C. The following day sections were given 3 x 5 min washes in PBS-Tween20 (0.05%) followed by 3 x 10 min washes in AP buffer 100 mM Tris HCL pH 9.5, 100 mM NaCl, 0.1% Tween 20). BM Purple AP (Roche) + 2 mM Tetrazolium (1000 x inhibitor) was then added to each section protected from light and left at room temperature until colour development (8 - 48 h). Slides were then given 3 x 5 min washes in PBS-T, rinsed for 5 min in running tap water, mounted with aqueous mounting solution and edges sealed with clear nail varnish (Boots, Byres Road UK)

2.16 Image Analysis

2.16.1 Image Acquisition and Analysis

Images of tissue sections obtained with QCapture software were taken using a Qimaging Micropublisher 3.3 RTV camera with mounted on an upright Olympus BX 40 microscope. Both morphometry and staining analysis was conducted using ImagePro software. Figure 2-16 demonstrates morphological analysis in a stented section with a large neointima. Figure 2-17 shows an example of staining quantification within the area of interest used for all stains except re-endothelialisation, which was calculated as a percentage of luminal circumference. Prior to image acquisition and analysis, slides were anonymised by removing all identifiable information and the allocation of random numbers by an independent researcher from within the Baker group. Following analysis the genetic identity of the samples was unblinded in order that conclusions could be drawn from the data obtained.

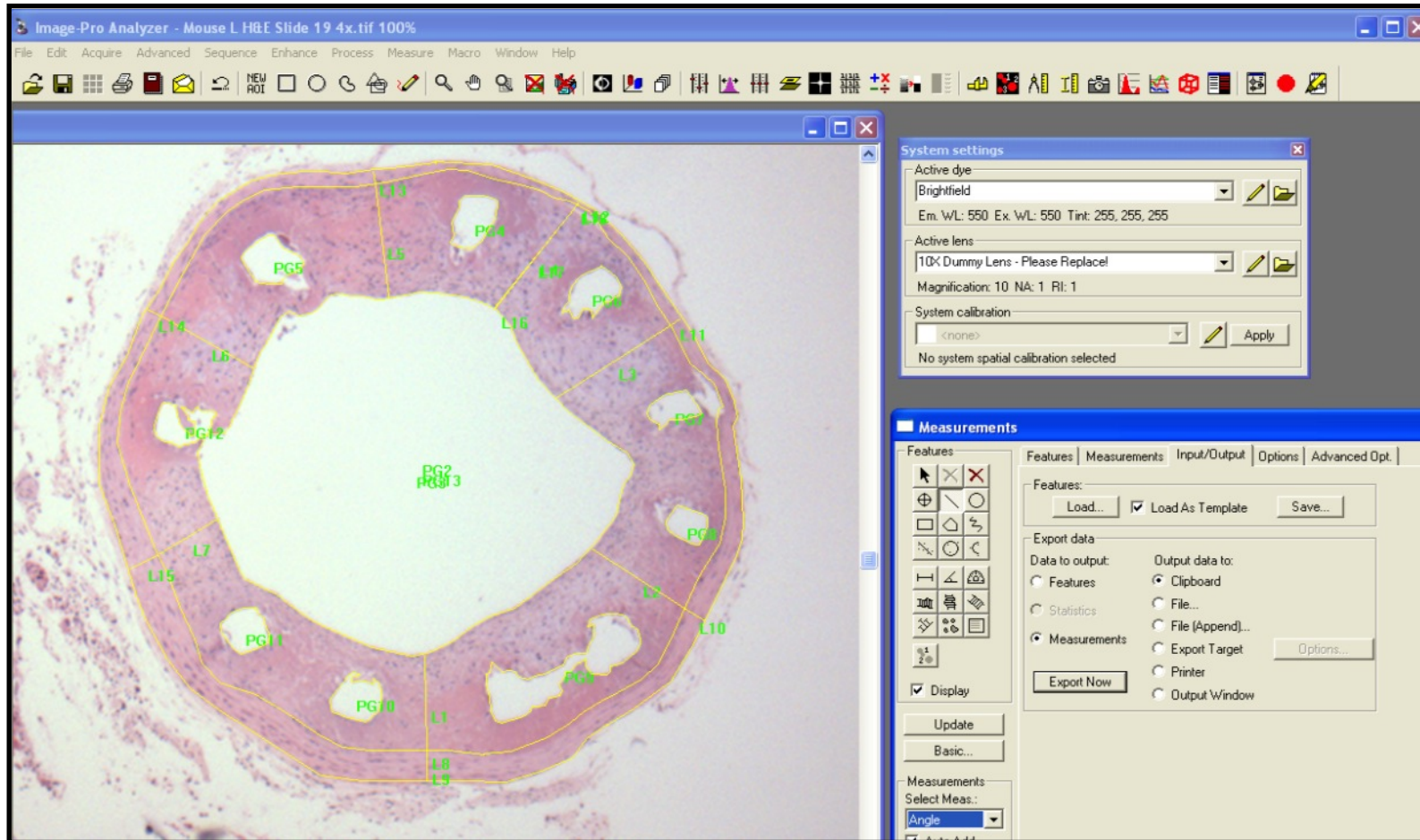


Figure 2-16. Example of Morphological Analysis. Measurements highlighted in yellow including total vessel, luminal, medial and neointimal areas.

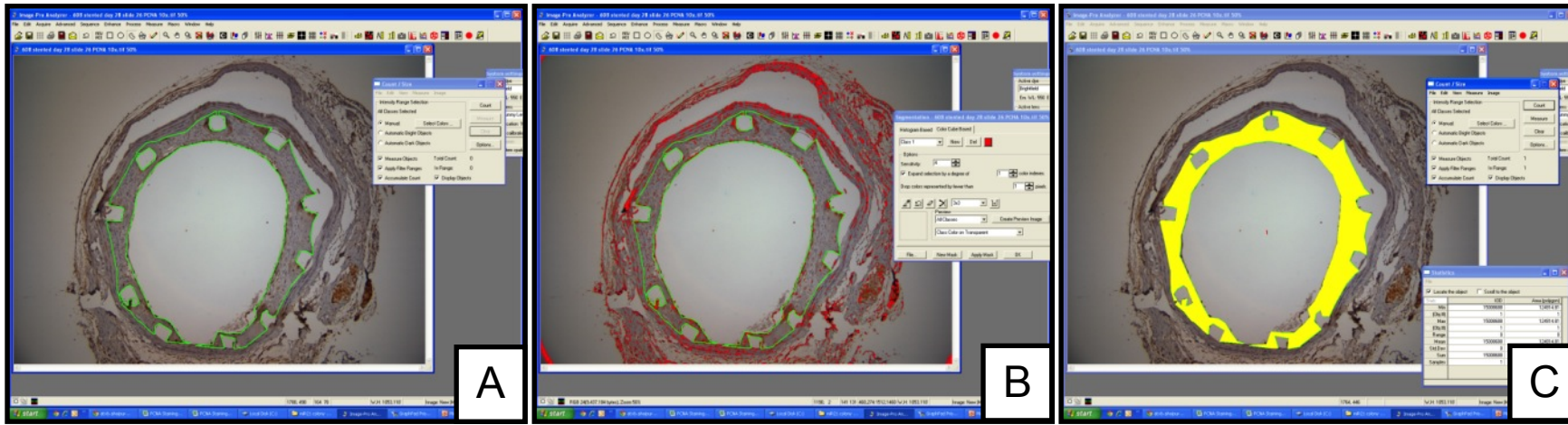


Figure 2-17. A, Area of interest (neointima) highlighted in green. B & C, Areas of staining highlighted (red) and quantified as percentage of total area of interest

2.17 Statistical analysis

Data is presented as mean \pm SEM unless otherwise stated. *In vivo* experiments were conducted from n = 3 - 12 animals per group. *In vitro* experiments were conducted in biological triplicate on three independent occasions except for Luminex assay, which was conducted once.

All statistical analysis was carried out using GraphPad Prism 4. Data was assessed for normality. Parametric data was analysed by Student's t-test when comparing two groups or one way ANOVA with Bonferroni's correction for multiple testing when comparing more than two groups. A p value <0.05 was considered significant.

3 Refinement of the Mouse Model of ISR and Stent Electrolysis

3.1 Introduction

Vascular disease is a complex pathological process involving the interaction, proliferation and migration of multiple cell types including inflammatory cells, endothelial cells, smooth muscle cells and fibroblasts among others (Ross, 1999). Additionally, a significant role is played by cytokines, growth factors and proteases released from these cell types which act in both an autocrine and paracrine fashion (reviewed in (Ross, 1999).

Adding further to the complexity of vascular pathology is that rather than being a single process it has become clear vascular disease is a heterogeneous group of pathologies, several of which are iatrogenic in their aetiology. Thus vascular disease encompasses a group of conditions including native vessel atherosclerosis, arteriosclerosis obliterans, cardiac allograft vasculopathy, vein graft neointimal hyperplasia and in-stent restenosis (Mehran et al., 1999, Motwani and Topol, 1998, Mancini et al., 2003).

The accurate and relevant replication of such a complex pathology *in vitro* is not possible; hence many studies of vascular pathology involve *in vivo* investigations using animal models (Waksman et al., 2012). Indeed many different animal models have been developed to mimic the variety of vascular pathologies noted above. Models of restenosis have been developed in several different species including large animals such as dog, pig, rabbit and non-human primates (Roubin et al., 1987, Ragosta et al., 1994, Ialenti et al., 2011, Geary et al., 1996). These models are attractive due to the comparable size of the target artery with human coronary arteries. However, none perfectly replicate human disease and have other associated problems. Dogs do not easily develop atherosclerosis and exhibit only a mild reaction upon balloon angioplasty or stenting (Roubin et al., 1987, Schwartz et al., 1994).

While rabbits can develop atherosclerosis when placed on high fat diets, many of the injury models use a two stage process involving air desiccation or balloon abrasion prior to angioplasty; thus calling into question how well they actually replicate human disease (Wilensky et al., 1995, Ragosta et al., 1994). In addition the neointima formed in rabbits following stenting contains a large proportion of

foam cells, which is not seen in human vessels following stenting (Feldman et al., 2000).

The porcine single injury model of angioplasty and stenting is well utilised and produces a significant neointimal lesion proportional to the degree of injury in both the carotid and coronary arteries (Steele et al., 1985, Schwartz et al., 1990, Ialenti et al., 2011). While the neointimal lesion formed resembles that in humans, with a high proportion of VSMCs present, the degree of injury inflicted is far greater than that seen in clinical practice. However, due to thrombotic complications observed in pigs they are, like humans, maintained on dual antiplatelet therapy following percutaneous intervention (Ialenti et al., 2011).

Non-human primate models are rarely utilised despite their close evolutionary link due to cost, the long period required for atherosclerosis development and difficulties with animal handling (Geary et al., 1996).

Small animal models of vascular injury have been far more widely used to study the development of NIH as they are cheap, easy to undertake and allow consistent lesion generation. The 1970s saw the earliest small animal models of vascular injury being developed with rat carotid arteries being subjected to air desiccation along their luminal surface, producing endothelial denudation and subsequent NIH (Fishman et al., 1975). The lack of clinical relevance with the air induced injury model resulted in the development of two other models. Firstly, a balloon injury model was developed whereby a balloon catheter was passed into the common carotid via a branch of the external carotid and inflated three times (Clowes and Clowes, 1986). This not only denuded the vessel lumen but also damaged the vessel media eliciting a large neointimal hyperplastic response. In order to dissect out the relative contributions of platelet aggregation, thrombosis and medial injury to the development of neointimal hyperplasia a third model of vascular injury was devised. By passing a 5/0 nylon monofilament along the luminal surface of the carotid artery three times, almost complete endothelial denudation could be achieved (Fingerle et al., 1990). This produced a smaller neointimal response than observed with balloon injury due to sparing of internal elastic lamina and VSMCs within the vessel media from damage. Unfortunately, while the above models of vascular injury have been well utilised

they have failed to fully reveal the molecular mechanisms underlying NIH following vessel injury.

Attracted by the huge number of transgenic and knockout mouse strains available, researchers have developed several mouse models of vascular injury. These have allowed scientists to elucidate the contribution from individual cells, cytokines, growth factors and proteases to the development of NIH (Ikeda et al., 1991, Zimmerman et al., 2002). With the exception of carotid artery ligation these models, including wire or filament injury, electrical injury, and adventitial cuff placement have been directly adapted from the rat or other animal species (Moroi et al., 1998, Lindner et al., 1993, Hui, 2008, Kumar and Lindner, 1997, Carmeliet et al., 1997). Despite the wealth of knowledge gained from these mouse models they still do not accurately mimic human disease.

The routine use of stents, coronary artery bypass grafting and increasing prevalence of heart transplantation within clinical practice has pushed researchers to develop more clinically relevant small animal models. Many of these more complex models mimicking specific clinical situations have intentionally been developed in mice. Indeed models of vein grafting and cardiac allograft vasculopathy were the next to be successfully developed. Almost a decade after the publication of the first mouse vein grafting model and seven years after the publication of the first allograft vasculopathy model a stenting model was finally developed which could be used in mice. This first stenting model, developed in the Channon laboratory, is based on the carotid interposition grafting models mentioned above (Ali et al., 2007). A small custom made stent is deployed within the aorta of a donor mouse and then grafted into the carotid artery of a recipient mouse using plastic cuffs to aid the creation of vascular anastomoses.

Despite the development of several murine stenting models histological analysis remains challenging due to the inability to cut tissues containing metal stents on standard microtomes. Although tissue resin embedding can be undertaken, cutting requires the use of a diamond tipped saw and laborious polishing of sections, disrupting the tissue architecture (Watt et al., 2013). In addition, in depth immunohistochemical analysis cannot be undertaken due to the inability of antibodies to penetrate the resin (Malik et al., 1998, Torgersen et al., 2009).

These obstacles have limited the widespread use of such stenting models and our knowledge of the molecular mechanisms underlying ISR development.

3.2 Aims

1. To introduce to our lab the mouse model of stenting pioneered in the Channon Laboratory Oxford.
2. To develop a reliable method of electrochemical dissolution of the metal stent *ex vivo* and allow the in-depth characterisation of neointimal content by immunohistochemistry.

3.3 Results

3.3.1 Replication and Complications of the Stenting Model

The *in vivo* stenting model developed by the Channon laboratory (Ali et al., 2007) was successfully replicated but not without difficulty mainly due to the high degree of surgical skill required. The highest mortality was encountered during the early stages of this study when attempting recovery surgery but by the end of the complete study programme all cause mortality in recipient mice had decreased to 4% within the final cohort (n = 50).

The *in vivo* procedure was initially undertaken in 50 mice (25 donors and 25 recipients). Two recipient mice suffered carotid rupture, 10 mice could not be recovered due to anastomotic failure. All were schedule one culled while under general anaesthesia. Two died of anaesthetic overdose. Of those recovered two mice were culled by schedule one method at day 1 and day 6 due to poor condition and visible distress. At post mortem one was found to have graft thrombosis the other a neck abscess. Nine animals were successfully recovered and stented grafts harvested at 28 days post operatively. All of these successful operations were undertaken towards the end of the operating list. Of the 9 animals surviving to 28 days, 2 grafts were found to have occluded. Examination of the occluded grafts showed in-stent thrombosis likely due to under deployment of the stent resulting in malaposition with the vessel wall. Inspection of tissue sections revealed concentric layers of thrombus interspersed with inflammatory cells. In some grafts infiltration of thrombus by VSMCs was observed. Figure 3-18 shows graft thrombosis and thrombus architecture. Figure 3-19 demonstrates macrophage staining within a thrombosed graft.

Complications observed were divided into early (peri-operatively and up to 1 day post-operatively) and late (>1 day postoperatively). Early complications included minor haemorrhage, major haemorrhage and death under anaesthesia. Minor haemorrhage was usually due to capillary rupture during tissue manipulation and was treated with direct manual pressure using gauze or a cotton bud. Major haemorrhage, either from failure to maintain haemostasis during carotid manipulation or failure of either anastomosis, commonly resulted in death. Where haemostasis could not be regained and death due to major haemorrhage

was deemed inevitable cervical dislocation was used to humanely kill the animal. Another early complication of surgery was death due to overdose of anaesthesia resulting from additional doses of injectable anaesthetics being administered intra-operatively in an attempt maintain an appropriate depth of anaesthesia for the duration of the operation. This complication was initially abrogated by the use of supplemental oxygen with additional doses and eventually completely eliminated by the reduction in operation duration from 1 hour 20 minutes to 30 minutes. Late complications also included haemorrhage, usually due to a persistent small leak, stroke due to graft thrombosis with embolisation and rarely infection.

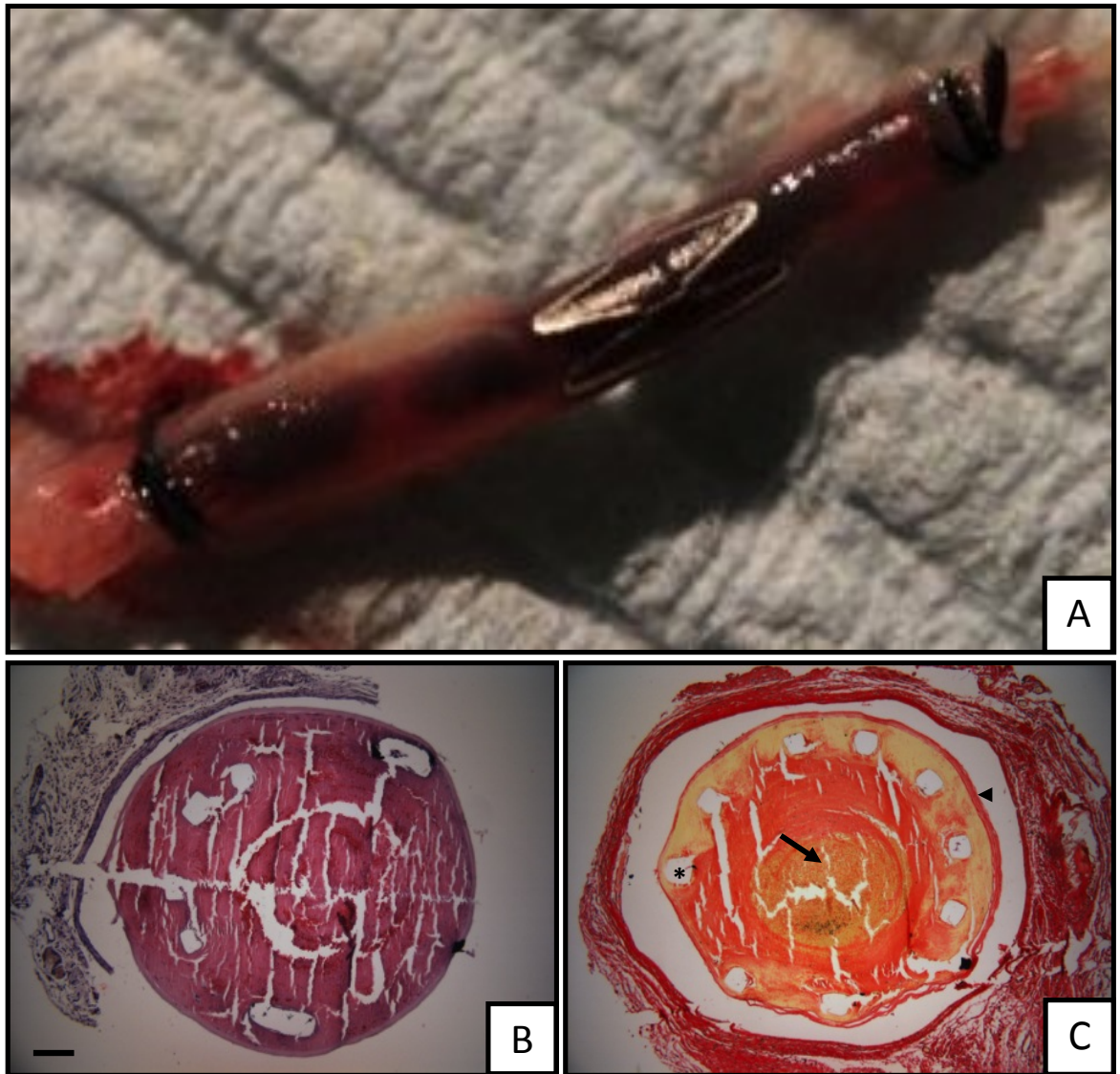


Figure 3-18. Graft Thrombosis. A, Harvested graft with thrombus visible underlying stent. B, Thrombosed stented section demonstrating malposition of stent against vessel wall (H&E) 10x. C, In-Stent Thrombosis stained with picro-sirus red showing the gradual build-up of thrombus in layers encroaching on the vessel lumen 10x. * - Stent strut location, Arrow - thrombus, Arrowhead - media. Scale bar = 100 μ m. Representative sections from n=1.

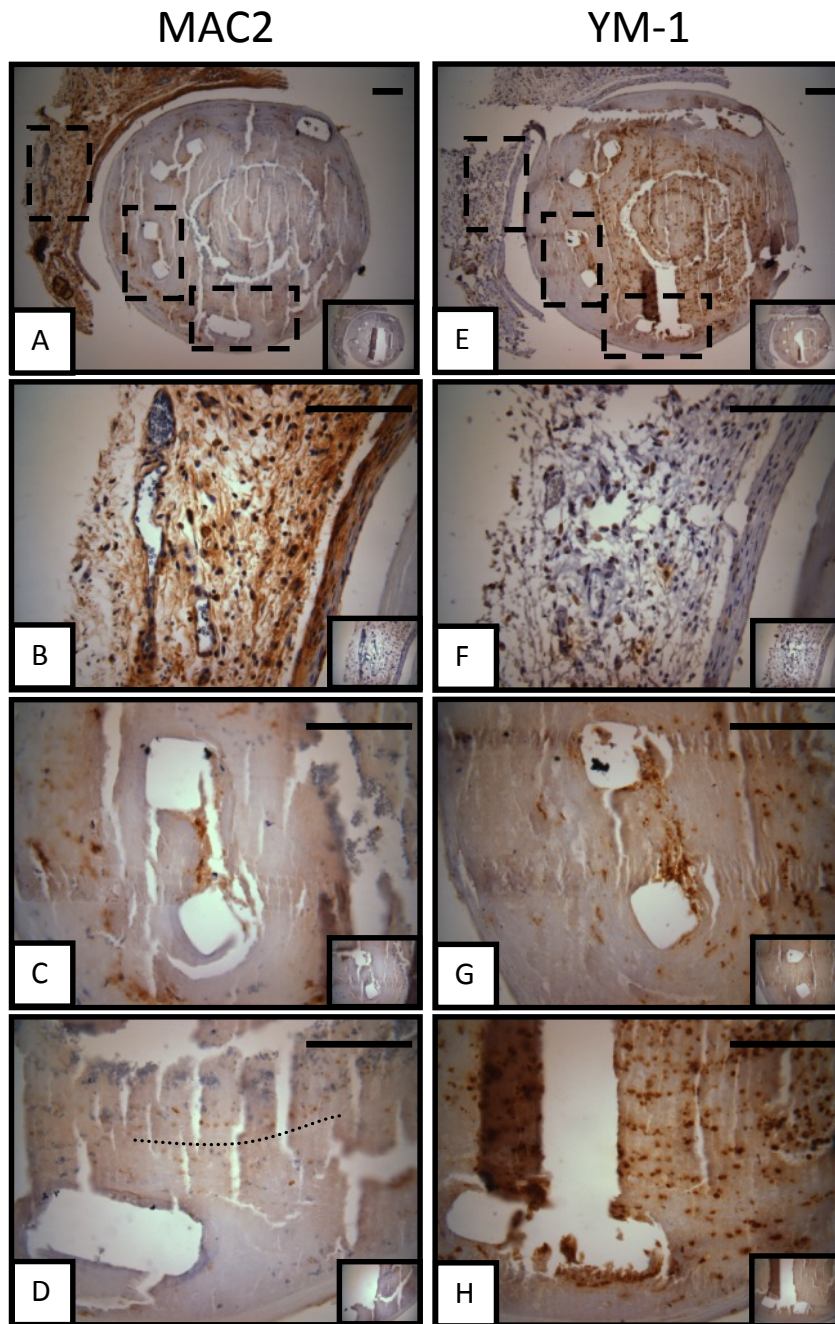


Figure 3-19. Macrophage Staining. A, B, C and D, Total macrophage staining with MAC-2. Macrophages present within the adventitia and within layers of thrombus (D dotted line). E, F, G and H, Alternatively activated macrophages predominate around stent struts and are less populous within adventitia. (Inserts-IgG control). Positive staining represented by brown colour. Boxes in panels A and E represent areas of higher magnification depicted in other panels. Scale bar = 100 μ m. Representative sections from n=1.

3.3.2 Optimisation of Stent Electrolysis Protocol and Staining

Following fixation in 4% PFA, electrochemical dissolution of the metallic stent to allow tissue sectioning was undertaken as described in Chapter 2. The five main variables requiring optimisation were the:

1. Containment apparatus.
2. Solution used in the electrolysis process.
3. Solution in which tissues were stored.
4. Electrodes/connection.
5. Voltage delivered by the DC power pack.

3.3.2.1 Containment Apparatus

Initially a 500 mL plastic mineral water bottle was used as the containment vessel and successfully dissolved a bare metal stent (Driver 3.0 x 24 mm, Medtronic) that was not encased in tissue. Progressively smaller containment vessels were investigated until a 5 mL bijou was found optimal. This allowed for more accurate mounting, easier manipulation and better visualisation of murine tissue. In addition, precise alteration of fluid level and conformation of a conducting circuit by the identification of ionic stream and gaseous bubble production was facilitated using a bijou.

3.3.2.2 Solution used in electrolysis process

Three citric acid/sodium chloride solutions were investigated at differing weight to volume concentrations, 1% (w/v), 5% (w/v) and 10% (w/v). All were found to complete the electrical circuit when bare metal electrodes were used. However, only the solutions above 1 % were found to conduct well when tissue samples were tried. Thus a solution of citric acid 5% (w/v) and sodium chloride 5% (w/v) pH 2, with 50:50 relative proportion of each chosen for all further work.

3.3.2.3 Storage solution for tissue

Standard lab protocol suggests storage of tissue in either PBS or 70% ethanol following fixation. Tissues stored in PBS allowed conduction to take place with bubbles of gas formed at the copper cathode but a stream of metallic ions was not observed. Examination of the stented tissue after 10 minutes revealed the stent remained almost completely intact and that any degradation of the stent occurred randomly across the stent. Stented tissues stored in 70% ethanol for at least 24 hours showed more complete stent dissolution and in a more predictable manner from the portion of the stent touching the citric saline solution up towards its connection with the anode. This is most likely due to the PBS infused tissue conducting in addition to the stent itself, while for tissues those stored in 70% ethanol only the stent conducted electricity.

3.3.2.4 Electrodes and connectors

Formation of a robust connection between the stent and the anode was found to be key to maintaining the electric circuit. Several materials were trialled including the central stilet from Mini Trek™ coronary balloon, microelectronic clip, tightly coiled spring, spring from propelling pen and fine wire. Initially both copper and silver wires were used as they are less reactive than the stent and should therefore only electrolyse after the stainless steel stent. However, a firm connection between wire and stent could not be maintained. Instead the optimal electrode-stent connector was found to be a stainless steel spring from a ball point pen, which was itself electrolysed into a sharp shallow point and wedged in the end of stent loop.

3.3.2.5 Voltage

Between 3 and 12 Volts were applied from the DC power pack. Twelve Volts allowed stent dissolution but excessive heat production caused tissue charring and altered staining, Figure 3-20. Below 5 Volts incomplete stent dissolution occurred and metallic debris could be seen within tissue sections. Metallic fragments tore and distorted tissue architecture, Figure 3-20B and C. Optimum stent dissolution was obtained in day 0 and 28 day samples using between 5 and 8 Volts.

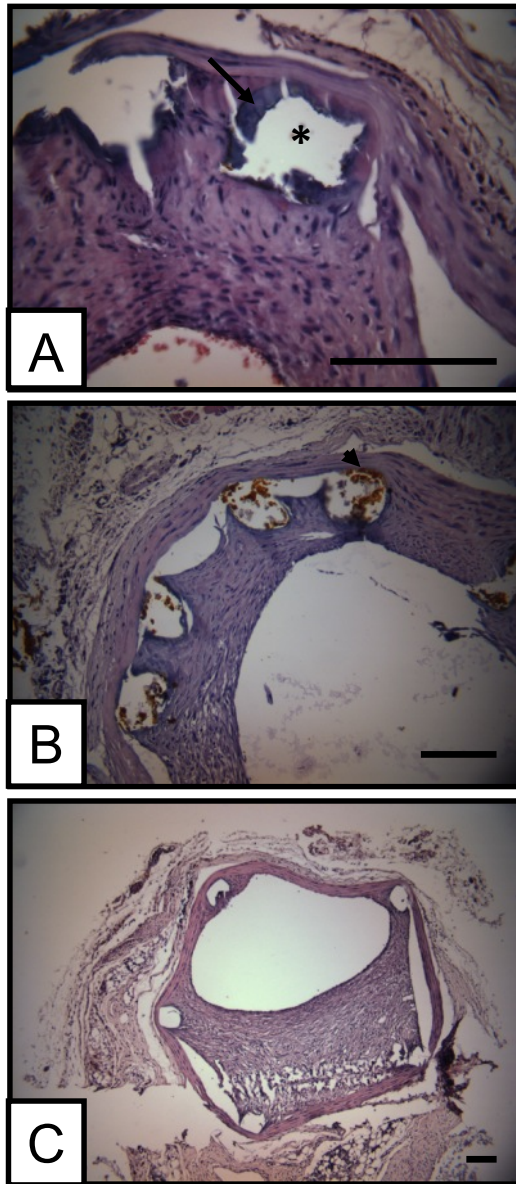


Figure 3-20. Optimisation of Stent Electrolysis. A, Charring of tissue around stent strut location due to excessive heat from electric circuit. * - stent strut location, Arrow – charred area, 40x. B, Incomplete dissolution of stent struts with metallic debris remaining. Arrowhead – metallic debris. 20x. C, H&E stained section showing tearing of tissue during cutting on microtome due to presence of metal debris 10x. Scale bar = 100 μ m. Representative sections from n=5.

3.3.3 Optimisation of Histochemical and Immunohistochemical Staining

3.3.3.1 Effect of Electrolysis on Tissue Staining

The electrolysis protocol did not impair tissue staining with either H&E or EVG. Error! Reference source not found. and 3-Figure 3-22 show tissue sections from an aortic graft harvested at day 28. No difference was observed in staining of stented sections, which were subjected to electrolysis, compared to sections both proximal and distal to the stent that were not. Similarly tissues harvested at day 0 were equally able to take up these standard stains, Figure 3-23.

Figure 3-23Figure 3-24 andFigure 3-25 demonstrate representative examples of staining for a panel of cell markers in stented (electrolysed) sections of the aortic graft at day 0 and day 28, respectively. Electrolysis did not inhibit tissues undergoing immunohistochemical staining at either time point. The panel of antibodies chosen not only assessed the composition of neointima but also ensured electrolysis did not alter the ability to stain for cell surface, cytoplasmic and nuclear antigens.

Several observations were noted from immunohistochemistry performed on day 0 and day 28 tissues. Sections stained for CD31 (an endothelial marker) showed there was almost complete endothelial denudation due to balloon and stent injury at day 0 and that by day 28 re-endothelialisation was almost complete, Figure 3-25. Few macrophages were identified in grafts at day 0 but were abundant in the adventitia, media and neointima at day 28. Similarly when stained with PCNA, proliferating cells were almost completely absent at day 0 but easily identified throughout the vessel wall by day 28.

Sections cut from the vascular anastomosis containing the plastic cuff were also examined. This revealed considerable neointimal development with extensive cellular infiltration and proliferation within the aorta and around the plastic cuff. These cells were confirmed to be VSMCs and macrophages by smooth muscle α -actin and MAC2 staining, respectively, Figure 3-9.

3.3.3.2 Staining for YM-1 within Tissues

YM-1, also known as Chitinase 3-like-3 (Chi3L3), is a murine marker of the alternatively activated (M2) macrophage (Raes et al., 2002). Expression of YM-1 is induced by exposure of macrophages to IL-4 or IL-13 both well-known drivers of M2 polarisation (Raes et al., 2002, Nair et al., 2003). Identification of M2 polarised macrophages in tissue sections has not previously been conducted within the Baker Laboratory but was achieved using a variety of tissues known to contain macrophages in different polarisation states as positive controls. Figure 3-26 shows YM-1 staining within sections of both mouse spleen and vein graft.

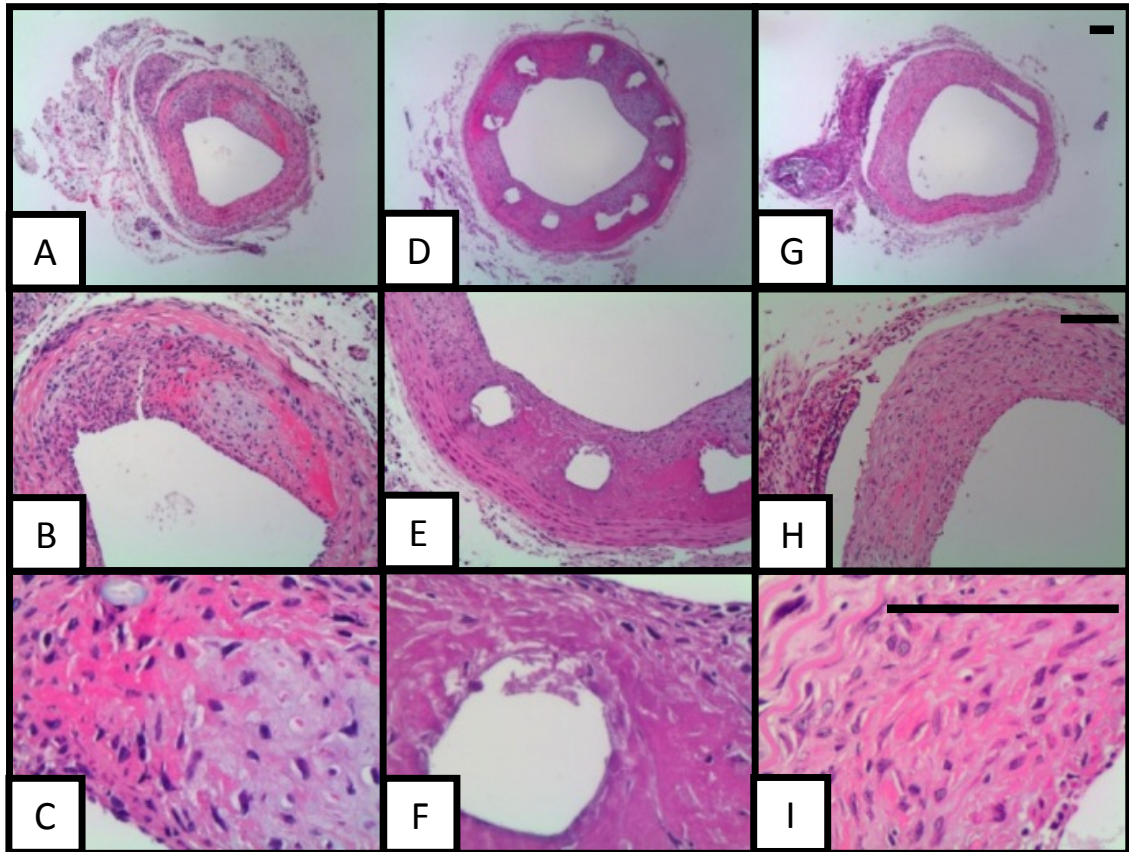


Figure 3-21. H&E Staining of Tissues Harvested at Day 28. A, B and C Proximal Graft (H&E 4x, 10x, 40x). D, E, and F, Stented Graft (H&E 4x, 10x, 40x). G, H and I Distal Graft (H&E 4x, 10x, 40x). Scale bar = 100 μ m. Representative sections from n=5.

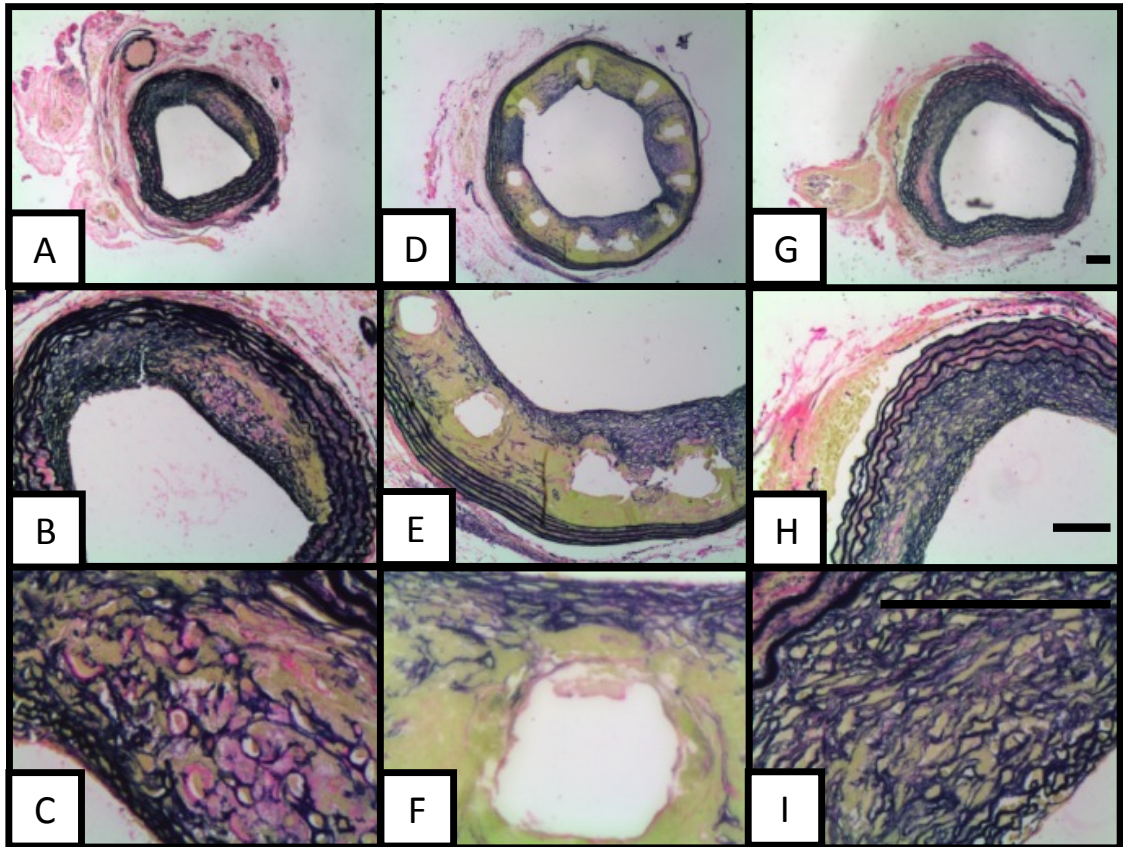


Figure 3-22. EVG Staining of Tissues Harvested at Day 28. A, B and C Proximal Graft (EVG 4x, 10x, 40x). D, E, and F, Stented Graft (EVG 4x, 10x, 40x). G, H and I Distal Graft (EVG 4x, 10x, 40x). Scale bar = 100 μ m. Representative sections from n=5.

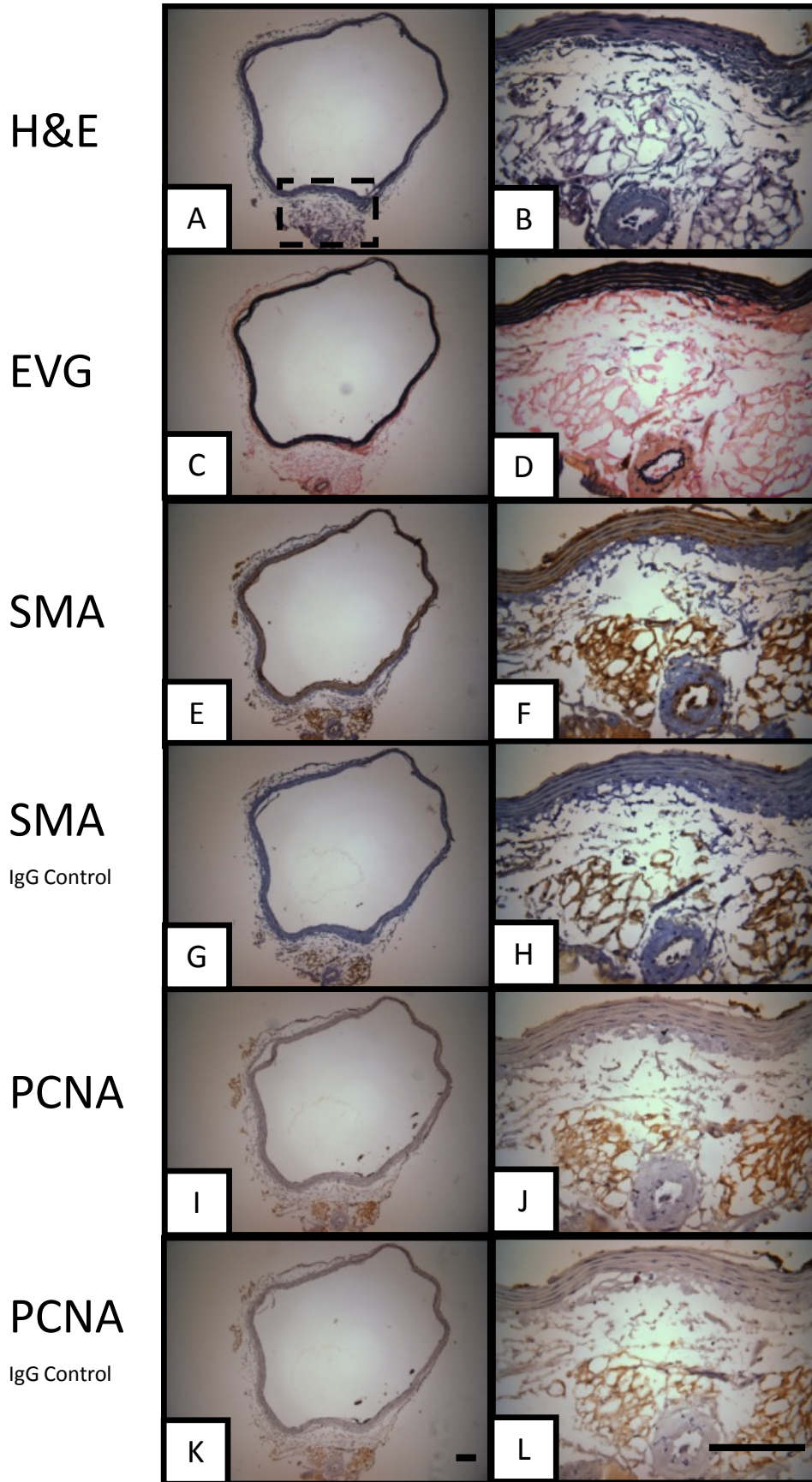


Figure 3-23. Histochemistry and Immunohistochemistry of stented graft harvested at day 0. A and B, H&E (10x, 40x). C and D, EVG (10x, 40x), E and F, SMA (10x, 40x). G and H, SMA IgG control (10x, 40x). I and J, PCNA (10x, 40x). K and L, PCNA IgG control (10x, 40x). Hatched box, magnified area of interest. Scale bar = 100 μ m. Representative sections from n=8.

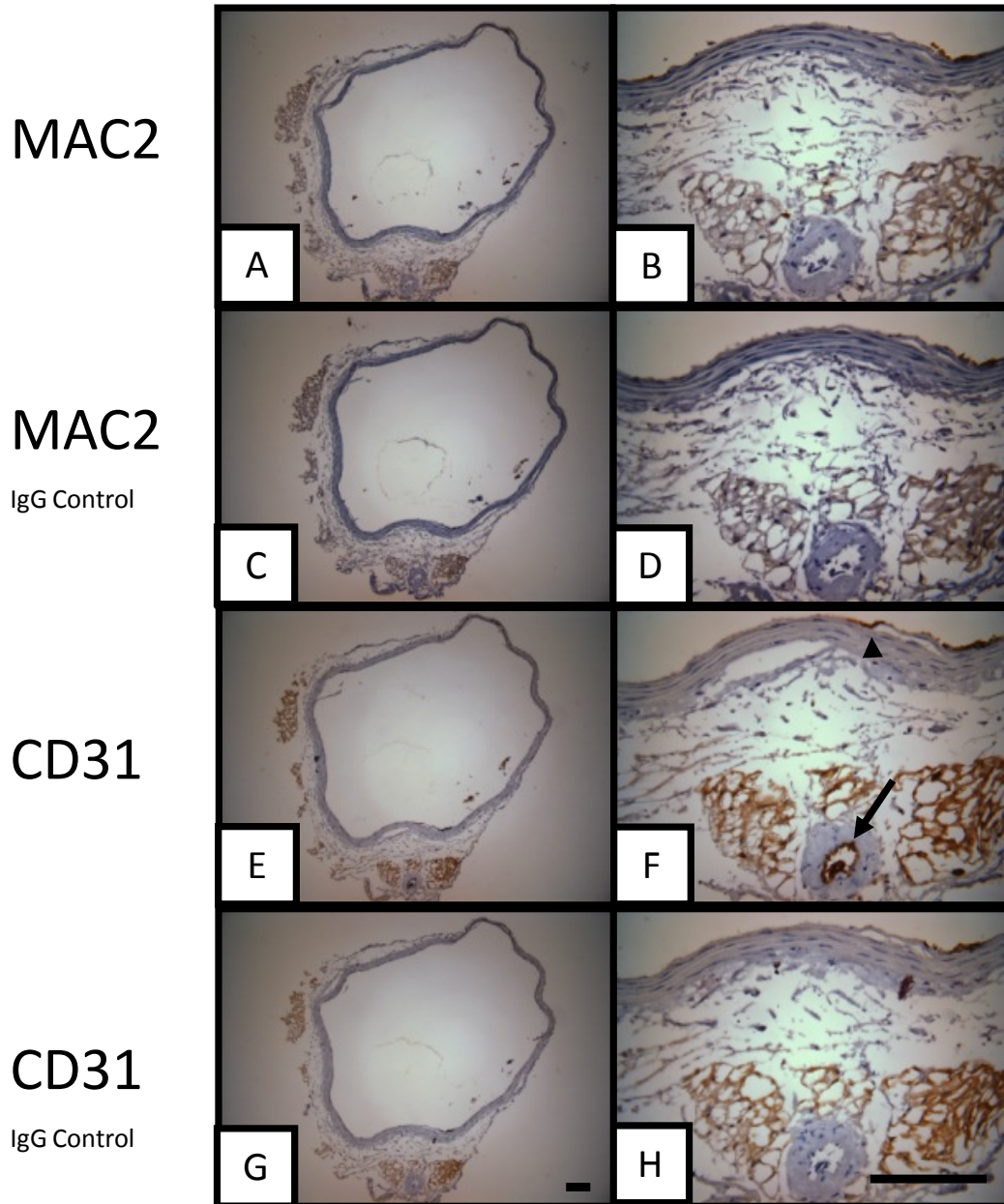


Figure 3-24. Immunohistochemistry of stented graft harvested at day 0. A and B, MAC2 (10x, 40x). C and D, MAC2 IgG control (10x, 40x), E, CD31 staining (10x) and F, CD31 demonstrating sparse endothelial cells in aortic intima following stenting (arrowhead), endothelium intact within blood vessels of vaso vasorum (arrow) (10x, 40x). G and H, CD31 IgG control (10x, 40x). Hatched box, magnified area of interest. Scale bar = 100 μ m. Representative sections from n=8.

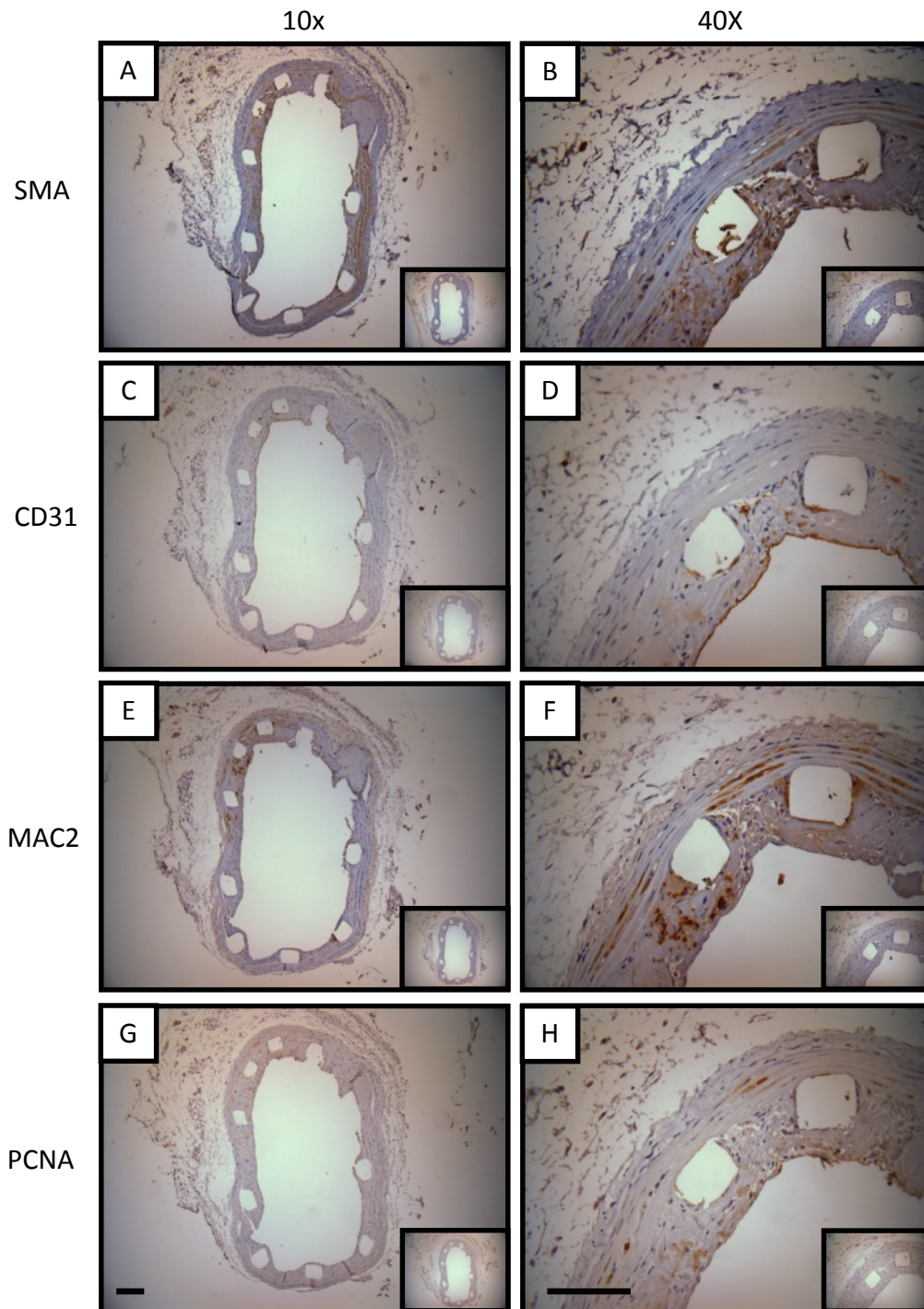


Figure 3-25. Immunohistochemistry of Stented Graft Harvested at Day 28. A and B, SMA (10x, 40x). C and D, CD 31 (10x, 40x). E and F, MAC2 (10x, 40x), G and H PCNA (10x, 40x). (Inserts-IgG controls). Scale bar = 100 μ m. Representative sections from n=5.

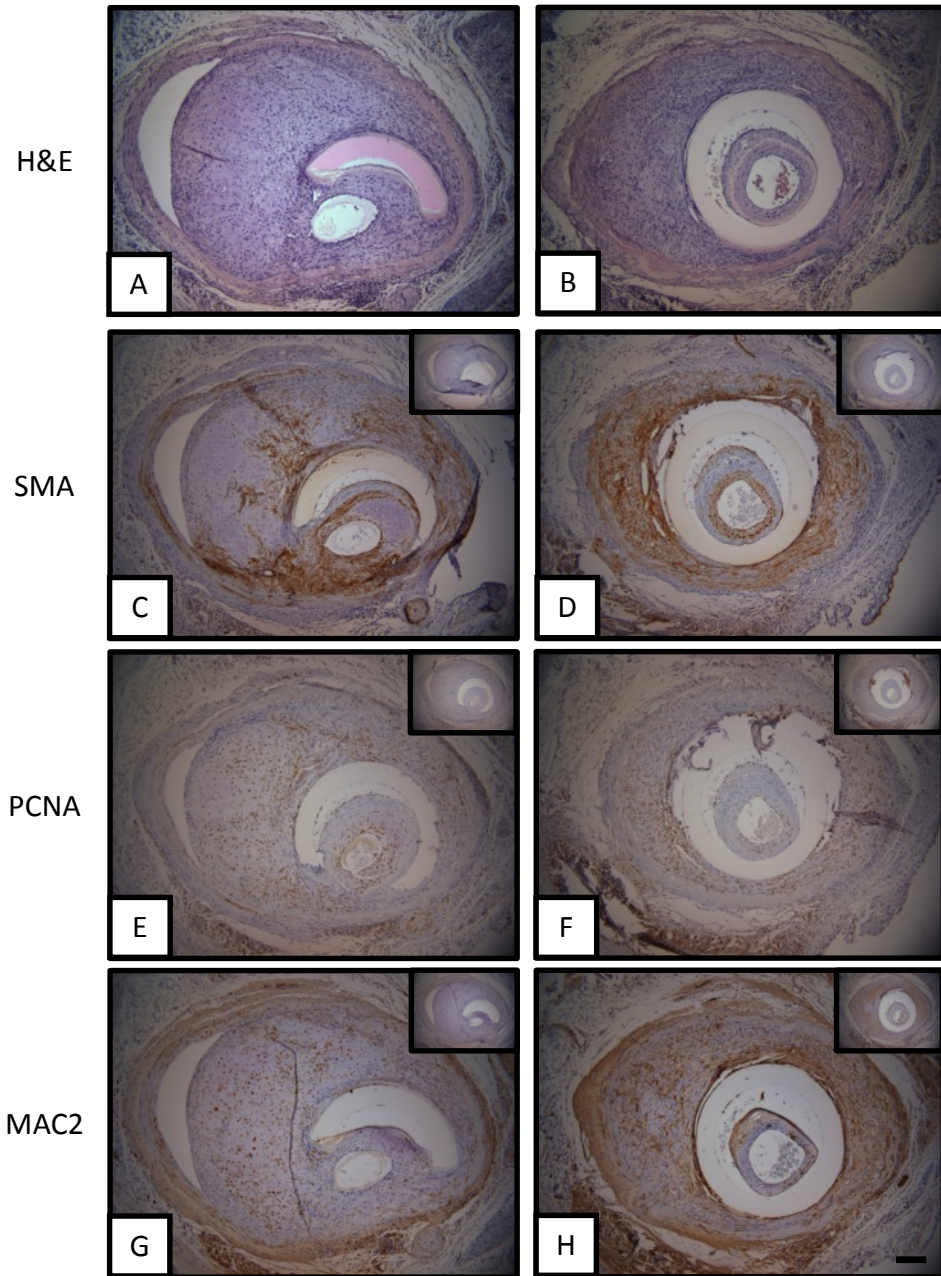


Figure 3-9 Staining of unstented non-electrolysed portion of graft containing the anastomosis forming cuff. A and B, H&E (10x). C and D SMA (10x). E and F, PCNA (10x). G and H, MAC2 (10x). Scale bar = 100 μ m. Representative sections from n=5.

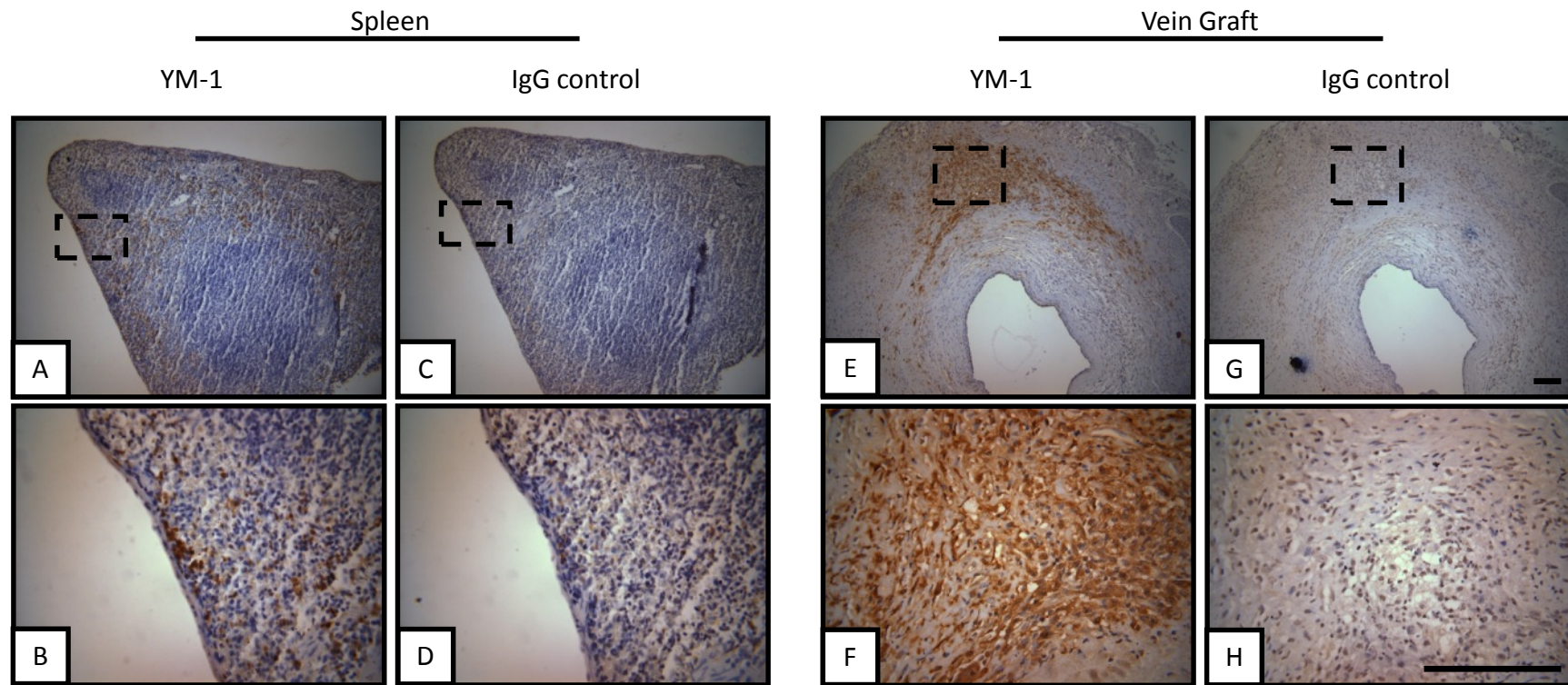


Figure 3-26. YM-1 immunohistochemistry M2 Macrophage staining in different tissues. A & B, Spleen (10x & 40x). C & D, IgG controls (10x & 40x). E & F, Vein graft (10x & 40x). G & H, IgG controls(10x & 40x). Scale bar = 100 μ m. Representative sections from n=3.

3.3.4 C57BL6 Mice Produce a Significant Neointima at Day 28.

Morphological analysis of stented grafts taken from C57BL6 mice at day 0 and day 28 and showed that no significant difference in either total vessel area ($0.46 \pm 0.03 \text{ mm}^2$ vs. $0.53 \pm 0.09 \text{ mm}^2$) or medial area ($0.07 \pm 0.005 \text{ mm}^2$ vs. $0.08 \pm 0.01 \text{ mm}^2$) respectively. However, there was a significant difference in medial thickness between day 0 and day 28 grafts ($0.024 \pm 0.002 \text{ mm}^2$ vs $0.03 \pm 0.002 \text{ mm}^2$, $p < 0.001$, respectively), Table 3-7. This represents the medial compression seen at time of stenting and subsequent medial remodelling.

Luminal area was significantly reduced from day 0 to day 28 ($0.38 \pm 0.023 \text{ mm}^2$ vs. $0.26 \pm 0.018 \text{ mm}^2$, $p < 0.05$, respectively). This was paralleled by an increase in neointimal area and thickness over the same period. When measured by area or thickness neointima was greater than 2 fold larger than the corresponding media. In addition significant neointimal coverage of stent struts had developed, Table 3-7.

Table 3-7. Morphometry from C57BL6 mice at day 0 and 28 following stenting.

C57BL6	Day 0 (n=8)	Day28 (n=5)	p value
	Mean (SEM)	Mean (SEM)	
Total Vessel Area (mm ²)	0.46 (0.03)	0.53 (0.09)	ns
Luminal Area (mm ²)	0.37 (0.07)	0.26 (0.05)	<0.05
Medial Area (mm ²)	0.07 (0.005)	0.08 (0.01)	ns
Neointimal Area (mm ²)	0	0.17 (0.04)	<0.001
N:M Area Ratio	-	2.26 (0.29)	-
Medial Thickness (mm)	0.024 (0.002)	0.03 (0.002)	<0.001
Neointimal Thickness (mm)	0	0.086 (0.017)	<0.001
N:M Thickness Ratio	-	2.66 (0.49)	-
Strut Depth (mm)	0	0.034 (0.009)	<0.001

The results presented in this chapter demonstrate the refinement of a previously developed mouse stenting model. Stented grafts were shown to develop a significant neointima and resultant ISR. In addition, successful electrochemical dissolution of the metal stent within the vessel wall allowed *in situ* hybridisation to be performed and several immunohistochemical stains to be used, facilitating the identification of macrophages, smooth muscle cells and endothelial cells.

3.4 Discussion

The current study successfully replicated the first murine aortic stenting model, pioneered by the Channon laboratory and demonstrated the development of ISR over a 28 day period. In addition this is the first study in any small animal model to utilise electrochemical stent dissolution during tissue processing.

Small animal air desiccation, wire and cuff injury models been used for decades to investigate the effects different genetic mutations and therapies have on vascular pathology (Lindner et al., 1993, Moroi et al., 1998). The popularity of these models is undoubtedly due to their ease of reproduction, requiring minimal surgical skill and low cost. The clinical relevance of such injury models is dubious, leading scientists and clinicians to develop both balloon injury models simulating the effects of balloon angioplasty in humans and more recently small animal models of stenting (Gabeler et al., 2002). Several models of carotid and aortic stenting have been published in rats with differing degrees of success and vascular access routes (Indolfi et al., 2000, Roks et al., 2002, Lowe et al., 2005). However, the inability to manipulate the rat genome has undoubtedly impeded their use in the investigation of ISR.

The first murine model of stenting, replicated here in this study, was based on previously published vein graft and aortic allograft models (Dietrich et al., 2000, Zou et al., 1998). This allowed Investigators for the first time to demonstrate that the use of an over the balloon stent in a C57BL6 mouse produces a significantly larger neointimal with a greater inflammatory response than with a balloon angioplasty alone (Ali et al., 2007). Investigators were also able to study the effect of genetic manipulation on in-stent restenosis. It was shown that the atherosclerosis prone ApoE $-/-$ mouse developed a significantly larger neointima than a WT mouse from the same genetic background (Ali et al., 2007). Our study was also conducted in C57BL6/J mice and produced far larger neointimal lesions than those originally observed by Ali et al (Ali et al., 2007). Several reasons may account for this, including that while learning the surgical technique grafts were subjected to rougher handling and a longer anoxic time. The mice used in our study were obtained from a commercial breeder and on arrival we were not able to verify they were transported in family groups. Thus while an inbred mouse strain was used we were not able to ensure grafting between littermates to

minimise any immune mediated allograft vasculopathy. Additionally, although we used the same stent as the original study, our balloon catheter was from a different manufacturer. Subtle differences in balloon compliance may, through differences in the degree of vessel damage, account in part for the discrepancy observed in neointimal : media ratio between studies.

While the use of an over the balloon stent makes the model used in the present study more clinically relevant than simpler injury models it is not without criticism. A high degree of operator skill is required in order to form two vascular anastomoses; with practice the failure rate can be reduced to around 4%. The requirement of two mice per procedure adds to the number of animals required. Concerns have also been noted that disruption of the vaso vasorum will produce anoxia within the vessel wall. The vaso vasorum and adventitia has been shown to play an important role in vessel remodelling following injury (Gabeler et al., 2002).

Three other mouse models of stenting have been published. Chamberlain et al used a single animal procedure with a self-expanding nitinol wire coil stent inserted into the infra-renal aorta via the femoral artery (Chamberlain et al., 2010). Initially, major haemorrhage due to vessel perforation upon stent deployment was reduced by the addition of a round bead to the advancing tip of the stent. With this tip modification the procedural failure rate was significantly reduced to a level similar to our study. However, the lower rate of thrombotic stent occlusion in this single animal model may be in part due to absence of vascular anastomoses and the use of dual antiplatelet therapy. Temporary or permanent hind limb paralysis was observed in over 50% of animals, due to the proximity of the femoral nerve and inadvertent damage during femoral artery manipulation. In addition while nitinol stents have been trialled in humans concerns have been raised regarding cytotoxicity and neither they nor self-expanding stents are used in routine coronary intervention thus limiting its clinical applicability.

Another murine stenting model described also stented the aorta *in situ* but access was achieved by infra renal aortic incision (Rodriguez-Menocal et al., 2010). In this model the aorta was predilated prior to stent placement. While a clinically relevant over the balloon stent was used, achieving haemostasis proved

difficult with a >35% failure rate (Rodriguez-Menocal et al., 2010). In addition despite using a stent with the same dimensions as our own the authors demonstrated far less neointimal development than both ourselves and Ali et al (Rodriguez-Menocal et al., 2010, Ali et al., 2007). While this may be due to differences in blood flow between models it may also be in part due to less vessel damage from the lower deployment pressures used. We observed that lower balloon pressures resulted in incomplete expansion, malaposition of stent and a propensity to develop an occlusive thrombus.

The latest published model of small animal stenting utilised a nitinol self-expanding coil stent deployed directly into the mouse carotid (Simseyilmaz et al., 2013). While the authors of this model can be commended for their technical skill, the massive amount of damage caused by the stent within such a small artery gave the investigators difficulty in the accurate identification of IEL and EEL during tissue analysis (Simseyilmaz et al., 2013). The vessels lack of vaso vasorum, the type of stent used and the degree of the vessel injury means that despite this model being novel is not necessarily more clinically relevant than the other published models.

A key reason that stenting models have not been as popular as simpler injury models is due to tissue processing after harvesting. Processing of tissue containing metal has traditionally been done by resin embedding tissues followed by cutting sections using a diamond tipped saw which can be done to 20 microns followed by polishing of sections to between 5 and 10 microns (Watt et al., 2013). These processes not only require expensive specialist equipment but are extremely labour intensive and require considerable operator skill to polish sections evenly. Tissue loss during the sawing and grinding process results in far fewer sections than would be obtained from paraffin embedding and cutting on a standard microtome (Malik et al., 1998). In situ hybridisation is impossible to perform on resin embedded tissues and IHC is also limited to a few antibodies compared to paraffin embedded tissues (Torgersen et al., 2009). In addition, the process of grinding also causes tissue distortion causing difficulty in image interpretation (Torgersen et al., 2009, Malik et al., 1998).

In order to reduce tissue waste and maximise section yield tungsten carbide blades mounted on a standard rotary microtome have been used to cut resin

embedded tissues into 5 microns thick sections (Rippstein et al., 2006). Another benefit of using these blades was a reduction in tissue distortion (Rippstein et al., 2006)

Despite an improvement in preservation of tissue architecture the use of tungsten carbide blades are prohibitively expensive and just as time consuming as traditional sawing and grinding. Optimisation of electrochemical stent dissolution was undertaken to allow tissues to be paraffin embedded and sections cut on a standard rotary microtome with stainless steel blades. This allowed both IHC and ISH to be conducted with high quality images able to be obtained. Electrolysis of coronary stents has been documented previously in human tissues but this represents the first time it has been utilised in any small animal model (Bradshaw et al., 2009). During the optimisation process it was found that the minimal citric acid saline solution to conduct with tissue embedded samples was 5% (w/v) this is in concordance previous reports (Bradshaw et al., 2009). Also key to complete stent dissolution was for only the very end of the stent distal to the anode to be submerged in the citric acid saline solution.

By storing tissues in 70% ethanol rather than PBS almost complete dissolution could be achieved. This is most likely as a result of ethanol's inability to conduct electricity. Conversely tissues saturated with PBS would allow conduction not only through the stent but also the surrounding tissue thus producing the uneven and incomplete stent dissolution observed.

The development of a suitable connector between anode and stent proved difficult. The use of a crocodile clip which had been successful for the larger human stents was not appropriate due to size (Bradshaw et al., 2009). Initially fine wires of metals less reactive than the stainless steel stent were investigated. However, fashioning a robust connection could only be achieved with a pen spring due to its rigidity.

The application of high voltages to the stent (12V) demonstrated the rapid production of a visible stream of ions released from the distal stent into solution. However, charring due to excess heat production in tissues surrounding the stent struts occurred. Optimal results were obtained by gradually increasing

the voltage from 3V to between 5 and 8V when both gas bubbles and a yellow/brown stream of ions were visible.

Having optimised stent electrolysis we were able to show it did not interfere with a wider range of histological and immunohistochemical stains than has been previously documented regardless of antigen location. Some stains such as CD31 for endothelial cell identification cannot be accomplished on resin embedded tissues. In addition this study represents the first time successful ISH (results presented in chapter 5) has been documented following electrolysis.

In summary the results presented in this chapter show the efficient replication of a mouse model of stenting with the production of ISR. In addition, the efficient electrochemical dissolution of the metal stent to allow cutting of paraffin embedded sections on a standard microtome facilitated the optimisation of several immunochemical stains within stented sections which have not previously been able to be conducted on resin embedded stented tissues.

4 Investigation of Multiple Strategies to Manipulate MicroRNA-21 Expression and the Impact on the Development of In-stent Restenosis.

4.1 Introduction

Percutaneous Coronary Intervention using stents as a scaffold to hold open a diseased and narrowed artery has in many cases superseded the use of balloon angioplasty, which was plagued by the issues of acute elastic recoil, vessel occlusion and the need for repeat revascularisation (Serruys et al., 1994). Indeed, stents have been shown to be a safe and effective treatment for both stable coronary artery disease and in the emergency situation of complete vessel occlusion during ST elevation myocardial infarction (De Bruyne et al., 2012, Andersen et al., 2003). However, the use of stents has been hindered by the development of ISR. ISR occurs following stent deployment due to a cascade of events as a result of damage to the vessel wall whereby denudation of the endothelium and disruption of the elastic lamina and VSMCs results in platelet aggregation and leukocyte adhesion (Virmani and Farb, 1999). The release of inflammatory cytokines and mitogenic growth factors such as IL-1, IL-6 and PDGF- β from a variety of cells in response to stent deployment acts to perpetuate inflammation, the proliferation of VSMCs and the deposition of connective tissue forming a neointimal layer (Costa and Simon, 2005, Indolfi et al., 2003). The resulting encroachment on the vessel lumen limits blood flow and results in the return of clinical symptoms (Dangas et al., 2010).

The development of DES, metal stents coated in a polymer, which is impregnated with a cytotoxic drug to limit VSMC proliferation, has been a second major advance in PCI, significantly reducing ISR (Bavry and Bhatt, 2008). However, DES have been associated with a significantly greater incidence of late stent thrombosis (LST) compared to BMS due to delayed arterial healing characterised by persistent fibrin around stent struts, incomplete re-endothelialisation and the presence of eosinophils (McFadden et al., 2004, Joner et al., 2006). Evidence from atherectomy specimens isolated from patients with LST and from animal models suggest that the non-erodible polymers utilised in first generation stents were responsible for the inflammation and hypersensitivity reaction rather than the cytotoxic drugs used (Virmani et al., 2004, Nebeker et al., 2006).

Despite the development of new generation of polymer-free drug eluting stents there is still a need to further elucidate the molecular mechanisms involved in

the complex vascular process of ISR. This may in turn lead to the development of novel therapies to promote healing and re-endothelialisation following stent deployment while inhibiting ISR. The discovery of non-coding RNAs and the important roles they play in fine-tuning many biological and pathological processes has alerted researchers to a putative role for these molecules in the development of ISR (Pauli et al., 2011, Esteller, 2011). MicroRNAs are one class of such non-coding RNA, which have yet to be investigated with respect to the development of ISR.

MicroRNAs are short 19-25 nucleotide RNA molecules which upon binding in a complementary fashion to the 3'UTR of mRNAs repress their translation (Bartel, 2009). Over 1000 miRNAs have now been identified within the human genome and are thought to regulate around 30% of all protein coding mRNA (Friedman et al., 2009). A single miRNA may have numerous mRNA targets at different points within multiple biological pathways or act upon a single target to mediate a disease phenotype (Aurora et al., 2012, Bang et al., 2014).

Several miRNAs including miR-133a, miR-143, miR-145, miR-195 and miR-663 have been studied in the setting of vascular injury with some promoting and others inhibiting NIH development and vessel remodelling. Two recent studies have been published looking at the role of miRNAs in patients with vascular disease. MiR-21 was shown to be up regulated in the intima and serum of patients with Arteriosclerosis Obliterans (Wang et al., 2011). In addition, the Tampere Vascular Study demonstrated miR-21 was up regulated within human atherosclerotic plaques (Raitoharju et al., 2011). In humans miR-21 is located on chromosome 17q23.1 within the eleventh intron of the TMEM49 gene it is transcribed independently by its own promoter (Fujita et al., 2008, Cai et al., 2004). Its actions have been found to prevent apoptosis, induce cellular growth, proliferation and migration (Iliopoulos et al., 2010, Han et al., 2012). The Baker laboratory has recently shown that miR-21 can play very important, yet distinctly different roles in the vessel wall (White et al., 2014). We demonstrated that global loss of miR-21 led to a substantial reduction in neointima formation *in vivo* using a murine vein grafting model and human *ex vivo* specimens (McDonald et al., 2013). Conversely, miR-21 loss in the endothelial compartment of small pulmonary vessels led to exacerbation of pulmonary hypertension (White et al., 2014). Hence, we therefore sought to

understand the expression, location and function of miR-21 in the context of vascular stenting, and its role in vessel remodelling, inflammation and endothelial damage.

4.2 Aims

To investigate the role played by miR-21 on the development of ISR using three *in vivo* strategies:

1. Genetic deletion,
2. Pharmacological knock-down,
3. Genetic over-expression.

To investigate the role played by miR-21 on VSMC proliferation and migration.

4.3 Results

4.3.1 Effect of Genetic Deletion of microRNA-21 on the Development of In-Stent Restenosis

MicroRNA-21 WT and KO animals underwent isogenic aortic stenting and carotid interposition grafting as described previously, chapter 2 (Ali et al., 2007). Mice were culled and grafts harvested for analysis at day 0 and day 28 following surgery.

At baseline (day 0) no significant difference was observed between miR-21 WT and KO animals, within the stented grafts for any of the parameters measured. Table 4-8 summarises all measured parameters for WT and KO grafts at day 0.

Comparing miR-21 WT grafts at day 0 and day 28 no significant difference was seen in total vessel area ($0.58 \pm 0.09 \text{ mm}^2$ vs $0.52 \pm 0.03 \text{ mm}^2$) or medial area ($0.11 \pm 0.03 \text{ mm}^2$ vs $0.09 \pm 0.005 \text{ mm}^2$). However, luminal area was significantly reduced at 28 days compared to day 0, ($0.46 \pm 0.07 \text{ mm}^2$ vs $0.22 \pm 0.02 \text{ mm}^2$) as a direct consequence of the developing neointima. No neointima was present at day 0 but by 28 days one was clearly present. Table 4-9 summarises all measured parameters for WT mice at day 0 and day 28.

Table 4-8. Baseline (Day 0) Characteristics of Stented Grafts for miR 21 WT and KO mice.

Day 0	WT (n=9)	KO (n=3)	p value
	Mean (SEM)	Mean (SEM)	
Total Vessel Area (mm ²)	0.58 (0.09)	0.45 (0.05)	ns
Luminal Area (mm ²)	0.46 (0.07)	0.39 (0.05)	ns
Medial Area (mm ²)	0.11 (0.03)	0.06 (0.04)	ns
Medial Thickness (mm)	0.035 (0.005)	0.025 (0.001)	ns
Vessel Injury (Schwartz Score)	0.58 (0.15)	0.52 (0.06)	ns

Table 4-9. Characteristics of Stented Grafts for miR 21 WT at Day 0 and Day 28.

	WT Day 0 (n=9)	WT Day 28 (n=12)	p value
	Mean (SEM)	Mean (SEM)	
Total Vessel Area (mm ²)	0.58 (0.09)	0.52 (0.03)	ns
Luminal Area (mm ²)	0.46 (0.07)	0.22 (0.02)	<0.01
Medial Area (mm ²)	0.11 (0.03)	0.09 (0.005)	ns
Neointimal Area (mm ²)	0	0.18 (0.02)	<0.001
N:M Area Ratio	-	2.11 (0.17)	-
Medial Thickness (mm)	0.035 (0.005)	0.038 (0.002)	ns
Neointimal Thickness (mm)	0	0.092 (0.009)	<0.001
N:M Thickness Ratio	-	2.51 (0.27)	-
Strut Depth (mm)	0	0.072 (0.011)	<0.001
Vessel Injury (Schwartz Score)	0.58 (0.15)	0.33 (0.14)	ns

Comparing miR-21 WT and KO mice at day 28 no significant difference was observed in total vessel area ($0.52 \pm 0.03 \text{ mm}^2$ vs. $0.55 \pm 0.03 \text{ mm}^2$, $p > 0.05$, respectively). Nor was a significant difference observed between WT and KO mice for medial area ($0.09 \pm 0.005 \text{ mm}^2$ vs. $0.08 \pm 0.005 \text{ mm}^2$, $p > 0.05$, respectively) or medial thickness ($0.038 \pm 0.002 \text{ mm}$ vs. $0.036 \pm 0.003 \text{ mm}$, $p > 0.05$, respectively), Figure 4-27. However, neointimal area was significantly larger in the WT than KO mice ($0.18 \pm 0.02 \text{ mm}^2$ vs. $0.12 \pm 0.02 \text{ mm}^2$, $p < 0.05$, respectively) as was neointimal thickness ($0.092 \pm 0.009 \text{ mm}$ vs. $0.057 \pm 0.012 \text{ mm}$, $p < 0.01$, respectively). Neointimal : Media area ratio was significantly greater in WT than KO mice, (2.11 ± 0.17 vs. 1.37 ± 0.18 , $p < 0.05$, respectively,) this was concordant with Neointimal : Media thickness ratios, Figure 4-27.

The significantly greater neointima observed within WT vs. KO mice resulted in a significantly smaller luminal area ($0.22 \pm 0.02 \text{ mm}^2$ vs. $0.30 \pm 0.02 \text{ mm}^2$, respectively, $p < 0.01$, respectively) and hence greater percentage stenosis ($41.7 \pm 2.9\%$ vs $24.1 \pm 2.6\%$, $p < 0.01$, respectively), Figure 4-27 and Figure 4-28.

Measurements of strut depth (the thickness of neointima covering each stent strut) were concordant with the findings for neointimal area and thickness, with greater strut depth found in WT compared to KO grafts ($0.072 \pm 0.011 \text{ mm}$ vs $0.03 \pm 0.007 \text{ mm}$, $p < 0.05$, respectively), Figure 4-28. Importantly no significant difference was observed in Schwartz Injury Score between WT and KO mice (0.33 ± 0.14 vs. 0.44 ± 0.15 , $p > 0.05$, respectively). Figure 4-28 shows representative sections from WT and KO grafts at 28 days.

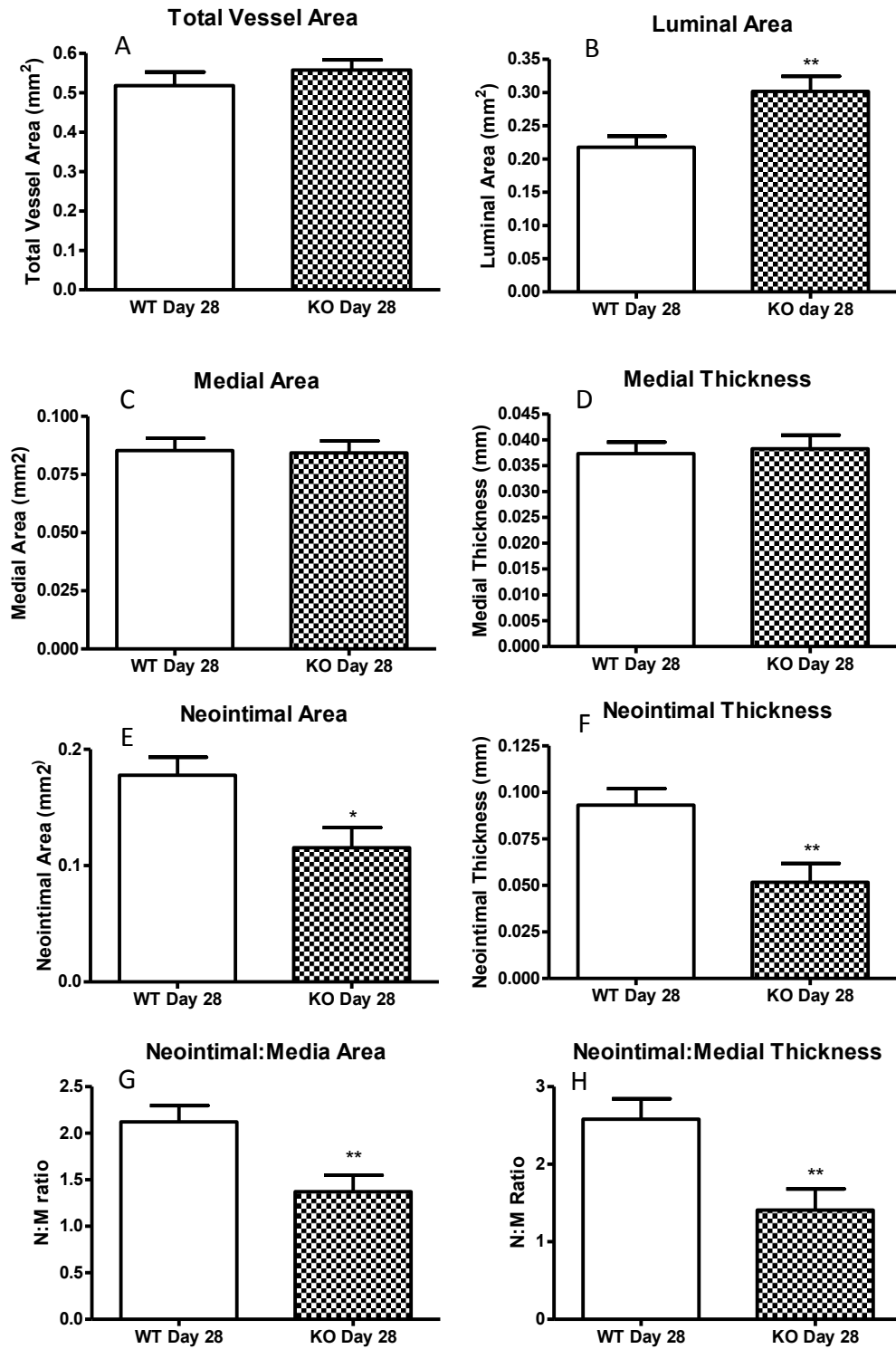


Figure 4-27. Characteristics of Stented Grafts from miR 21 WT and KO mice at Day 28. A, Total Vessel Area. B, Luminal Area. C, Medial Area. D, Medial Thickness. E, Neointimal Area. F, Neointimal Thickness. G, Neointimal:Media Area ratio. H, Neointimal:Media Thickness ratio. WT n=12, KO n=11. *p<0.05, **p<0.01 vs. WT Day 28.

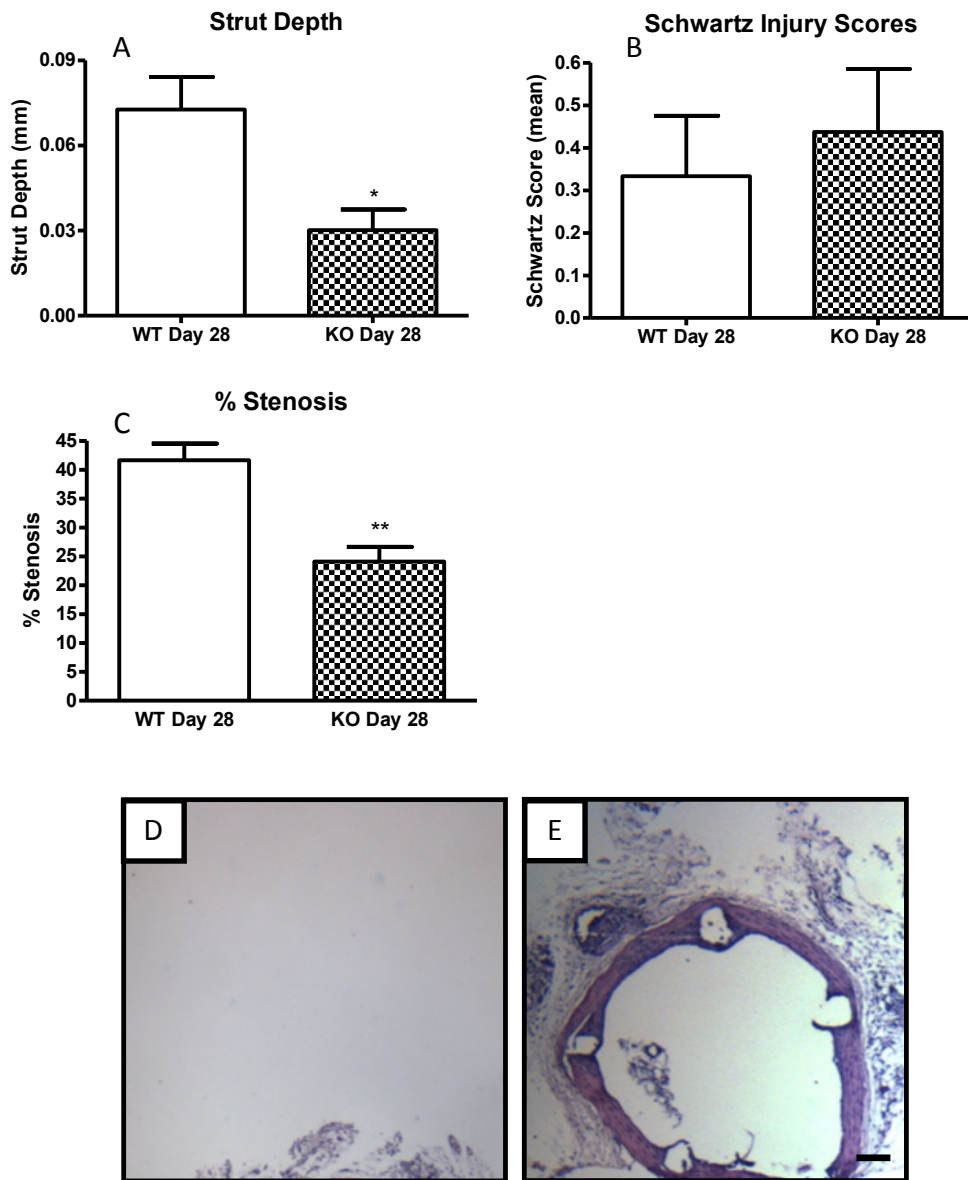


Figure 4-28. Further Characteristics of Stented Grafts from miR 21 WT and KO mice at Day 28. A, Strut Depth. B, Schwartz Injury Score. C, Percentage Stenosis. D and E representative H&E sections from WT and KO grafts, respectively. WT n=12, KO n=11. * $p < 0.05$, ** $p < 0.01$. 10x. Scale bar = 100 μm .

4.3.2 Comparison of Neointimal Composition between microRNA-21 WT and KO mice.

Having identified a significant difference in neointimal size at 28 days, further characterisation of neointimal composition was undertaken by staining for a variety of cellular markers and connective tissue.

Examination of neointimal composition revealed more smooth muscle cell α -actin staining in the WT compared to KO grafts expressed as a percentage of neointimal area ($28 \pm 2.4\%$ vs. $14 \pm 3.7\%$, $p < 0.01$, respectively), Figure 4-29A, B and C. Elastin van Geison staining revealed neointima of WT mice had an almost two-fold greater elastin content compared to KO mice ($21.1 \pm 1.2\%$ vs $11.5 \pm 3.4\%$, $p < 0.01$, respectively). In addition, acellular areas comprised of residual fibrin deposits were evident within the neointima formed by miR-21 KO mice, Figure 4-29D, E and F.

Staining for Proliferating Cell Nuclear Antigen (PCNA) was successful but failed to demonstrate a significant difference in the number of proliferating cells within the neointimal layers of WT and KO mice ($3.6 \pm 0.8\%$ vs $3.3 \pm 0.7\%$, respectively), Figure 4-29G, H and I.

Additionally no significant difference was observed in re-endothelialisation between WT and KO groups ($91.0 \pm 3.9\%$ vs $88.7 \pm 2.9\%$, respectively). Re-endothelialisation assessed as a percentage of the luminal surface staining positive for CD31 (Platelet Endothelial Cell Adhesion Molecule, PECAM), Figure 4-29J, K and L.

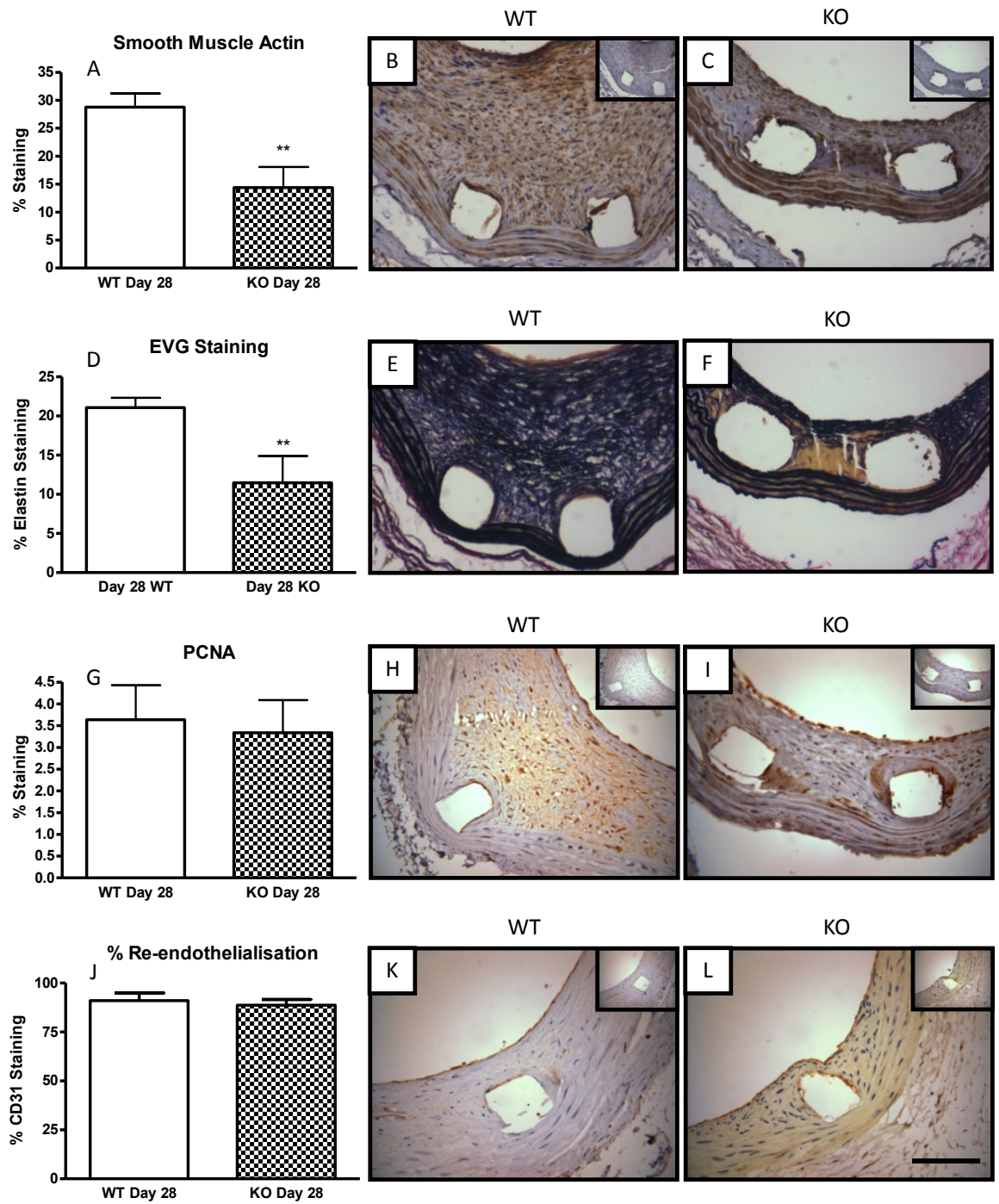


Figure 4-29. Neointimal Composition. A, B and C Smooth Muscle Actin Staining. D, E and F Elastin van Gieson Staining. G, H and I, Proliferating Cell Nuclear Antigen Staining. J, K, and L, CD31 (PECAM) Staining. Inserts IgG control. WT n=12, KO n=11. * $p < 0.05$, ** $p < 0.01$. 40x. Scale bar = 100 μm .

4.3.3 Macrophage Presence and Polarisation within microRNA-21 WT and KO Grafts

Identification of macrophages within the neointima was investigated by IHC. In addition the polarisation state of macrophages was also investigated. The anti-inflammatory macrophage marker MAC2 (Galectin3) revealed the majority of macrophages were located around the stent struts with lower percentage staining observed within the WT than KO grafts (0.79 ± 0.23 % vs. 2.54 ± 0.75 % $p < 0.05$, respectively), Figure 4-30A, B and C. Further characterisation of macrophage polarisation was undertaken by staining for YM-1, a validated marker of the alternatively activated (M2) macrophage (Raes et al., 2002). YM-1 staining demonstrated fewer M2 macrophages were present within WT than KO grafts (0.50 ± 0.21 % vs, 1.93 ± 0.54 %, $p < 0.01$, respectively), Figure 4-30D, E and F. Both of these stains demonstrate higher levels of anti inflammatory or alternatively activated (M2) macrophages are present within the grafts of miR-21 KO mice.

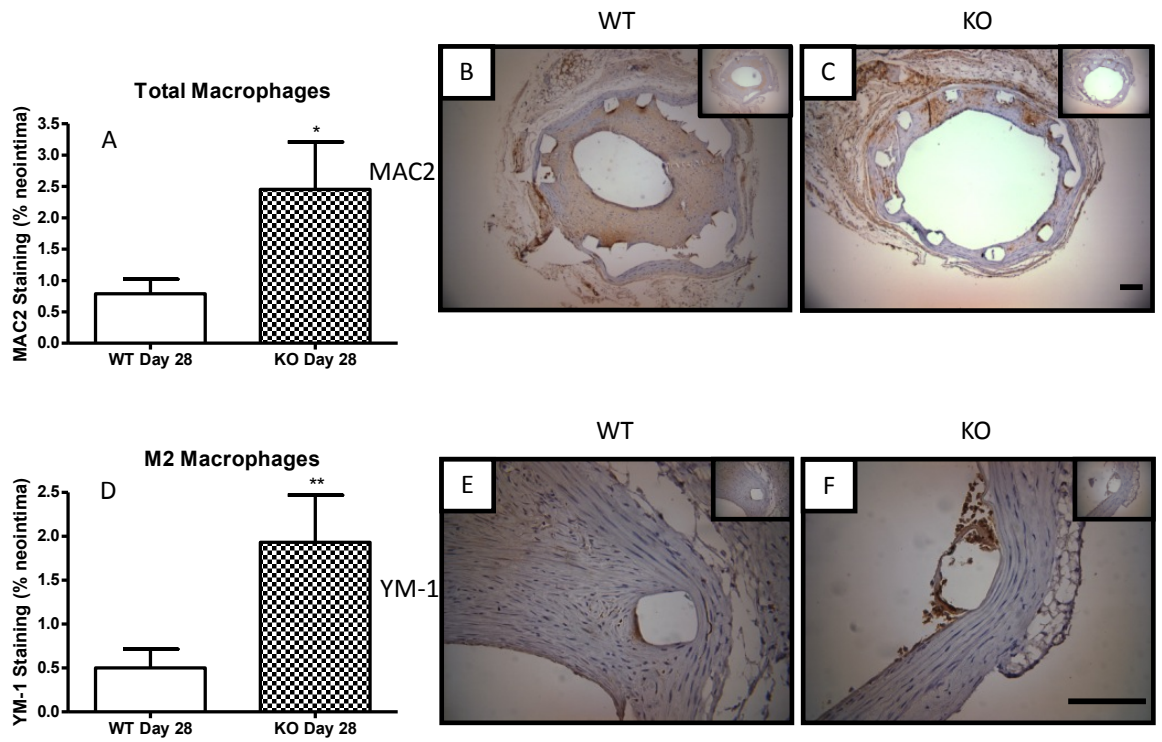


Figure 4-30. Macrophage Staining. A, B, and C Macrophage staining with MAC2 in WT and KO grafts 10x. D, E and F, Macrophage staining for YM-1. Inserts IgG control. 40x. WT n=12, KO n=11. * $p < 0.05$, ** $p < 0.01$. Scale bars = 100 μm .

4.3.4 Localisation of microRNA-21 within Graft

In situ hybridisation for miR-21 was conducted to establish its distribution within vascular tissues. In unstented sections of aorta from WT mice miR-21 was easily detected within the media and adventitial layers indicating its expression within VSMCs and possibly adventitial fibroblasts, Figure 4-31A-D. Within the stented graft miR-21 staining could be identified, indicating that the electrolysis process to which it had been subjected prohibited neither IHC nor *in situ* hybridisation. Surprisingly low levels of staining were identified within the media of the stented graft compared to unstented aorta. However, within the neointima strong miR-21 staining was present around the luminal surface and subluminal area in addition to having a marked peri-stent distribution, Figure 4-31. By comparing these findings with those from IHC described in sections 4.3.2 and 4.3.3 it is reasonable to suggest miR-21 is up regulated within endothelium, sub-luminal VSMCs of the neointima and also within the macrophages surrounding the stent struts.

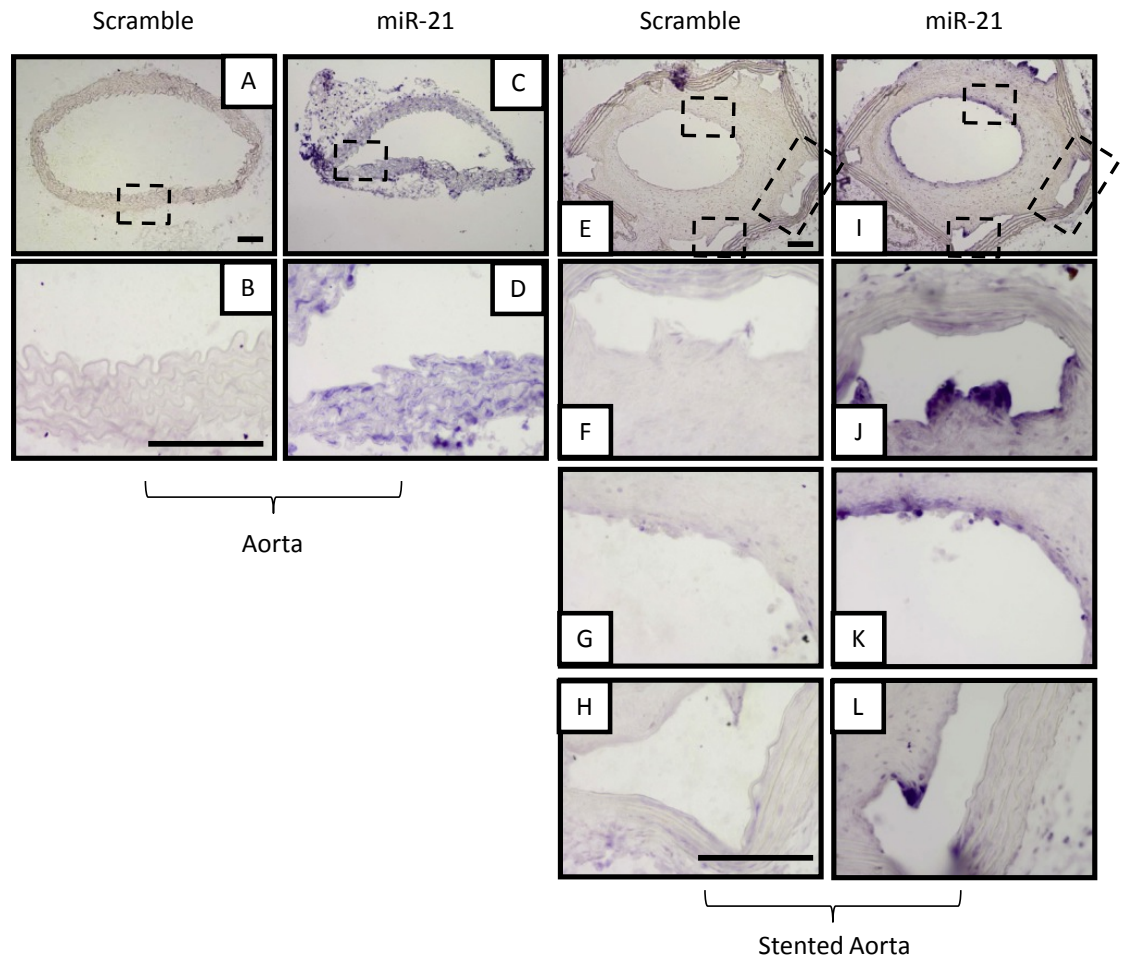


Figure 4-31. *In situ* Hybridisation for miR-21 in WT mice. A and B, Unstented aorta scramble probe (10x and 40x respectively). C and D, Unstented aorta miR-21 probe (10x and 40x respectively). E, Stented graft scramble probe (10x). F, G and H Stented graft scramble probe (40x). I, Stented graft miR-21 probe (10x). J, K, and L Stented graft miR-21 probe (40x). hatched boxes represent magnified areas of interest. Scale bars = 100 μ m.

4.3.5 *In vitro* Characterisation of miR-21 WT and KO VSMCs Proliferative and Migratory Phenotype.

Having identified a difference in neointimal size and smooth muscle α -actin staining between miR-21 WT and KO animals in the model of in-stent restenosis, *in vitro* analysis of aortic VSMCs isolated from both WT and KO mice was undertaken. VSMCs are one of the main cell types responsible for the development of a neointima due to their proliferation and migration towards the vessel lumen following vessel injury (Gabeler et al., 2002).

4.3.5.1 VSMC Proliferation

BrdU incorporation assay was used to assess the proliferative response of WT and KO aortic VSMCs which had been quiesced for 24 hours prior to use as described in Chapter 2. Media containing 0.2% FCS was used as a negative control and BrdU incorporation expressed relative to this.

When cultured in media containing 10% FCS, BrdU incorporation increased over two-fold in both WT and KO VSMCs compared to 0.2% FCS, $p < 0.05$ for both, Figure 4-32. When exposed to increasing concentrations of PDGF, proliferation was significantly greater in WT compared to KO VSMCs at both 20 ng/mL (2.00 ± 0.06 vs. 1.31 ± 0.02 , $p < 0.05$) and 50 ng/mL, (3.02 ± 0.09 vs. 1.40 ± 0.02 , $p < 0.01$), Figure 4-32. Thus genetic deletion of miR-21 appeared to have no effect on proliferative response to 10% FCS but resulted in a diminished response to PDGF when compared to WT controls.

4.3.5.2 VSMC Migration

Assessment of the migratory capacity of cells can be conducted by various methods (Liang et al., 2007). Scratch assay is an accepted and well documented method of assessing cellular migration by making a linear scratch in a cellular monolayer and then observing the movement of cells back into the wound (Liang et al., 2007).

Confluent VSMCs were quiesced in media containing 0.2% FCS for 24 hours prior to creating a linear wound in the cellular monolayer. Cells were then either maintained in media containing 10% FCS or PDGF 20 ng/mL. Media containing

0.2% FCS was used as control. As expected, cells maintained in control media containing 0.2% FCS exhibited minimal migration over 24 hours and no significant difference was observed between WT and KO VSMCs at 6 hours ($42.30 \pm 9.25 \mu\text{m}$ vs $28.08 \pm 7.57 \mu\text{m}$, respectively), 12 hours ($78.46 \pm 9.25 \mu\text{m}$ vs. $59.18 \pm 17.76 \mu\text{m}$, respectively) or 24 hours ($140.8 \pm 20.3 \mu\text{m}$ vs. $96.60 \pm 14.49 \mu\text{m}$, respectively), Figure 4-33A. Representative photographs of cellular migration under control conditions are presented in Figure 4-33B.

Cells stimulated with media containing 10% FCS showed marked wound closure over 24 hours. However, no difference was observed and KO VSMCs at 6 hours ($76.27 \pm 7.19 \mu\text{m}$ vs $63.85 \pm 20.68 \mu\text{m}$, 12 hours ($136.2 \pm 5.89 \mu\text{m}$ vs. $139.7 \pm 7.10 \mu\text{m}$, respectively) or 24 $\pm 4.9 \mu\text{m}$ vs. $225.9 \pm 32.36 \mu\text{m}$, respectively),

Figure 4-34A. Representative photographs of cellular migration when stimulated with 10% FCS are presented in

Figure 4-34B.

As with media containing 10% FCS, WT VSMCs stimulated with 20 ng/mL of PDGF exhibited profound migration and wound closure. However, the migration of VSMCs derived from WT mice was significantly greater than their KO counterparts at all time-points, 6 hours ($89.61 \pm 10.01 \mu\text{m}$ vs $41.66 \pm 9.86 \mu\text{m}$, respectively, $p < 0.01$), 12 hours ($141.5 \pm 15.72 \mu\text{m}$ vs. $101.3 \pm 4.59 \mu\text{m}$, respectively, $p < 0.05$) and 24 hours ($237.8 \pm 20.51 \mu\text{m}$ vs. $163.3 \pm 0.96 \mu\text{m}$, respectively, $p < 0.001$), Figure 4-35A. Representative photographs of cell migration when stimulated with PDGF 20 ng/mL are presented in Figure 4-35B

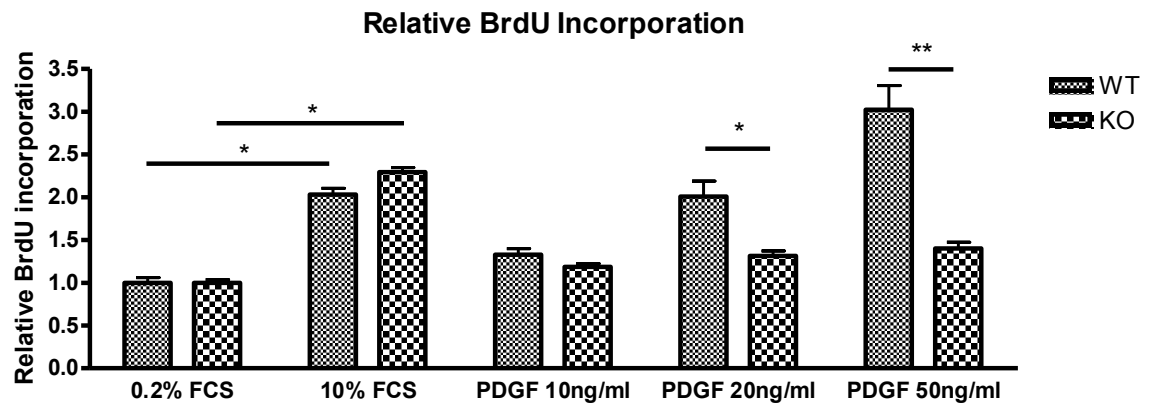


Figure 4-32. Proliferation Assay. BrdU incorporation within miR-21 WT and KO VSMCs relative to 0.2% FCS. n=3. *p<0.05, **p<0.01.

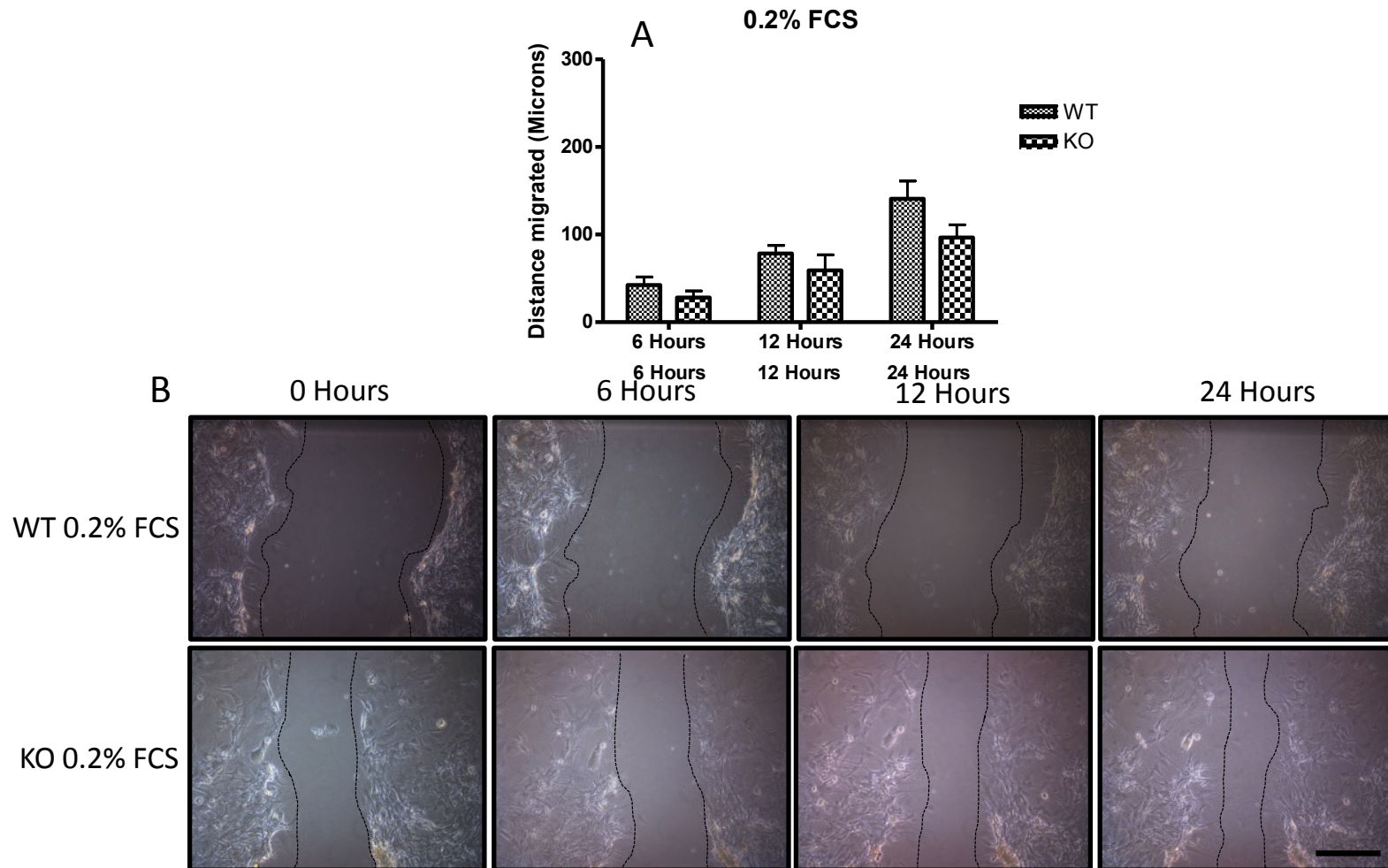


Figure 4-33. VSMC Migration Assay. 0.2% FCS. A, distance migrated by miR-21 WT and KO VSMCs in 6, 12 hours and 24 hours. B Representative photographs of VSMC migration. Biological triplicate, technical duplicate. Statistics performed on biological triplicate data. Scale bar = 100 μ m.

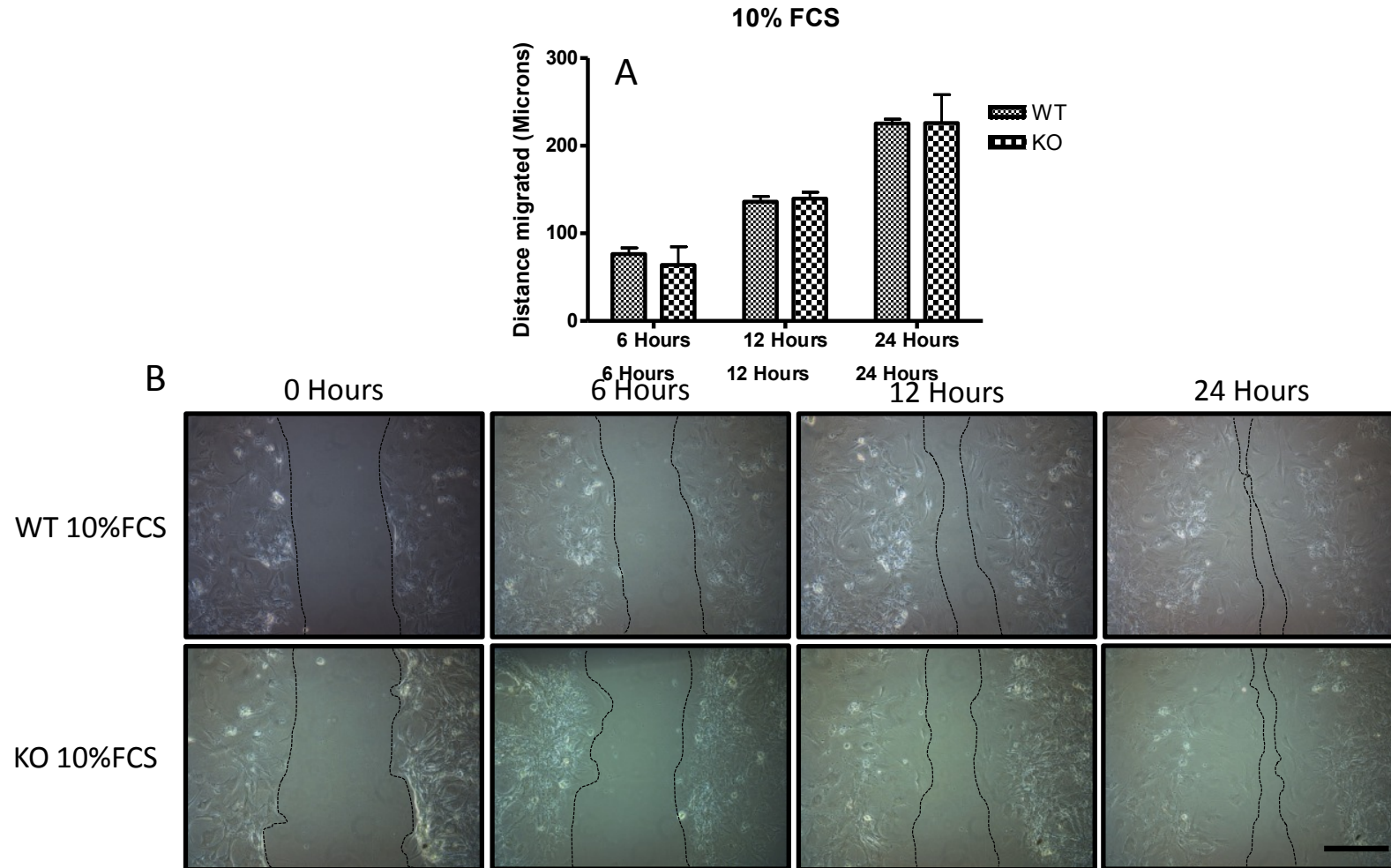


Figure 4-34. VSMC Migration Assay. 10% FCS. A distance migrated by miR-21 WT and KO VSMCs in 6, 12 and 24 hours. **B** Representative photographs of VSMC migration. Biological triplicate, technical duplicate. Statistics performed on biological triplicate data. Scale bar = 100 μ m

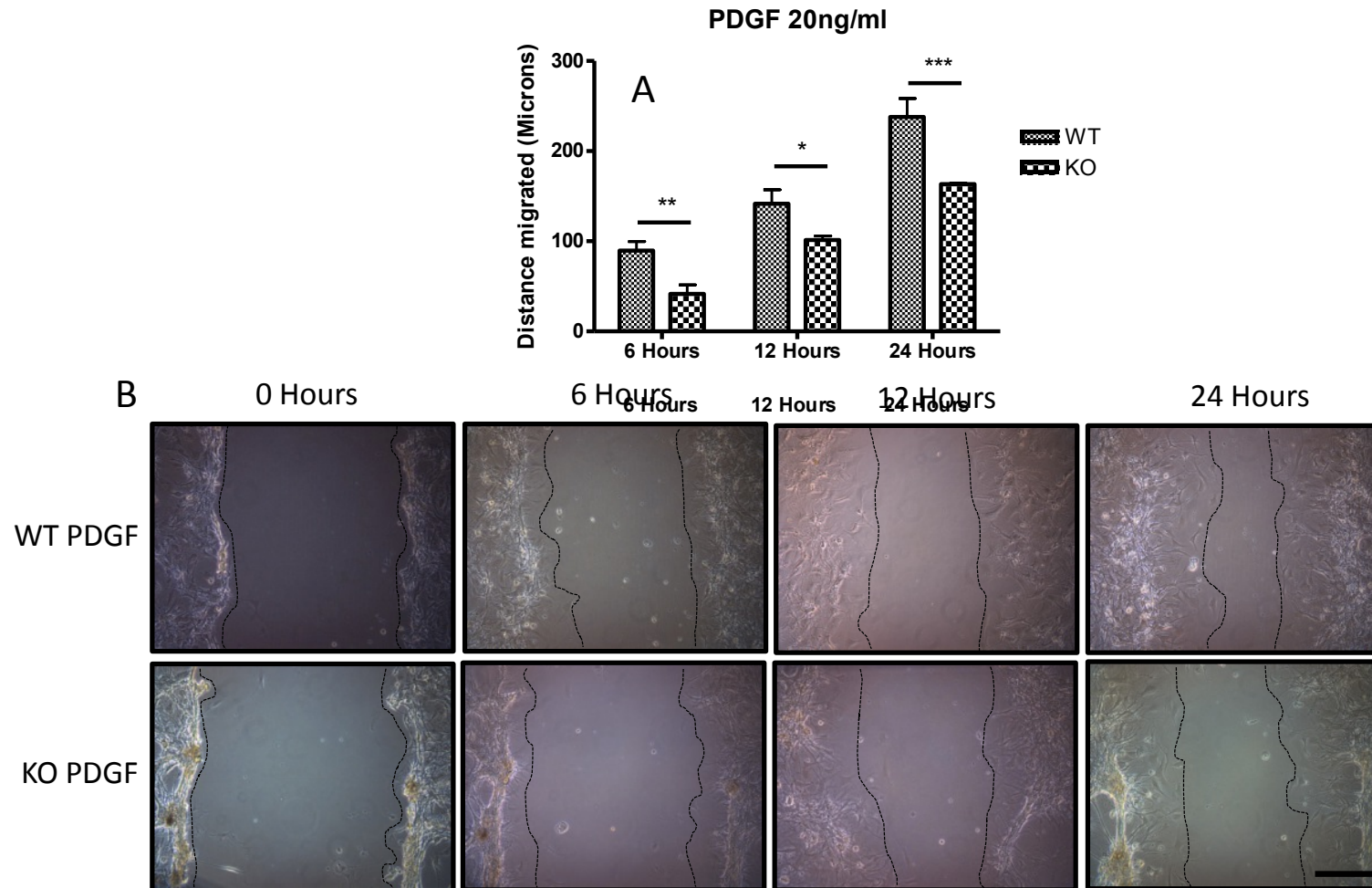


Figure 4-35. VSMC Migration Assay. PDGF 20ng/mL. A distance migrated by miR-21 WT and KO VSMCs in 6, 12 and 24 hours. B Representative photographs , VSMC migration. Biological triplicate, technical duplicate. Statistics performed on biological triplicate data. Scale bar = 100 μ m. *p<0.05, **p<0.01, *p<0.001.**

4.3.6 MicroRNA-21 expression within VSMCs is elevated following stimulation.

In order to determine if the effect of PDGF 20 ng/mL and 10% FCS on VSMC proliferation and migration may be mediated by an up-regulation of miR-21, expression levels of both miR-21(-5p) and miR-21-3p were determined by RT-qPCR. VSMCs quiesced in 0.2% FCS were used as control.

Stimulation of WT VSMCs with 10% FCS resulted in a significant 3.73 (\pm 1.27) fold increase in miR-21(-5p), $p < 0.01$. While exposure to PDGF 20 ng/mL also resulted in a significant 3.03 (\pm 0.23) fold increase in miR-21(-5p) expression, $p < 0.05$. No significant difference was observed in miR-21(-5p) expression comparing 10% FCS and PDGF stimulation, Figure 4-36A. No significant difference in miR-21(-5p) expression was observed between FCS and PDGF treated VSMCs

Neither 10% FCS nor PDGF 20 ng/mL had any significant effect on miR-21-3p levels found within stimulated VSMCs compared to control (1.04 ± 0.15 and 1.18 ± 0.89 , $p > 0.05$ for both, respectively). However, it was noted that compared to miR-21(-5p), miR-21-3p levels were markedly lower, with average cycle threshold values of ~ 25 versus ~ 35 , respectively.

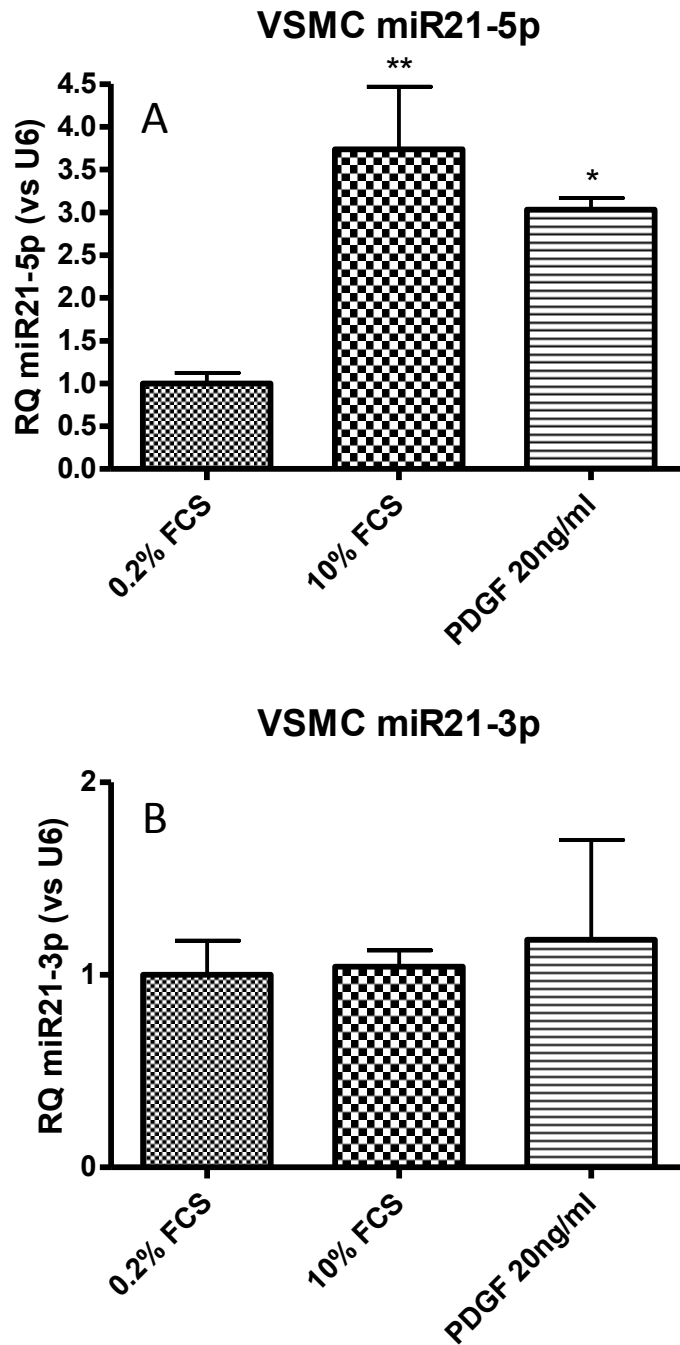


Figure 4-36. miR-21 Expression. WT VSMCs stimulated with 10% FCS or PDGF 20ng/mL relative to quiesced cells (0.2% FCS). A, miR-21-5p. B miR-21-3p (miR-21*). vs U6 housekeeper. Biological triplicate, technical duplicate. Statistics performed on biological triplicate data. * $p < 0.05$, ** $p < 0.01$ vs 0.2% FCS. RQ = Relative Quantity.

4.3.7 Effect of microRNA-21 up-regulation in VSMCs on known targets.

Having shown that miR-21 is up regulated in VSMCs following stimulation with 10% FCS and PDGF 20 ng/mL further evidence of its role through target repression was sought.

4.3.7.1 Investigation Potential Housekeeping genes in murine VSMCs

RT-qPCR was conducted on RNA isolated from VSMCs used during the migration assay in section 4.3.5.2. The constant expression of three potential housekeeping genes 18S, GAPDH and Tbp were assessed and were found to have mean cycle thresholds (\pm standard deviation) of, 12.48 (\pm 0.71), 20.36 (\pm 0.72), 28.34 (\pm 0.46), respectively, Figure 4-37. Tbp had the smallest standard deviation (<0.5) and was thus taken forward for use as housekeeper when quantifying gene expression in VSMCs from miR-21 WT and KO mice.

4.3.7.2 Effect of raised microRNA-21 levels on a panel of targets in stimulated VSMCs

RT-qPCR was conducted on a panel of known miR-21 targets validated in various cell types including cells present within the cardiovascular system.

The expression of PDCD4, a miR-21 target validated in VSMCs, was reduced in WT VSMCs stimulated with both 10% FCS (0.81 ± 0.04 , vs quiesced) and PDGF 20 ng/mL (0.68 ± 0.03 vs quiesced, $p < 0.05$). Importantly this reduction in PDCD4 was not observed in stimulated KO VSMCs. In fact stimulation with 10% FCS and PDGF 20 ng/mL induced a significant increase in PDCD4 (1.45 ± 0.08 and 1.42 ± 0.05 vs. quiesced, $p < 0.01$ for both, respectively), Figure 4-38.

STAT3 expression in WT VSMCs stimulated with PDGF 20 ng/mL was found to be significantly decreased (0.51 ± 0.03 vs. quiesced, $p < 0.001$) However, no change was observed in WT VSMCs stimulated with 10% FCS, nor was any change seen in KO VSMCs, Figure 4-38.

BMPR2, PPAR α , PTEN and TIMP3 did not change significantly upon stimulation with 10% FCS or PDGF in miR-21 WT or KO VSMCs. IL-12p35 could not be detected in RNA extracted from WT or KO VSMCs, Figure 4-39.

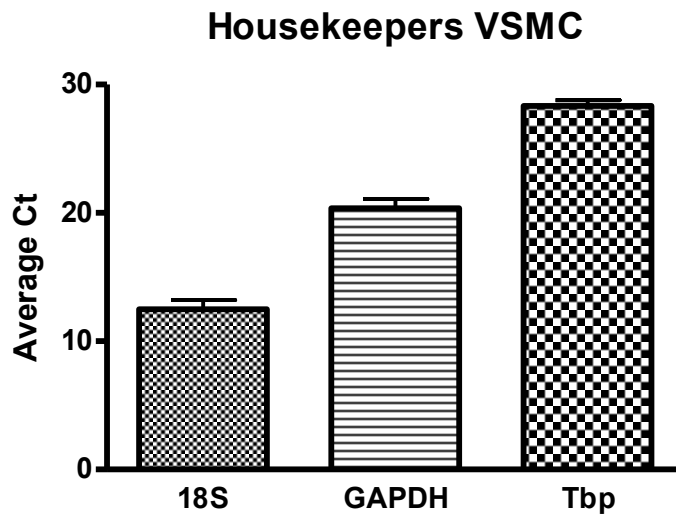


Figure 4-37. VSMC Housekeeper gene expression. Average Cycle Threshold (Ct) values for three housekeeping genes in miR-21 WT and KO VSMCs. Data presented mean \pm -SD. Biological n=5, technical duplicates. Tbp, Tata box binding protein.

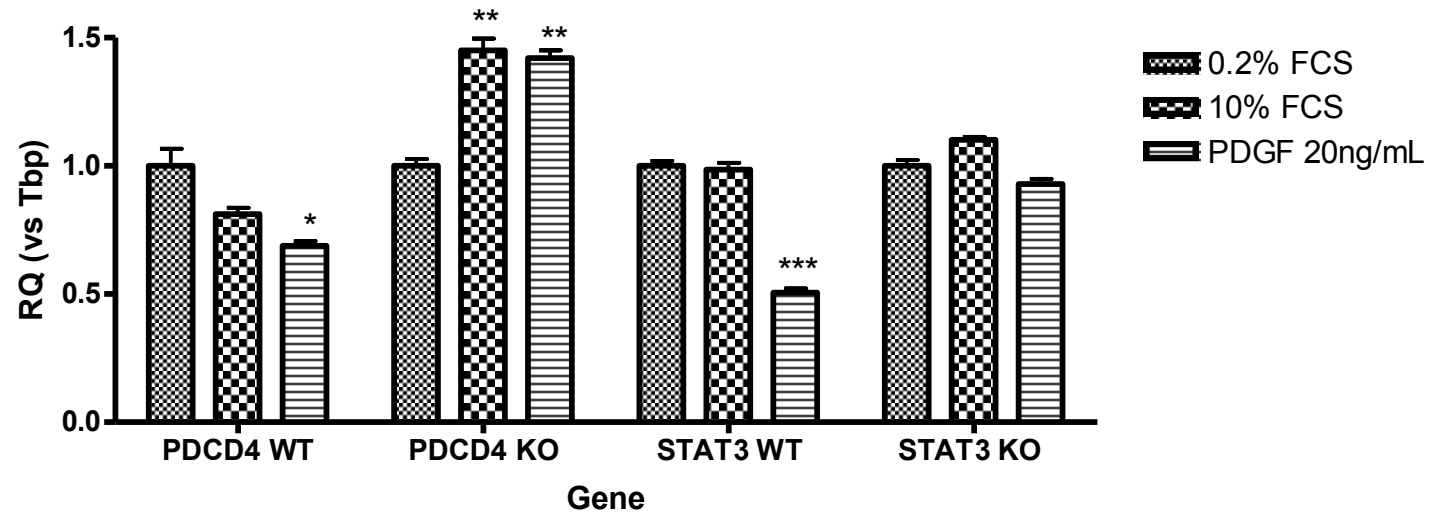


Figure 4-38. MiR-21 Target Expression. Relative expression of PDCD4 and STAT3 in miR-21 WT and KO VSMCs stimulated with 10% FCS or PDGF 20ng/mL. RQ+/-rqmax (vs. 0.2% FCS). Biological n=5, technical triplicates. Statistics performed on biological data. Scale bar = 100 μ m.n=5. *p<0.05, **p<0.01, ***p<0.001. RQ = Relative Quantity.

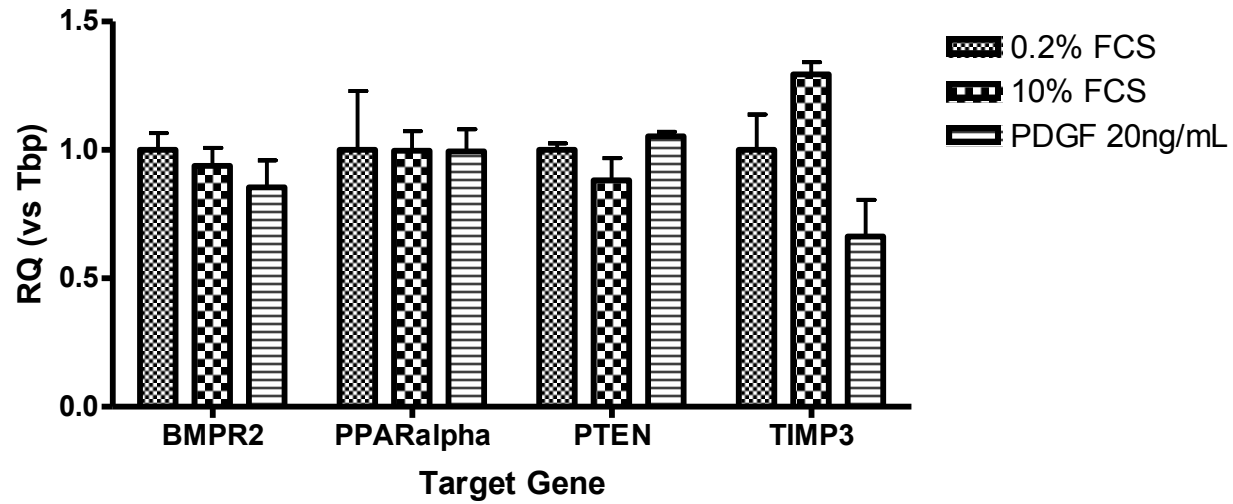


Figure 4-39. MiR-21 Target Expression. Relative expression of known miR-21 targets which did not significantly change in stimulated miR-21 WT VSMCs. RQ +/-rqmax (vs. 0.2% FCS). Biological n=5, technical triplicates. Statistics performed on biological data. RQ = Relative Quantity.

4.3.8 Effect of Knockdown of microRNA-21 using AntimiR-21 on the Development of In-Stent Restenosis

C57BL6 mice 15 weeks of age were dosed at 25 mg/kg with antimiR-21 or scramble antimiR by subcutaneous injection on a weekly basis for three weeks prior to undergoing isogenic aortic stenting and carotid interposition grafting as described in Chapter 2. Dose selection was made following the review of previously published work by (Patrick et al., 2010). It should be noted that the mice used in this experiment are not the same strain as the miR-21 WT and KO mice used previously which had been cross bred with S129 mice. Recipient mice were given a further dose immediately post operatively and on three further occasions at weekly intervals. Mice were culled and grafts harvested for analysis at day 28 following surgery. Figure 4-40 outlines the antimiR-21 treatment and operating schedule.

Morphological analysis of antimiR-21 and scramble treated mice at day 28 showed no significant difference in total vessel area ($0.49 \pm 0.02 \text{ mm}^2$ vs. $0.49 \pm 0.03 \text{ mm}^2$, $p > 0.05$, respectively). Nor was a significant difference observed in medial area ($0.06 \pm 0.008 \text{ mm}^2$ vs. $0.07 \pm 0.007 \text{ mm}^2$, $p > 0.05$, respectively) or medial thickness ($0.033 \pm 0.004 \text{ mm}$ vs. $0.029 \pm 0.003 \text{ mm}$, $p > 0.05$, respectively), Figure 4-41. Additionally, neointimal area and thickness in the antimiR-21 and scramble groups were not significantly different ($0.18 \pm 0.01 \text{ mm}^2$ vs. $0.15 \pm 0.02 \text{ mm}^2$, and $0.085 \pm 0.006 \text{ mm}$ vs. $0.074 \pm 0.011 \text{ mm}$, $p > 0.05$ for both, respectively), Figure 4-41. As a consequence neointimal : media area and thickness ratios did not differ significantly between antimiR-21 and scramble treated groups (2.78 ± 0.28 vs. 2.17 ± 0.20 and 2.74 ± 0.30 vs. 2.58 ± 0.32 , $p > 0.05$ for both, respectively) See Figure 4-41G and H.

Luminal area and calculated percentage stenosis were concordant with previously documented measurements from the grafts of antimiR-21 and scramble treated mice with no significant difference observed ($0.22 \pm 0.02 \text{ mm}^2$ vs. $0.24 \pm 0.02 \text{ mm}^2$ and $41.7 \pm 2.9\%$ vs $24.1 \pm 2.6\%$, $p > 0.05$ for both, respectively), Figure 4-41 and Figure 4-42.

Schwartz injury scores did not differ between antimiR-21 and scramble treated mice (0.41 ± 0.07 vs. 0.29 ± 0.06 , $p > 0.05$, respectively). Figure 4-42 shows representative sections from antimiR-21 and scramble grafts.

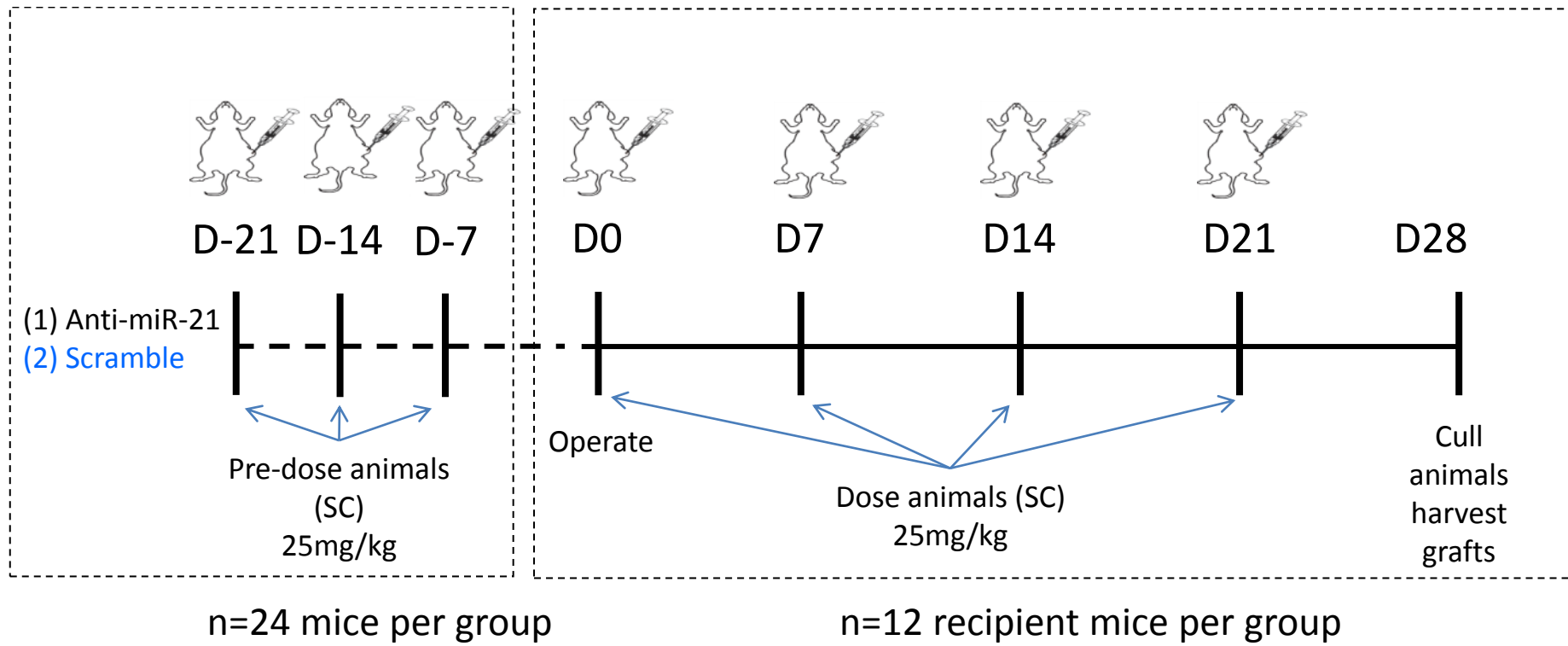


Figure 4-40. AntimiR-21 Dosing and Operation Schedule.

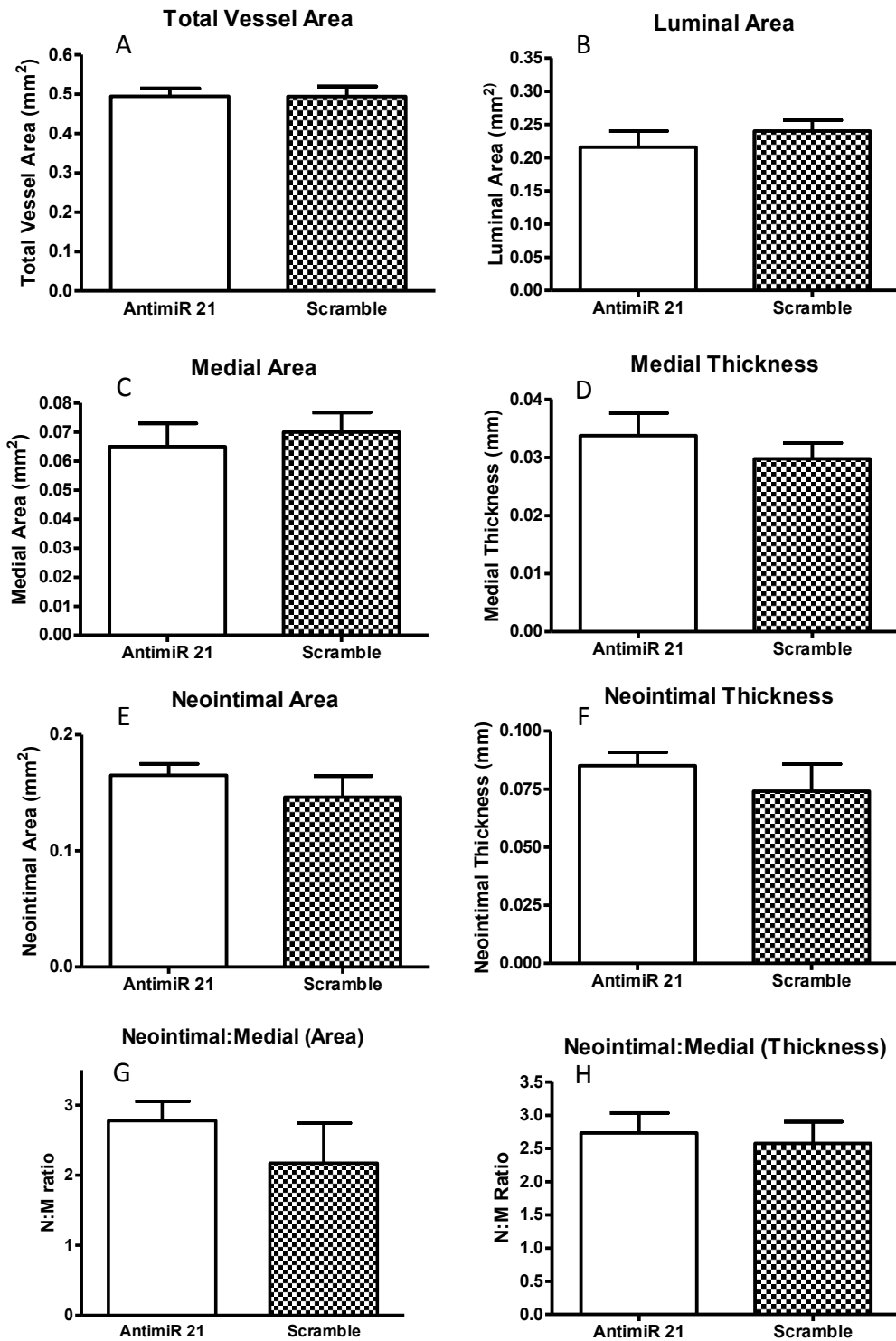


Figure 4-41. Morphometry of AntimiR-21 Treated Mice. Characteristics of Stented Grafts from antimiR-21 and scramble treated mice at Day 28. A, Total Vessel Area. B, Luminal Area. C, Medial Area. D, Medial Thickness. E, Neointimal Area. F, Neointimal Thickness. G, Neointimal:Media Area ratio. H, Neointimal:Media Thickness ratio. AntimiR-21 n=11, Scramble n=8.

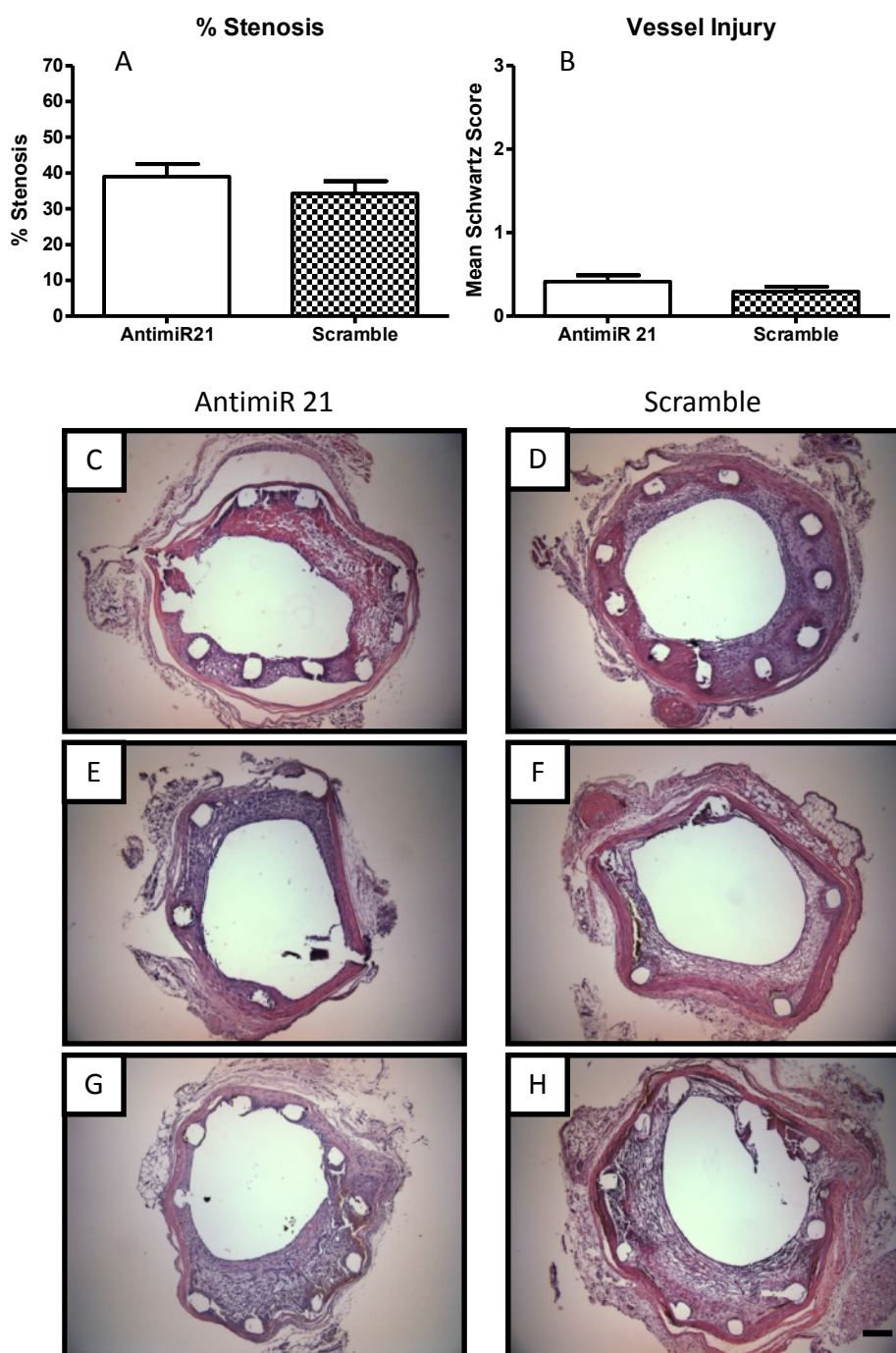


Figure 4-42. AntimiR-21 Treated Grafts. Further characterisation of stented grafts for antimiR-21 and scramble treated mice at Day 28. **A**, Percentage Stenosis. **B**, Schwartz Injury Score. **C**, **E** and **G** representative sections from antimiR-21 treated mice. **D**, **F** and **H** representative sections from scramble treated mice. Scale bar = 100 μ m. AntimiR-21 n=11, Scramble n=8.

4.3.9 Effect of microRNA-21 over expression on the Development of In-Stent Restenosis

4.3.9.1 miR-21 overexpression within vascular and non-vascular tissues

Significant overexpression of miR-21 in the CAG-miR-21 containing transgenic mouse strain used in this study has been previously confirmed in a variety of tissues by both RT-qPCR and Northern blotting (Hatley et al., 2010). However, while overexpression has been documented in the heart, expression levels have not been previously confirmed in the aorta (Hatley et al., 2010). Therefore, we first set out to confirm this prior to using these mice in the stenting model.

Identification of wild-type (WT +/+) and heterozygous CAG-miR-21 (HET +/+) transgenic mice was first confirmed by conventional PCR for the presence or absence of the reporter gene EGFP located within the transgenic construct as described in Chapter 2. RT-qPCR was then conducted on RNA isolated from the three different tissues: aorta, heart and liver.

MiR-21(-5p) levels in the aorta, heart and liver were found to be significantly elevated in HET +/+ mice (4.4 ± 0.8 fold, 24.4 ± 2.6 fold and 4.1 ± 0.5 fold vs. WT +/+ mice, $p < 0.01$, $p < 0.0001$ and $p < 0.001$, respectively), Figure 4-43.

In addition miR-21(star)-3p levels in the aorta, heart and liver were also found to be elevated in HET +/+ mice (3.6 ± 1.5 fold, 45.7 ± 7.9 fold and 4.2 ± 1.0 fold vs WT +/+ mice, respectively). However, this only reached significance in the heart and liver ($p < 0.001$ and $p < 0.05$, respectively), Figure 4-43.

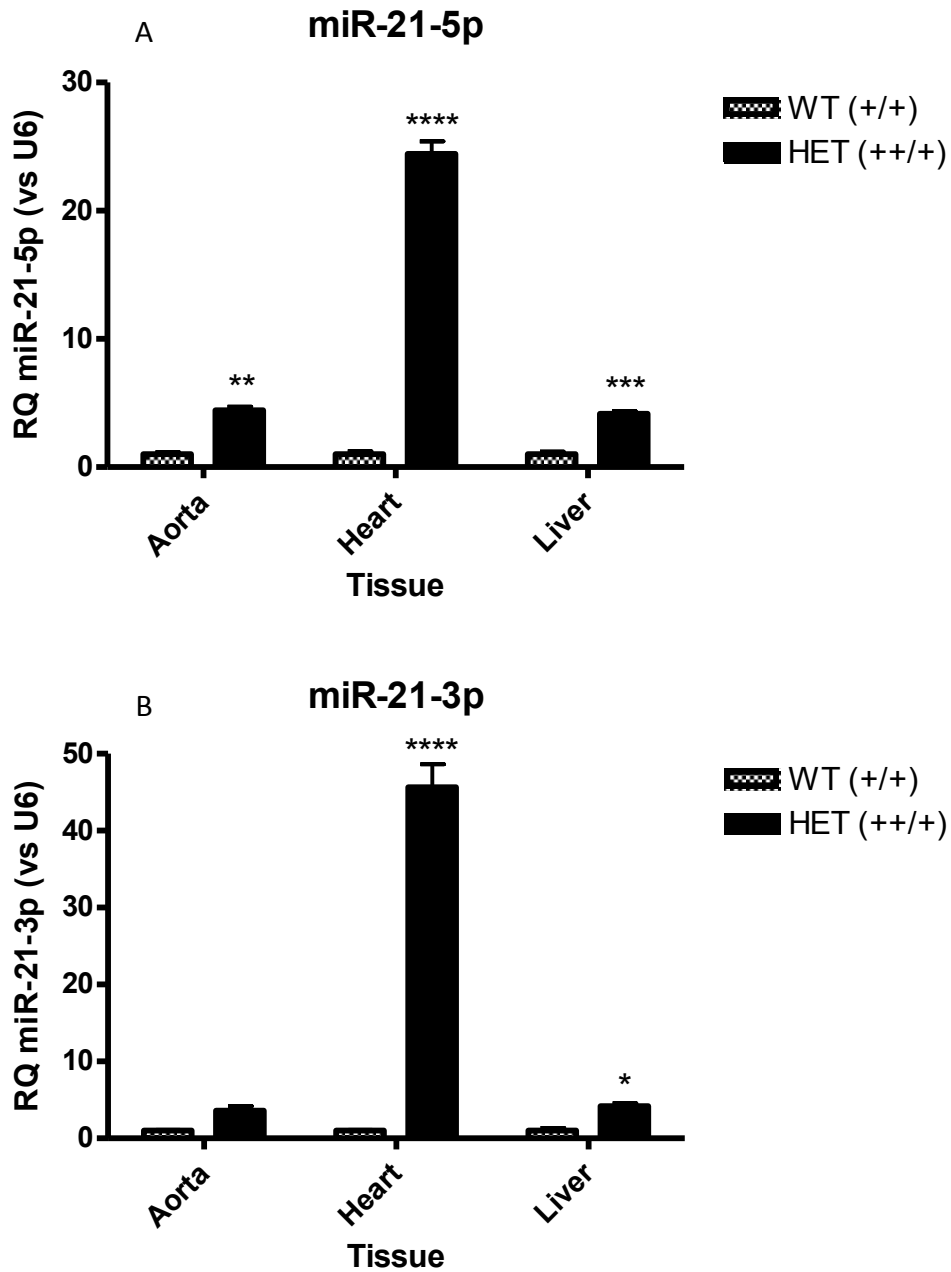


Figure 4-43. MicroRNA-21 Expression. MiR-21 expression in aorta, heart and liver samples from Transgenic CAG-miR-21 mice and WT littermates. A miR-21-5p. B, miR-21-3p. * $p < 0.05$, ** $p < 0.01$, *** $p < 0.001$, **** $p < 0.0001$ vs WT (+/+). WT +/+ and HET +/+ biological $n = 5$ for both, technical triplicates. Statistics performed on biological data. RQ = Relative Quantity.

4.3.10 Morphometry of stented grafts from heterozygous miR-21 over expressing mice and wild-type littermates

Total vessel area was significantly smaller in WT +/+ compared to HET +/+ mice at day 28 ($0.49 \pm 0.03 \text{ mm}^2$ vs $0.55 \pm 0.02 \text{ mm}^2$, $p < 0.05$, respectively). No significant difference was observed between WT +/+ compared to HET +/+ for medial area ($0.08 \pm 0.01 \text{ mm}^2$ vs. $0.08 \pm 0.01 \text{ mm}^2$, $p > 0.05$, respectively) or medial thickness ($0.037 \pm 0.003 \text{ mm}$ vs. $0.034 \pm 0.002 \text{ mm}$, $p > 0.05$, respectively), Figure 4-44. However, neointimal area was significantly smaller in the WT +/+ than HET +/+ group ($0.10 \pm 0.02 \text{ mm}^2$ vs. $0.16 \pm 0.02 \text{ mm}^2$, $p < 0.05$, respectively), Figure 4-44. Similarly neointimal thickness was less in the WT +/+ than HET +/+ group but this did not reach significance ($0.05 \pm 0.008 \text{ mm}$ vs. $0.08 \pm 0.016 \text{ mm}$, respectively). Neointimal : Media area and thickness ratios were greater in WT +/+ than HET +/+ mice but neither reached significance, (1.46 ± 0.31 vs. 2.15 ± 0.30 , and 1.48 ± 0.32 vs. 2.55 ± 0.49 , respectively), Figure 4-44.

While measurements of strut depth were concordant with the findings for neointimal area and thickness, with greater strut depth found in WT +/+ vs HET +/+ grafts, this also failed to reach significance ($0.03 \pm 0.004 \text{ mm}$ vs $0.06 \pm 0.018 \text{ mm}$, respectively), Figure 4-45.

Although WT +/+ had a significantly smaller neointimal area than HET +/+ mice no significant difference was observed in luminal area ($0.27 \pm 0.02 \text{ mm}^2$ vs. $0.25 \pm 0.03 \text{ mm}^2$, respectively, respectively), Figure 4-44. This is likely due to the difference in total vessel area. When total vessel area was corrected for, no significant difference was noted in percentage stenosis, calculated as: $(\text{Area within IEL} - \text{Luminal Area}) / \text{Area within IEL} \times 100$, (WT +/+ vs. HET +/+, $24.8 \pm 4.0 \%$ vs $35.5 \pm 3.5 \%$, respectively), Figure 4-45.

Importantly no significant difference was observed in Schwartz Injury Score between WT +/+ and HET +/+ mice (0.39 ± 0.07 vs. 0.34 ± 0.07 , respectively), Figure 4-45. Representative sections from WT +/+ and HET +/+ grafts at 28 days are shown in Figure 4-45.

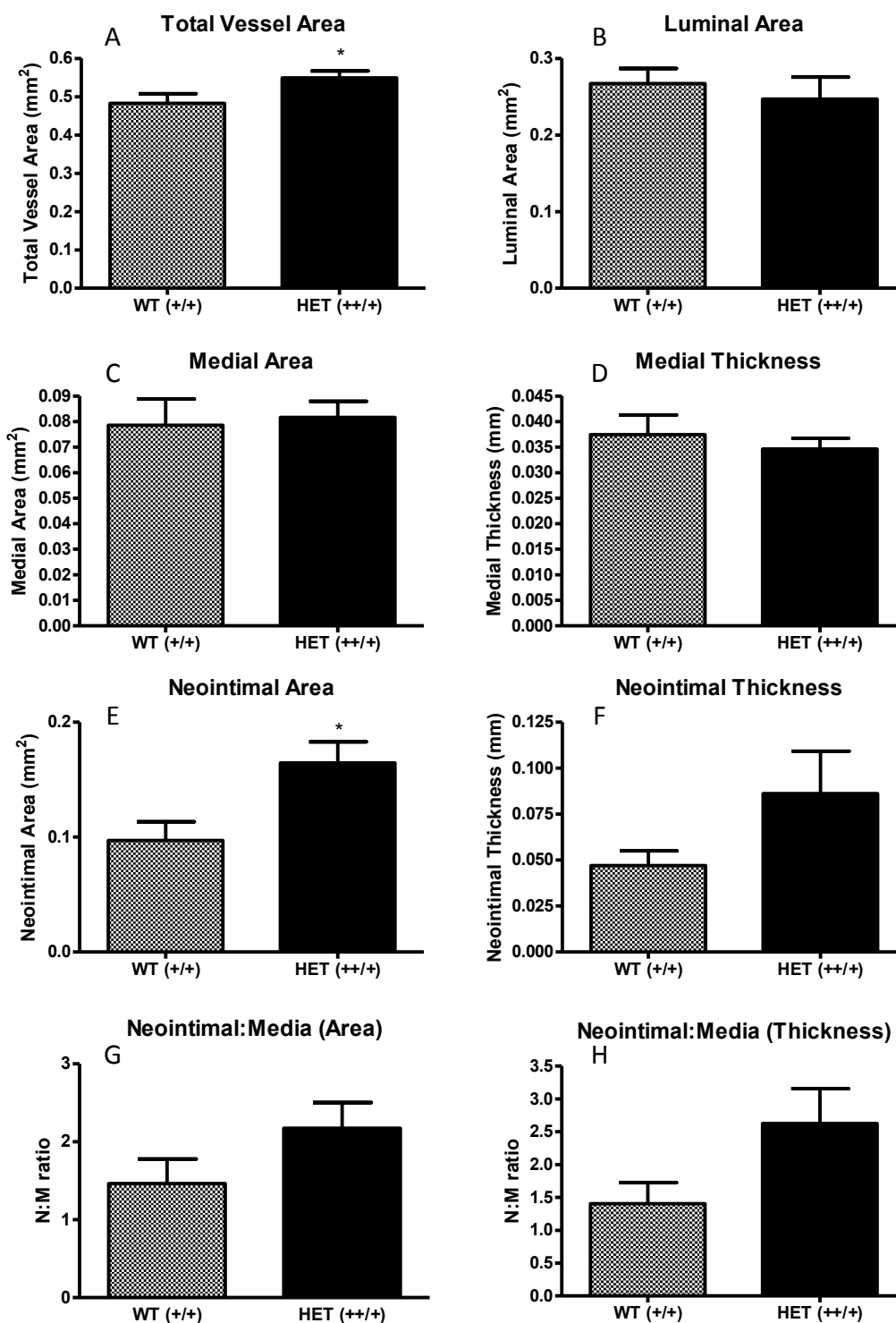


Figure 4-44. Characteristics of Stented Grafts from WT +/+ and HET +/+ mice at Day 28. A, Total Vessel Area. B, Luminal Area. C, Medial Area. D, Medial Thickness. E, Neointimal Area. F, Neointimal Thickness. G, Neointimal:Media Area ratio. H, Neointimal:Media Thickness ratio. * $p < 0.05$. WT +/+ $n = 6$, HET +/+ $n = 11$.

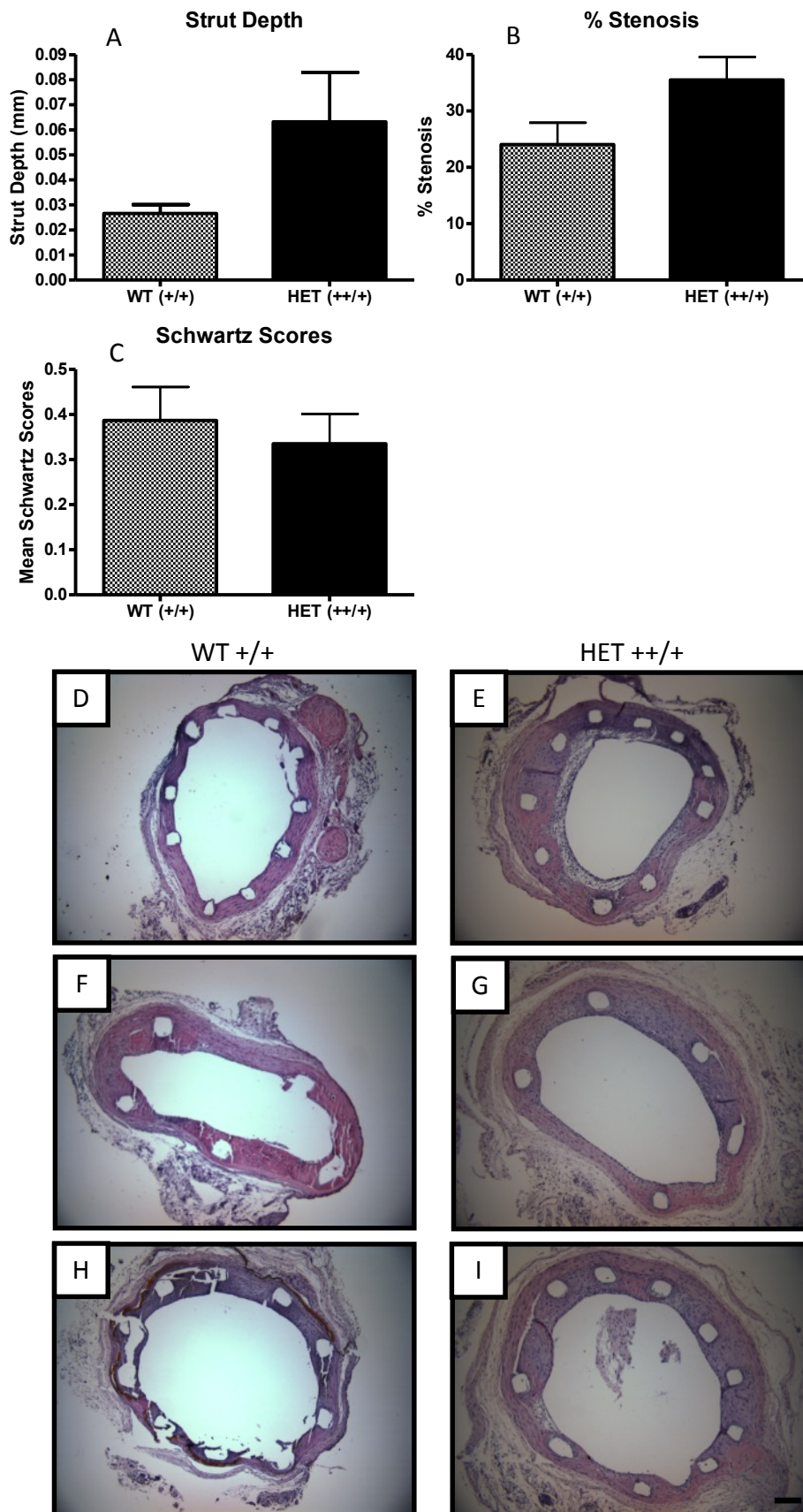


Figure 4-45. Further Characteristics of Stented Grafts from WT +/+ and HET +/+ mice at Day 28. A, Strut Depth. B, Percentage Stenosis. C, Schwartz Injury Score. D, F and H representative sections from WT +/+ mice. E, G and I representative sections from HET +/+ grafts. Scale bar = 100 μ m. WT +/+ n=6, HET +/+ n=11.

The data presented above demonstrate that the genetic deletion of miR-21 in a mouse model of stenting reduced the formation of neointima and hence the development of ISR without affecting re-endothelialisation of the stented segments. Reduced proliferative and migratory capacities were observed in VSMCs in which miR-21 had been deleted. In addition, an altered macrophage polarisation state was observed between miR-21 WT and KO stented grafts.

Neither pharmacological knockdown nor overexpression of miR-21 significantly altered the size of neointima formed.

4.4 Discussion

The results presented within this chapter demonstrate that genetic deletion of miR-21 resulted in a significant reduction in neointimal formation and importantly in-stent stenosis at 28 days following aortic stenting in this mouse model. In addition, loss of the miR-21 stem loop in knockout mice blocked neointimal formation through effects on VSMC proliferation and migration but had no effect on the re-endothelialisation of grafts. The altered inflammatory phenotype with an enhancement of anti-inflammatory (M2) macrophages in response to stenting was also evident within grafts from miR-21 KO mice and may contribute towards a reduction in the neointima observed.

This study is the first to investigate the role of microRNAs on the development of in-stent stenosis and to document the deleterious effects of miR-21 on the development of neointimal hyperplasia following stent placement. We found that genetic deletion of miR-21 resulted in a reduction in the development of NIH and importantly in-stent stenosis at 28 days following stenting. These results are in keeping with our previously published studies of miR-21 in a murine vein grafting model where genetic deletion of miR-21 resulted in an 80% reduction in NIH (McDonald et al., 2013). Indeed it was also shown that the genetic deletion of miR-21 within the vein graft itself was responsible for the reduction in NIH rather than presence or absence of miR-21 within the recipient animal as evidenced by grafting between genotypes (McDonald et al., 2013). The results presented in this chapter are concordant with those from other *in vivo* models of vascular injury. Two independent groups have demonstrated, in rat models of carotid and iliac artery balloon injury, inhibition of miR-21 results in a reduction in NIH by approximately two thirds. In both of these studies knockdown of miR-21 was achieved by the local delivery of antagomirs suspended in a poloxamer gel (Ji et al., 2007, Wang et al., 2012a). Compared to these balloon injury models it is tempting to suggest that the more profound reduction in NIH seen within the vein-grafting model is likely to result from the complete absence of miR-21 due to its genetic deletion rather than the temporary knockdown of miR-21. However, within the current study which utilised a miR-21 knockout strategy the reduction in NIH was even less than that seen in the knockdown studies mentioned above. Thus while the strategy used to inhibit miR-21 may indeed play a role in the reduction of NIH observed, accurate conclusions cannot be

drawn by comparing such strategies between injury models due to differing type and severity of injury as well as the presence of the stent.

The current study demonstrated up regulation of miR-21 expression by *in situ* hybridisation within the neointima, particularly around the luminal surface and subluminal areas. In addition, staining also identified a marked peri-stent distribution. Immunohistochemical staining of sequential sections for markers such as α -actin, CD31 and MAC2 strongly suggests high miR-21 expression was present within the endothelium, neointimal VSMCs, and macrophages surrounding stent struts. Our results are not surprising given the findings of other studies, which have demonstrated by both *in situ* hybridisation and RT-qPCR an elevated expression of miR-21 not only following vascular injury but also in atherosclerotic plaques and in failed human vein grafts (Ji et al., 2007, Wang et al., 2012a, Raitoharju et al., 2011). In addition, elevated expression of miR-21 was identified within samples obtained from patients with Arteriosclerosis Obliterans (Wang et al., 2011). Interestingly the greatest expression was not found in lesions with the greatest stenosis but within lesions displaying up to 50% stenosis, suggesting up regulation of miR-21 may be an early phenomenon (Wang et al., 2011). Within a porcine coronary stenting model we have also demonstrated, by RT-qPCR, elevated miR-21 expression in the artery wall (McDonald et al., 2015). *In situ* hybridisation confirmed elevated levels of miR-21 in all three layers of the vessel wall. Interestingly miR-21 expression was greatest at 7 days but remained elevated to a lesser degree at 28 days (McDonald et al., 2015). Taken together these findings suggest miR-21 induction is an early event following vascular injury and may play a role in the development of stenotic lesions.

The mechanisms underpinning miR-21 up regulation following stenting in these complex *in vivo* models is likely to be multifactorial, related to mechanical and chemical factors such as hypoxia, oxidative stress and growth factor release. Differing from balloon or wire injury models, stent placement against the vessel induces a constant rather than transient radial force. *In vitro* studies have identified stretch to be a key stimulus of miR-21 transcription in a variety of cell types (Song et al., 2012). Stretch in the form of both unidirectional and oscillatory shear stress has been shown to induce up regulation of miR-21 in

endothelial cells with the later producing an increase in binding of c-Jun to the AP-1 binding site on the miR-21 promoter (Weber et al., 2010); (Zhou et al., 2011). In human aortic smooth muscle cells cultured *in vitro*, stretch itself was shown to induce miR-21 transcription due to an increase in phosphorylation and hence activity of the transcription factor c-Jun, an important component of the AP-1 heterodimer (Song et al., 2012). AP-1 has in VSMCs been demonstrated to promote proliferation following vascular balloon injury (Yasumoto et al., 2001). *In vivo* models of cardiac pressure overload using trans-aortic constriction which increase left ventricular end diastolic pressure have also been shown to induce miR-21 expression in cardiac fibroblasts (Thum et al., 2008).

Local hypoxia due to stent compression and disruption of blood flow within the vaso vasorum may also play a role in the modulation of miR-21 within the vessel wall. However, the role of hypoxia in modulating miR-21 expression remains controversial. While it has been reported that hypoxia induces miR-21 transcription, others have found the opposite in a hypoxic lung injury model (Sarkar et al., 2010, Yang et al., 2012, Caruso et al., 2010). Thus while it is conceivable that local hypoxia within the vessel wall due to stent compression may play a role in the up regulation of miR-21, confirmation would require further investigation in this particular experimental setting.

In the current study not only did size of neointima differ between miR-21 WT and KO mice but neointimal composition also differed significantly. Neointima from WT mice were found to contain significantly more smooth muscle cell alpha actin than that of KO counterparts. PDGF is a key growth factor released from platelets and endothelial cells following vascular injury, promoting VSMC proliferation and migration (Jackson et al., 1993). PDGF inhibition has been shown to dramatically reduce NIH (Ferns et al., 1991). *In vitro* analysis demonstrated that in response to PDGF stimulation, the reduction in smooth muscle staining observed within the neointima of miR-21 KO mice was likely a consequence of both reduced VSMC proliferation and migration. These findings are not surprising given that upon injury, miR-21 has been shown by several groups to induce VSMC proliferation, migration and to protect against apoptosis (Ji et al., 2007, Wang et al., 2011, Lin et al., 2009). It has previously been shown that miR-21 is a key molecular switch in the signalling pathway of PDGF, which increases miR-21 expression indirectly via activation of HIF-1 α (Wang et

al., 2011). In addition, PDGF stimulation of miR-21 WT VSMCs demonstrated both an up regulation of miR-21 and repression PDCD4 and STAT3. PDCD4 is a known target of miR-21 previously validated in the setting of vascular injury (Wang et al., 2011, Maegdefessel et al., 2012). The results of the current study are in keeping with previously published data showing PDCD4 is down regulated following both vascular injury and PDGF stimulation (Liu et al., 2010). Additionally, over-expression of PDCD4 using an adenoviral vector has been shown to attenuate the proliferative response as well as augmenting the induction of apoptosis within VSMCs (Liu et al., 2010). Interestingly, within the current study PDCD4 was also found to be elevated in VSMCs taken from miR-21 KO mice adding further weight to the idea that PDCD4 may be a key miR-21 target involved in the development of ISR.

Within the current study the apparent discrepancy between the *in vivo* IHC analysis of PCNA staining, which failed to show a difference in proliferation between miR-21 WT and KO mice and the *in vitro* analysis using BrdU could at least in part be explained by the fact that a far earlier time point was analysed *in vitro*. Greatest proliferative response is seen immediately following injury and quickly reduces to basal levels by 28 days when healing is complete (Touchard and Schwartz, 2006). Interestingly, using pharmacological knockdown of miR-21 *in vivo* other groups have been able to demonstrate a difference in proliferation at 14 days following both balloon injury and within a murine AAA model (Ji et al., 2007, Maegdefessel et al., 2012). Thus had the *in vivo* analysis been conducted at an earlier time point following stenting, a difference in proliferation may have been observed.

Following stenting greater elastin deposition was observed within the neointima of miR-21 WT mice compared to their KO counterparts. Our results are in keeping with other injury models demonstrating that up regulation of miR-21 following injury induces ECM deposition and sequestration of miR-21 attenuates such a response. Thum et al (Thum et al., 2008) demonstrated up regulation of miR-21 within cardiac fibroblasts in a trans-aortic constriction model of cardiac hypertrophy. This resulted in increased cardiac fibrosis. In addition they showed the intravenous administration of antagomir-21 de-repressed SPRY1 protein levels, which via a resultant decrease in ERK-MAPK signalling inhibited deposition of ECM molecules including collagens (Thum et al., 2008).

Interestingly, it has been shown under non-stressed conditions that selective deletion of miR-21 from endothelial cells results in both structural and functional remodelling of the thoracic aorta with age (Song et al., 2012). In particular a reduction in elastin, collagen I and III expression were observed within the vessel media compared to WT mice (Song et al., 2012). Song et al (Song et al., 2012) attribute these effects to an increase in endothelial cell SMAD7 and consequently inhibition of TGF β 1-induced ECM expression. However, they fail to demonstrate whether these effects are due to endothelial to mesenchymal transition or a paracrine signalling effect on cells classically involved in ECM synthesis. Under non-stressed conditions neither the Olsen laboratory nor we identified any gross phenotypic vascular abnormality in the miR-21 KO mouse used within this study (McDonald et al., 2013, Hatley et al., 2010). In addition, at baseline no cardiac abnormality could be demonstrated in miR-21 KO mice compared to their WT littermates (Patrick et al., 2010). Further work is required to fully understand the differences noted between mice where miR-21 has been selectively deleted from ECs and completely removed from all cell types.

Re-endothelialisation following stenting in the model used in the current study has been demonstrated to be dependent on both cells originating from bone marrow (endothelial progenitor cells) and from those of the adjacent intact vasculature (Douglas et al., 2013). Our study did not demonstrate a difference in re-endothelialisation between WT and KO mice, which was virtually complete at 28 days. The complex role of miR-21 in endothelial cell apoptosis, proliferation and migration has been extensively investigated. Sabatel et al (Sabatel et al., 2011) demonstrated that over expression of miR-21 in ECs reduced proliferation, migration and tubulogenesis by targeting of RhoB, which has previously been implicated in EC migration. Furthermore, up regulation of miR-21 within ECs by rapamycin has been shown via RhoB repression to be involved the inhibitory effects of this drug on EC proliferation and migration (Jin et al., 2013). Concordant with these findings it has also been shown in early passage HUVECs that miR-21 overexpression impairs angiogenesis and cell proliferation by targeting CDC25A and nuclear factor 1 B-type (Dellago et al., 2013). Down regulation of these targets in turn resulted in an increase in the cell cycle

inhibitor p21 and a failure to dephosphorylate CDK2 and thus drive the cell through the G1/S phase checkpoint (Dellago et al., 2013).

While the Inflammatory response has been shown to be important to the development of NIH in both balloon injury and stenting models, significant differences have been identified in the innate immune response to each model. Balloon injury induces a transient neutrophil predominant infiltration of the vessel wall (Welt et al., 2000) while stenting has been shown to produce a more prolonged inflammatory response dominated by macrophages (Horvath et al., 2002). The majority of the macrophage population originate from bone marrow-derived circulating monocytes, which infiltrate the tissue via the luminal and adventitial surfaces (Tuleta et al., 2008). Significant differences in macrophage polarisation were evident with grafts from miR-21 KO mice containing more anti-inflammatory (M2) macrophages than miR-21 WT mice. These findings are concordant with those of other investigators who have independently shown miR-21 promotes M1 macrophage polarisation by targeting STAT3 and that genetic deletion of miR-21 results in enhanced M2 polarisation in a STAT3 dependent manner (Wang et al., 2015). M2 or alternatively activated macrophages are thought to suppress inflammation, facilitate tissue healing by differences in their phagocytic capacity and the cytokines secreted (Murray and Wynn, 2011). Lavin et al (Lavin et al., 2014) have recently demonstrated greater neointimal lesion formation following balloon injury in NOS3 deficient mice due to higher M1:M2 ratios within the vascular wall. They also demonstrated that conditioned media from NOS3 deficient endothelial cells could induce repolarisation of macrophages from an M2 to an M1 phenotype. In addition, they found conditioned media from M1 macrophages induced both greater proliferation and migration within VSMCs (Lavin et al., 2014).

Taken together our findings and those of other groups suggest miR-21 may play an important role in modulating the inflammatory response following vascular stenting. Thus further experiments were devised to investigate the effect the absence of miR-21 has on macrophage biology and in particular the potential consequences on neointimal development and are reported in chapter 5.

Having shown that genetic deletion of miR-21 reduces NIH development, further experiments were undertaken to establish if suppression of miR-21 using a knock

down strategy would have a similar effect. Unfortunately no significant differences were observed between antimiR-21 and scramble treated mice for any of the morphological parameters measured. This is in stark contrast to several other studies, which have shown the inhibition of miR-21 following vascular injury could significantly impact vascular remodelling (Ji et al., 2007, Maegdefessel et al., 2012, Wang et al., 2012a). One reason, which may account for the current findings may be the model itself. Partial suppression of miR-21 may not sufficiently de-repress the mRNA targets in order to alter the vascular pathology observed within the stenting model.

Aside from the model itself the method of delivery, dose, dosing schedule and chemistry of the antimiR used are all likely to contribute to the results observed. The current study used a systemic delivery method in contrast to two successful studies, which topically applied antagomir-21 suspended within a poloxamer gel to the vessel's adventitial surface at the time of balloon injury (Wang et al., 2012a, Ji et al., 2007). Thus, failure of the antimiR-21 to reach the stented graft is a possible explanation in addition to the fact that the majority of antimiR is known to be sequestered by the liver. Against this theory is that excellent biodistribution of antimiRs have been demonstrated by others (Krutzfeldt et al., 2005). With the sole exception being the central nervous system, which appears difficult to penetrate following systemic injection (Krutzfeldt et al., 2005). In addition within an elastase infusion model, a single systemic tail vein injection of antimiR-21 significantly augmented the development of AAA by de-repressing PTEN (Maegdefessel et al., 2012). Thus it would seem unlikely that the method of delivery would on its own account for lack of effect within the current study.

The dose of antimiR is a further putative explanation for the results observed. Indeed the first *in vivo* antagomir study was conducted in mice to suppress miR-122 within the liver and used three different intravenous doses, 80, 160 and 240 mg/kg (Krutzfeldt et al., 2005). By using these three doses a dose response relationship was observed. While the maximum dose used by Krutzfeldt et al (Krutzfeldt et al., 2005) is almost 10 fold greater than the dose of antimiR-21 used in the current study, a dose of 25 mg/kg has been shown to de-repress PDCD4 expression levels within the heart (Patrick et al., 2010). Although others

have previously demonstrated it took a dose of 80 mg/kg to alter phenotype (Thum et al., 2011).

The differing chemistries of miR inhibitors have caused great debate regarding stability and efficacy *in vivo*. The earliest oligonucleotides, termed antagomirs were similar in length to the mature miR and conjugated to cholesterol at their 3' ends to facilitate cellular uptake and in addition contain O-methyl groups conjugated to the second oxygen of the ribose sugar within each nucleotide. Thum et al (Thum et al., 2008) utilised such antagomirs to inhibit cardiac fibrosis following trans-aortic banding. Various other modifications have also been added to the 2'-O (Thum et al., 2011, Dangwal et al., 2012). More novel antimiRs have been developed between 8 and 15 nucleotides in length with fully lock nucleic acids to enhance stability and affinity individual miRs (Montgomery et al., 2011). AntimiR-21 and scramble control used within the current study were gifts from miRagen™ (Boulder, Colorado USA) the exact chemistry of which is commercially sensitive and was not revealed to ourselves. However, it is likely that the gifted compounds are similar to those used in the Olsen Laboratory (Patrick et al., 2010).

Patrick et al showed maximal target de-repression three weeks following the first antimiR-21 dose (Patrick et al., 2010). It should be noted that while they demonstrated target de-repression of PDCD4 they failed to show phenotypic change. One possible explanation is commencement of trans-aortic banding 6 weeks before commencement of antimiR-21 resulted in pathological remodelling which was irreversible by the time of antimiR delivery. The dosing schedule chosen for the current study of weekly antimiR injections commencing 3 weeks prior to stenting and continued until harvesting of the graft was devised to establish target de-repression prior to stenting and maintain this effect throughout the course of the experiment. Due to the requirement for histological analysis the current study did not confirm target de-repression within the stented graft.

While every effort was undertaken to optimise the antimiR study protocol it is likely that a combination of the above mentioned variables in antimiR delivery, dose, regimen and chemistry contributed to the lack of effect observed within this study. In addition, other unknown counter-regulatory responses to both

antimiR presence and target expression may have contributed to the outcome. Further work would be required to investigate this.

Within VSMCs, over-expression of miR-21 *in vitro* and *in vivo* using commercially available premiR-21 or lentivirus encoding premiR-21, respectively, have both been shown to increase proliferation, vessel wall thickness and reduce apoptosis (Maegdefessel et al., 2012). We therefore investigated the effect on ISR development in a transgenic mouse overexpressing miR-21. We first confirmed that miR-21 was over expressed in different cardiovascular and non-cardiovascular tissues from heterozygous mice containing CAG-miR-21 gene. An increase of 4.4 fold in miR-21 expression was observed within the aorta compared to WT mice. This is in keeping with previous reports of miR-21 over expression in CAG-miR-21 transgenic mice (Hatley et al., 2010). A small but significant increase in neointimal area was observed in heterozygous miR-21 $+/+$ mice compared to WT $+/+$ mice. However, total vessel area was also greater in heterozygous miR-21 $+/+$ mice and upon correcting for this finding no difference was observed in percentage stenosis nor was there a significant difference in luminal area. Thus it can be concluded that heterozygous over-expression of miR-21 in our model did not result in significantly greater ISR than WT littermates. It would initially appear reasonable to suggest that had homozygote miR-21 $+/+$ over-expressing mice been used, a significant difference in ISR may have been observed. However, we did not measure relative expression in homozygous miR-21 $+/+$ mice, nor did we measure miR-21 expression within the heterozygous miR-21 $+/+$ grafts at the end of the study period. One putative reason, for the findings presented in this study, is that while following stenting there is likely to be up regulation of miR-21 expression from native miR-21 alleles, counter regulatory (negative) feedback loops involving the AP-1/miR-21/PDCD4 axis may actually suppress increased miR-21 expression from native alleles within heterozygous miR-21 $+/+$ mice (Talotta et al., 2009). Consequently the relative difference in miR-21 expression at baseline between heterozygous miR-21 $+/+$ mice and miR-21 WT mice may be diminished following intervention. Interestingly when these over expressing mice were studied in the setting of non-small-cell lung cancer miR-21 over-expression alone was not enough to induce tumourigenesis. Indeed investigators noted that a “second hit” in the form of K-Ras mutation was required to induce tumour

progression and metastasis (Hatley et al., 2010). Importantly gain-of-function K-Ras mutations induce miR-21 by up regulation of AP-1 activity circumventing the negative feedback loop involving AP-1/miR-21/PDCD4 (Hatley et al., 2010, Talotta et al., 2009). This could explain the lack of effect on ISR in the current study but would require further investigation.

In conclusion, genetic deletion of miR-21 significantly reduces neointimal formation but crucially did not impair re-endothelialisation of stent struts. The underlying mechanisms are likely to be multifactorial involving a reduced migratory and proliferative capacity of miR-21 deficient VSMCs in response to de-repression of PDCD4. Mir-21 also appears to alter macrophage polarisation within stented arteries and may also play a significant role in modulating the development of ISR. The failure of both antimir-21 and overexpression strategies to diminish and augment ISR, respectively are disappointing and suggests counter regulatory mechanisms involving miR-21 and its targets are complex and robust. Further work is required to develop therapeutically viable strategies to mirror the effect of miR-21 deletion.

5 Effects of microRNA-21 on macrophage polarisation and function in the development of in-stent restenosis.

5.1 Introduction

Macrophages are key cellular components of the innate immune system functioning in both health and disease (Sica and Mantovani, 2012). One of their key roles is to function as part of the host's defence system against invading pathogens including bacteria, viruses, and parasites (Mosser and Edwards, 2008). However, they also play important roles in organ development, tissue remodelling and repair (Mantovani et al., 2013). In addition the importance of macrophages in allergy, metabolism and many cancers has been extensively investigated (Biswas and Mantovani, 2010, Robbe et al., 2015).

In order to accomplish the wide array of tasks required, macrophages exhibit extraordinary plasticity to adapt to their local environment (Sica and Mantovani, 2012, Wolfs et al., 2011). Upon stimulation macrophages polarise to different phenotypes by altering their gene expression profile. Classical (M1) activation occurs following stimulation with IFN γ or LPS triggering IFN receptor and TLR4 activation, respectively (Sica and Mantovani, 2012). Through cooperative signalling cascades involving NF κ B and STAT1 pro-inflammatory cytokines are up regulated including IL-1, IL-6, IL-12 and TNF α (Mantovani et al., 2013). M1 polarised macrophages are predominantly involved in microbial killing and are viewed as pro-inflammatory (Mosser and Edwards, 2008). Alternatively activated (M2) macrophages are induced by IL-4 or IL-13 stimulation and through STAT6 signalling up regulate genes such as Retnla, YM-1, PPAR γ and IL-10 (Raes et al., 2002, Odegaard and Chawla, 2011, Szanto et al., 2010). M2 macrophages are commonly viewed as anti-inflammatory, functioning to suppress inflammation while promoting tissue repair (Mantovani et al., 2013). Recently further subdivision of M2 macrophages into M2a, M2b and M2c phenotypes has been proposed with more subtle but distinct functional characteristics being elucidated (Lucas et al., 2010). Polarisation should be viewed as a complex phenotypic continuum, which has been shown to be reversible in many circumstances upon changing local environmental stimuli (Guiducci et al., 2005).

The role played by miRs in macrophage polarisation has already been investigated. Initial studies demonstrated that following polarisation numerous miRs and their passenger stands were up or down regulated. In addition, miR expression varied according to polarisation state (Graff et al., 2012). Further

work has demonstrated that individual miRs such as miR-125a-5p and let-7c are also able to influence initial polarisation as well as drive macrophages from one polarisation state to another (Banerjee et al., 2013a, Banerjee et al., 2013b). Interestingly, let-7c has also been shown to modulate both phagocytic and bactericidal activity of polarised macrophages (Banerjee et al., 2013b).

Following stent placement macrophages play a far greater role in the development of ISR than in NIH following balloon angioplasty (Welt et al., 2000). Macrophage presence within the neointima has been positively correlated with increasing ISR (Rogers et al., 1996). Conversely, within a rabbit stenting model transient depletion of macrophages by the systemic administration of a single dose of liposomal alendronate significantly reduced neointimal size (Danenberg et al., 2003). Not only do the presence of macrophages contribute to neointimal bulk but also the liberation of reactive oxygen species, growth factors and cytokines which promote VSMC proliferation and ECM deposition (Chen et al., 2004). More recently, the polarisation state of macrophages within the neointima has been demonstrated to be of considerable importance in the generation of NIH. Higher M1 to M2 ratio have been associated with an increase in NIH following vascular injury (Lavin et al., 2014). Concordantly, where defective M2 polarisation has been induced by genetic manipulation, an increase in NIH has also been observed (Lavin et al., 2014).

The findings presented in chapter 4 demonstrated an altered inflammatory phenotype within the stented grafts of miR-21 KO mice. We hypothesised that the absence of miR-21 may be responsible for not only the altered inflammatory response but consequently the reduction in neointima observed in miR-21 KO mice. Therefore, further work was undertaken to elucidate the role played by miR-21 in macrophage polarisation and function.

5.2 Aims

Characterise the response to polarisation of macrophages taken from miR-21 WT and KO mice.

Assess the effect of polarisation on the expression of miR-21 and its targets in M1 and M2 macrophages.

Determine any differences in cytokine production and the putative effect on other cell types present within the developing neointima.

5.3 Methods

5.3.1 Characterisation of bone marrow derived macrophages from miR-21 WT and KO mice.

Bone marrow derived monocytes were isolated and cultured as described in Chapter 2 followed by polarisation into an M1 or M2 state using LPS or IL-4, respectively unless otherwise stated. Characterisation of macrophages in different polarisation states was undertaken in order to identify differences between those macrophages derived from miR-21 WT and KO mice as outlined in Figure 5-46, using the following techniques;

1. Assessment of validated gene expression markers of polarisation by RT-qPCR.
2. Determination of cell surface marker expression by flow cytometry.
3. Assessment of cytokine production.
4. Effect of conditioned media from macrophages on proliferation of VSMCs.
5. Assess expression of miR-21 and its targets by RT-qPCR.

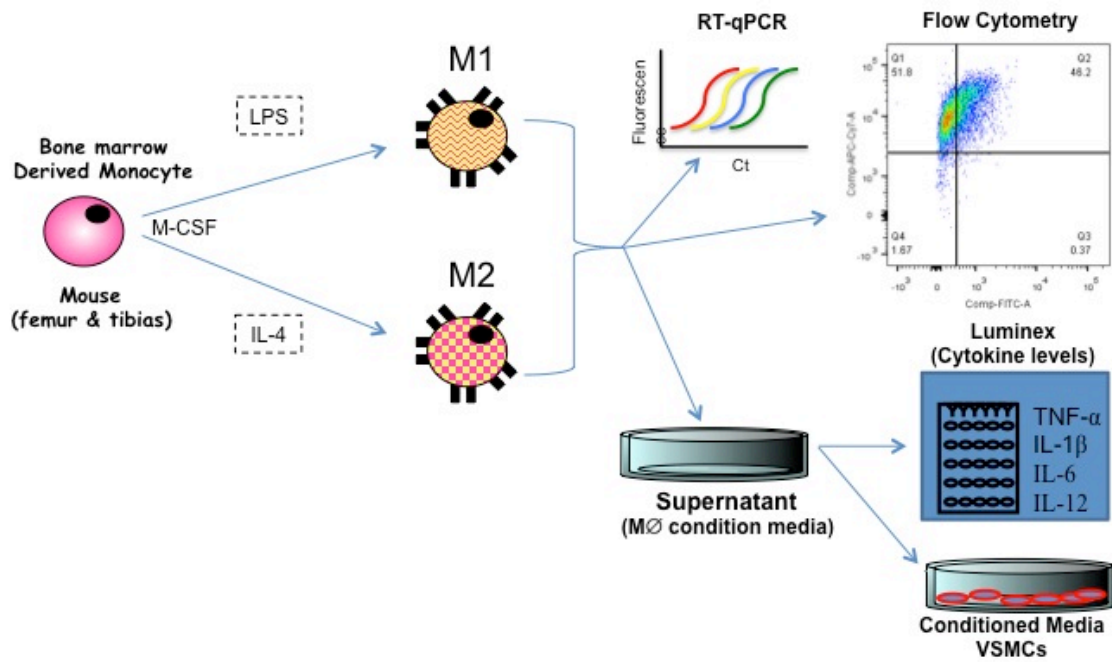


Figure 5-46. Investigation of miR-21 WT and KO Macrophages. Bone marrow derived monocytes were isolated and cultured in presence of M-CSF to produce macrophages. Macrophages then polarised to M1 or M2 states with LPS and IL-4, respectively. Cells and supernatants assessed by flow cytometry, Luminex assay, and RT-qPCR.

5.4 Results

5.4.1 Assessment of validated gene expression markers of polarisation by RT-qPCR.

No obvious difference was observed by light microscopy between miR-21 WT and KO bone marrow derived macrophages in either their unpolarised (M0), M1 or M2 polarised states, Figure 5-47.

5.4.1.1 Investigation of Potential Housekeeping genes in murine macrophages

RT-qPCR was conducted on RNA isolated from macrophages cultured from miR-21 WT and KO mice. The constant expression of three potential housekeeping genes: 18S, GAPDH and Tbp were assessed and were found to have mean cycle thresholds (+/-standard deviation) of, 11.52 (\pm 0.56), 15.83 (\pm 0.87), 24.75 (\pm 0.39), respectively, Figure 5-48. GAPDH was more highly expressed in macrophages than VSMCs (Ct \sim 20), see Chapter 4, but had the greatest standard deviation. Tbp had the smallest standard deviation ($<$ 0.5) and was thus taken forward for use as housekeeper when quantifying gene expression in macrophages from the miR-21 WT and KO colony, Figure 5-48.

5.4.1.2 Relative Expression of Macrophage Polarisation Markers

Successful polarisation of bone marrow derived macrophages to either an M1 or M2 state with LPS or IL-4, respectively, was confirmed by the expression of a panel of validated markers by RT-qPCR, Figure 5-49. M1 polarised macrophages showed appropriate up-regulation of inducible nitric oxide synthase (NOS2) and down-regulation of PPAR γ , while up-regulation YM-1 and Retnla was observed in M2 polarised macrophages, Figure 5-49.

M0 unstimulated miR-21 KO macrophages had significantly higher PPAR γ (M2 marker) expression than their WT counterparts (2.54 ± 0.46 fold higher vs. WT, $p < 0.01$), Figure 5-50.

In addition, a significant difference was observed in the NOS2 : Arginase1 mRNA expression ratio, with the ratio in miR-21 WT being significantly greater than that in KO macrophages (20.6 ± 6.52 fold vs 2.7 ± 1.24 , $p < 0.001$), Figure 5-50.

The significant differences noted at baseline in PPAR γ expression levels and in NOS2 : Arginase1 ratio in response to LPS indicates miR-21 KO macrophages shift towards an M2 polarisation state and are less responsive to traditional stimuli of M1 polarisation. This may at least partially account for the preponderance of M2 macrophages identified within neointima of miR-21 KO stented grafts, see Chapter 4.

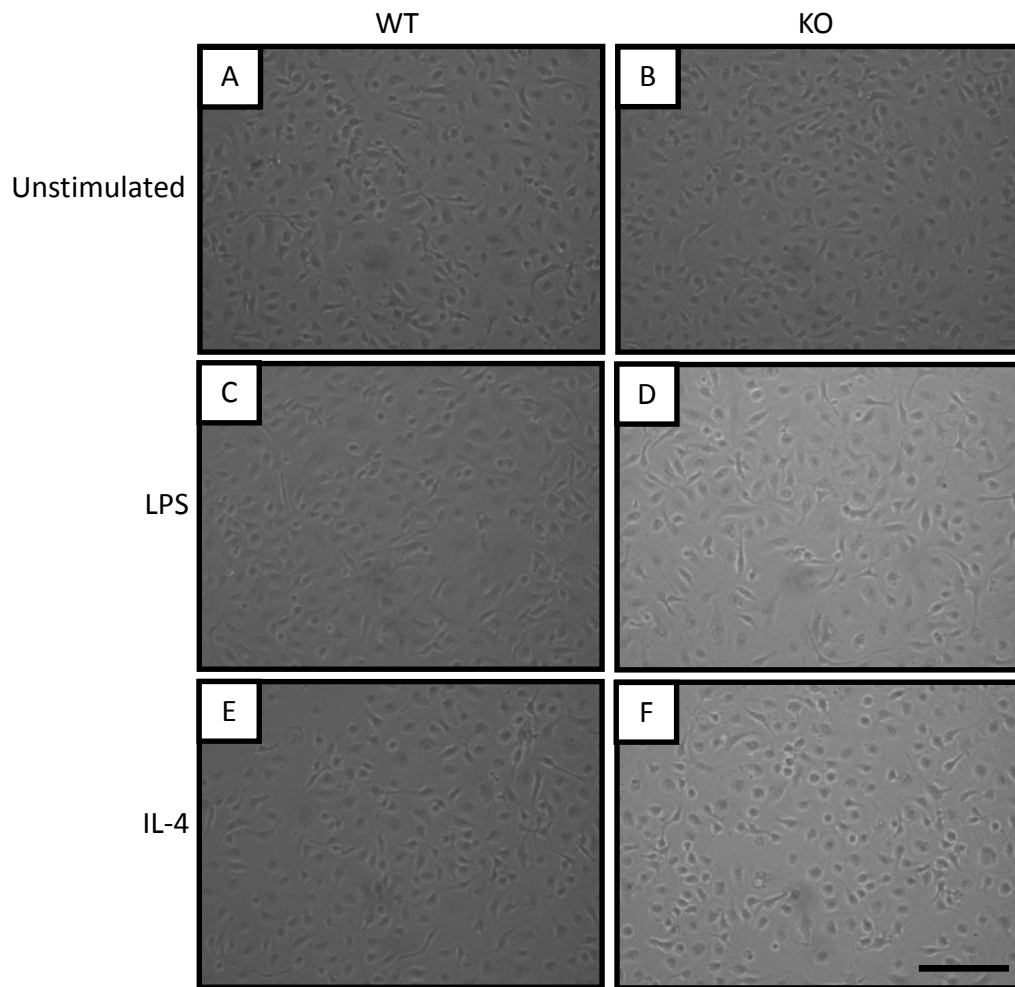


Figure 5-47. miR-21 WT and KO Macrophages. Light microscopy of bone marrow derived macrophages cultured for 6 days then stimulated with LPS or IL-4. A and B, Unstimulated controls (M0) miR-21 WT and KO respectively. C and D, LPS stimulated (M1) miR-21 WT and KO, respectively. E and F, IL-4 stimulated (M2) miR-21 WT and KO, respectively. Scale bar = 100 μ m.

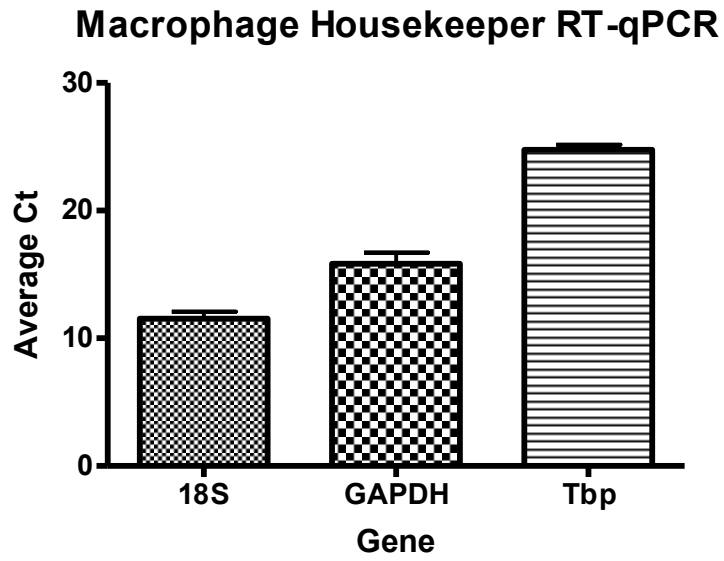


Figure 5-48. Macrophage House Keeper Gene RT-qPCR. Average cycle threshold (Ct) values for three housekeeping genes in miR-21 WT and KO macrophages. Data presented mean \pm SD. Tbp, Tata-box binding protein. Biological n=5, technical triplicates. Statistics performed on biological data.

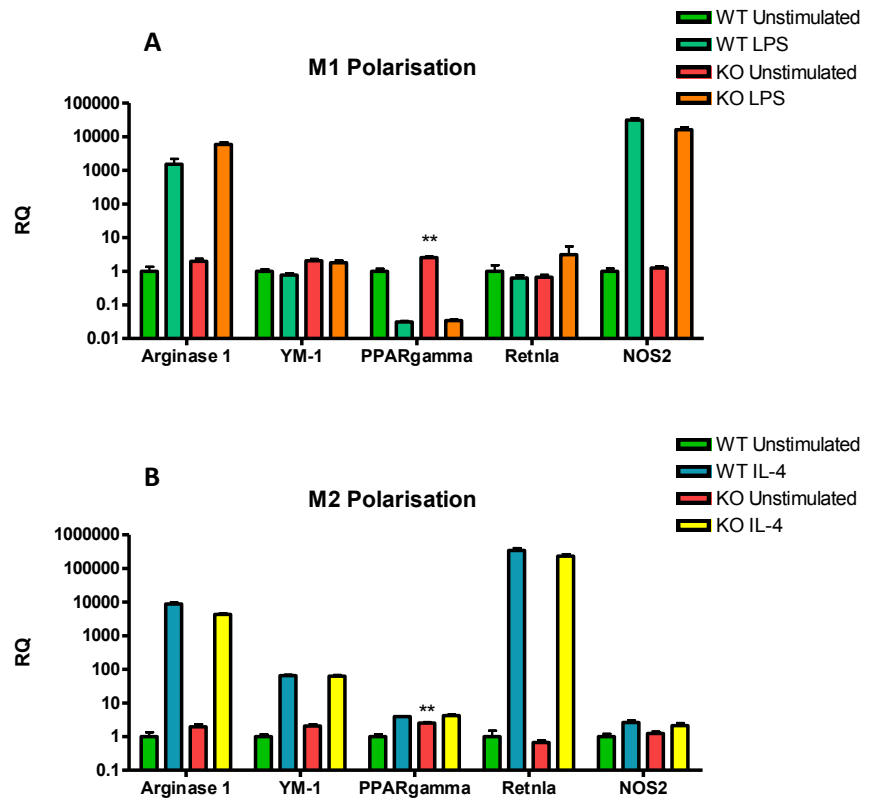


Figure 5-49. Macrophage Polarisation Markers. A, Relative polarisation marker expression following LPS stimulation by RT-qPCR. B, Relative polarisation marker expression following IL-4 stimulation by RT-qPCR. RQ = Relative Quantity. Biological n=5, technical triplicates. Statistics performed on biological data. **p<0.01, vs. WT unstimulated.

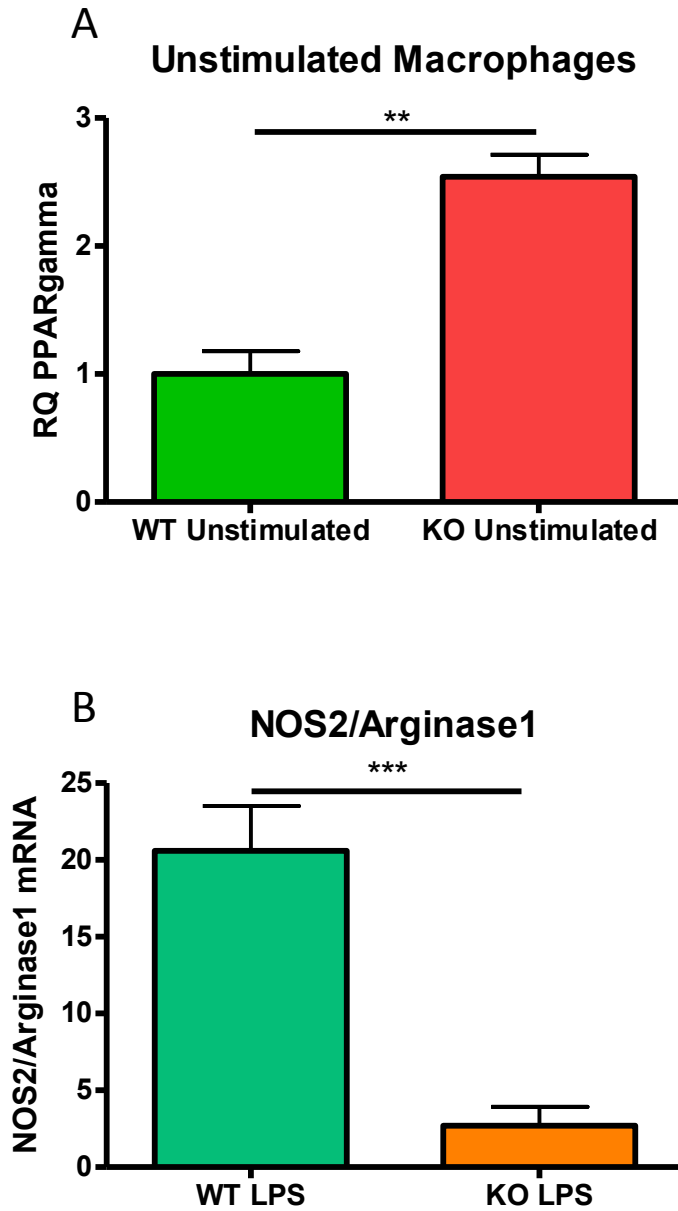


Figure 5-50. Macrophage Polarisation. A, PPAR γ expression in unstimulated macrophages. C, NOS2/Arginase1 ratio miR-21 WT and KO macrophages stimulated with LPS. Biological n=5, technical triplicates. Statistics performed on biological data. **p<0.01, ***p<0.001 vs. WT.

5.4.2 Cell Surface Marker Expression on miR-21 WT and KO Macrophages Following Polarisation with LPS or IL-4.

Flow cytometry was used to investigate the expression of a panel of cell surface markers commonly associated with M1 and M2 polarisation. Figure 5-51 shows the gating strategy used to identify macrophages.

As with genomic markers detailed in section 5.4.1.2, staining showed appropriate changes in cell surface expression according to macrophage polarisation state. M1 macrophages up regulated MHC II, the co-stimulatory molecule CD86, TLR2, and CD69. M2 macrophages demonstrated elevated expression of CD206 and CD11c, with a reduction in TLR2.

A significant difference in CD69 expression between miR-21 WT and KO polarised macrophages was observed, with CD69 being more highly expressed in miR-21 WT compared to KO M1 macrophages (1.8 fold, $p < 0.05$), see Figure 5-52. Interestingly CD69 is an early activation marker induced in macrophages in response to TLR signalling by miR-21 (Fabbri et al., 2012). Representative scatter plots for CD69 are shown **Error! Reference source not found.**

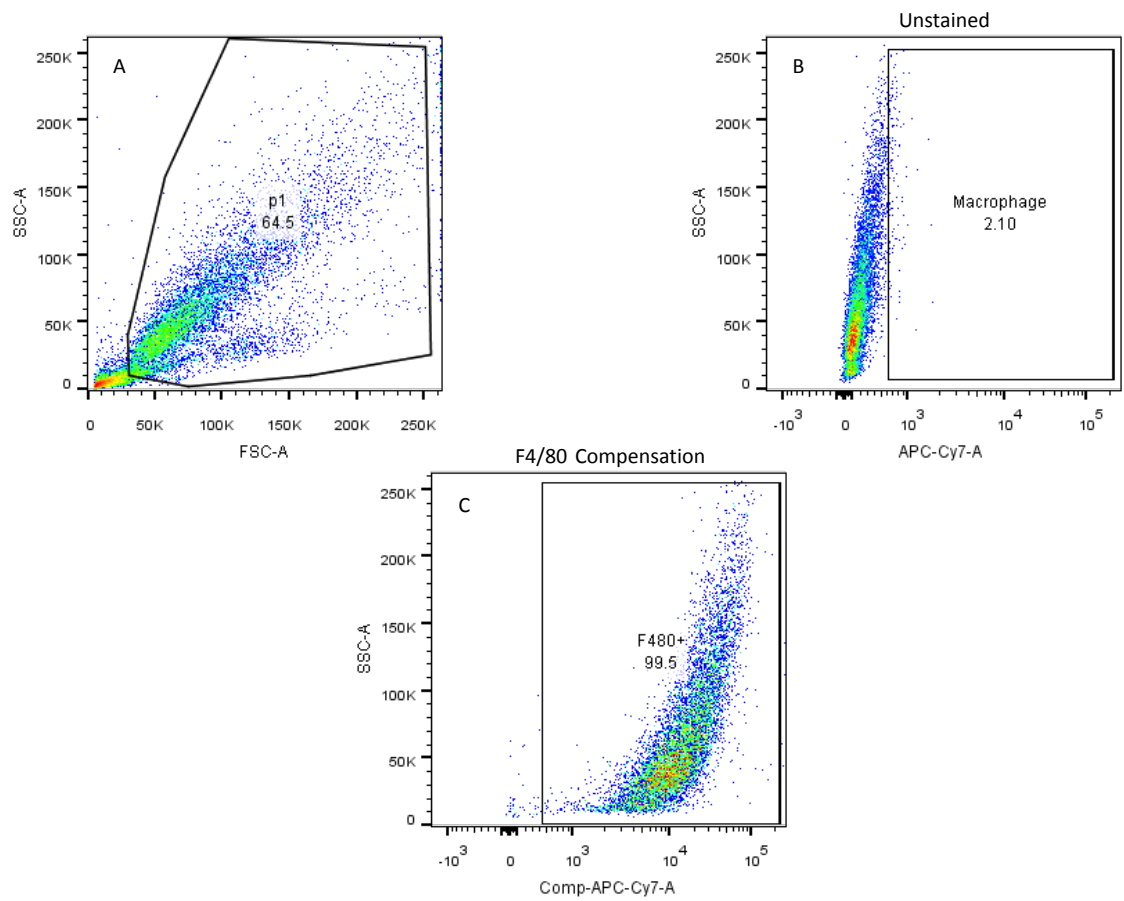


Figure 5-51. Macrophage Flow Cytometry Gating Strategy. A, Total events with gate around cells of interest. B, Unstained sample. C, Macrophages stained with anti F4/80-APC-Cy7.

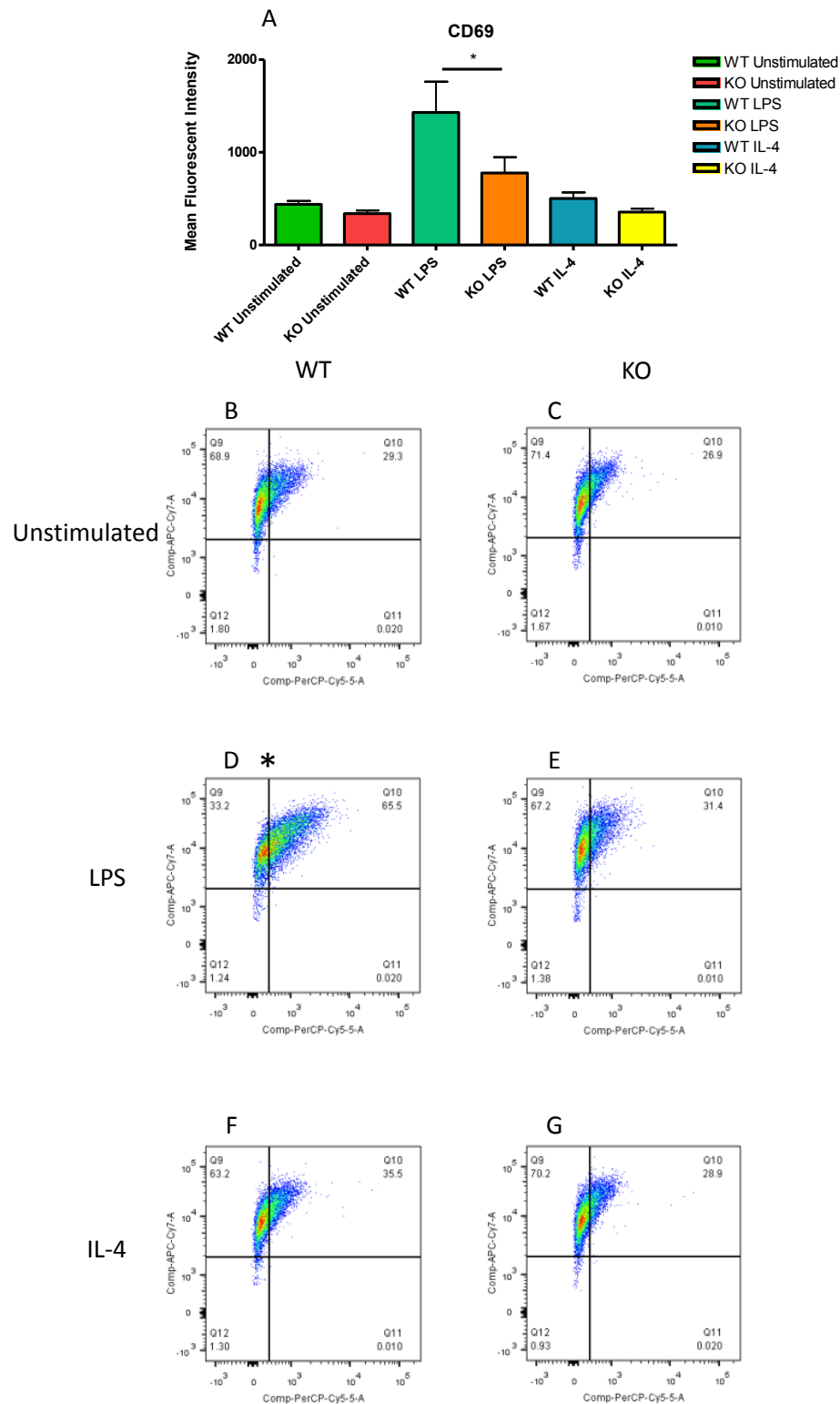


Figure 5-52. CD69 macrophage staining. A. Mean fluorescent intensity of cell surface markers on miR-21 WT and KO macrophages. Representative Scatterplots. **B** and **C**, unstimulated WT and KO, respectively. **D** and **E**, LPS stimulated WT and KO, respectively. **F** and **G**, IL-4 stimulated WT and KO, respectively. * $p < 0.05$ vs LPS. X-axis CD69-PerCP-Cy5.5, y-axis F4/80-APC-Cy7. Biological $n = 9$ for both WT and KO groups, technical duplicates. Statistics performed on biological data. * $p < 0.05$.

5.4.3 Cytokine Production from miR-21 WT and KO Macrophages

Cytokine levels were measured in media from unstimulated (M0), M1 (LPS treated) and M2 (IL-4 treated) macrophages from miR-21 WT and KO mice.

As expected, the level of many pro-inflammatory cytokines was increased upon LPS stimulation including IL-1 α and β , IL-6, IL-12, IP-10, KC, MCP-1 and TNF α ,

Figure 5-53.

Several cytokines known to play a role in stimulating fibrosis and VSMC proliferation were expressed more highly by LPS treated macrophages from miR-21 WT than KO mice. IL-1 α , IL-1 β and MIP-1 α concentrations were greater within media from WT compared to KO macrophages (203 ± 50 pg/mL vs. 86 ± 23 pg/mL, $p < 0.01$) (111 ± 21 vs. 56 ± 7.5 pg/mL, $p < 0.01$) and (21556 ± 4291 pg/mL vs 12056 ± 3107 pg/mL, $p < 0.05$),

Figure 5-53. Interleukin-6, IL-12 and TNF α were also higher from WT than KO macrophages (3340 ± 461 pg/mL vs. 2098 ± 511 pg/mL, $p < 0.05$), (1323 ± 280 pg/mL vs. 540 ± 126 pg/mL, $p < 0.001$), (6772 ± 1544 pg/mL vs. 3584 ± 821 pg/mL, $p < 0.05$),

Figure 5-53. Additionally the IL-12 : IL-10 ratio for LPS-stimulated miR-21 WT macrophages was almost double that of KO macrophages (24 vs. 13).

A statistically significant difference in MIG concentrations between miR-21 WT and KO macrophages was also observed (25.3 ± 8.0 pg/mL vs. 7.8 ± 2.7 pg/mL, respectively, $p < 0.05$), in many samples, from both WT and KO macrophages, the concentration was below the level of detection and thus its biological significance is uncertain.

Unstimulated macrophages, as well as those stimulated with IL-4, exhibited minimal cytokine production with no significant difference noted between genotypes, Table 5-10.

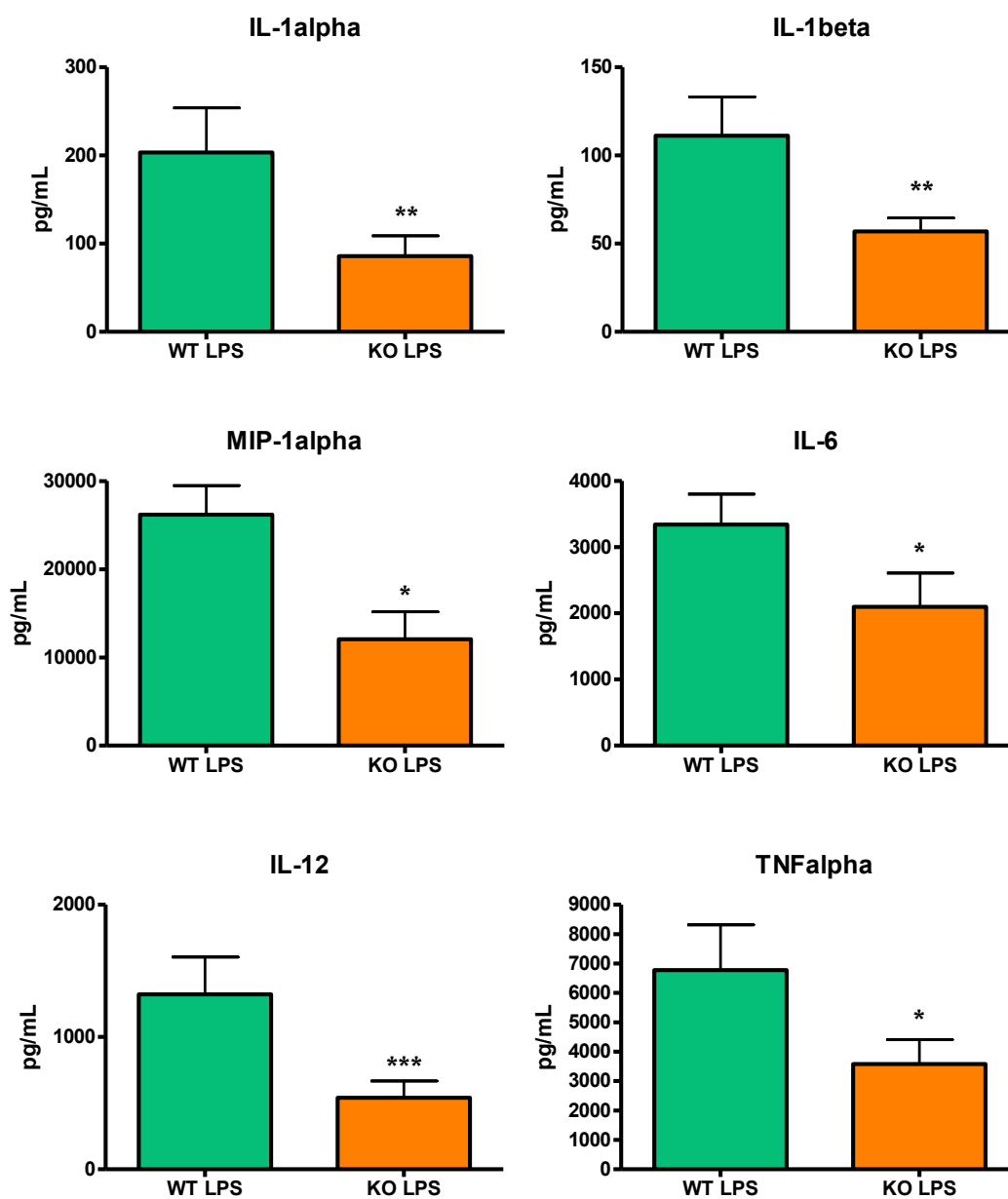


Figure 5-53. Cytokine production from LPS stimulated macrophages. Measured by Luminex assay. Biological n=9 for both WT and KO groups, technical triplicates. Statistics performed on biological data. *p<0.05, **p<0.01, ***p<0.001 vs. WT.

Table 5-10. Cytokine Production from WT and KO macrophages

Cytokine	WT Untimulated	KO Unstimulated	WT IL-4	KO IL-4
IL-1alpha	12.9	12.9	12.9	12.9
IL-1beta	10.3	6.9	14.1	10.2
IL-2	2.4	2.4	2.4	2.8
IL-4	28.4	13.8	2781.6	2255.3
IL-5	12.1	13.9	77.0	166.3
IL-6	9.4	9.8	8.2	9.8
IL-10	15.9	16.3	15.9	20.2
IL-12	4.9	5.0	19.5	33.1
IL-13	6.4	8.2	7.5	8.2
IL-17	2.4	2.4	2.4	2.4
FGFbasic	84.7	56.7	85.3	64.6
GM-CSF	6.2	6.2	6.2	6.2
IFN-gamma	5.3	5.3	8.5	6.1
IP-10	14.9	39.9	14.9	16.7
KC	29.6	26.1	22.6	22.6
MCP-1	10.2	13.9	95.5	204.1
MIG	3.3	2.7	3.5	3.0
MIP-1alpha	17.8	14.7	24.1	22.3
TNFalpha	14.7	15.3	22.8	17.2
VEGF	4.1	8.0	1.5	1.6

Biological n=9 for both WT and KO groups, technical triplicates. All measurements in pg/mL.

5.4.4 Effect of conditioned media from cultured miR 21 WT and KO macrophages on VSMC

Quiesced VSMCs from miR-21 WT and KO mice were used to assess the effect of conditioned media from polarised WT and KO macrophages on proliferation. BrdU incorporation as a surrogate marker of proliferation was conducted as described in Chapter 2. 0.2% FCS and 10% FCS were used as negative and positive controls, respectively.

Figure 5-54 shows BrdU incorporation relative to VSMCs quiesced in 0.2% FCS. As expected an increase in BrdU incorporation was observed in VSMCs stimulated with 10% FCS. Exposure of VSMCs to conditioned macrophage media taken from all experimental conditions resulted in poor BrdU incorporation. No significant difference in proliferation was observed when comparing conditioned media from miR-21 WT and KO macrophages in VSMCs of either genotype,

Figure 5-54.

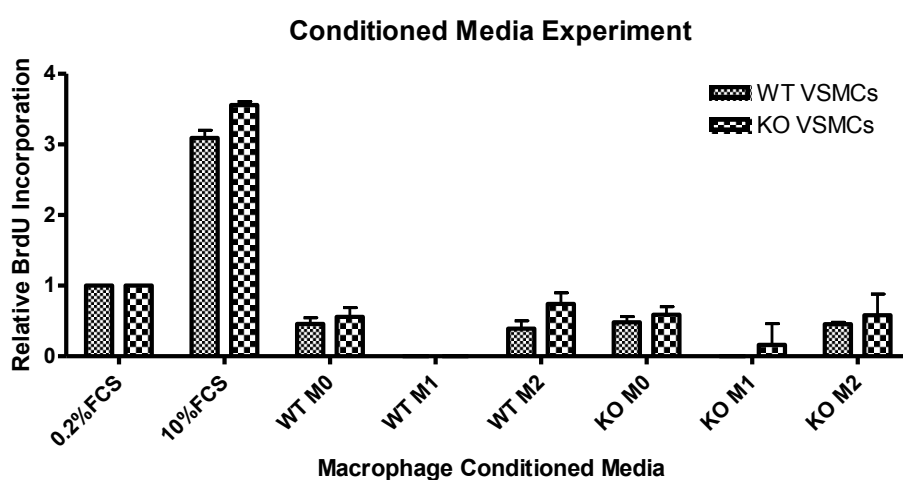


Figure 5-54. Effect of conditioned media from miR-21 WT and KO macrophages on the proliferation of VSMCs. Biological triplicates for both WT and KO groups, technical duplicates. Statistics performed on biological data.

5.4.5 Effect of macrophage polarisation on miR-21 expression

The effect of LPS and IL-4 polarisation on miR-21 expression was also studied. Relative to unstimulated macrophages, LPS and IL-4 both induced an up-regulation of miR-21(-5p) (3.00 ± 0.23 fold, $p < 0.05$ and 4.74 ± 0.13 fold, $p < 0.01$, respectively), Figure 5-55. Additionally, relative to untreated macrophages significant increases in miR-21-3p was also observed with LPS and IL-4 treatment (4.38 ± 0.52 fold and 4.88 ± 0.43 fold, respectively, $p < 0.05$ for both), Figure 5-55.

No difference was observed between LPS or IL-4 treatments for miR-21(-5p) or miR-21-3p levels. However, it was noted that compared to miR-21(-5p), miR-21-3p levels were markedly lower, with average cycle threshold values of ~ 20 compared to ~ 33 , respectively.

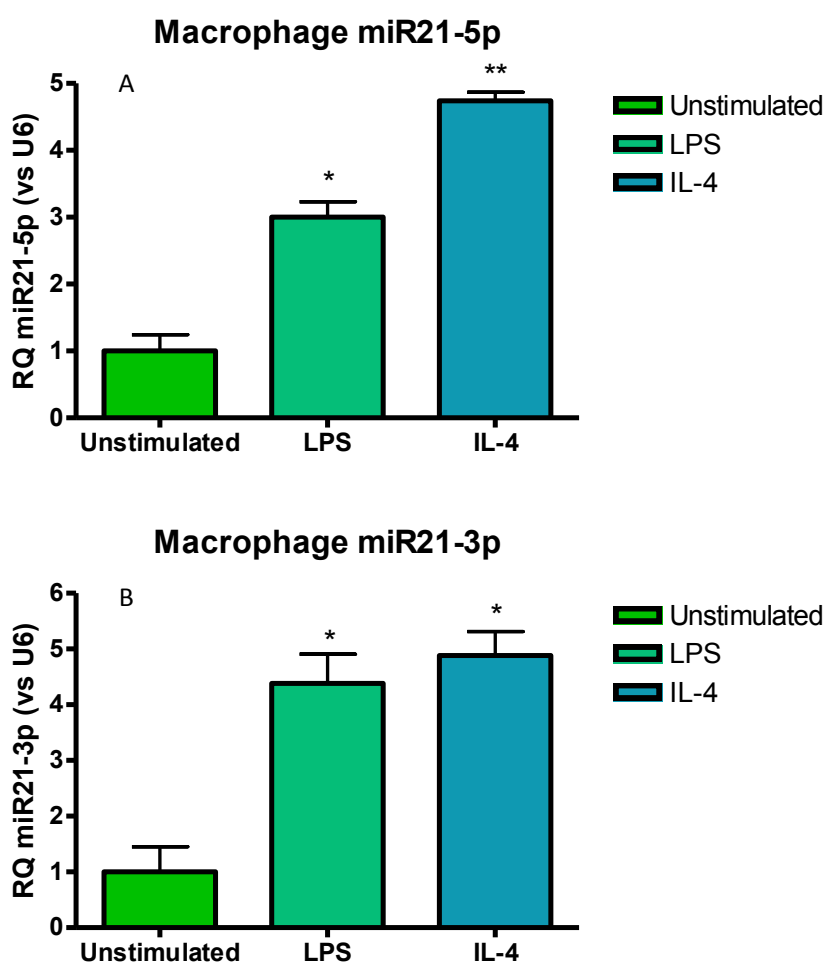


Figure 5-55. MiR-21 Expression. RT-qPCR for miR-21. A, miR-21(-5p). B, miR-21-3p(star). * $p < 0.05$, ** $p < 0.01$ vs. unstimulated. Biological triplicates, technical triplicates. Statistics performed on biological data.

5.4.6 Effect of LPS and IL-4 induced up-regulation of miR-21 in macrophages on known targets.

Having shown that miR-21 is up-regulated in macrophages following LPS and IL-4 treatment, further evidence of its role in mediating the effects through target repression was sought. RT-qPCR was conducted on a panel of known miR-21(-5p) targets validated in various cell types. Of these target genes PDCD4, PTEN and IL-12p35 have been previously validated in macrophages. Additionally, the relative expression of these targets was also evaluated in LPS and IL-4 treated macrophages from miR-21 KO mice.

Upon LPS stimulation, miR-21 WT and KO macrophages demonstrated greater than 3700-fold and 1700-fold increases in IL-12p35, respectively. STAT 3 was also up regulated by LPS exposure in miR-21 WT and KO macrophages, 4.9-fold and 3.6-fold, respectively. No significant difference was found between genotype, Figure 56.

While PDCD4 was down-regulated following LPS stimulation in miR-21 WT macrophages compared to unstimulated controls, a similar pattern was also observed in miR-21 KO macrophages, (88% and 82% reduction, respectively, $p < 0.001$ for both), Figure 56.

Four targets genes BMPR2, PPAR α , TIMP3 and PTEN showed no significant change in their expression levels despite an increase in miR-21.

No significant difference in putative target gene expression was observed between miR-21 WT and KO macrophages.

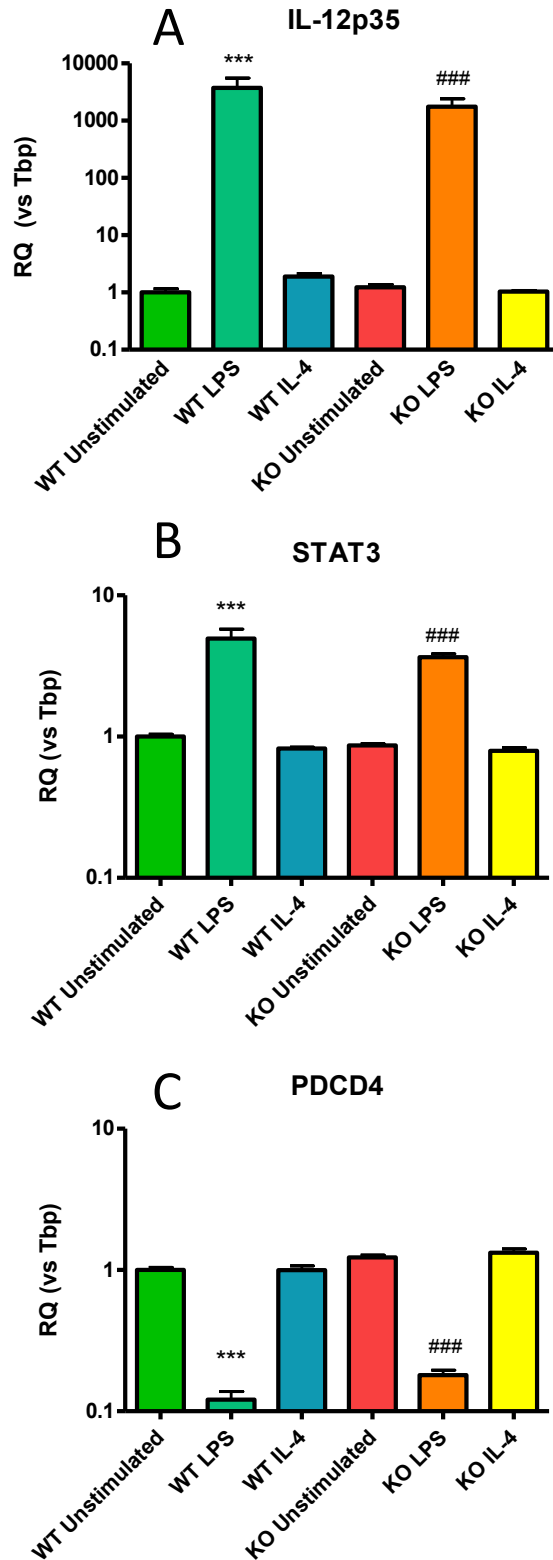


Figure 56. Macrophage miR-21(-5p) target expression. Unstimulated, LPS stimulated, IL-4 stimulated miR-21 WT and KO macrophages. A, IL-12p35. B, STAT3. C, PDCD4, Data RQ+/-rqmax *p<0.001 vs. WT unstimulated. ###p<0.001 vs. KO unstimulated. Biological n=5, technical triplicates for both WT and KO. Statistics performed on biological data.**

5.4.7 Cell surface marker expression on miR-21 WT and KO macrophages following culture in presence of stainless steel

Having assessed cell surface marker expression in M1 and M2 polarised macrophages, following exposure to classic polarising stimuli (LPS and IL-4), a pilot experiment (n=1, for each, miR-21 WT and KO) was conducted to assess if these markers would change in the presence of metal. To mimic, *in vitro*, the effect a bare metal stent may have on macrophage polarisation *in vivo*, stainless steel metal discs were placed in the wells of 6 well plates used during the generation of macrophages and during polarisation. M1 polarisation was achieved with the addition of LPS (100 ng/mL) and IFN γ (100 units/mL) rather than LPS alone. M2 polarisation was conducted as before with IL-4 (2 ng/mL).

Figure 5-12 shows representative photographs of macrophages at day 4 of culture with and without metal discs. Clumping of macrophages around the edge of the metal disc was observed. Figure 5-13 shows representative photographs from miR-21 WT and KO polarised macrophages at day 7 with and without the presence of the metal disc.

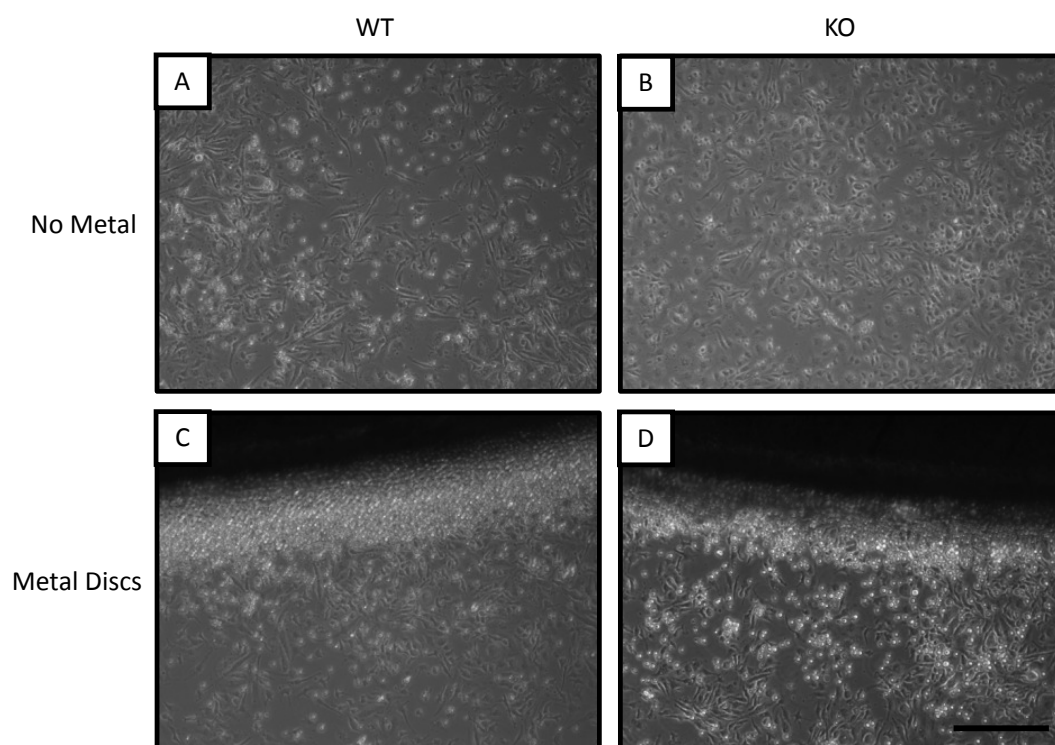


Figure 5-12. Macrophage culture. Unpolarised macrophages, day 4 in M-CSF, with and without presence of stainless steel metal discs. A and B, No metal discs, miR-21 WT and KO, respectively. C and D, Metal discs (black), miR-21 WT and KO, respectively. Scale bar = 100 μ m.

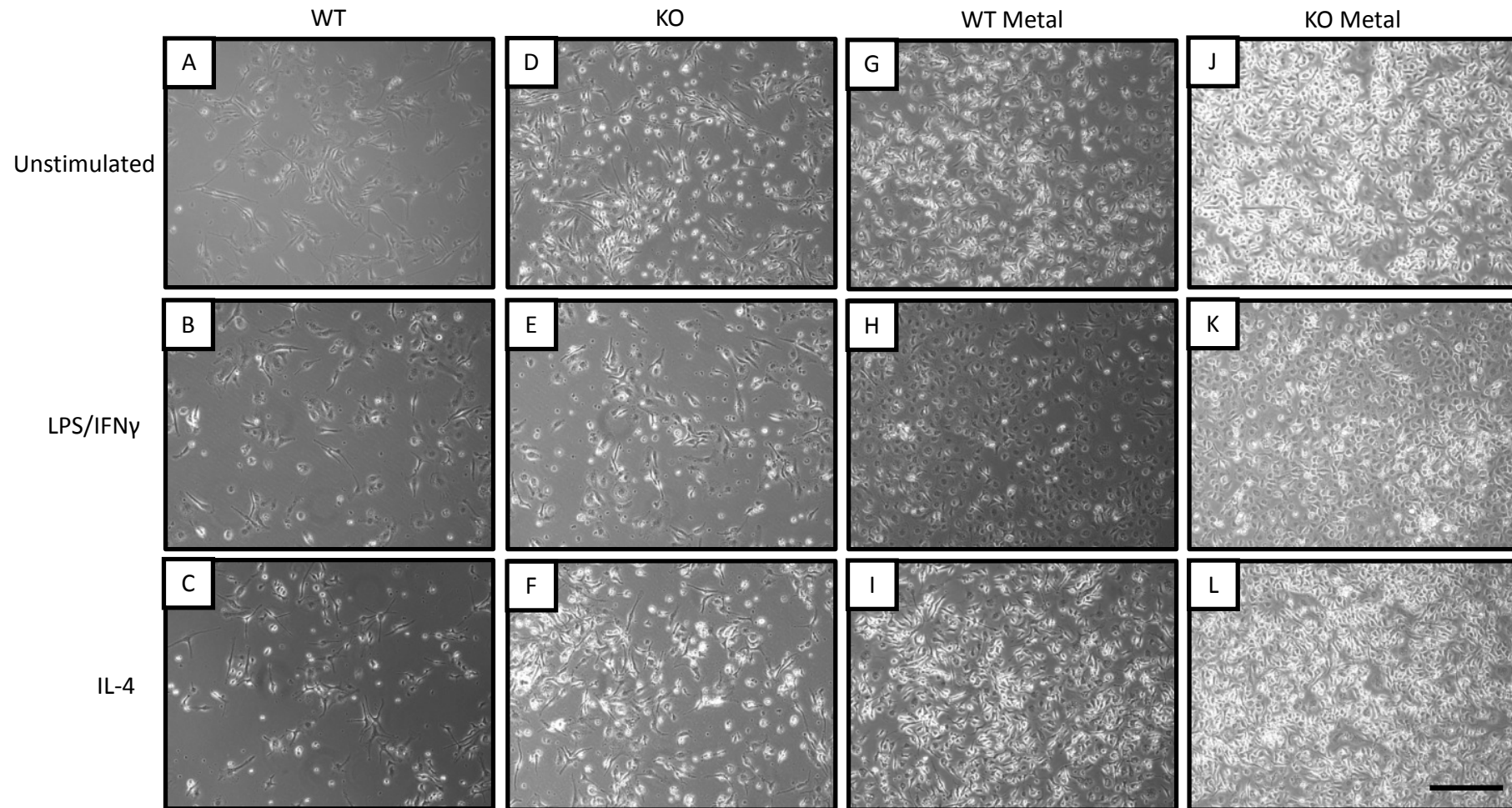


Figure 5-13. Polarised macrophages with and without presence of stainless steel. A, B and C, miR-21 WT unstimulated, LPS/IFN γ and IL-4, respectively. D, E and F miR-21 KO unstimulated, LPS/IFN γ and IL-4, respectively. G, H and I, miR-21 WT with stainless steel, unstimulated, LPS/IFN γ and IL-4, respectively. J, K and L, miR-21 KO with stainless steel, unstimulated, LPS/IFN γ and IL-4, respectively. Scale bar = 100 μ m.

Analysis of cell surface marker expression was undertaken by flow cytometry as in section 0.

Mean fluorescent intensity analysis demonstrated that across polarisation stimuli and genotype the presence of metal discs either had little effect on, or diminished the expression of CD86, TLR2, MHCII, CD11c and CD69. Using CD69 as a representative example, Figure 5-57 demonstrates cell surface marker staining in the presence and absence of metal.

This pilot data would require to be repeated in order to ascertain any effect the stainless steel may have on macrophage polarisation.

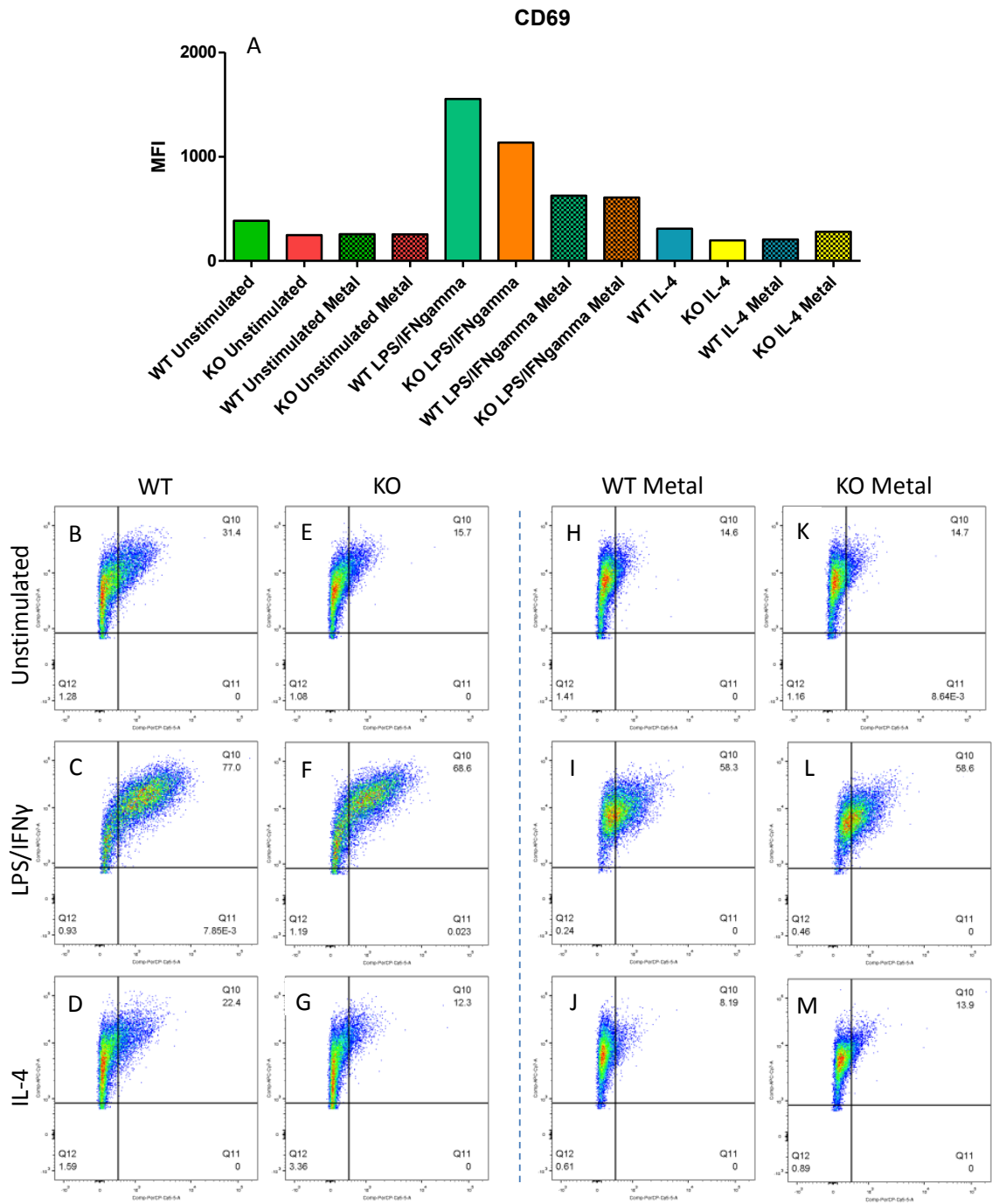


Figure 5-57. CD69 Expression. MFI of cell surface marker on miR-21 WT and KO macrophages in presence and absence of stainless steel discs. **A**, Summary data. **B**, **C** and **D**, WT without metal, unstimulated, LPS/IFN γ , and IL-4, respectively. **E**, **F** and **G** KO without metal, unstimulated, LPS/IFN γ , and IL-4, respectively. **H**, **I** and **J**, WT with metal, unstimulated, LPS/IFN γ , and IL-4, respectively. **K**, **L** and **M**, KO with metal, unstimulated, LPS/IFN γ , and IL-4, respectively. X-axis CD69-PerCP-Cy5.5, y-axis F4/80-APC-Cy7. Biological n=1 for both WT and KO, technical duplicate.

The results presented above demonstrate that unstimulated miR-21 KO macrophages express lower levels of PPAR γ than miR-21 WT macrophages. In addition, miR-21 WT macrophages stimulated with the classical M1 stimulus LPS expressed significantly higher levels of CD69 and several pro-inflammatory cytokines including IL-1 α and β , IL-6, IL-12, IP-10, KC, MCP-1 and TNF α than their miR-21 KO counterparts.

5.5 Discussion

The data presented within this chapter show that although stimulation with LPS and IL-4 did not significantly alter M1 and M2 polarisation marker expression between miR-21 WT and KO, the absence of miR-21 alters the inflammatory cytokine response of bone marrow derived macrophages. These findings suggest miR-21 modulates macrophage phenotype, its absence directs them away from an inflammatory bactericidal role towards an anti-inflammatory (M2) tissue healing state.

Characterisation of unstimulated macrophages demonstrated an increase in basal expression of the validated M2 marker PPAR γ , in mir-21 KO macrophages compared to their WT counterparts. These findings are particularly relevant in the setting of inflammatory vascular disease since a number of studies suggest that activation of PPAR γ can diminish the inflammatory response in both macrophages and VSMCs (Jiang et al., 1998, Marx et al., 1998, Shu et al., 2000). Activation of PPAR γ in human macrophages reduces MMP-9 activity and inhibits IL-1 β , IL-6, TNF α expression. Furthermore, a number of groups have reported that PPAR- γ agonists inhibit the development of atherosclerosis and reduce inflammatory markers in ApoE KO mice (Collins et al., 2001, Li et al., 2000).

Additionally, the response of miR-21 KO macrophages to LPS, a classical (M1) inflammatory stimuli is attenuated as evidenced by a reduction in NOS2:Arg1 ratio. NOS2:Arg1 ratio is a commonly reported parameter of macrophage polarisation state and its relative reduction suggests miR-21 KO macrophages display a less extreme M1 phenotype upon LPS stimulation. Despite early studies showing a direct correlation between macrophage content and neointimal size recent evidence suggests macrophages play an important role in the healing process and that polarisation state may be as or more important than merely their presence. Recently published work has identified key roles played by macrophages in EC differentiation and the prevention of thrombosis (Wong et al., 2014). It has also been found that M1 macrophages, in particular the presence of high M1 to M2 ratios, are likely to contribute to the development of larger neointima (Lavin et al., 2014). In addition, investigators determined that either defective M2 polarisation or the repolarisation of macrophages from a M2 to M1 phenotype increased NIH size (Lavin et al., 2014).

Cytokine profiling of M1 polarised macrophages following LPS stimulation showed a reduced capacity of miR-21 KO macrophages to secrete numerous pro-inflammatory cytokines including IL-1, IL-6, TNF α and IL-12. These results may explain the effect of altered macrophage phenotype between miR-21 WT and KO mice and hence differences in NIH development presented in chapter 4. Interleukin-1 α stimulation of VSMCs has been shown to induce the expression of a cascade of proinflammatory cytokines including, IL-6 and TNF α (Clarke et al., 2010). Interleukin-1 β has not only been shown to increase VSMC proliferation but also to stimulate the expression of fibronectin, an ECM component known to aid the transformation of VSMCs from contractile to synthetic state (Forsyth et al., 1997). Additionally, IL-6 and TNF α have been shown to stimulate the proliferation and migration of VSMCs, respectively (Ikeda et al., 1991, Goetze et al., 1999). Thus within the current study the reduction in cytokine release from miR-21 KO macrophages is likely to contribute to the reduction in VSMC proliferation, ECM deposition and NIH size observed.

Furthermore, phenotyping of surface receptors from BMDM also demonstrated a reduction in the expression of CD69 in miR-21 KO macrophages. It has been shown that miRs including miR-21 can activate Toll-like receptors (Fabbri et al., 2012). TLR7 and its human equivalent TLR8 are intracellular TLRs functioning to identify ssRNA which, via NF κ B signalling induce the expression of CD69 as well as cytokines such as IL-6 and TNF α (Fabbri et al., 2012). Thus the absence of miR-21 and hence TLR7/8 activation may account for the reduced CD69 expression, IL-6 and TNF α observed. In addition, the reduction in CD69 may also contribute to the reduction in inflammatory cytokine secretion since previous studies have reported that activation of CD69 mediates a number of inflammatory processes such as nitric oxide production and release of TNF α from murine macrophages and T-cells (Marzio et al., 1997, Santis et al., 1992).

The use of unconcentrated conditioned media likely containing low absolute concentrations of cytokines may have resulted in the poor proliferative response observed. Further experiments utilising concentrated media may increase proliferation observed. An alternative approach would be to utilise co-culture experiments in order to assess the effect of paracrine signalling between macrophages and VSMCs with respect to genotype.

Both M1 and M2 polarised macrophages demonstrated up regulation of miR-21. The work presented in this chapter confirms that of others who have demonstrated that LPS stimulation increases miR-21 levels (Sheedy et al., 2010, Zhou et al., 2010). It is important to note that only the mature form of miR-21 was assessed in the current study. While it could be surmised that the increase in miR-21 may be as a result of increased transcription from the LPS-induced NF κ B binding to the miR-21 promoter, an increase in miR-21 due to pre-miR-21 processing cannot be excluded. In addition, IL-4 stimulation was also found to increase miR-21 expression. Taken together these findings suggest miR-21 expression may be increased upon immune activation rather than polarisation to a specific state.

Despite up regulation of miR-21 upon LPS and IL-4 stimulation no differential change in the expression of known targets between miR-21 WT and KO macrophages could be demonstrated. This was clearly illustrated in the assessment of PDCD4 which, while being significantly down regulated in LPS stimulated WT macrophages was also significantly lower in corresponding miR-21 KO samples. In addition, no reduction in PDCD4 was observed in M2 polarised WT macrophages that would have been expected given the increase in miR-21 expression. Thus within macrophages it is likely that the down regulation of PDCD4 by LPS is through a miR-21 independent mechanism. These findings would appear to contradict data from previously published studies showing, in both a murine macrophage cell line and human peripheral blood mononuclear cells, miR-21 was key to down regulation of PDCD4 following LPS stimulation (Sheedy et al., 2010). Investigators demonstrated that upon LPS stimulation the addition of anti-miR-21 increased PDCD4 expression and conversely the addition of a miR-21 mimic reduced PDCD4 (Sheedy et al., 2010). It would appear LPS can reduce PDCD4 expression by both miR-21-dependent and -independent pathways; the relative contribution of each may be highly dependent on the cell type and setting.

Strikingly, over a 1000-fold rise in IL-12 RNA of was observed following LPS stimulation of both miR-21 WT and KO macrophages. This is concordant with the findings of cytokine profiling demonstrating an increase of similar magnitudes at a protein level. Thus, while IL-12 has previously been validated as a miR-21

target within macrophages in a murine model of asthma it is not one within the present model of vascular stenting (Lu et al., 2011).

The pathophysiological relevance of LPS and IL-4 stimulation strategies to mimic the effects on macrophage polarisation *in vivo* within the murine stenting model is questionable and is a significant limitation of this study. Therefore, a pilot experiment investigating the effect of a metal stent on macrophage polarisation was undertaken. This revealed no obvious morphological differences in macrophages following exposure to stainless steel. While much work has been published on the effect of metal implants on macrophage cytokine release, little data on their effect on cell surface expression markers has been published. Investigating the effects of soluble and particulate stainless steel implants on innate immunity has been undertaken in the field of orthopaedic prosthetics. It has previously been demonstrated that soluble cobalt, chromium, and molybdenum (all constituents of stainless steel) induce the production of a cascade of pro-inflammatory cytokines through NF κ B activation (Lu et al., 2011). In addition, careful investigation has shown that within macrophages, metal salts as well as cobalt-chromium-molybdenum alloy particles induce reactive oxygen species generation, activating the inflammasome, which in turn activates caspase-1 and promotes the conversion of pro-IL-1 β to IL-1 β (Caicedo et al., 2009). It is likely that the stimulation of macrophages by metal implants is a diverse and complex process likely to result in a multitude of different and mixed polarisation states dependent on type of metal and tissue involved. It should be noted that the data presented in the current study is from a n=1 and would require to be repeated if any conclusions are to be drawn.

In summary, the results presented within this chapter demonstrate that the absence of miR-21 results in a propensity for macrophages to polarise towards an M2 phenotype. In addition, genetic deletion of miR-21 resulted in a reduction in the secretion of several pro-inflammatory cytokines upon classical M1 polarisation. While it was not possible to demonstrate a direct effect on putative target mRNA within macrophages, the effects could at least in part be explained by a reduction in intracellular TLR signalling with consequent reduction in IL-6, TNF α and CD69 expression due to the absence of miR-21. However, further work

would be required to confirm whether these effects are maintained *in vivo* and in the presence of metallic stents.

6 General Discussion.

This thesis contains research data demonstrating a significant increase in the understanding of the development of ISR. Firstly, the refinement of the murine stenting model and establishment within the Baker laboratory substantially increases our ability to study the development of ISR. In addition, refining the stent electrolysis and tissue processing in a small animal stenting model facilitates the discovery of novel cellular and molecular mechanisms responsible for the development of ISR. This is the first study to examine the role of microRNAs in the development of ISR and using miR-21 KO animals we were able to identify a crucial role played by miR-21 in the development of ISR. Careful *ex vivo* and *in vitro* analysis revealed putative mechanisms involving miR-21 in both VSMCs and the immune system, which contributed to the differences in ISR observed between miR-21 WT and KO animals.

Despite a significant reduction in its incidence across many western societies IHD remains an important cause of morbidity and mortality globally. Indeed within the UK IHD continues to place an enormous burden on the NHS. With an aging population this burden is only likely to increase (Bhatnagar et al., 2015). The two major manifestations of IHD, angina and myocardial infarction are commonly treated with a combination of pharmacological therapy and revascularisation. Significant changes in the revascularisation strategy adopted for many patients now means that far more undergo PCI rather than CABG. Indeed, recent figures show that over the last decade the number of CABG procedures performed in the UK has fallen by over one third. While over the same period PCI procedures have more than doubled to over 92,000 per year (BHF, 2014). This has been due not only to substantial improvements in interventional techniques and technologies but also increasing patient age and the presence of comorbidities, which have a significant impact on surgical mortality.

Early interventional procedures were dominated by balloon angioplasty, with the use of stents to prevent elastic recoil and acute vessel occlusion more widely adopted after the publication of the BENESTENT trial (Serruys et al., 1994). However, bare metal stent use appeared only to substitute the problem of elastic recoil for that of ISR, which often necessitated target vessel revascularisation. The development of drug eluting stents was heralded as a major advance in stent technology but their use was complicated by late stent thrombosis as a result of delayed and incomplete re-endothelialisation (Joner et

al., 2006). In addition, the initial polymers on which the antiproliferative drugs were impregnated caused a chronic inflammatory reaction as evidenced by a persistent local eosinophilia (Nebeker et al., 2006). Prevention of late stent thrombosis was achieved by prolonged dual antiplatelet use at the expense of an increased bleeding risk (Joner et al., 2006). Since the introduction TAXUS and Cypher first generation DES considerable advances in stent technology have been made, including the development of thinner stent struts, new antiproliferative medication and improvements in polymer biocompatibility as well as the development of biodegradable polymers (Puricel et al., 2015). More recently polymer free DESs have been developed (Urban et al., 2013). Taken together these improvements have been associated with reduced inflammation, thrombus formation and increased re-endothelialisation as well as allowing far shorter duration of dual antiplatelet use.

However, despite the improvements mentioned above ISR remains an important clinical problem particularly in those with diabetes (Abizaid et al., 1998). Treatment of ISR can be challenging and although several therapies have been trialled including cutting balloons, drug eluting balloons and further deployment of DES with the original stent no consensus has been reached as to optimal therapy (Lee et al., 2015).

Improved understanding of the pathophysiology of ISR may allow the development of novel preventative strategies to reduce its occurrence or therapies to treat this iatrogenic problem. It is likely that any such strategy would be combined with current DES technology rather than as a standalone measure. The use of pre-clinical animal models has already improved our understanding of vascular injury but this has not always been translated into clinical practice. Numerous reasons for this exist, not least differences between humans and animals in healing, inflammation and coagulation cascades (Touchard and Schwartz, 2006). Moreover, until now the majority of animal models, especially those in small animals have been non-stenting injury models, which poorly replicate the clinical problem in humans. The later issue was directly addressed in chapter 3 where we refined a mouse model of stenting for use within the Baker laboratory. Importantly we used a miniaturised BMS and a balloon catheter used in the clinical setting. In addition, the electrochemical dissolution of stents led to substantially improved tissue processing, increasing

the range of immunohistochemical stains available as well as being able to undertake *in situ* hybridisation for microRNAs. The improvements in model and tissue processing allowed further in depth study of ISR development, inflammation and re-endothelialisation. Until now assessment of re-endothelialisation has necessitated transgene use and bone marrow transfer studies (Douglas et al., 2013).

Since the discovery of microRNAs and their role in the coordination of tissue development their importance in disease has also been recognised. Indeed, miRs have been found to be dysregulated in numerous cardiovascular diseases including atherosclerosis, arteriosclerosis obliterans, AAA and following balloon angioplasty. Targeting multiple mRNAs and fine-tuning their expression across multiple points in biological pathways miRs appear attractive targets for therapeutic manipulation in the treatment of disease.

Given the known role of miR-21 in promoting cellular proliferation and migration in many cancers we hypothesised that it is likely to be important in many proliferative cardiovascular diseases including ISR (Meng et al., 2007). Within chapter 4, miR-21 was demonstrated to be highly expressed in the neointima of stented tissue taken from the mouse model used. Within the Baker laboratory we have also shown a post stenting increase in miR-21 expression within both a large animal model and most importantly within diseased human coronary arteries following stenting. These data suggested miR-21 is dysregulated following stent injury and that this is conserved across species. Further work was undertaken in order to determine if the up regulation of miR-21 played an important role in the development of ISR. The use of KO mice demonstrated *in vivo*, that miR-21 has a deleterious effect on the development of ISR with a reduction in neointimal size, VSMC and fibrous tissue content observed following genetic deletion. *In vitro* analysis revealed these findings maybe in part due to the reduced proliferative and migratory response of miR-21 KO VSMCs to PDGF, a key mitogen released from various cell types upon stent deployment (Chaabane et al., 2013). Furthermore, investigation revealed that the deleterious effects of miR-21 in VSMCs may be due to PDCD4 targeting.

In addition, *in vivo* investigation demonstrated the macrophages present within miR-21 KO stented tissue had an altered inflammatory state. This finding

suggested a potentially novel mechanism by which miR-21 may influence ISR development. The data presented within Chapter 5 demonstrated significant differences in macrophage cytokine release between miR-21 WT and KO macrophages. It is not inconceivable that these differences may be responsible for the reduction in ISR observed in KO mice as a result of changes to direct macrophage - VSMC interaction and or paracrine signalling mechanisms via effects on proliferation, migration and ECM secretion. Adding further weight to this immune mediated hypothesis is the work of others within the Baker group who have demonstrated significant differences in monocytes, T and B-cells between miR-21 WT and KO mice (McDonald et al., 2015). Both T and B-cells have been implicated in the development of ISR (Chaabane et al., 2013).

Despite our initial and unsuccessful attempt to therapeutically manipulate miR-21 in the setting of ISR, pharmacological manipulation remains an attractive therapy for many diseases. Indeed, other researchers have had success in miR manipulation within several preclinical models of cardiovascular disease (Ji et al., 2007, Maegdefessel et al., 2012, Wang et al., 2011). Several key considerations need to be examined when deciding upon the therapeutic manipulation of miRs. Firstly, identification of an appropriate miR or miRs which are actively involved in the disease process is important. Various strategies can be employed to modulate miR levels within tissues. Up regulation of specific miRs can be achieved by several methods including the use of miR mimics or vectors such as adenovirus and lentivirus containing miR expression cassettes. Down regulation of miRs can be achieved by siRNAs, antimiRs (of various chemistries) and more recently by the use of miR sponges (van Rooij et al., 2012).

Route of delivery is another key consideration in miR modulation and may be determined by the ease of access to site or sites required in order to gain a therapeutic effect. Local delivery methods have been extensively used in pre-clinical models and may be clinically relevant in numerous surgical settings. Indeed during CABG surgery saphenous veins are harvested and stored for a short period prior to grafting, during which miR-modulating therapy could be delivered. However, the local delivery methods used in pre-clinical models of stenting including the adventitial application of a poloxamer containing antimiR

or Adenovirus are not clinically applicable. Instead the use of miR mimics or viral vectors conjugated to stents are likely to be necessary to achieve local delivery.

Systemic delivery either by intravenous, intramuscular or subcutaneous routes are possible for miR manipulation. Intravenous administration on antimiR-21 has been successful in pre-clinical models of vascular disease (Maegdefessel et al., 2012). As evidenced in gene therapy trials, these approaches would appear particularly useful if trying to target multiple sites, the reticuloendothelial system or the liver. However, it is also important to note that systemic delivery may require high doses of therapeutic agent and thus risks the development of a systemic inflammatory response.

Another important therapeutic consideration is the potential for off target effects following miR manipulation. These include targeting of miRs in unintended tissues, which may be more likely following systemic delivery. However, local delivery may also result in targeting within unintended cell types. This may be very important as individual miRs play multiple roles within the body, often having tissue specific effects. Indeed, opposing effects have been documented including that of miR-21 in endothelial cells and VSMCs (Lin et al., 2009, Sabatel et al., 2011). Other concerns surrounding miR manipulation include the alteration of homeostatic mechanisms within non-diseased tissues and the unmasking of disease or the acceleration of disease progression such as cancer. Even within intended target tissues therapeutic modulation of miRs may alter the expression of genes not normally targeted within that tissue, resulting in the unintended alteration of bystander biological pathways (van Rooij and Olson, 2012).

Despite the inherent difficulties with the development of miR based therapeutics, a recent phase 2 clinical study of antimiR-122 subcutaneously administered for the treatment of Hepatitis C has shown considerable promise in the reduction of viral load. Importantly the therapeutic regimen appeared to be well tolerated with no excess of adverse events noted between antimiR-122 and placebo treated groups (Janssen et al., 2013).

In addition, an on going clinical trial is currently investigating the potential of MRX34 in several types of cancer including primary liver cancer, lung cancer and

several haematological malignancies (McClure, 2015). Importantly this trial plans to recruit those with metastatic disease burden for whom there are often little therapeutic options. MRX34 is a miR-34 mimic formulated within a liposomal preparation for intravenous administration (McClure, 2015). Mir-34 has been shown to be reduced in several types of cancer and has a dramatic effect on many cancers by inducing cell cycle arrest at the G1 checkpoint by targeting CDK4/6, cyclin E2 and Bcl-2 (Sun et al., 2008). Interestingly the tumour suppressor p53 has been found to induce miR-34 expression and its mutation blocks the induction of a positive feedback loop between itself and miR-34 (Corney et al., 2007). Despite being a phase 1 trial the above study offers some hope to those with metastatic cancer.

MiR-29 has been shown in various settings to through inhibition of TGF β signalling to reduce fibrosis and ECM deposition (Xiao et al., 2012, Chung et al., 2013). Its potential in the treatment of cutaneous scleroderma is currently being investigated in a phase 1 clinical trial using the miR-29 mimic MRG-201 administered by intradermal injection. This trial is due to report in late 2016 (Rodman, 2015).

In summary, the work contained within this thesis demonstrates that miR-21 is important in the development of ISR. In addition, genetic deletion of miR-21 reduced ISR, most likely by affecting the proliferative and migratory response of VSMC as well as altering the immune cell function. However, this study is not without its limitations. It is important to note the genetic deficiency of miR-21 was present prior to stenting and may alter the response to injury in these mice. In addition, lack of efficacy upon pharmacological knockdown requires further investigation including detailed analysis of miR-21 activity and that of mRNA targets.

References

- ABIZAID, A., KORNOWSKI, R., MINTZ, G. S., HONG, M. K., ABIZAID, A. S., MEHRAN, R., PICHARD, A. D., KENT, K. M., SATLER, L. F., WU, H., POPMA, J. J. & LEON, M. B. 1998. The influence of diabetes mellitus on acute and late clinical outcomes following coronary stent implantation. *J Am Coll Cardiol*, 32, 584-9.
- AGEMA, W. R., MONRAATS, P. S., ZWINDERMAN, A. H., DE WINTER, R. J., TIO, R. A., DOEVENDANS, P. A., WALTEBERGER, J., DE MAAT, M. P., FRANTS, R. R., AT SMA, D. E., VAN DER LAARSE, A., VAN DER WALL, E. E. & JUKEMA, J. W. 2004. Current PTCA practice and clinical outcomes in The Netherlands: the real world in the pre-drug-eluting stent era. *Eur Heart J*, 25, 1163-70.
- ALBINSSON, S., SKOURA, A., YU, J., DILORENZO, A., FERNANDEZ-HERNANDO, C., OFFERMANN, S., MIANO, J. M. & SESSA, W. C. 2011. Smooth muscle miRNAs are critical for post-natal regulation of blood pressure and vascular function. *PLoS One*, 6, e18869.
- ALBINSSON, S., SUAREZ, Y., SKOURA, A., OFFERMANN, S., MIANO, J. M. & SESSA, W. C. 2010. MicroRNAs are necessary for vascular smooth muscle growth, differentiation, and function. *Arterioscler Thromb Vasc Biol*, 30, 1118-26.
- ALI, Z. A., ALP, N. J., LUPTON, H., ARNOLD, N., BANNISTER, T., HU, Y., MUSSA, S., WHEATCROFT, M., GREAVES, D. R., GUNN, J. & CHANNON, K. M. 2007. Increased in-stent stenosis in ApoE knockout mice: insights from a novel mouse model of balloon angioplasty and stenting. *Arterioscler Thromb Vasc Biol*, 27, 833-40.
- ANDERSEN, H. R., NIELSEN, T. T., RASMUSSEN, K., THUESEN, L., KELBAEK, H., THAYSEN, P., ABILDGAARD, U., PEDERSEN, F., MADSEN, J. K., GRANDE, P., VILLADSEN, A. B., KRUSELL, L. R., HAGHFELT, T., LOMHOLT, P., HUSTED, S. E., VIGHOLT, E., KJAERGARD, H. K., MORTENSEN, L. S. & INVESTIGATORS, D.-. 2003. A comparison of coronary angioplasty with fibrinolytic therapy in acute myocardial infarction. *N Engl J Med*, 349, 733-42.
- ANDO, Y., YANG, G. X., KENNY, T. P., KAWATA, K., ZHANG, W., HUANG, W., LEUNG, P. S., LIAN, Z. X., OKAZAKI, K., ANSARI, A. A., HE, X. S., INVERNIZZI, P., RIDGWAY, W. M., LU, Q. & GERSHWIN, M. E. 2013. Overexpression of microRNA-21 is associated with elevated pro-inflammatory cytokines in dominant-negative TGF-beta receptor type II mouse. *J Autoimmun*, 41, 111-9.
- ASANGANI, I. A., RASHEED, S. A., NIKOLOVA, D. A., LEUPOLD, J. H., COLBURN, N. H., POST, S. & ALLGAYER, H. 2008. MicroRNA-21 (miR-21) post-transcriptionally downregulates tumor suppressor Pcd4 and stimulates invasion, intravasation and metastasis in colorectal cancer. *Oncogene*, 27, 2128-36.
- AURORA, A. B., MAHMOUD, A. I., LUO, X., JOHNSON, B. A., VAN ROOIJ, E., MATSUZAKI, S., HUMPHRIES, K. M., HILL, J. A., BASSEL-DUBY, R., SADEK, H. A. & OLSON, E. N. 2012. MicroRNA-214 protects the mouse heart from ischemic injury by controlling Ca(2)(+) overload and cell death. *J Clin Invest*, 122, 1222-32.
- AUTHORS/TASK FORCE, M., WINDECKER, S., KOLH, P., ALFONSO, F., COLLET, J. P., CREMER, J., FALK, V., FILIPPATOS, G., HAMM, C., HEAD, S. J., JUNI, P., KAPPETEIN, A. P., KASTRATI, A., KNUUTI, J., LANDMESSER, U., LAUFER, G., NEUMANN, F. J., RICHTER, D. J., SCHAUERTE, P., SOUSA

- UVA, M., STEFANINI, G. G., TAGGART, D. P., TORRACCA, L., VALGIMIGLI, M., WIJNS, W. & WITKOWSKI, A. 2014. 2014 ESC/EACTS Guidelines on myocardial revascularization: The Task Force on Myocardial Revascularization of the European Society of Cardiology (ESC) and the European Association for Cardio-Thoracic Surgery (EACTS) Developed with the special contribution of the European Association of Percutaneous Cardiovascular Interventions (EAPCI). *Eur Heart J*, 35, 2541-619.
- BANERJEE, S., CUI, H., XIE, N., TAN, Z., YANG, S., ICYUZ, M., THANNICKAL, V. J., ABRAHAM, E. & LIU, G. 2013a. miR-125a-5p regulates differential activation of macrophages and inflammation. *J Biol Chem*, 288, 35428-36.
- BANERJEE, S., XIE, N., CUI, H., TAN, Z., YANG, S., ICYUZ, M., ABRAHAM, E. & LIU, G. 2013b. MicroRNA let-7c regulates macrophage polarization. *J Immunol*, 190, 6542-9.
- BANG, C., BATKAI, S., DANGWAL, S., GUPTA, S. K., FOINQUINOS, A., HOLZMANN, A., JUST, A., REMKE, J., ZIMMER, K., ZEUG, A., PONIMASKIN, E., SCHMIEDL, A., YIN, X., MAYR, M., HALDER, R., FISCHER, A., ENGELHARDT, S., WEI, Y., SCHOBER, A., FIEDLER, J. & THUM, T. 2014. Cardiac fibroblast-derived microRNA passenger strand-enriched exosomes mediate cardiomyocyte hypertrophy. *J Clin Invest*, 124, 2136-46.
- BARTEL, D. P. 2004. MicroRNAs: genomics, biogenesis, mechanism, and function. *Cell*, 116, 281-97.
- BARTEL, D. P. 2009. MicroRNAs: target recognition and regulatory functions. *Cell*, 136, 215-33.
- BASKERVILLE, S. & BARTEL, D. P. 2005. Microarray profiling of microRNAs reveals frequent coexpression with neighboring miRNAs and host genes. *RNA*, 11, 241-7.
- BAVRY, A. A. & BHATT, D. L. 2008. Appropriate use of drug-eluting stents: balancing the reduction in restenosis with the concern of late thrombosis. *Lancet*, 371, 2134-43.
- BERNSTEIN, E., KIM, S. Y., CARMELL, M. A., MURCHISON, E. P., ALCORN, H., LI, M. Z., MILLS, A. A., ELLEDGE, S. J., ANDERSON, K. V. & HANNON, G. J. 2003. Dicer is essential for mouse development. *Nat Genet*, 35, 215-7.
- BHATNAGAR, P., WICKRAMASINGHE, K., WILLIAMS, J., RAYNER, M. & TOWNSEND, N. 2015. The epidemiology of cardiovascular disease in the UK 2014. *Heart*.
- BHF 2014. CARDIOVASCULAR DISEASE STATISTICS 2014. UK: BHF.
- BISWAS, S. K. & MANTOVANI, A. 2010. Macrophage plasticity and interaction with lymphocyte subsets: cancer as a paradigm. *Nat Immunol*, 11, 889-96.
- BLOMKALNS, A. L., GAVRILA, D., THOMAS, M., NELTNER, B. S., BLANCO, V. M., BENJAMIN, S. B., MCCORMICK, M. L., STOLL, L. L., DENNING, G. M., COLLINS, S. P., QIN, Z., DAUGHERTY, A., CASSIS, L. A., THOMPSON, R. W., WEISS, R. M., LINDOWER, P. D., PINNEY, S. M., CHATTERJEE, T. & WEINTRAUB, N. L. 2013. CD14 directs adventitial macrophage precursor recruitment: role in early abdominal aortic aneurysm formation. *J Am Heart Assoc*, 2, e000065.
- BOETTGER, T., BEETZ, N., KOSTIN, S., SCHNEIDER, J., KRUGER, M., HEIN, L. & BRAUN, T. 2009. Acquisition of the contractile phenotype by murine arterial smooth muscle cells depends on the Mir143/145 gene cluster. *J Clin Invest*, 119, 2634-47.
- BRADSHAW, S. H., KENNEDY, L., DEXTER, D. F. & VEINOT, J. P. 2009. A practical method to rapidly dissolve metallic stents. *Cardiovasc Pathol*, 18, 127-33.

- CAI, X., HAGEDORN, C. H. & CULLEN, B. R. 2004. Human microRNAs are processed from capped, polyadenylated transcripts that can also function as mRNAs. *RNA*, 10, 1957-66.
- CAI, X., YIN, Y., LI, N., ZHU, D., ZHANG, J., ZHANG, C. Y. & ZEN, K. 2012. Repolarization of tumor-associated macrophages to pro-inflammatory M1 macrophages by microRNA-155. *J Mol Cell Biol*, 4, 341-3.
- CAICEDO, M. S., DESAI, R., MCALLISTER, K., REDDY, A., JACOBS, J. J. & HALLAB, N. J. 2009. Soluble and particulate Co-Cr-Mo alloy implant metals activate the inflammasome danger signaling pathway in human macrophages: a novel mechanism for implant debris reactivity. *J Orthop Res*, 27, 847-54.
- CALVO-GARRIDO, J., CARILLA-LATORRE, S., LAZARO-DIEGUEZ, F., EGEEA, G. & ESCALANTE, R. 2008. Vacuole membrane protein 1 is an endoplasmic reticulum protein required for organelle biogenesis, protein secretion, and development. *Mol Biol Cell*, 19, 3442-53.
- CARMELIET, P., MOONS, L., STASSEN, J. M., DE MOL, M., BOUCHE, A., VAN DEN OORD, J. J., KOCKX, M. & COLLEN, D. 1997. Vascular wound healing and neointima formation induced by perivascular electric injury in mice. *Am J Pathol*, 150, 761-76.
- CARROZZA, J. P., JR., KUNTZ, R. E., LEVINE, M. J., POMERANTZ, R. M., FISHMAN, R. F., MANSOUR, M., GIBSON, C. M., SENERCHIA, C. C., DIVER, D. J., SAFIAN, R. D. & ET AL. 1992. Angiographic and clinical outcome of intracoronary stenting: immediate and long-term results from a large single-center experience. *J Am Coll Cardiol*, 20, 328-37.
- CARUSO, P., MACLEAN, M. R., KHANIN, R., MCCLURE, J., SOON, E., SOUTHGATE, M., MACDONALD, R. A., GREIG, J. A., ROBERTSON, K. E., MASSON, R., DENBY, L., DEMPSIE, Y., LONG, L., MORRELL, N. W. & BAKER, A. H. 2010. Dynamic changes in lung microRNA profiles during the development of pulmonary hypertension due to chronic hypoxia and monocrotaline. *Arterioscler Thromb Vasc Biol*, 30, 716-23.
- CELERMAJER, D. S., SORENSEN, K. E., BULL, C., ROBINSON, J. & DEANFIELD, J. E. 1994. Endothelium-dependent dilation in the systemic arteries of asymptomatic subjects relates to coronary risk factors and their interaction. *J Am Coll Cardiol*, 24, 1468-74.
- CHAABANE, C., OTSUKA, F., VIRMANI, R. & BOCHATON-PIALLAT, M. L. 2013. Biological responses in stented arteries. *Cardiovasc Res*, 99, 353-63.
- CHAMBERLAIN, J., EVANS, D., KING, A., DEWBERRY, R., DOWER, S., CROSSMAN, D. & FRANCIS, S. 2006. Interleukin-1beta and signaling of interleukin-1 in vascular wall and circulating cells modulates the extent of neointima formation in mice. *Am J Pathol*, 168, 1396-403.
- CHAMBERLAIN, J., WHEATCROFT, M., ARNOLD, N., LUPTON, H., CROSSMAN, D. C., GUNN, J. & FRANCIS, S. 2010. A novel mouse model of in situ stenting. *Cardiovasc Res*, 85, 38-44.
- CHEN, J. F., MURCHISON, E. P., TANG, R., CALLIS, T. E., TATSUGUCHI, M., DENG, Z., ROJAS, M., HAMMOND, S. M., SCHNEIDER, M. D., SELZMAN, C. H., MEISSNER, G., PATTERSON, C., HANNON, G. J. & WANG, D. Z. 2008. Targeted deletion of Dicer in the heart leads to dilated cardiomyopathy and heart failure. *Proc Natl Acad Sci U S A*, 105, 2111-6.
- CHEN, T., HUANG, Z., WANG, L., WANG, Y., WU, F., MENG, S. & WANG, C. 2009. MicroRNA-125a-5p partly regulates the inflammatory response, lipid uptake, and ORP9 expression in oxLDL-stimulated monocyte/macrophages. *Cardiovasc Res*, 83, 131-9.
- CHEN, Z., KEANEY, J. F., JR., SCHULZ, E., LEVISON, B., SHAN, L., SAKUMA, M., ZHANG, X., SHI, C., HAZEN, S. L. & SIMON, D. I. 2004. Decreased

- neointimal formation in Nox2-deficient mice reveals a direct role for NADPH oxidase in the response to arterial injury. *Proc Natl Acad Sci U S A*, 101, 13014-9.
- CHENG, Y., LIU, X., YANG, J., LIN, Y., XU, D. Z., LU, Q., DEITCH, E. A., HUO, Y., DELPHIN, E. S. & ZHANG, C. 2009. MicroRNA-145, a novel smooth muscle cell phenotypic marker and modulator, controls vascular neointimal lesion formation. *Circ Res*, 105, 158-66.
- CHO, A. & REIDY, M. A. 2002. Matrix metalloproteinase-9 is necessary for the regulation of smooth muscle cell replication and migration after arterial injury. *Circ Res*, 91, 845-51.
- CHUNG, A. C., DONG, Y., YANG, W., ZHONG, X., LI, R. & LAN, H. Y. 2013. Smad7 suppresses renal fibrosis via altering expression of TGF-beta/Smad3-regulated microRNAs. *Mol Ther*, 21, 388-98.
- CLARKE, M. C., TALIB, S., FIGG, N. L. & BENNETT, M. R. 2010. Vascular smooth muscle cell apoptosis induces interleukin-1-directed inflammation: effects of hyperlipidemia-mediated inhibition of phagocytosis. *Circ Res*, 106, 363-72.
- CLOWES, A. W. & CLOWES, M. M. 1986. Kinetics of cellular proliferation after arterial injury. IV. Heparin inhibits rat smooth muscle mitogenesis and migration. *Circ Res*, 58, 839-45.
- COHEN, M., DEMERS, C., GURFINKEL, E. P., TURPIE, A. G., FROMELL, G. J., GOODMAN, S., LANGER, A., CALIFF, R. M., FOX, K. A., PREMMEREUR, J. & BIGONZI, F. 1997. A comparison of low-molecular-weight heparin with unfractionated heparin for unstable coronary artery disease. Efficacy and Safety of Subcutaneous Enoxaparin in Non-Q-Wave Coronary Events Study Group. *N Engl J Med*, 337, 447-52.
- COLLINS, A. R., MEEHAN, W. P., KINTSCHER, U., JACKSON, S., WAKINO, S., NOH, G., PALINSKI, W., HSUEH, W. A. & LAW, R. E. 2001. Troglitazone inhibits formation of early atherosclerotic lesions in diabetic and nondiabetic low density lipoprotein receptor-deficient mice. *Arterioscler Thromb Vasc Biol*, 21, 365-71.
- CORDES, K. R., SHEEHY, N. T., WHITE, M. P., BERRY, E. C., MORTON, S. U., MUTH, A. N., LEE, T. H., MIANO, J. M., IVEY, K. N. & SRIVASTAVA, D. 2009. miR-145 and miR-143 regulate smooth muscle cell fate and plasticity. *Nature*, 460, 705-10.
- CORNEY, D. C., FLESKEN-NIKITIN, A., GODWIN, A. K., WANG, W. & NIKITIN, A. Y. 2007. MicroRNA-34b and MicroRNA-34c are targets of p53 and cooperate in control of cell proliferation and adhesion-independent growth. *Cancer Res*, 67, 8433-8.
- COSTA, M. A. & SIMON, D. I. 2005. Molecular basis of restenosis and drug-eluting stents. *Circulation*, 111, 2257-73.
- CRISBY, M., KALLIN, B., THYBERG, J., ZHIVOTOVSKY, B., ORRENIUS, S., KOSTULAS, V. & NILSSON, J. 1997. Cell death in human atherosclerotic plaques involves both oncosis and apoptosis. *Atherosclerosis*, 130, 17-27.
- DA COSTA MARTINS, P. A., BOURAJAJ, M., GLADKA, M., KORTLAND, M., VAN OORT, R. J., PINTO, Y. M., MOKKENTIN, J. D. & DE WINDT, L. J. 2008. Conditional dicer gene deletion in the postnatal myocardium provokes spontaneous cardiac remodeling. *Circulation*, 118, 1567-76.
- DAEMEN, M. J., LOMBARDI, D. M., BOSMAN, F. T. & SCHWARTZ, S. M. 1991. Angiotensin II induces smooth muscle cell proliferation in the normal and injured rat arterial wall. *Circ Res*, 68, 450-6.
- DANENBERG, H. D., GOLOMB, G., GROOTHUIS, A., GAO, J., EPSTEIN, H., SWAMINATHAN, R. V., SEIFERT, P. & EDELMAN, E. R. 2003. Liposomal

- alendronate inhibits systemic innate immunity and reduces in-stent neointimal hyperplasia in rabbits. *Circulation*, 108, 2798-804.
- DANGAS, G. D., CLAESSEN, B. E., CAIXETA, A., SANIDAS, E. A., MINTZ, G. S. & MEHRAN, R. 2010. In-stent restenosis in the drug-eluting stent era. *J Am Coll Cardiol*, 56, 1897-907.
- DANGWAL, S., BANG, C. & THUM, T. 2012. Novel techniques and targets in cardiovascular microRNA research. *Cardiovasc Res*, 93, 545-54.
- DAVIS, B. N., HILYARD, A. C., LAGNA, G. & HATA, A. 2008. SMAD proteins control DROSHA-mediated microRNA maturation. *Nature*, 454, 56-61.
- DAVIS, B. N., HILYARD, A. C., NGUYEN, P. H., LAGNA, G. & HATA, A. 2009. Induction of microRNA-221 by platelet-derived growth factor signaling is critical for modulation of vascular smooth muscle phenotype. *J Biol Chem*, 284, 3728-38.
- DAVIS, M. J., TSANG, T. M., QIU, Y., DAYRIT, J. K., FREIJ, J. B., HUFFNAGLE, G. B. & OLSZEWSKI, M. A. 2013. Macrophage M1/M2 polarization dynamically adapts to changes in cytokine microenvironments in *Cryptococcus neoformans* infection. *MBio*, 4, e00264-13.
- DAVIS-DUSENBERY, B. N., CHAN, M. C., RENO, K. E., WEISMAN, A. S., LAYNE, M. D., LAGNA, G. & HATA, A. 2011a. down-regulation of Kruppel-like factor-4 (KLF4) by microRNA-143/145 is critical for modulation of vascular smooth muscle cell phenotype by transforming growth factor-beta and bone morphogenetic protein 4. *J Biol Chem*, 286, 28097-110.
- DAVIS-DUSENBERY, B. N. & HATA, A. 2011. Smad-mediated miRNA processing: a critical role for a conserved RNA sequence. *RNA Biol*, 8, 71-6.
- DAVIS-DUSENBERY, B. N., WU, C. & HATA, A. 2011b. Micromanaging vascular smooth muscle cell differentiation and phenotypic modulation. *Arterioscler Thromb Vasc Biol*, 31, 2370-7.
- DE BRUYNE, B., PIJLS, N. H., KALESAN, B., BARBATO, E., TONINO, P. A., PIROTH, Z., JAGIC, N., MOBIUS-WINKLER, S., RIOUFOL, G., WITT, N., KALA, P., MACCARTHY, P., ENGSTROM, T., OLDROYD, K. G., MAVROMATIS, K., MANOHARAN, G., VERLEE, P., FROBERT, O., CURZEN, N., JOHNSON, J. B., JUNI, P., FEARON, W. F. & INVESTIGATORS, F. T. 2012. Fractional flow reserve-guided PCI versus medical therapy in stable coronary disease. *N Engl J Med*, 367, 991-1001.
- DEAN, C. J., MORTON, A. C., ARNOLD, N. D., HOSE, D. R., CROSSMAN, D. C. & GUNN, J. 2005. Relative importance of the components of stent geometry to stretch induced in-stent neointima formation. *Heart*, 91, 1603-4.
- DELLAGO, H., PRESCHITZ-KAMMERHOFER, B., TERLECKI-ZANIEWICZ, L., SCHREINER, C., FORTSCHEGGER, K., CHANG, M. W., HACKL, M., MONTEFORTE, R., KUHNEL, H., SCHOSSERER, M., GRUBER, F., TSCHACHLER, E., SCHEIDELER, M., GRILLARI-VOGLAUER, R., GRILLARI, J. & WIESER, M. 2013. High levels of oncomiR-21 contribute to the senescence-induced growth arrest in normal human cells and its knock-down increases the replicative lifespan. *Aging Cell*, 12, 446-58.
- DIETRICH, H., HU, Y., ZOU, Y., DIRNHOFER, S., KLEINDIENST, R., WICK, G. & XU, Q. 2000. Mouse model of transplant arteriosclerosis: role of intercellular adhesion molecule-1. *Arterioscler Thromb Vasc Biol*, 20, 343-52.
- DONNERS, M. M., WOLFS, I. M., STOGER, L. J., VAN DER VORST, E. P., POTTGENS, C. C., HEYMANS, S., SCHROEN, B., GIJBELS, M. J. & DE WINTHER, M. P. 2012. Hematopoietic miR155 deficiency enhances atherosclerosis and decreases plaque stability in hyperlipidemic mice. *PLoS One*, 7, e35877.

- DOUGLAS, G., BENDALL, J. K., CRABTREE, M. J., TATHAM, A. L., CARTER, E. E., HALE, A. B. & CHANNON, K. M. 2012. Endothelial-specific Nox2 overexpression increases vascular superoxide and macrophage recruitment in ApoE(-)/(-) mice. *Cardiovasc Res*, 94, 20-9.
- DOUGLAS, G., VAN KAMPEN, E., HALE, A. B., MCNEILL, E., PATEL, J., CRABTREE, M. J., ALI, Z., HOERR, R. A., ALP, N. J. & CHANNON, K. M. 2013. Endothelial cell repopulation after stenting determines in-stent neointima formation: effects of bare-metal vs. drug-eluting stents and genetic endothelial cell modification. *Eur Heart J*, 34, 3378-88.
- DOYLE, J. T., DAWBER, T. R., KANNEL, W. B., HESLIN, A. S. & KAHN, H. A. 1962. Cigarette smoking and coronary heart disease. Combined experience of the Albany and Framingham studies. *N Engl J Med*, 266, 796-801.
- DU, F., YU, F., WANG, Y., HUI, Y., CARNEVALE, K., FU, M., LU, H. & FAN, D. 2014. MicroRNA-155 deficiency results in decreased macrophage inflammation and attenuated atherogenesis in apolipoprotein E-deficient mice. *Arterioscler Thromb Vasc Biol*, 34, 759-67.
- EGUCHI, S., MATSUMOTO, T., MOTLEY, E. D., UTSUNOMIYA, H. & INAGAMI, T. 1996. Identification of an essential signaling cascade for mitogen-activated protein kinase activation by angiotensin II in cultured rat vascular smooth muscle cells. Possible requirement of Gq-mediated p21ras activation coupled to a Ca²⁺/calmodulin-sensitive tyrosine kinase. *J Biol Chem*, 271, 14169-75.
- ELIA, L., QUINTAVALLE, M., ZHANG, J., CONTU, R., COSSU, L., LATRONICO, M. V., PETERSON, K. L., INDOLFI, C., CATALUCCI, D., CHEN, J., COURTNEIDGE, S. A. & CONDORELLI, G. 2009. The knockout of miR-143 and -145 alters smooth muscle cell maintenance and vascular homeostasis in mice: correlates with human disease. *Cell Death Differ*, 16, 1590-8.
- ESTELLER, M. 2011. Non-coding RNAs in human disease. *Nat Rev Genet*, 12, 861-74.
- EULALIO, A., HUNTZINGER, E., NISHIHARA, T., REHWINKEL, J., FAUSER, M. & IZAUERRALDE, E. 2009. Deadenylation is a widespread effect of miRNA regulation. *RNA*, 15, 21-32.
- FABBRI, M., PAONE, A., CALORE, F., GALLI, R., GAUDIO, E., SANTHANAM, R., LOVAT, F., FADDA, P., MAO, C., NUOVO, G. J., ZANESI, N., CRAWFORD, M., OZER, G. H., WERNICKE, D., ALDER, H., CALIGIURI, M. A., NANA-SINKAM, P., PERROTTI, D. & CROCE, C. M. 2012. MicroRNAs bind to Toll-like receptors to induce prometastatic inflammatory response. *Proc Natl Acad Sci U S A*, 109, E2110-6.
- FELDMAN, L. J., AGUIRRE, L., ZIOL, M., BRIDOU, J. P., NEVO, N., MICHEL, J. B. & STEG, P. G. 2000. Interleukin-10 inhibits intimal hyperplasia after angioplasty or stent implantation in hypercholesterolemic rabbits. *Circulation*, 101, 908-16.
- FERNS, G. A., RAINES, E. W., SPRUGEL, K. H., MOTANI, A. S., REIDY, M. A. & ROSS, R. 1991. Inhibition of neointimal smooth muscle accumulation after angioplasty by an antibody to PDGF. *Science*, 253, 1129-32.
- FINGERLE, J., AU, Y. P., CLOWES, A. W. & REIDY, M. A. 1990. Intimal lesion formation in rat carotid arteries after endothelial denudation in absence of medial injury. *Arteriosclerosis*, 10, 1082-7.
- FISCHMAN, D. L., LEON, M. B., BAIM, D. S., SCHATZ, R. A., SAVAGE, M. P., PENN, I., DETRE, K., VELTRI, L., RICCI, D., NOBUYOSHI, M. & ET AL. 1994. A randomized comparison of coronary-stent placement and balloon angioplasty in the treatment of coronary artery disease. Stent Restenosis Study Investigators. *N Engl J Med*, 331, 496-501.

- FISHMAN, J. A., RYAN, G. B. & KARNOVSKY, M. J. 1975. Endothelial regeneration in the rat carotid artery and the significance of endothelial denudation in the pathogenesis of myointimal thickening. *Lab Invest*, 32, 339-51.
- FORSTERMANN, U., CLOSS, E. I., POLLOCK, J. S., NAKANE, M., SCHWARZ, P., GATH, I. & KLEINERT, H. 1994. Nitric oxide synthase isozymes. Characterization, purification, molecular cloning, and functions. *Hypertension*, 23, 1121-31.
- FORSYTH, E. A., ALY, H. M., NEVILLE, R. F. & SIDAWY, A. N. 1997. Proliferation and extracellular matrix production by human infragenicular smooth muscle cells in response to interleukin-1 beta. *J Vasc Surg*, 26, 1002-7; discussion 1007-8.
- FRIEDMAN, R. C., FARH, K. K., BURGE, C. B. & BARTEL, D. P. 2009. Most mammalian mRNAs are conserved targets of microRNAs. *Genome Res*, 19, 92-105.
- FUJITA, S., ITO, T., MIZUTANI, T., MINOGUCHI, S., YAMAMICHI, N., SAKURAI, K. & IBA, H. 2008. miR-21 Gene expression triggered by AP-1 is sustained through a double-negative feedback mechanism. *J Mol Biol*, 378, 492-504.
- FURGESON, S. B., SIMPSON, P. A., PARK, I., VANPUTTEN, V., HORITA, H., KONTOS, C. D., NEMENOFF, R. A. & WEISER-EVANS, M. C. 2010. Inactivation of the tumour suppressor, PTEN, in smooth muscle promotes a pro-inflammatory phenotype and enhances neointima formation. *Cardiovasc Res*, 86, 274-82.
- GABELER, E. E., VAN HILLEGERSBERG, R., STATIUS VAN EPS, R. G., SLUITER, W., GUSSENHOVEN, E. J., MULDER, P. & VAN URK, H. 2002. A comparison of balloon injury models of endovascular lesions in rat arteries. *BMC Cardiovasc Disord*, 2, 16.
- GALIS, Z. S., SUKHOVA, G. K., LARK, M. W. & LIBBY, P. 1994. Increased expression of matrix metalloproteinases and matrix degrading activity in vulnerable regions of human atherosclerotic plaques. *J Clin Invest*, 94, 2493-503.
- GARASIC, J. M., EDELMAN, E. R., SQUIRE, J. C., SEIFERT, P., WILLIAMS, M. S. & ROGERS, C. 2000. Stent and artery geometry determine intimal thickening independent of arterial injury. *Circulation*, 101, 812-8.
- GEARY, R. L., WILLIAMS, J. K., GOLDEN, D., BROWN, D. G., BENJAMIN, M. E. & ADAMS, M. R. 1996. Time course of cellular proliferation, intimal hyperplasia, and remodeling following angioplasty in monkeys with established atherosclerosis. A nonhuman primate model of restenosis. *Arterioscler Thromb Vasc Biol*, 16, 34-43.
- GILABERT, M., VACCARO, M. I., FERNANDEZ-ZAPICO, M. E., CALVO, E. L., TURRINI, O., SECQ, V., GARCIA, S., MOUTARDIER, V., LOMBERK, G., DUSETTI, N., URRUTIA, R. & IOVANNA, J. L. 2013. Novel role of VMP1 as modifier of the pancreatic tumor cell response to chemotherapeutic drugs. *J Cell Physiol*, 228, 1834-43.
- GOETZE, S., XI, X. P., KAWANO, Y., KAWANO, H., FLECK, E., HSUEH, W. A. & LAW, R. E. 1999. TNF-alpha-induced migration of vascular smooth muscle cells is MAPK dependent. *Hypertension*, 33, 183-9.
- GORITZKA, M., DURANT, L. R., PEREIRA, C., SALEK-ARDAKANI, S., OPENSHAW, P. J. & JOHANSSON, C. 2014. Alpha/beta interferon receptor signaling amplifies early proinflammatory cytokine production in the lung during respiratory syncytial virus infection. *J Virol*, 88, 6128-36.
- GOUGH, P. J., GOMEZ, I. G., WILLE, P. T. & RAINES, E. W. 2006. Macrophage expression of active MMP-9 induces acute plaque disruption in apoE-deficient mice. *J Clin Invest*, 116, 59-69.

- GRAF, K., XI, X. P., YANG, D., FLECK, E., HSUEH, W. A. & LAW, R. E. 1997. Mitogen-activated protein kinase activation is involved in platelet-derived growth factor-directed migration by vascular smooth muscle cells. *Hypertension*, 29, 334-9.
- GRAFF, J. W., DICKSON, A. M., CLAY, G., MCCAFFREY, A. P. & WILSON, M. E. 2012. Identifying functional microRNAs in macrophages with polarized phenotypes. *J Biol Chem*, 287, 21816-25.
- GRUNTZIG, A. 1978. Transluminal dilatation of coronary-artery stenosis. *Lancet*, 1, 263.
- GUIDUCCI, C., VICARI, A. P., SANGALETTI, S., TRINCHIERI, G. & COLOMBO, M. P. 2005. Redirecting in vivo elicited tumor infiltrating macrophages and dendritic cells towards tumor rejection. *Cancer Res*, 65, 3437-46.
- GUNN, J., ARNOLD, N., CHAN, K. H., SHEPHERD, L., CUMBERLAND, D. C. & CROSSMAN, D. C. 2002. Coronary artery stretch versus deep injury in the development of in-stent neointima. *Heart*, 88, 401-5.
- GUO, H., INGOLIA, N. T., WEISSMAN, J. S. & BARTEL, D. P. 2010. Mammalian microRNAs predominantly act to decrease target mRNA levels. *Nature*, 466, 835-40.
- HAN, L., YUE, X., ZHOU, X., LAN, F. M., YOU, G., ZHANG, W., ZHANG, K. L., ZHANG, C. Z., CHENG, J. Q., YU, S. Z., PU, P. Y., JIANG, T. & KANG, C. S. 2012. MicroRNA-21 expression is regulated by beta-catenin/STAT3 pathway and promotes glioma cell invasion by direct targeting RECK. *CNS Neurosci Ther*, 18, 573-83.
- HATLEY, M. E., PATRICK, D. M., GARCIA, M. R., RICHARDSON, J. A., BASSEL-DUBY, R., VAN ROOIJ, E. & OLSON, E. N. 2010. Modulation of K-Ras-dependent lung tumorigenesis by MicroRNA-21. *Cancer Cell*, 18, 282-93.
- HEAD, S. J., HOLMES, D. R., JR., MACK, M. J., SERRUYS, P. W., MOHR, F. W., MORICE, M. C., COLOMBO, A., KAPPETEIN, A. P. & INVESTIGATORS, S. 2012. Risk profile and 3-year outcomes from the SYNTAX percutaneous coronary intervention and coronary artery bypass grafting nested registries. *JACC Cardiovasc Interv*, 5, 618-25.
- HO, V. W. & SLY, L. M. 2009. Derivation and characterization of murine alternatively activated (M2) macrophages. *Methods Mol Biol*, 531, 173-85.
- HORVATH, C., WELT, F. G., NEDELMAN, M., RAO, P. & ROGERS, C. 2002. Targeting CCR2 or CD18 inhibits experimental in-stent restenosis in primates: inhibitory potential depends on type of injury and leukocytes targeted. *Circ Res*, 90, 488-94.
- HUI, D. Y. 2008. Intimal hyperplasia in murine models. *Curr Drug Targets*, 9, 251-60.
- HUMPHREYS, D. T., WESTMAN, B. J., MARTIN, D. I. & PREISS, T. 2005. MicroRNAs control translation initiation by inhibiting eukaryotic initiation factor 4E/cap and poly(A) tail function. *Proc Natl Acad Sci U S A*, 102, 16961-6.
- HUTCHESON, R., TERRY, R., CHAPLIN, J., SMITH, E., MUSIYENKO, A., RUSSELL, J. C., LINCOLN, T. & ROCIC, P. 2013. MicroRNA-145 restores contractile vascular smooth muscle phenotype and coronary collateral growth in the metabolic syndrome. *Arterioscler Thromb Vasc Biol*, 33, 727-36.
- IALENTI, A., GRASSIA, G., GORDON, P., MADDALUNO, M., DI LAURO, M. V., BAKER, A. H., GUGLIELMOTTI, A., COLOMBO, A., BIONDI, G., KENNEDY, S. & MAFFIA, P. 2011. Inhibition of in-stent stenosis by oral administration of bindarit in porcine coronary arteries. *Arterioscler Thromb Vasc Biol*, 31, 2448-54.

- IKEDA, U., IKEDA, M., OOHARA, T., OGUCHI, A., KAMITANI, T., TSURUYA, Y. & KANO, S. 1991. Interleukin 6 stimulates growth of vascular smooth muscle cells in a PDGF-dependent manner. *Am J Physiol*, 260, H1713-7.
- ILIOPOULOS, D., JAEGER, S. A., HIRSCH, H. A., BULYK, M. L. & STRUHL, K. 2010. STAT3 activation of miR-21 and miR-181b-1 via PTEN and CYLD are part of the epigenetic switch linking inflammation to cancer. *Mol Cell*, 39, 493-506.
- INDOLFI, C., ESPOSITO, G., STABILE, E., CAVUTO, L., PISANI, A., COPPOLA, C., TORELLA, D., PERRINO, C., DI LORENZO, E., CURCIO, A., PALOMBINI, L. & CHIARIELLO, M. 2000. A new rat model of small vessel stenting. *Basic Res Cardiol*, 95, 179-85.
- INDOLFI, C., MONGIARDO, A., CURCIO, A. & TORELLA, D. 2003. Molecular mechanisms of in-stent restenosis and approach to therapy with eluting stents. *Trends Cardiovasc Med*, 13, 142-8.
- IRVINE, K. M., ANDREWS, M. R., FERNANDEZ-ROJO, M. A., SCHRODER, K., BURNS, C. J., SU, S., WILKS, A. F., PARTON, R. G., HUME, D. A. & SWEET, M. J. 2009. Colony-stimulating factor-1 (CSF-1) delivers a proatherogenic signal to human macrophages. *J Leukoc Biol*, 85, 278-88.
- JACKSON, C. L., RAINES, E. W., ROSS, R. & REIDY, M. A. 1993. Role of endogenous platelet-derived growth factor in arterial smooth muscle cell migration after balloon catheter injury. *Arterioscler Thromb*, 13, 1218-26.
- JANSSEN, H. L., REESINK, H. W., LAWITZ, E. J., ZEUZEM, S., RODRIGUEZ-TORRES, M., PATEL, K., VAN DER MEER, A. J., PATICK, A. K., CHEN, A., ZHOU, Y., PERSSON, R., KING, B. D., KAUPPINEN, S., LEVIN, A. A. & HODGES, M. R. 2013. Treatment of HCV infection by targeting microRNA. *N Engl J Med*, 368, 1685-94.
- JEREMY, J. Y., ROWE, D., EMSLEY, A. M. & NEWBY, A. C. 1999. Nitric oxide and the proliferation of vascular smooth muscle cells. *Cardiovasc Res*, 43, 580-94.
- JI, R., CHENG, Y., YUE, J., YANG, J., LIU, X., CHEN, H., DEAN, D. B. & ZHANG, C. 2007. MicroRNA expression signature and antisense-mediated depletion reveal an essential role of MicroRNA in vascular neointimal lesion formation. *Circ Res*, 100, 1579-88.
- JIANG, C., TING, A. T. & SEED, B. 1998. PPAR-gamma agonists inhibit production of monocyte inflammatory cytokines. *Nature*, 391, 82-6.
- JIN, C., ZHAO, Y., YU, L., XU, S. & FU, G. 2013. MicroRNA-21 mediates the rapamycin-induced suppression of endothelial proliferation and migration. *FEBS Lett*, 587, 378-85.
- JOHNSON, J. L., DWIVEDI, A., SOMERVILLE, M., GEORGE, S. J. & NEWBY, A. C. 2011. Matrix metalloproteinase (MMP)-3 activates MMP-9 mediated vascular smooth muscle cell migration and neointima formation in mice. *Arterioscler Thromb Vasc Biol*, 31, e35-44.
- JONER, M., FINN, A. V., FARB, A., MONT, E. K., KOLODGIE, F. D., LADICH, E., KUTYS, R., SKORIJA, K., GOLD, H. K. & VIRMANI, R. 2006. Pathology of drug-eluting stents in humans: delayed healing and late thrombotic risk. *J Am Coll Cardiol*, 48, 193-202.
- KANG, H., DAVIS-DUSENBERY, B. N., NGUYEN, P. H., LAL, A., LIEBERMAN, J., VAN AELST, L., LAGNA, G. & HATA, A. 2012. Bone morphogenetic protein 4 promotes vascular smooth muscle contractility by activating microRNA-21 (miR-21), which down-regulates expression of family of dedicator of cytokinesis (DOCK) proteins. *J Biol Chem*, 287, 3976-86.
- KANNEL, W. B., DAWBER, T. R., KAGAN, A., REVOTSKIE, N. & STOKES, J., 3RD 1961. Factors of risk in the development of coronary heart disease--six

- year follow-up experience. The Framingham Study. *Ann Intern Med*, 55, 33-50.
- KANNEL, W. B. & MCGEE, D. L. 1979. Diabetes and cardiovascular risk factors: the Framingham study. *Circulation*, 59, 8-13.
- KASAOKA, S., TOBIS, J. M., AKIYAMA, T., REIMERS, B., DI MARIO, C., WONG, N. D. & COLOMBO, A. 1998. Angiographic and intravascular ultrasound predictors of in-stent restenosis. *J Am Coll Cardiol*, 32, 1630-5.
- KASTRATI, A., DIBRA, A., MEHILLI, J., MAYER, S., PINIECK, S., PACHE, J., DIRSCHINGER, J. & SCHOMIG, A. 2006. Predictive factors of restenosis after coronary implantation of sirolimus- or paclitaxel-eluting stents. *Circulation*, 113, 2293-300.
- KASTRATI, A., MEHILLI, J., DIRSCHINGER, J., DOTZER, F., SCHUHLEN, H., NEUMANN, F. J., FLECKENSTEIN, M., PFAFFEROTT, C., SEYFARTH, M. & SCHOMIG, A. 2001. Intracoronary stenting and angiographic results: strut thickness effect on restenosis outcome (ISAR-STERO) trial. *Circulation*, 103, 2816-21.
- KIM, I., MOON, S. O., KIM, S. H., KIM, H. J., KOH, Y. S. & KOH, G. Y. 2001. Vascular endothelial growth factor expression of intercellular adhesion molecule 1 (ICAM-1), vascular cell adhesion molecule 1 (VCAM-1), and E-selectin through nuclear factor-kappa B activation in endothelial cells. *J Biol Chem*, 276, 7614-20.
- KIM, Y. K. & KIM, V. N. 2007. Processing of intronic microRNAs. *EMBO J*, 26, 775-83.
- KING, S. B., 3RD 1998. The development of interventional cardiology. *J Am Coll Cardiol*, 31, 64B-88B.
- KITCHENS, W. H., CHASE, C. M., UEHARA, S., CORNELL, L. D., COLVIN, R. B., RUSSELL, P. S. & MADSEN, J. C. 2007. Macrophage depletion suppresses cardiac allograft vasculopathy in mice. *American Journal of Transplantation*, 7, 2675-2682.
- KORNOWSKI, R., HONG, M. K., TIO, F. O., BRAMWELL, O., WU, H. & LEON, M. B. 1998. In-stent restenosis: contributions of inflammatory responses and arterial injury to neointimal hyperplasia. *J Am Coll Cardiol*, 31, 224-30.
- KRUTZFELDT, J., RAJEWSKY, N., BRAICH, R., RAJEEV, K. G., TUSCHL, T., MANOHARAN, M. & STOFFEL, M. 2005. Silencing of microRNAs in vivo with 'antagomirs'. *Nature*, 438, 685-9.
- KUEHBACHER, A., URBICH, C., ZEIHNER, A. M. & DIMMELER, S. 2007. Role of Dicer and Drosha for endothelial microRNA expression and angiogenesis. *Circ Res*, 101, 59-68.
- KUMAR, A. & LINDNER, V. 1997. Remodeling with neointima formation in the mouse carotid artery after cessation of blood flow. *Arterioscler Thromb Vasc Biol*, 17, 2238-44.
- KUNJATHOOR, V. V., FEBBRAIO, M., PODREZ, E. A., MOORE, K. J., ANDERSSON, L., KOEHN, S., RHEE, J. S., SILVERSTEIN, R., HOFF, H. F. & FREEMAN, M. W. 2002. Scavenger receptors class A-I/II and CD36 are the principal receptors responsible for the uptake of modified low density lipoprotein leading to lipid loading in macrophages. *J Biol Chem*, 277, 49982-8.
- LAVIN, B., GOMEZ, M., PELLO, O. M., CASTEJON, B., PIEDRAS, M. J., SAURA, M. & ZARAGOZA, C. 2014. Nitric Oxide Prevents Aortic Neointimal Hyperplasia by Controlling Macrophage Polarization. *Arterioscler Thromb Vasc Biol*.
- LEE, J. M., PARK, J., KANG, J., JEON, K. H., JUNG, J. H., LEE, S. E., HAN, J. K., KIM, H. L., YANG, H. M., PARK, K. W., KANG, H. J., KOO, B. K. & KIM, H. S. 2015. Comparison among drug-eluting balloon, drug-eluting stent, and

- plain balloon angioplasty for the treatment of in-stent restenosis: a network meta-analysis of 11 randomized, controlled trials. *JACC Cardiovasc Interv*, 8, 382-94.
- LEE, R. C., FEINBAUM, R. L. & AMBROS, V. 1993. The *C. elegans* heterochronic gene *lin-4* encodes small RNAs with antisense complementarity to *lin-14*. *Cell*, 75, 843-54.
- LEE, Y., AHN, C., HAN, J., CHOI, H., KIM, J., YIM, J., LEE, J., PROVOST, P., RADMARK, O., KIM, S. & KIM, V. N. 2003. The nuclear RNase III Drosha initiates microRNA processing. *Nature*, 425, 415-9.
- LEE, Y., JEON, K., LEE, J. T., KIM, S. & KIM, V. N. 2002. MicroRNA maturation: stepwise processing and subcellular localization. *EMBO J*, 21, 4663-70.
- LEITINGER, N. & SCHULMAN, I. G. 2013. Phenotypic polarization of macrophages in atherosclerosis. *Arterioscler Thromb Vasc Biol*, 33, 1120-6.
- LI, A. C., BROWN, K. K., SILVESTRE, M. J., WILLSON, T. M., PALINSKI, W. & GLASS, C. K. 2000. Peroxisome proliferator-activated receptor gamma ligands inhibit development of atherosclerosis in LDL receptor-deficient mice. *J Clin Invest*, 106, 523-31.
- LI, J., LI, P., ZHANG, Y., LI, G. B., ZHOU, Y. G., YANG, K. & DAI, S. S. 2013a. c-Ski inhibits the proliferation of vascular smooth muscle cells via suppressing Smad3 signaling but stimulating p38 pathway. *Cell Signal*, 25, 159-67.
- LI, J., ZHAO, L., HE, X., YANG, T. & YANG, K. 2014. MiR-21 inhibits c-Ski signaling to promote the proliferation of rat vascular smooth muscle cells. *Cell Signal*, 26, 724-9.
- LI, L., MIANO, J. M., CSERJESI, P. & OLSON, E. N. 1996. SM22 alpha, a marker of adult smooth muscle, is expressed in multiple myogenic lineages during embryogenesis. *Circ Res*, 78, 188-95.
- LI, P., LIU, Y., YI, B., WANG, G., YOU, X., ZHAO, X., SUMMER, R., QIN, Y. & SUN, J. 2013b. MicroRNA-638 is highly expressed in human vascular smooth muscle cells and inhibits PDGF-BB-induced cell proliferation and migration through targeting orphan nuclear receptor NOR1. *Cardiovasc Res*, 99, 185-93.
- LI, P., ZHU, N., YI, B., WANG, N., CHEN, M., YOU, X., ZHAO, X., SOLOMIDES, C. C., QIN, Y. & SUN, J. 2013c. MicroRNA-663 regulates human vascular smooth muscle cell phenotypic switch and vascular neointimal formation. *Circ Res*, 113, 1117-27.
- LI, T., CAO, H., ZHUANG, J., WAN, J., GUAN, M., YU, B., LI, X. & ZHANG, W. 2011. Identification of miR-130a, miR-27b and miR-210 as serum biomarkers for atherosclerosis obliterans. *Clin Chim Acta*, 412, 66-70.
- LIANG, C. C., PARK, A. Y. & GUAN, J. L. 2007. In vitro scratch assay: a convenient and inexpensive method for analysis of cell migration in vitro. *Nat Protoc*, 2, 329-33.
- LIMA, W. F., WU, H., NICHOLS, J. G., SUN, H., MURRAY, H. M. & CROOKE, S. T. 2009. Binding and cleavage specificities of human Argonaute2. *J Biol Chem*, 284, 26017-28.
- LIN, Y., LIU, X., CHENG, Y., YANG, J., HUO, Y. & ZHANG, C. 2009. Involvement of MicroRNAs in hydrogen peroxide-mediated gene regulation and cellular injury response in vascular smooth muscle cells. *J Biol Chem*, 284, 7903-13.
- LINDNER, V., FINGERLE, J. & REIDY, M. A. 1993. Mouse model of arterial injury. *Circ Res*, 73, 792-6.
- LIU, X., CHENG, Y., YANG, J., KRALL, T. J., HUO, Y. & ZHANG, C. 2010. An essential role of PDCD4 in vascular smooth muscle cell apoptosis and

- proliferation: implications for vascular disease. *Am J Physiol Cell Physiol*, 298, C1481-8.
- LIU, X., CHENG, Y., ZHANG, S., LIN, Y., YANG, J. & ZHANG, C. 2009. A necessary role of miR-221 and miR-222 in vascular smooth muscle cell proliferation and neointimal hyperplasia. *Circ Res*, 104, 476-87.
- LIVAK, K. J. & SCHMITTGEN, T. D. 2001. Analysis of relative gene expression data using real-time quantitative PCR and the 2^{-Delta Delta C(T)} Method. *Methods*, 25, 402-8.
- LOFFLER, D., BROCKE-HEIDRICH, K., PFEIFER, G., STOCSITS, C., HACKERMULLER, J., KRETZSCHMAR, A. K., BURGER, R., GRAMATZKI, M., BLUMERT, C., BAUER, K., CVIJIC, H., ULLMANN, A. K., STADLER, P. F. & HORN, F. 2007. Interleukin-6 dependent survival of multiple myeloma cells involves the Stat3-mediated induction of microRNA-21 through a highly conserved enhancer. *Blood*, 110, 1330-3.
- LOWE, H. C., JAMES, B. & KHACHIGIAN, L. M. 2005. A novel model of in-stent restenosis: rat aortic stenting. *Heart*, 91, 393-5.
- LU, T. X., HARTNER, J., LIM, E. J., FABRY, V., MINGLER, M. K., COLE, E. T., ORKIN, S. H., ARONOW, B. J. & ROTHENBERG, M. E. 2011. MicroRNA-21 limits in vivo immune response-mediated activation of the IL-12/IFN-gamma pathway, Th1 polarization, and the severity of delayed-type hypersensitivity. *J Immunol*, 187, 3362-73.
- LUCAS, T., WAISMAN, A., RANJAN, R., ROES, J., KRIEG, T., MULLER, W., ROERS, A. & EMING, S. A. 2010. Differential roles of macrophages in diverse phases of skin repair. *J Immunol*, 184, 3964-77.
- LUTGENS, E., GIJBELS, M., SMOOK, M., HEERINGA, P., GOTWALS, P., KOTELIANSKY, V. E. & DAEMEN, M. J. 2002. Transforming growth factor-beta mediates balance between inflammation and fibrosis during plaque progression. *Arterioscler Thromb Vasc Biol*, 22, 975-82.
- MAEGDEFESSEL, L., AZUMA, J., TOH, R., DENG, A., MERK, D. R., RAIESDANA, A., LEEPER, N. J., RAAZ, U., SCHOELMERICH, A. M., MCCONNELL, M. V., DALMAN, R. L., SPIN, J. M. & TSAO, P. S. 2012. MicroRNA-21 blocks abdominal aortic aneurysm development and nicotine-augmented expansion. *Sci Transl Med*, 4, 122ra22.
- MALIK, N., GUNN, J., HOLT, C. M., SHEPHERD, L., FRANCIS, S. E., NEWMAN, C. M., CROSSMAN, D. C. & CUMBERLAND, D. C. 1998. Intravascular stents: a new technique for tissue processing for histology, immunohistochemistry, and transmission electron microscopy. *Heart*, 80, 509-16.
- MANCINI, D., PINNEY, S., BURKHOFF, D., LAMANCA, J., ITESCU, S., BURKE, E., EDWARDS, N., OZ, M. & MARKS, A. R. 2003. Use of rapamycin slows progression of cardiac transplantation vasculopathy. *Circulation*, 108, 48-53.
- MANTOVANI, A., BISWAS, S. K., GALDIERO, M. R., SICA, A. & LOCATI, M. 2013. Macrophage plasticity and polarization in tissue repair and remodelling. *J Pathol*, 229, 176-85.
- MANTOVANI, A. & LOCATI, M. 2013. Tumor-associated macrophages as a paradigm of macrophage plasticity, diversity, and polarization: lessons and open questions. *Arterioscler Thromb Vasc Biol*, 33, 1478-83.
- MARX, N., SCHONBECK, U., LAZAR, M. A., LIBBY, P. & PLUTZKY, J. 1998. Peroxisome proliferator-activated receptor gamma activators inhibit gene expression and migration in human vascular smooth muscle cells. *Circ Res*, 83, 1097-103.

- MARZIO, R., JIRILLO, E., RANSIJN, A., MAUEL, J. & CORRADIN, S. B. 1997. Expression and function of the early activation antigen CD69 in murine macrophages. *J Leukoc Biol*, 62, 349-55.
- MCCLURE, P. 2015. *A Multicenter Phase I Study of MRX34, MicroRNA miR-RX34 Liposomal Injection* [Online]. Available: <https://clinicaltrials.gov/ct2/show/NCT01829971>.
- MCDONALD, R. A., HALLIDAY, C. A., MILLER, A. M., DIVER, L. A., DAKIN, R. S., MONTGOMERY, J., MCBRIDE, M. W., KENNEDY, S., MCCLURE, J. D., ROBERTSON, K. E., DOUGLAS, G., CHANNON, K. M., OLDROYD, K. G. & BAKER, A. H. 2015. Reducing In-Stent Restenosis: Therapeutic Manipulation of miRNA in Vascular Remodeling and Inflammation. *J Am Coll Cardiol*, 65, 2314-27.
- MCDONALD, R. A., WHITE, K. M., WU, J., COOLEY, B. C., ROBERTSON, K. E., HALLIDAY, C. A., MCCLURE, J. D., FRANCIS, S., LU, R., KENNEDY, S., GEORGE, S. J., WAN, S., VAN ROOIJ, E. & BAKER, A. H. 2013. miRNA-21 is dysregulated in response to vein grafting in multiple models and genetic ablation in mice attenuates neointima formation. *Eur Heart J*, 34, 1636-43.
- MCFADDEN, E. P., STABILE, E., REGAR, E., CHENEAU, E., ONG, A. T., KINNAIRD, T., SUDDATH, W. O., WEISSMAN, N. J., TORGUSON, R., KENT, K. M., PICHARD, A. D., SATLER, L. F., WAKSMAN, R. & SERRUYS, P. W. 2004. Late thrombosis in drug-eluting coronary stents after discontinuation of antiplatelet therapy. *Lancet*, 364, 1519-21.
- MEGURO, T., NAKASHIMA, H., KAWADA, S., TOKUNAGA, K. & OHMOTO, T. 2000. Effect of external stenting and systemic hypertension on intimal hyperplasia in rat vein grafts. *Neurosurgery*, 46, 963-9; discussion 969-70.
- MEHRAN, R., DANGAS, G., ABIZAID, A. S., MINTZ, G. S., LANSKY, A. J., SATLER, L. F., PICHARD, A. D., KENT, K. M., STONE, G. W. & LEON, M. B. 1999. Angiographic patterns of in-stent restenosis: classification and implications for long-term outcome. *Circulation*, 100, 1872-8.
- MENG, F., HENSON, R., WEHBE-JANEK, H., GHOSHAL, K., JACOB, S. T. & PATEL, T. 2007. MicroRNA-21 regulates expression of the PTEN tumor suppressor gene in human hepatocellular cancer. *Gastroenterology*, 133, 647-58.
- MIANO, J. M. 2010. Vascular smooth muscle cell differentiation-2010. *J Biomed Res*, 24, 169-80.
- MIANO, J. M., CSERJESI, P., LIGON, K. L., PERIASAMY, M. & OLSON, E. N. 1994. Smooth muscle myosin heavy chain exclusively marks the smooth muscle lineage during mouse embryogenesis. *Circ Res*, 75, 803-12.
- MICKELSON, J. K., LAKKIS, N. M., VILLARREAL-LEVY, G., HUGHES, B. J. & SMITH, C. W. 1996. Leukocyte activation with platelet adhesion after coronary angioplasty: a mechanism for recurrent disease? *J Am Coll Cardiol*, 28, 345-53.
- MONTALESCOT, G., SECHTEM, U., ACHENBACH, S., ANDREOTTI, F., ARDEN, C., BUDAJ, A., BUGIARDINI, R., CREA, F., CUISSET, T., DI MARIO, C., FERREIRA, J. R., GERSH, B. J., GITT, A. K., HULOT, J. S., MARX, N., OPIE, L. H., PFISTERER, M., PRESCOTT, E., RUSCHITZKA, F., SABATE, M., SENIOR, R., TAGGART, D. P., VAN DER WALL, E. E., VRINTS, C. J., ZAMORANO, J. L., BAUMGARTNER, H., BAX, J. J., BUENO, H., DEAN, V., DEATON, C., EROL, C., FAGARD, R., FERRARI, R., HASDAI, D., HOES, A. W., KIRCHHOF, P., KNUUTI, J., KOLH, P., LANCELLOTTI, P., LINHART, A., NIHOYANNOPOULOS, P., PIEPOLI, M. F., PONIKOWSKI, P., SIRNES, P. A., TAMARGO, J. L., TENDERA, M., TORBICKI, A., WIJNS, W., WINDECKER, S., VALGIMIGLI, M., CLAEYS, M. J., DONNER-BANZHOF, N., FRANK, H.,

- FUNCK-BRENTANO, C., GAEMPERLI, O., GONZALEZ-JUANATEY, J. R., HAMILOS, M., HUSTED, S., JAMES, S. K., KERVINEN, K., KRISTENSEN, S. D., MAGGIONI, A. P., PRIES, A. R., ROMEO, F., RYDEN, L., SIMOONS, M. L., STEG, P. G., TIMMIS, A. & YILDIRIR, A. 2013. 2013 ESC guidelines on the management of stable coronary artery disease: the Task Force on the management of stable coronary artery disease of the European Society of Cardiology. *Eur Heart J*, 34, 2949-3003.
- MONTGOMERY, R. L., HULLINGER, T. G., SEMUS, H. M., DICKINSON, B. A., SETO, A. G., LYNCH, J. M., STACK, C., LATIMER, P. A., OLSON, E. N. & VAN ROOIJ, E. 2011. Therapeutic inhibition of miR-208a improves cardiac function and survival during heart failure. *Circulation*, 124, 1537-47.
- MOORE, K. J., SHEEDY, F. J. & FISHER, E. A. 2013. Macrophages in atherosclerosis: a dynamic balance. *Nat Rev Immunol*, 13, 709-21.
- MORICE, M. C., SERRUYS, P. W., SOUSA, J. E., FAJADET, J., BAN HAYASHI, E., PERIN, M., COLOMBO, A., SCHULER, G., BARRAGAN, P., GUAGLIUMI, G., MOLNAR, F., FALOTICO, R. & LESIONS, R. S. G. R. S. W. T. S.-C. B. V. B.-E. S. I. T. T. O. P. W. D. N. N. C. A. 2002. A randomized comparison of a sirolimus-eluting stent with a standard stent for coronary revascularization. *N Engl J Med*, 346, 1773-80.
- MOROI, M., ZHANG, L., YASUDA, T., VIRMANI, R., GOLD, H. K., FISHMAN, M. C. & HUANG, P. L. 1998. Interaction of genetic deficiency of endothelial nitric oxide, gender, and pregnancy in vascular response to injury in mice. *J Clin Invest*, 101, 1225-32.
- MOSSER, D. M. & EDWARDS, J. P. 2008. Exploring the full spectrum of macrophage activation. *Nat Rev Immunol*, 8, 958-69.
- MOTWANI, J. G. & TOPOL, E. J. 1998. Aortocoronary saphenous vein graft disease: pathogenesis, predisposition, and prevention. *Circulation*, 97, 916-31.
- MURRAY, P. J. & WYNN, T. A. 2011. Protective and pathogenic functions of macrophage subsets. *Nat Rev Immunol*, 11, 723-37.
- NAIR, M. G., COCHRANE, D. W. & ALLEN, J. E. 2003. Macrophages in chronic type 2 inflammation have a novel phenotype characterized by the abundant expression of Ym1 and Fizz1 that can be partly replicated in vitro. *Immunol Lett*, 85, 173-80.
- NAZARI-JAHANTIGH, M., WEI, Y., NOELS, H., AKHTAR, S., ZHOU, Z., KOENEN, R. R., HEYLL, K., GREMSE, F., KIESSLING, F., GROMMES, J., WEBER, C. & SCHOBER, A. 2012. MicroRNA-155 promotes atherosclerosis by repressing Bcl6 in macrophages. *J Clin Invest*, 122, 4190-202.
- NEBEKER, J. R., VIRMANI, R., BENNETT, C. L., HOFFMAN, J. M., SAMORE, M. H., ALVAREZ, J., DAVIDSON, C. J., MCKOY, J. M., RAISCH, D. W., WHISENANT, B. K., YARNOLD, P. R., BELKNAP, S. M., WEST, D. P., GAGE, J. E., MORSE, R. E., GLIGORIC, G., DAVIDSON, L. & FELDMAN, M. D. 2006. Hypersensitivity cases associated with drug-eluting coronary stents: a review of available cases from the Research on Adverse Drug Events and Reports (RADAR) project. *J Am Coll Cardiol*, 47, 175-81.
- NEUMANN, F. J., OTT, I., GAWAZ, M., PUCHNER, G. & SCHOMIG, A. 1996. Neutrophil and platelet activation at balloon-injured coronary artery plaque in patients undergoing angioplasty. *J Am Coll Cardiol*, 27, 819-24.
- NI, C. W., QIU, H. & JO, H. 2011. MicroRNA-663 upregulated by oscillatory shear stress plays a role in inflammatory response of endothelial cells. *Am J Physiol Heart Circ Physiol*, 300, H1762-9.

- NICHOLS, M., TOWNSEND, N., SCARBOROUGH, P. & RAYNER, M. 2014. Cardiovascular disease in Europe 2014: epidemiological update. *Eur Heart J*, 35, 2929.
- NICOLI, S., KNYPHAUSEN, C. P., ZHU, L. J., LAKSHMANAN, A. & LAWSON, N. D. 2012. miR-221 is required for endothelial tip cell behaviors during vascular development. *Dev Cell*, 22, 418-29.
- O'SULLIVAN, J. F., MARTIN, K. & CAPLICE, N. M. 2011. Microribonucleic acids for prevention of plaque rupture and in-stent restenosis: "a finger in the dam". *J Am Coll Cardiol*, 57, 383-9.
- ODEGAARD, J. I. & CHAWLA, A. 2011. Alternative macrophage activation and metabolism. *Annu Rev Pathol*, 6, 275-97.
- ODEGAARD, J. I., RICARDO-GONZALEZ, R. R., GOFORTH, M. H., MOREL, C. R., SUBRAMANIAN, V., MUKUNDAN, L., RED EAGLE, A., VATS, D., BROMBACHER, F., FERRANTE, A. W. & CHAWLA, A. 2007. Macrophage-specific PPARgamma controls alternative activation and improves insulin resistance. *Nature*, 447, 1116-20.
- OROM, U. A., NIELSEN, F. C. & LUND, A. H. 2008. MicroRNA-10a binds the 5'UTR of ribosomal protein mRNAs and enhances their translation. *Mol Cell*, 30, 460-71.
- OWENS, G. K., KUMAR, M. S. & WAMHOFF, B. R. 2004. Molecular regulation of vascular smooth muscle cell differentiation in development and disease. *Physiol Rev*, 84, 767-801.
- PAGANO, P. J., ITO, Y., TORNHEIM, K., GALLOP, P. M., TAUBER, A. I. & COHEN, R. A. 1995. An NADPH oxidase superoxide-generating system in the rabbit aorta. *Am J Physiol*, 268, H2274-80.
- PAN, Y., BALAZS, L., TIGYI, G. & YUE, J. 2011. Conditional deletion of Dicer in vascular smooth muscle cells leads to the developmental delay and embryonic mortality. *Biochem Biophys Res Commun*, 408, 369-74.
- PASQUINELLI, A. E., REINHART, B. J., SLACK, F., MARTINDALE, M. Q., KURODA, M. I., MALLER, B., HAYWARD, D. C., BALL, E. E., DEGNAN, B., MULLER, P., SPRING, J., SRINIVASAN, A., FISHMAN, M., FINNERTY, J., CORBO, J., LEVINE, M., LEAHY, P., DAVIDSON, E. & RUVKUN, G. 2000. Conservation of the sequence and temporal expression of let-7 heterochronic regulatory RNA. *Nature*, 408, 86-9.
- PATRICK, D. M., MONTGOMERY, R. L., QI, X., OBAD, S., KAUPPINEN, S., HILL, J. A., VAN ROOIJ, E. & OLSON, E. N. 2010. Stress-dependent cardiac remodeling occurs in the absence of microRNA-21 in mice. *J Clin Invest*, 120, 3912-6.
- PAULI, A., RINN, J. L. & SCHIER, A. F. 2011. Non-coding RNAs as regulators of embryogenesis. *Nat Rev Genet*, 12, 136-49.
- PEIRO, C., REDONDO, J., RODRIGUEZ-MARTINEZ, M. A., ANGULO, J., MARIN, J. & SANCHEZ-FERRER, C. F. 1995. Influence of endothelium on cultured vascular smooth muscle cell proliferation. *Hypertension*, 25, 748-51.
- PIDKOVKA, N. A., CHEREPANOVA, O. A., YOSHIDA, T., ALEXANDER, M. R., DEATON, R. A., THOMAS, J. A., LEITINGER, N. & OWENS, G. K. 2007. Oxidized phospholipids induce phenotypic switching of vascular smooth muscle cells in vivo and in vitro. *Circ Res*, 101, 792-801.
- PILLAI, R. S., BHATTACHARYYA, S. N., ARTUS, C. G., ZOLLER, T., COUGOT, N., BASYUK, E., BERTRAND, E. & FILIPOWICZ, W. 2005. Inhibition of translational initiation by Let-7 MicroRNA in human cells. *Science*, 309, 1573-6.
- POLYAK, K., LEE, M. H., ERDJUMENT-BROMAGE, H., KOFF, A., ROBERTS, J. M., TEMPST, P. & MASSAGUE, J. 1994. Cloning of p27Kip1, a cyclin-dependent

- kinase inhibitor and a potential mediator of extracellular antimitogenic signals. *Cell*, 78, 59-66.
- PRITCHARD, K. A., JR., GROSZEK, L., SMALLEY, D. M., SESSA, W. C., WU, M., VILLALON, P., WOLIN, M. S. & STEMERMAN, M. B. 1995. Native low-density lipoprotein increases endothelial cell nitric oxide synthase generation of superoxide anion. *Circ Res*, 77, 510-8.
- PURICEL, S., ARROYO, D., CORPATAUX, N., BAERISWYL, G., LEHMANN, S., KALLINIKOU, Z., MULLER, O., ALLARD, L., STAUFFER, J. C., TOGNI, M., GOY, J. J. & COOK, S. 2015. Comparison of everolimus- and biolimus-eluting coronary stents with everolimus-eluting bioresorbable vascular scaffolds. *J Am Coll Cardiol*, 65, 791-801.
- QUINN, M. T., PARTHASARATHY, S., FONG, L. G. & STEINBERG, D. 1987. Oxidatively modified low density lipoproteins: a potential role in recruitment and retention of monocyte/macrophages during atherogenesis. *Proc Natl Acad Sci U S A*, 84, 2995-8.
- RAES, G., DE BAETSELIER, P., NOEL, W., BESCHIN, A., BROMBACHER, F. & HASSANZADEH GH, G. 2002. Differential expression of FIZZ1 and Ym1 in alternatively versus classically activated macrophages. *J Leukoc Biol*, 71, 597-602.
- RAGOSTA, M., GIMPLE, L. W., GERTZ, S. D., DUNWIDDIE, C. T., VLASUK, G. P., HABER, H. L., POWERS, E. R., ROBERTS, W. C. & SAREMBOCK, I. J. 1994. Specific factor Xa inhibition reduces restenosis after balloon angioplasty of atherosclerotic femoral arteries in rabbits. *Circulation*, 89, 1262-71.
- RAITOHARJU, E., LYYTIKAINEN, L. P., LEVULA, M., OKSALA, N., MENNANDER, A., TARKKA, M., KLOPP, N., ILLIG, T., KAHONEN, M., KARHUNEN, P. J., LAAKSONEN, R. & LEHTIMAKI, T. 2011. miR-21, miR-210, miR-34a, and miR-146a/b are up-regulated in human atherosclerotic plaques in the Tampere Vascular Study. *Atherosclerosis*, 219, 211-7.
- RANGREZ, A. Y., MASSY, Z. A., METZINGER-LE MEUTH, V. & METZINGER, L. 2011. miR-143 and miR-145: molecular keys to switch the phenotype of vascular smooth muscle cells. *Circ Cardiovasc Genet*, 4, 197-205.
- REINHART, B. J., SLACK, F. J., BASSON, M., PASQUINELLI, A. E., BETTINGER, J. C., ROUGVIE, A. E., HORVITZ, H. R. & RUVKUN, G. 2000. The 21-nucleotide let-7 RNA regulates developmental timing in *Caenorhabditis elegans*. *Nature*, 403, 901-6.
- RIBAS, J., NI, X., CASTANARES, M., LIU, M. M., ESOPPI, D., YEGNASUBRAMANIAN, S., RODRIGUEZ, R., MENDELL, J. T. & LUPOLD, S. E. 2012. A novel source for miR-21 expression through the alternative polyadenylation of VMP1 gene transcripts. *Nucleic Acids Res*, 40, 6821-33.
- RIPPSTEIN, P., BLACK, M. K., BOIVIN, M., VEINOT, J. P., MA, X., CHEN, Y. X., HUMAN, P., ZILLA, P. & O'BRIEN, E. R. 2006. Comparison of processing and sectioning methodologies for arteries containing metallic stents. *J Histochem Cytochem*, 54, 673-81.
- ROBBE, P., DRAIJER, C., BORG, T. R., LUINGE, M., TIMENS, W., WOUTERS, I. M., MELGERT, B. N. & HYLKEMA, M. N. 2015. Distinct macrophage phenotypes in allergic and nonallergic lung inflammation. *Am J Physiol Lung Cell Mol Physiol*, 308, L358-67.
- ROBBINS, C. S., HILGENDORF, I., WEBER, G. F., THEURL, I., IWAMOTO, Y., FIGUEIREDO, J. L., GORBATOV, R., SUKHOVA, G. K., GERHARDT, L. M., SMYTH, D., ZAVITZ, C. C., SHIKATANI, E. A., PARSONS, M., VAN ROOIJEN, N., LIN, H. Y., HUSAIN, M., LIBBY, P., NAHRENDORF, M., WEISSLEDER, R. & SWIRSKI, F. K. 2013. Local proliferation dominates lesional macrophage accumulation in atherosclerosis. *Nat Med*, 19, 1166-72.

- RODMAN, D. 2015. Safety, Tolerability and Pharmacokinetic Study of MRG-201 in Healthy Volunteers and Patients With Cutaneous Scleroderma.
- RODRIGUEZ, A., GRIFFITHS-JONES, S., ASHURST, J. L. & BRADLEY, A. 2004. Identification of mammalian microRNA host genes and transcription units. *Genome Res*, 14, 1902-10.
- RODRIGUEZ-MENOCAL, L., WEI, Y., PHAM, S. M., ST-PIERRE, M., LI, S., WEBSTER, K., GOLDSCHMIDT-CLERMONT, P. & VAZQUEZ-PADRON, R. I. 2010. A novel mouse model of in-stent restenosis. *Atherosclerosis*, 209, 359-66.
- ROGERS, C., WELT, F. G., KARNOVSKY, M. J. & EDELMAN, E. R. 1996. Monocyte recruitment and neointimal hyperplasia in rabbits. Coupled inhibitory effects of heparin. *Arterioscler Thromb Vasc Biol*, 16, 1312-8.
- ROKS, A. J., HENNING, R. H., VAN BOVEN, A. J., TIO, R. A. & VAN GILST, W. H. 2002. Rat abdominal aortic stenting: a simple model displaying in-stent restenosis. *Am J Cardiol*, 89, 1149-50.
- ROQUE, M., KIM, W. J., GAZDOIN, M., MALIK, A., REIS, E. D., FALLON, J. T., BADIMON, J. J., CHARO, I. F. & TAUBMAN, M. B. 2002. CCR2 deficiency decreases intimal hyperplasia after arterial injury. *Arterioscler Thromb Vasc Biol*, 22, 554-9.
- ROSS, R. 1999. Atherosclerosis--an inflammatory disease. *N Engl J Med*, 340, 115-26.
- ROUBIN, G. S., ROBINSON, K. A., KING, S. B., 3RD, GIANTURCO, C., BLACK, A. J., BROWN, J. E., SIEGEL, R. J. & DOUGLAS, J. S., JR. 1987. Early and late results of intracoronary arterial stenting after coronary angioplasty in dogs. *Circulation*, 76, 891-7.
- RYAN, T. J. 2002. The coronary angiogram and its seminal contributions to cardiovascular medicine over five decades. *Circulation*, 106, 752-6.
- SABATEL, C., MALVAUX, L., BOVY, N., DEROANNE, C., LAMBERT, V., GONZALEZ, M. L., COLIGE, A., RAKIC, J. M., NOEL, A., MARTIAL, J. A. & STRUMAN, I. 2011. MicroRNA-21 exhibits antiangiogenic function by targeting RhoB expression in endothelial cells. *PLoS One*, 6, e16979.
- SANTIS, A. G., CAMPANERO, M. R., ALONSO, J. L., TUGORES, A., ALONSO, M. A., YAGUE, E., PIVEL, J. P. & SANCHEZ-MADRID, F. 1992. Tumor necrosis factor-alpha production induced in T lymphocytes through the AIM/CD69 activation pathway. *Eur J Immunol*, 22, 1253-9.
- SARKAR, J., GOU, D., TURAKA, P., VIKTOROVA, E., RAMCHANDRAN, R. & RAJ, J. U. 2010. MicroRNA-21 plays a role in hypoxia-mediated pulmonary artery smooth muscle cell proliferation and migration. *Am J Physiol Lung Cell Mol Physiol*, 299, L861-71.
- SASU, S. & BEASLEY, D. 2000. Essential roles of IkappaB kinases alpha and beta in serum- and IL-1-induced human VSMC proliferation. *Am J Physiol Heart Circ Physiol*, 278, H1823-31.
- SCHEE, K., BOYE, K., ABRAHAMSEN, T. W., FODSTAD, O. & FLATMARK, K. 2012. Clinical relevance of microRNA miR-21, miR-31, miR-92a, miR-101, miR-106a and miR-145 in colorectal cancer. *BMC Cancer*, 12, 505.
- SCHWARTZ, R. S., EDWARDS, W. D., BAILEY, K. R., CAMRUD, A. R., JORGENSEN, M. A. & HOLMES, D. R., JR. 1994. Differential neointimal response to coronary artery injury in pigs and dogs. Implications for restenosis models. *Arterioscler Thromb*, 14, 395-400.
- SCHWARTZ, R. S., HUBER, K. C., MURPHY, J. G., EDWARDS, W. D., CAMRUD, A. R., VLIETSTRA, R. E. & HOLMES, D. R. 1992. Restenosis and the proportional neointimal response to coronary artery injury: results in a porcine model. *J Am Coll Cardiol*, 19, 267-74.

- SCHWARTZ, R. S., MURPHY, J. G., EDWARDS, W. D., CAMRUD, A. R., VLIESTRA, R. E. & HOLMES, D. R. 1990. Restenosis after balloon angioplasty. A practical proliferative model in porcine coronary arteries. *Circulation*, 82, 2190-200.
- SERRUYS, P. W., DE JAEGERE, P., KIEMENEIJ, F., MACAYA, C., RUTSCH, W., HEYNDRIKX, G., EMANUELSSON, H., MARCO, J., LEGRAND, V., MATERNE, P. & ET AL. 1994. A comparison of balloon-expandable-stent implantation with balloon angioplasty in patients with coronary artery disease. Benestent Study Group. *N Engl J Med*, 331, 489-95.
- SETHUPATHY, P., BOREL, C., GAGNEBIN, M., GRANT, G. R., DEUTSCH, S., ELTON, T. S., HATZIGEORGIOU, A. G. & ANTONARAKIS, S. E. 2007. Human microRNA-155 on chromosome 21 differentially interacts with its polymorphic target in the AGTR1 3' untranslated region: a mechanism for functional single-nucleotide polymorphisms related to phenotypes. *Am J Hum Genet*, 81, 405-13.
- SHEEDY, F. J., PALSSON-MCDERMOTT, E., HENNESSY, E. J., MARTIN, C., O'LEARY, J. J., RUAN, Q., JOHNSON, D. S., CHEN, Y. & O'NEILL, L. A. 2010. Negative regulation of TLR4 via targeting of the proinflammatory tumor suppressor PDCD4 by the microRNA miR-21. *Nat Immunol*, 11, 141-7.
- SHI, C., LIANG, Y., YANG, J., XIA, Y., CHEN, H., HAN, H., YANG, Y., WU, W., GAO, R. & QIN, H. 2013. MicroRNA-21 knockout improve the survival rate in DSS induced fatal colitis through protecting against inflammation and tissue injury. *PLoS One*, 8, e66814.
- SHU, H., WONG, B., ZHOU, G., LI, Y., BERGER, J., WOODS, J. W., WRIGHT, S. D. & CAI, T. Q. 2000. Activation of PPARalpha or gamma reduces secretion of matrix metalloproteinase 9 but not interleukin 8 from human monocytic THP-1 cells. *Biochem Biophys Res Commun*, 267, 345-9.
- SICA, A. & MANTOVANI, A. 2012. Macrophage plasticity and polarization: in vivo veritas. *J Clin Invest*, 122, 787-95.
- SIGWART, U., PUEL, J., MIRKOVITCH, V., JOFFRE, F. & KAPPENBERGER, L. 1987. Intravascular stents to prevent occlusion and restenosis after transluminal angioplasty. *N Engl J Med*, 316, 701-6.
- SIMSEKYILMAZ, S., SCHREIBER, F., WEINANDY, S., GREMSE, F., SONMEZ, T. T. & LIEHN, E. A. 2013. A murine model of stent implantation in the carotid artery for the study of restenosis. *J Vis Exp*, e50233.
- SMALL, E. M. & OLSON, E. N. 2011. Pervasive roles of microRNAs in cardiovascular biology. *Nature*, 469, 336-42.
- SMITH, J. D., TROGAN, E., GINSBERG, M., GRIGAUX, C., TIAN, J. & MIYATA, M. 1995. Decreased atherosclerosis in mice deficient in both macrophage colony-stimulating factor (op) and apolipoprotein E. *Proc Natl Acad Sci U S A*, 92, 8264-8.
- SONG, J., HU, B., QU, H., BI, C., HUANG, X. & ZHANG, M. 2012. Mechanical stretch modulates microRNA 21 expression, participating in proliferation and apoptosis in cultured human aortic smooth muscle cells. *PLoS One*, 7, e47657.
- SONG, J. J., SMITH, S. K., HANNON, G. J. & JOSHUA-TOR, L. 2004. Crystal structure of Argonaute and its implications for RISC slicer activity. *Science*, 305, 1434-7.
- STAMLER, J., WENTWORTH, D. & NEATON, J. D. 1986. Is relationship between serum cholesterol and risk of premature death from coronary heart disease continuous and graded? Findings in 356,222 primary screenees of the Multiple Risk Factor Intervention Trial (MRFIT). *JAMA*, 256, 2823-8.

- STARY, H. C. 2000. Natural history and histological classification of atherosclerotic lesions: an update. *Arterioscler Thromb Vasc Biol*, 20, 1177-8.
- STEELE, P. M., CHESEBRO, J. H., STANSON, A. W., HOLMES, D. R., JR., DEWANJEE, M. K., BADIMON, L. & FUSTER, V. 1985. Balloon angioplasty. Natural history of the pathophysiological response to injury in a pig model. *Circ Res*, 57, 105-12.
- STEVENS, A. A. L., J 1999. *Human Histology*, Barcelona, Spain, Mosby.
- STOUT, R. W., BIERMAN, E. L. & ROSS, R. 1975. Effect of insulin on the proliferation of cultured primate arterial smooth muscle cells. *Circ Res*, 36, 319-27.
- SUAREZ, Y., FERNANDEZ-HERNANDO, C., POBER, J. S. & SESSA, W. C. 2007. Dicer dependent microRNAs regulate gene expression and functions in human endothelial cells. *Circ Res*, 100, 1164-73.
- SUAREZ, Y., FERNANDEZ-HERNANDO, C., YU, J., GERBER, S. A., HARRISON, K. D., POBER, J. S., IRUELA-ARISPE, M. L., MERKENSCHLAGER, M. & SESSA, W. C. 2008. Dicer-dependent endothelial microRNAs are necessary for postnatal angiogenesis. *Proc Natl Acad Sci U S A*, 105, 14082-7.
- SUN, F., FU, H., LIU, Q., TIE, Y., ZHU, J., XING, R., SUN, Z. & ZHENG, X. 2008. Downregulation of CCND1 and CDK6 by miR-34a induces cell cycle arrest. *FEBS Lett*, 582, 1564-8.
- SUN, J., MARX, S. O., CHEN, H. J., POON, M., MARKS, A. R. & RABBANI, L. E. 2001. Role for p27(Kip1) in Vascular Smooth Muscle Cell Migration. *Circulation*, 103, 2967-72.
- SUN, S. G., ZHENG, B., HAN, M., FANG, X. M., LI, H. X., MIAO, S. B., SU, M., HAN, Y., SHI, H. J. & WEN, J. K. 2011. miR-146a and Kruppel-like factor 4 form a feedback loop to participate in vascular smooth muscle cell proliferation. *EMBO Rep*, 12, 56-62.
- SUNDARESAN, M., YU, Z. X., FERRANS, V. J., IRANI, K. & FINKEL, T. 1995. Requirement for generation of H₂O₂ for platelet-derived growth factor signal transduction. *Science*, 270, 296-9.
- SUZUKI, H. I., YAMAGATA, K., SUGIMOTO, K., IWAMOTO, T., KATO, S. & MIYAZONO, K. 2009. Modulation of microRNA processing by p53. *Nature*, 460, 529-33.
- SZANTO, A., BALINT, B. L., NAGY, Z. S., BARTA, E., DEZSO, B., PAP, A., SZELES, L., POLISKA, S., OROS, M., EVANS, R. M., BARAK, Y., SCHWABE, J. & NAGY, L. 2010. STAT6 transcription factor is a facilitator of the nuclear receptor PPAR γ -regulated gene expression in macrophages and dendritic cells. *Immunity*, 33, 699-712.
- TALOTTA, F., CIMMINO, A., MATARAZZO, M. R., CASALINO, L., DE VITA, G., D'ESPOSITO, M., DI LAURO, R. & VERDE, P. 2009. An autoregulatory loop mediated by miR-21 and PDCD4 controls the AP-1 activity in RAS transformation. *Oncogene*, 28, 73-84.
- TAY, Y., ZHANG, J., THOMSON, A. M., LIM, B. & RIGOUTSOS, I. 2008. MicroRNAs to Nanog, Oct4 and Sox2 coding regions modulate embryonic stem cell differentiation. *Nature*, 455, 1124-8.
- THUM, T., CHAU, N., BHAT, B., GUPTA, S. K., LINSLEY, P. S., BAUERSACHS, J. & ENGELHARDT, S. 2011. Comparison of different miR-21 inhibitor chemistries in a cardiac disease model. *J Clin Invest*, 121, 461-2; author reply 462-3.
- THUM, T., GROSS, C., FIEDLER, J., FISCHER, T., KISSLER, S., BUSSEN, M., GALUPPO, P., JUST, S., ROTTBAUER, W., FRANTZ, S., CASTOLDI, M., SOUTSCHEK, J., KOTELIANSKY, V., ROSENWALD, A., BASSON, M. A., LICHT,

- J. D., PENA, J. T., ROUHANIFARD, S. H., MUCKENTHALER, M. U., TUSCHL, T., MARTIN, G. R., BAUERSACHS, J. & ENGELHARDT, S. 2008. MicroRNA-21 contributes to myocardial disease by stimulating MAP kinase signalling in fibroblasts. *Nature*, 456, 980-4.
- TORELLA, D., IACONETTI, C., CATALUCCI, D., ELLISON, G. M., LEONE, A., WARING, C. D., BOCHICCHIO, A., VICINANZA, C., AQUILA, I., CURCIO, A., CONDORELLI, G. & INDOLFI, C. 2011. MicroRNA-133 controls vascular smooth muscle cell phenotypic switch in vitro and vascular remodeling in vivo. *Circ Res*, 109, 880-93.
- TORGERSEN, J. S., TAKLE, H. & ANDERSEN, O. 2009. Localization of mRNAs and proteins in methyl methacrylate-embedded tissues. *J Histochem Cytochem*, 57, 825-30.
- TOUCHARD, A. G. & SCHWARTZ, R. S. 2006. Preclinical restenosis models: challenges and successes. *Toxicol Pathol*, 34, 11-8.
- TUGAL, D., LIAO, X. & JAIN, M. K. 2013. Transcriptional control of macrophage polarization. *Arterioscler Thromb Vasc Biol*, 33, 1135-44.
- TULETA, I., SKOWASCH, D., PEUSTER, M., NICKENIG, G. & BAURIEDEL, G. 2008. Cells of primarily extravascular origin in neointima formation following stent implantation: coordinated expression of endothelial progenitor, dendritic and neural crest-derived cells. *Cardiology*, 110, 199-205.
- URBAN, P., ABIZAID, A., CHEVALIER, B., GREENE, S., MEREDITH, I., MORICE, M. C. & POCOCCO, S. 2013. Rationale and design of the LEADERS FREE trial: A randomized double-blind comparison of the BioFreedom drug-coated stent vs the Gazelle bare metal stent in patients at high bleeding risk using a short (1 month) course of dual antiplatelet therapy. *Am Heart J*, 165, 704-9.
- VAN DER WAL, A. C., BECKER, A. E., VAN DER LOOS, C. M. & DAS, P. K. 1994. Site of intimal rupture or erosion of thrombosed coronary atherosclerotic plaques is characterized by an inflammatory process irrespective of the dominant plaque morphology. *Circulation*, 89, 36-44.
- VAN ROOIJ, E. & OLSON, E. N. 2012. MicroRNA therapeutics for cardiovascular disease: opportunities and obstacles. *Nat Rev Drug Discov*, 11, 860-72.
- VAN ROOIJ, E., PURCELL, A. L. & LEVIN, A. A. 2012. Developing microRNA therapeutics. *Circ Res*, 110, 496-507.
- VAN TITS, L. J., STIENSTRA, R., VAN LENT, P. L., NETEA, M. G., JOOSTEN, L. A. & STALENHOF, A. F. 2011. Oxidized LDL enhances pro-inflammatory responses of alternatively activated M2 macrophages: a crucial role for Kruppel-like factor 2. *Atherosclerosis*, 214, 345-9.
- VIRMANI, R. & FARB, A. 1999. Pathology of in-stent restenosis. *Curr Opin Lipidol*, 10, 499-506.
- VIRMANI, R., GUAGLIUMI, G., FARB, A., MUSUMECI, G., GRIECO, N., MOTTA, T., MIHALCSIK, L., TESPILI, M., VALSECCHI, O. & KOLODGIE, F. D. 2004. Localized hypersensitivity and late coronary thrombosis secondary to a sirolimus-eluting stent: should we be cautious? *Circulation*, 109, 701-5.
- WAKSMAN, R., PAKALA, R., BAFFOUR, R., SEABRON, R., HELLINGA, D., CHAN, R., SU, S. H., KOLODGIE, F. & VIRMANI, R. 2012. In vivo comparison of a polymer-free Biolimus A9-eluting stent with a biodegradable polymer-based Biolimus A9 eluting stent and a bare metal stent in balloon denuded and radiated hypercholesterolemic rabbit iliac arteries. *Catheter Cardiovasc Interv*, 80, 429-36.
- WALLENTIN, L., BECKER, R. C., BUDAJ, A., CANNON, C. P., EMANUELSSON, H., HELD, C., HORROW, J., HUSTED, S., JAMES, S., KATUS, H., MAHAFFEY, K. W., SCIRICA, B. M., SKENE, A., STEG, P. G., STOREY, R. F., HARRINGTON,

- R. A., INVESTIGATORS, P., FREIJ, A. & THORSEN, M. 2009. Ticagrelor versus clopidogrel in patients with acute coronary syndromes. *N Engl J Med*, 361, 1045-57.
- WANG, F., ZHAO, X. Q., LIU, J. N., WANG, Z. H., WANG, X. L., HOU, X. Y., LIU, R., GAO, F., ZHANG, M. X., ZHANG, Y. & BU, P. L. 2012a. Antagonist of microRNA-21 improves balloon injury-induced rat iliac artery remodeling by regulating proliferation and apoptosis of adventitial fibroblasts and myofibroblasts. *J Cell Biochem*, 113, 2989-3001.
- WANG, M., LI, W., CHANG, G. Q., YE, C. S., OU, J. S., LI, X. X., LIU, Y., CHEANG, T. Y., HUANG, X. L. & WANG, S. M. 2011. MicroRNA-21 regulates vascular smooth muscle cell function via targeting tropomyosin 1 in arteriosclerosis obliterans of lower extremities. *Arterioscler Thromb Vasc Biol*, 31, 2044-53.
- WANG, Y. S., WANG, H. Y., LIAO, Y. C., TSAI, P. C., CHEN, K. C., CHENG, H. Y., LIN, R. T. & JUO, S. H. 2012b. MicroRNA-195 regulates vascular smooth muscle cell phenotype and prevents neointimal formation. *Cardiovasc Res*, 95, 517-26.
- WANG, Z., BRANDT, S., MEDEIROS, A., WANG, S., WU, H., DENT, A. & SEREZANI, C. H. 2015. MicroRNA 21 is a homeostatic regulator of macrophage polarization and prevents prostaglandin E2-mediated M2 generation. *PLoS One*, 10, e0115855.
- WATT, J., KENNEDY, S., MCCORMICK, C., AGBANI, E. O., MCPHADEN, A., MULLEN, A., CZUDAJ, P., BEHNISCH, B., WADSWORTH, R. M. & OLDROYD, K. G. 2013. Succinobucol-eluting stents increase neointimal thickening and peri-strut inflammation in a porcine coronary model. *Catheter Cardiovasc Interv*, 81, 698-708.
- WEBER, M., BAKER, M. B., MOORE, J. P. & SEARLES, C. D. 2010. MiR-21 is induced in endothelial cells by shear stress and modulates apoptosis and eNOS activity. *Biochem Biophys Res Commun*, 393, 643-8.
- WEI, Y., NAZARI-JAHANTIGH, M., NETH, P., WEBER, C. & SCHOBER, A. 2013. MicroRNA-126, -145, and -155: a therapeutic triad in atherosclerosis? *Arterioscler Thromb Vasc Biol*, 33, 449-54.
- WELT, F. G., EDELMAN, E. R., SIMON, D. I. & ROGERS, C. 2000. Neutrophil, not macrophage, infiltration precedes neointimal thickening in balloon-injured arteries. *Arterioscler Thromb Vasc Biol*, 20, 2553-8.
- WELT, F. G., TSO, C., EDELMAN, E. R., KJELSBERG, M. A., PAOLINI, J. F., SEIFERT, P. & ROGERS, C. 2003. Leukocyte recruitment and expression of chemokines following different forms of vascular injury. *Vasc Med*, 8, 1-7.
- WHITE, K., DEMPSIE, Y., CARUSO, P., WALLACE, E., MCDONALD, R. A., STEVENS, H., HATLEY, M. E., VAN ROOIJ, E., MORRELL, N. W., MACLEAN, M. R. & BAKER, A. H. 2014. Endothelial Apoptosis in Pulmonary Hypertension Is Controlled by a microRNA/Programmed Cell Death 4/Caspase-3 Axis. *Hypertension*, 64, 185-94.
- WIDIMSKY, P., GROCH, L., ZELIZKO, M., ASCHERMANN, M., BEDNAR, F. & SURYAPRANATA, H. 2000. Multicentre randomized trial comparing transport to primary angioplasty vs immediate thrombolysis vs combined strategy for patients with acute myocardial infarction presenting to a community hospital without a catheterization laboratory. The PRAGUE study. *Eur Heart J*, 21, 823-31.
- WIENHOLDS, E., KOUDIJS, M. J., VAN EEDEN, F. J., CUPPEN, E. & PLASTERK, R. H. 2003. The microRNA-producing enzyme Dicer1 is essential for zebrafish development. *Nat Genet*, 35, 217-8.

- WIGHTMAN, B., HA, I. & RUVKUN, G. 1993. Posttranscriptional regulation of the heterochronic gene *lin-14* by *lin-4* mediates temporal pattern formation in *C. elegans*. *Cell*, 75, 855-62.
- WILENSKY, R. L., MARCH, K. L., GRADUS-PIZLO, I., SANDUSKY, G., FINEBERG, N. & HATHAWAY, D. R. 1995. Vascular injury, repair, and restenosis after percutaneous transluminal angioplasty in the atherosclerotic rabbit. *Circulation*, 92, 2995-3005.
- WOLFS, I. M., DONNERS, M. M. & DE WINTHER, M. P. 2011. Differentiation factors and cytokines in the atherosclerotic plaque micro-environment as a trigger for macrophage polarisation. *Thromb Haemost*, 106, 763-71.
- WONG, M. M., CHEN, Y., MARGARITI, A., WINKLER, B., CAMPAGNOLO, P., POTTER, C., HU, Y. & XU, Q. 2014. Macrophages control vascular stem/progenitor cell plasticity through tumor necrosis factor-alpha-mediated nuclear factor-kappaB activation. *Arterioscler Thromb Vasc Biol*, 34, 635-43.
- WONG, N. D. 2014. Epidemiological studies of CHD and the evolution of preventive cardiology. *Nat Rev Cardiol*, 11, 276-89.
- WONG, N. D. & LEVY, D. 2013. Legacy of the framingham heart study: rationale, design, initial findings, and implications. *Glob Heart*, 8, 3-9.
- WU, L., FAN, J. & BELASCO, J. G. 2006. MicroRNAs direct rapid deadenylation of mRNA. *Proc Natl Acad Sci U S A*, 103, 4034-9.
- XIAO, J., MENG, X. M., HUANG, X. R., CHUNG, A. C., FENG, Y. L., HUI, D. S., YU, C. M., SUNG, J. J. & LAN, H. Y. 2012. miR-29 inhibits bleomycin-induced pulmonary fibrosis in mice. *Mol Ther*, 20, 1251-60.
- XIN, M., SMALL, E. M., SUTHERLAND, L. B., QI, X., MCANALLY, J., PLATO, C. F., RICHARDSON, J. A., BASSEL-DUBY, R. & OLSON, E. N. 2009. MicroRNAs miR-143 and miR-145 modulate cytoskeletal dynamics and responsiveness of smooth muscle cells to injury. *Genes Dev*, 23, 2166-78.
- YANG, H. S., JANSEN, A. P., KOMAR, A. A., ZHENG, X., MERRICK, W. C., COSTES, S., LOCKETT, S. J., SONENBERG, N. & COLBURN, N. H. 2003. The transformation suppressor *Pcd4* is a novel eukaryotic translation initiation factor 4A binding protein that inhibits translation. *Mol Cell Biol*, 23, 26-37.
- YANG, K., HE, Y. S., WANG, X. Q., LU, L., CHEN, Q. J., LIU, J., SUN, Z. & SHEN, W. F. 2011. MiR-146a inhibits oxidized low-density lipoprotein-induced lipid accumulation and inflammatory response via targeting toll-like receptor 4. *FEBS Lett*, 585, 854-60.
- YANG, S., BANERJEE, S., FREITAS, A., CUI, H., XIE, N., ABRAHAM, E. & LIU, G. 2012. miR-21 regulates chronic hypoxia-induced pulmonary vascular remodeling. *Am J Physiol Lung Cell Mol Physiol*, 302, L521-9.
- YASUMOTO, H., KIM, S., ZHAN, Y., MIYAZAKI, H., HOSHIGA, M., KANEDA, Y., MORISHITA, R. & IWAO, H. 2001. Dominant negative c-jun gene transfer inhibits vascular smooth muscle cell proliferation and neointimal hyperplasia in rats. *Gene Ther*, 8, 1682-9.
- YI, C., WANG, Q., WANG, L., HUANG, Y., LI, L., LIU, L., ZHOU, X., XIE, G., KANG, T., WANG, H., ZENG, M., MA, J., ZENG, Y. & YUN, J. P. 2012. MiR-663, a microRNA targeting p21(WAF1/CIP1), promotes the proliferation and tumorigenesis of nasopharyngeal carcinoma. *Oncogene*, 31, 4421-33.
- YUSUF, S., HAWKEN, S., OUNPUU, S., DANS, T., AVEZUM, A., LANAS, F., MCQUEEN, M., BUDAJ, A., PAIS, P., VARIGOS, J., LISHENG, L. & INVESTIGATORS, I. S. 2004. Effect of potentially modifiable risk factors associated with myocardial infarction in 52 countries (the INTERHEART study): case-control study. *Lancet*, 364, 937-52.

- YUSUF, S., MEHTA, S. R., CHROLAVICIUS, S., AFZAL, R., POGUE, J., GRANGER, C. B., BUDAJ, A., PETERS, R. J., BASSAND, J. P., WALLENTIN, L., JOYNER, C., FOX, K. A. & GROUP, O.-T. 2006. Effects of fondaparinux on mortality and reinfarction in patients with acute ST-segment elevation myocardial infarction: the OASIS-6 randomized trial. *JAMA*, 295, 1519-30.
- YUSUF, S., ZHAO, F., MEHTA, S. R., CHROLAVICIUS, S., TOGNONI, G., FOX, K. K. & CLOPIDOGREL IN UNSTABLE ANGINA TO PREVENT RECURRENT EVENTS TRIAL, I. 2001. Effects of clopidogrel in addition to aspirin in patients with acute coronary syndromes without ST-segment elevation. *N Engl J Med*, 345, 494-502.
- ZENG, Y. & CULLEN, B. R. 2004. Structural requirements for pre-microRNA binding and nuclear export by Exportin 5. *Nucleic Acids Res*, 32, 4776-85.
- ZENG, Y. & CULLEN, B. R. 2005. Efficient processing of primary microRNA hairpins by Drosha requires flanking nonstructured RNA sequences. *J Biol Chem*, 280, 27595-603.
- ZETTLER, M. E., PROCIUK, M. A., AUSTRIA, J. A., MASSAELI, H., ZHONG, G. & PIERCE, G. N. 2003. OxLDL stimulates cell proliferation through a general induction of cell cycle proteins. *Am J Physiol Heart Circ Physiol*, 284, H644-53.
- ZHANG, R. N., ZHENG, B., LI, L. M., ZHANG, J., ZHANG, X. H. & WEN, J. K. 2014. Tongxinluo inhibits vascular inflammation and neointimal hyperplasia through blockade of the positive feedback loop between miR-155 and TNF-alpha. *Am J Physiol Heart Circ Physiol*, 307, H552-62.
- ZHOU, J., WANG, K. C., WU, W., SUBRAMANIAM, S., SHYY, J. Y., CHIU, J. J., LI, J. Y. & CHIEN, S. 2011. MicroRNA-21 targets peroxisome proliferators-activated receptor-alpha in an autoregulatory loop to modulate flow-induced endothelial inflammation. *Proc Natl Acad Sci U S A*, 108, 10355-60.
- ZHOU, R., HU, G., GONG, A. Y. & CHEN, X. M. 2010. Binding of NF-kappaB p65 subunit to the promoter elements is involved in LPS-induced transactivation of miRNA genes in human biliary epithelial cells. *Nucleic Acids Res*, 38, 3222-32.
- ZHU, S., PAN, W., SONG, X., LIU, Y., SHAO, X., TANG, Y., LIANG, D., HE, D., WANG, H., LIU, W., SHI, Y., HARLEY, J. B., SHEN, N. & QIAN, Y. 2012. The microRNA miR-23b suppresses IL-17-associated autoimmune inflammation by targeting TAB2, TAB3 and IKK-alpha. *Nat Med*, 18, 1077-86.
- ZIMMERMAN, M. A., SELZMAN, C. H., REZNIKOV, L. L., MILLER, S. A., RAEBURN, C. D., EMMICK, J., MENG, X. & HARKEN, A. H. 2002. Lack of TNF-alpha attenuates intimal hyperplasia after mouse carotid artery injury. *Am J Physiol Regul Integr Comp Physiol*, 283, R505-12.
- ZOU, Y., DIETRICH, H., HU, Y., METZLER, B., WICK, G. & XU, Q. 1998. Mouse model of venous bypass graft arteriosclerosis. *Am J Pathol*, 153, 1301-10.

Appendix



Reducing In-Stent Restenosis

Therapeutic Manipulation of miRNA in Vascular Remodeling and Inflammation

Robert A. McDonald, PhD,* Crawford A. Halliday, MChB,* Ashley M. Miller, PhD,* Louise A. Diver, PhD,* Rachel S. Dakin, PhD,* Jennifer Montgomery, PhD,* Martin W. McBride, PhD,* Simon Kennedy, PhD,* John D. McClure, PhD,* Keith E. Robertson, MChB,* Gillian Douglas, PhD,† Keith M. Channon, MD,† Keith G. Oldroyd, MD,‡ Andrew H. Baker, PhD*

ABSTRACT

BACKGROUND Drug-eluting stents reduce the incidence of in-stent restenosis, but they result in delayed arterial healing and are associated with a chronic inflammatory response and hypersensitivity reactions. Identifying novel interventions to enhance wound healing and reduce the inflammatory response may improve long-term clinical outcomes. Micro-ribonucleic acids (miRNAs) are noncoding small ribonucleic acids that play a prominent role in the initiation and resolution of inflammation after vascular injury.

OBJECTIVES This study sought to identify miRNA regulation and function after implantation of bare-metal and drug-eluting stents.

METHODS Pig, mouse, and in vitro models were used to investigate the role of miRNA in in-stent restenosis.

RESULTS We documented a subset of inflammatory miRNAs activated after stenting in pigs, including the miR-21 stem loop miRNAs. Genetic ablation of the miR-21 stem loop attenuated neointimal formation in mice post-stenting. This occurred via enhanced levels of anti-inflammatory M2 macrophages coupled with an impaired sensitivity of smooth muscle cells to respond to vascular activation.

CONCLUSIONS MiR-21 plays a prominent role in promoting vascular inflammation and remodeling after stent injury. miRNA-mediated modulation of the inflammatory response post-stenting may have therapeutic potential to accelerate wound healing and enhance the clinical efficacy of stenting. (J Am Coll Cardiol 2015;65:2314-27) © 2015 by the American College of Cardiology Foundation.

Coronary stenting has almost universally superseded the use of balloon angioplasty alone for the percutaneous treatment of coronary heart disease. Stenting solves the major problems of balloon angioplasty, including acute elastic recoil, occlusive dissection, and the need for repeat revascularization due to restenosis (1). Stenting is superior to balloon angioplasty alone in the setting of

both stable and unstable coronary artery disease (2,3). However, the vascular injury caused by stent implantation provokes neointimal hyperplasia due to aberrant vascular smooth muscle cell (SMC) proliferation and migration (4). The resulting encroachment on the vessel lumen may be sufficient to cause in-stent restenosis (ISR), recurrent ischemia, and a need for repeat revascularization in up to 20% of

From the *Institute of Cardiovascular and Medical Sciences, College of Medical, Veterinary and Life Sciences, University of Glasgow, Glasgow, Scotland; †West of Scotland Regional Heart & Lung Centre, Golden Jubilee National Hospital, Clydebank, Scotland; and the ‡Department of Cardiovascular Medicine, University of Oxford, John Radcliffe Hospital, Oxford, United Kingdom. This work was funded by the British Heart Foundation (program grants RG/09/005/27915, RG/14/3/30706, and FS11/12/28673). Dr. Baker is supported by the British Heart Foundation Chair of Translational Cardiovascular Sciences (CH/11/2/28733). Dr. Channon is supported by the National Institute for Health Research Oxford Biomedical Research Centre. Dr. Oldroyd has received honoraria from Biosensors. All other authors have reported that they have no relationships relevant to the contents of this paper to disclose. Drs. McDonald and Halliday contributed equally to this work.

Listen to this manuscript's audio summary by JACC Editor-in-Chief Dr. Valentin Fuster.

You can also listen to this issue's audio summary by JACC Editor-in-Chief Dr. Valentin Fuster.

Manuscript received February 16, 2015; accepted March 9, 2015.



patients treated with bare-metal stents (BMS) at 1 year. The development of metallic drug-eluting stents (DES) coated with an antiproliferative drug has substantially reduced ISR (5) but is associated with a significantly greater incidence of late stent thrombosis compared with BMS due to delayed arterial healing (6,7). Several clinical trials are currently evaluating fully bioresorbable nonmetallic DES, but early reports suggest that they may have higher rates of incomplete strut apposition and strut fracture (8,9). Collectively, these findings highlight the need to further improve our understanding of the events that control vascular healing responses with both BMS and DES.

SEE PAGE 2328

Noncoding ribonucleic acids (RNAs) play a pivotal role in many physiological and homeostatic processes (10,11). The best characterized are short, highly conserved RNA molecules called microRNAs (miRNAs), which mediate messenger RNA silencing through translational degradation or repression after complementary base pairing (12). More than 1,000 miRNAs are thought to regulate ~30% of all protein-coding messenger RNA (13). Thus, a single miRNA may have ≥ 1 messenger RNA targets at different points within multiple biological pathways to mediate a disease phenotype (14,15). In the setting of vascular injury, miRNAs are involved in inflammatory cell recruitment and activation and dedifferentiation of SMCs, key processes that drive the vessel response to injury. However, there has been no systematic analysis of miRNA regulation post-stent deployment.

The goal of the present study, therefore, was to define the expression pattern and function of miRNAs after stenting with BMS and DES to identify miRNAs with the potential to modulate vascular response to injury.

METHODS

Detailed methods are available in the [Online Appendix](#). In brief, male Landrace pigs (19 to 26 kg) were pre-dosed orally with aspirin and clopidogrel 24 h before surgery, and they were maintained on this dual antiplatelet therapy throughout the study to reduce the risk of in-stent thrombosis. Vascular access was obtained by femoral artery cutdown and the insertion of a 6-F transradial sheath (Arrow International, Reading, Pennsylvania). Coronary angiography was performed before the deployment of either BMS (Gazelle, Biosensors Europe SA, Morges, Switzerland) or Biolimus A9 eluting stents (BioMatrix Flex, Biosensors Europe SA) to achieve a target ratio

of stent to artery diameter of 1.2:1. Animals were euthanized after 7 or 28 days.

In the murine model, a stainless steel stent (5-cell, 2.5 mm \times 0.8 mm; strut thickness 0.06 mm; Cambus Medical, Galway, Ireland) was crimped onto a 1.20-mm \times 8-mm Mini-Trek balloon angioplasty catheter (Abbott Vascular, Abbott Park, Illinois) and deployed (10 atm for 30 s) into the thoracic aorta before engraftment into a recipient mouse. Mice were allowed to recover in heated chambers for 24 h and were returned to normal housing conditions, where they were maintained on aspirin-supplemented water and a normal chow diet for another 28 days before being killed. Murine aortas were harvested from male mice 8 to 12 weeks of age, and vascular SMCs were isolated and cultured. Cell migration was assessed via scratch assay. Bone marrow-derived macrophages (BMDM) were generated and bone marrow cells isolated from femurs and tibiae of wild-type (WT) and miR-21 knockout (KO) mice. Flow cytometry was performed by using a BD FACSCanto II or LSR II (BD Biosciences, San Jose, California).

Global profiling for miRNAs in the control unstented arteries and stented porcine coronary arteries was performed with miRNA quantification by using real-time polymerase chain reaction. For analysis, fold changes for each miRNA were normalized to U6 because this miRNA was the most suitable endogenous miRNA in porcine tissue. Data analysis was performed by using SDS software version 2.3 (Applied Biosystems, Carlsbad, California), and the baseline and threshold were automatically set. Data were normalized and then analyzed to identify miRNAs differentially expressed between the control (unstented) arteries and arteries subjected to stenting for 7 or 28 days. Data were analyzed by using Data-Assist software version 3 (Applied Biosystems).

All data are mean \pm SEM. Visual assessment was used to check for any lack of normality; because there was no evidence of this, 1-way analysis of variance followed by a Tukey multiple comparison test (for comparison of >2 groups) or Student *t* test (for comparison of 2 groups) were conducted. For all the quantitative polymerase chain reaction experiments, values are expressed as fold-change. All statistical analyses were conducted by using Prism version 4 (GraphPad Software, San Diego, California). The microRNA array data were analyzed in DataAssist software. Comparisons of in vitro SMC proliferation and migration were performed by using 2-way analysis of variance and Bonferroni post-hoc tests.

ABBREVIATIONS AND ACRONYMS

BMDM	= bone marrow-derived macrophages
BMS	= bare-metal stent(s)
CD	= cluster of differentiation
DES	= drug-eluting stent(s)
IL	= interleukin
ISR	= in-stent restenosis
KO	= knockout
LPS	= lipopolysaccharide
miRNA	= micro-ribonucleic acid
PDCD4	= programmed cell death protein 4
PDGF	= platelet-derived growth factor
PPAR	= peroxisome proliferator-activated receptor
RNA	= ribonucleic acid
SMC	= smooth muscle cell
WT	= wild-type

All animal procedures were performed in accordance with the United Kingdom Home Office Guidance on the operation of the Animals (Scientific Procedures) Act 1986 and institutional ethical approval.

RESULTS

The effects of BMS and DES on ISR were assessed in pig coronary arteries by using optical coherence tomography imaging (Figures 1A to 1D). The DES reduced neointima formation by 33% compared with BMS at 28 days (Figure 1A), leading to a significantly larger luminal diameter (Figure 1B) with no difference in stent expansion (Figure 1C).

We sought to identify aberrantly expressed miRNAs. At 7 days post-stenting, 116 miRNAs were differentially regulated in the BMS group, with 23 miRNAs remaining dysregulated at 28 days. At 7 days, multiple miRNAs associated with inflammatory cell infiltration and activation were altered (Online Table 1, Online Figure 1). Of note, miR-21-3p was substantially up-regulated in both BMS- and DES-treated arteries at 7 days, suggesting that the miR-21 stem loop (i.e., both lead and “passenger” strands) may be important post-stenting. The

expression profile of miR-21-3p and miR-21-5p were validated, and this revealed that miR-21-5p was significantly up-regulated in stented arteries at 7 days regardless of stent type and remained up-regulated at 28 days compared with unstented control arteries (Figure 2A). MiR-21-3p was also up-regulated at 7 and 28 days post-stenting in both groups (Figure 2B). We then identified the localization of expression of the miR-21 axis in the vessel wall after stenting, focusing on miR-21-5p (because the absolute levels of miR-21-3p are lower and below the detection threshold for in situ hybridization). In control coronary arteries, miR-21-5p was detected within the media (Figure 2C). In injured vessels 28 days post-stenting, increased signal intensity was observed in the medial layer and developing neointima, particularly around stent struts. To determine if this expression pattern is maintained in the clinical setting, in situ hybridization was performed in human coronary arteries 14 days post-stenting from tissue obtained from a heart transplant patient. In concordance with the staining pattern in porcine arteries, abundant miR-21 expression was observed in the developing neointima and infiltrating inflammatory cells (Figure 2D, Online Figure 2). Taken together, these findings

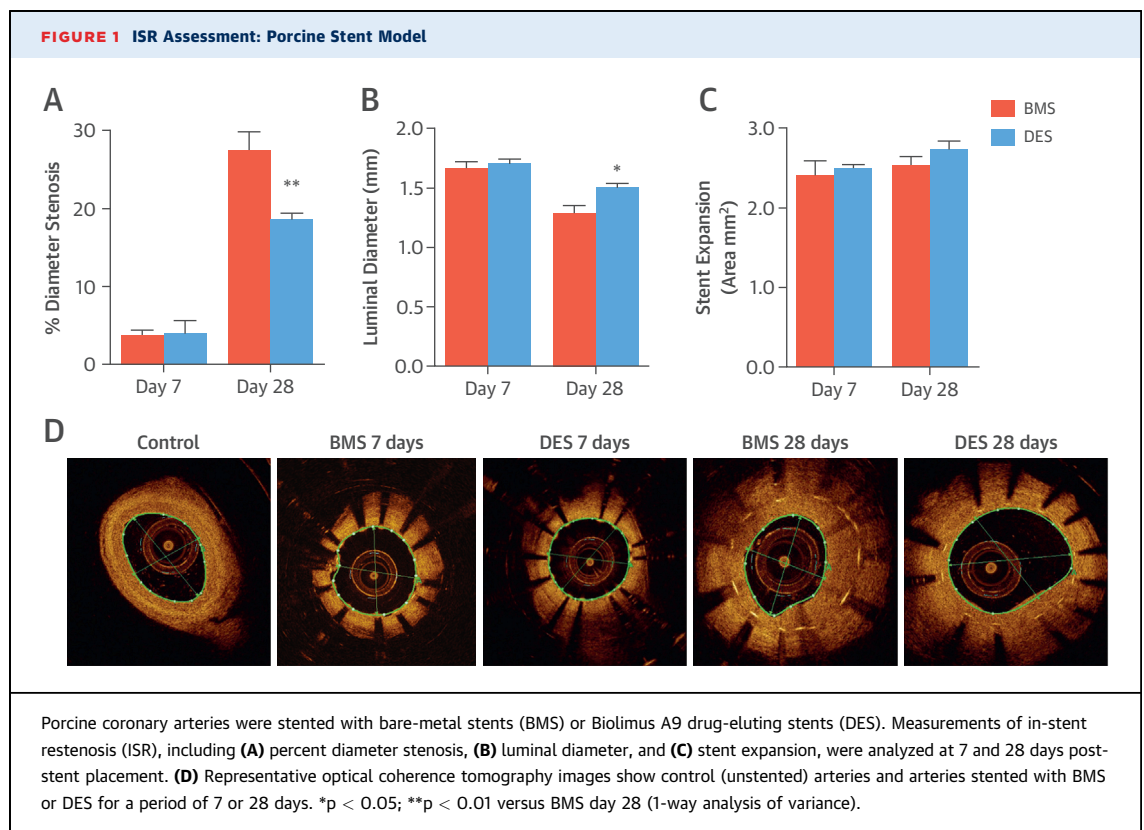
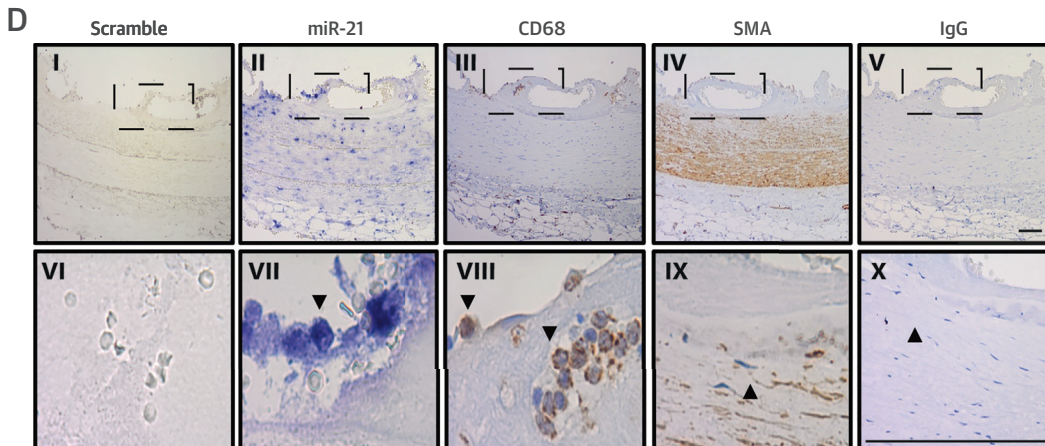
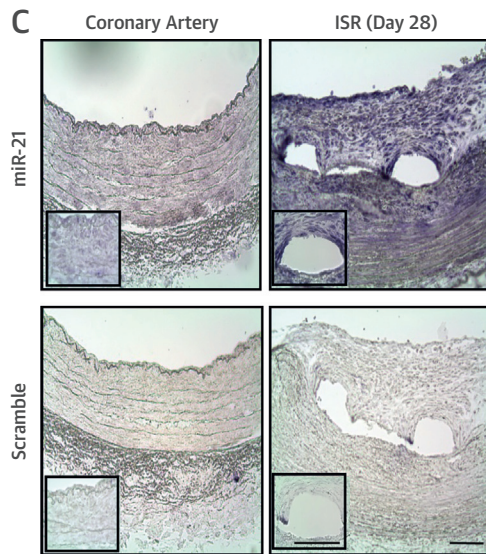
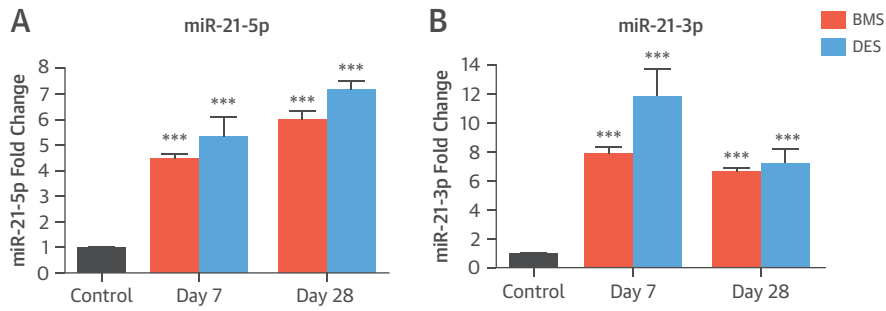


FIGURE 2 Regulation of miR-21-5p and -3p During ISR



Relative-fold change in **(A)** miR-21-5p and **(B)** miR-21-3p is expressed in control arteries or arteries stented with a BMS or DES for 7 or 28 days. *** $p < 0.001$ versus control arteries (1-way analysis of variance). Data are normalized to expression of U6. **(C)** In situ hybridization for miR-21 and scrambled control in unstented porcine coronary arteries and in BMS-stented vessels with ISR at day 28 (representative images, $n = 3$). Areas under enhanced magnification correspond to the regions highlighted by the hatched rectangles. Scale bar = 100 μm . **(D)** In situ hybridization for miR-21 and scrambled control in stented human coronary arteries and immunohistochemistry for smooth muscle actin (SMA) and cluster of differentiation (CD) 68 for smooth muscle cells and macrophages, respectively. Panels VI through X are higher magnification images of the hatch regions in panels I through V. Scale bar = 100 μm . IgG = immunoglobulin G; other abbreviations as in **Figure 1**.

suggest that miR-21-5p and miR-21-3p may be important in the development of post-stent pathological responses to injury.

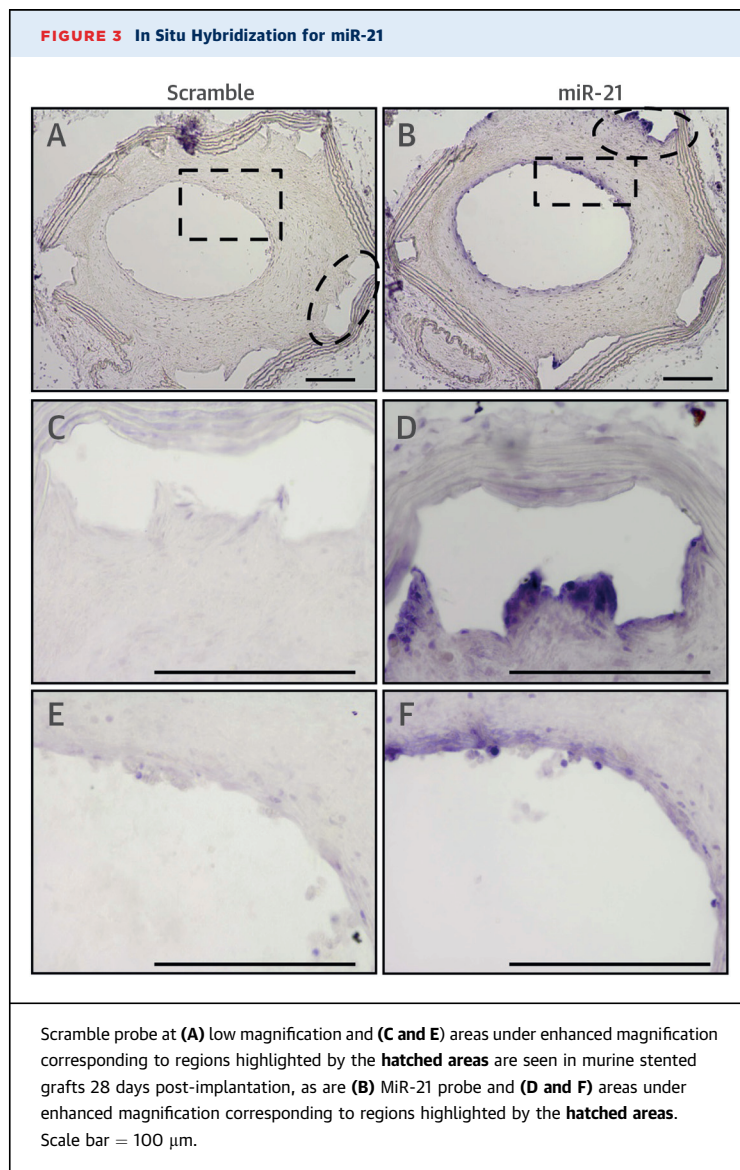
We used a murine interpositional graft model of stenting. In situ hybridization confirmed abundant miR-21-5p staining around the stent struts and developing neointima (Figure 3), consistent with the porcine data. Morphometric analysis found that miR-21 KO mice stent grafts had a reduced neointimal area, neointimal thickness, and neointima-to-medial ratio compared with WT controls (1.37 ± 0.18 [n = 8] vs. 2.11 ± 0.17 [n = 9]; $p < 0.05$) (Figures 4A and 4B, Online Table 2). Measurements of strut depth were concordant with greater strut depth in WT-stented grafts than in KO-stented grafts. A significant

reduction in luminal area in WT mice compared with miR-21 KO mice was also observed (Figures 4C and 4D, Online Table 2). There were no apparent differences in luminal, media, or total vessel area between WT and miR-21 KO mice at baseline (before stent injury), although an increased sample size would be needed to confirm this observation (Online Table 3). Furthermore, the total vessel area did not differ significantly at 28 days (Figure 4E), and no differences were observed in unstented vessels at baseline (Online Table 3).

The neointimal lesions from miR-21 KO mice contained significantly less α -actin-positive SMCs ($28 \pm 2.4\%$ [n = 8] vs. $14 \pm 3.7\%$ [n = 9]; $p < 0.01$) (Figures 5A and 5B). Lesions in WT mice contained 50% more elastin than in KO mice (Figures 5C and 5D, Online Table 2). No difference in cell proliferation was observed after quantification of cells in the neointima (Figures 5E and 5F, Online Table 2). We assessed vessel reendothelialization and, importantly, found no significant difference between miR-21 KO and WT mice ($91.0 \pm 3.9\%$ vs. $88.7 \pm 2.9\%$, respectively) (Figures 5G and 5H). No differences were observed at baseline (i.e., unstented vessels) (Online Table 3).

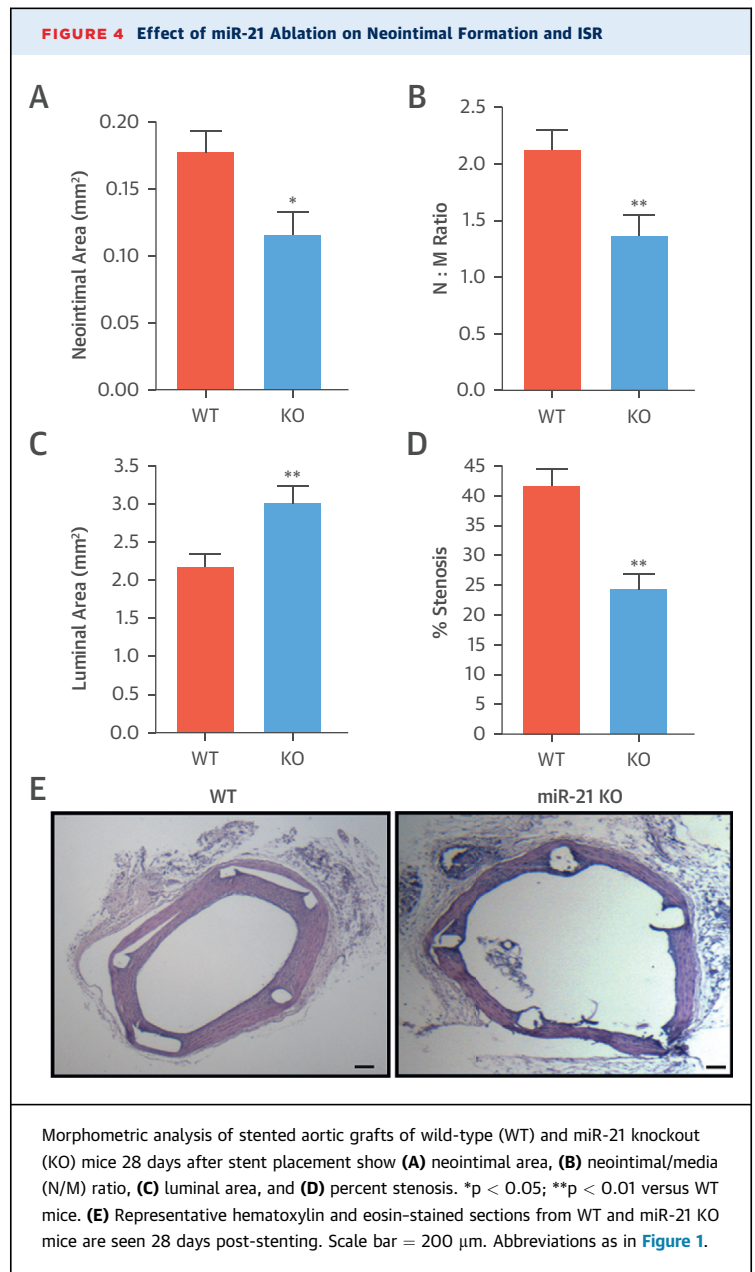
To explore the mechanisms responsible for the reduction in neointima formation in miR-21 KO mice, proliferation and wound healing assays were performed. The proliferative response of miR-21 KO SMC was dramatically attenuated in response to platelet-derived growth factor (PDGF) (Figure 6A), as was migration in response to PDGF (Figures 6B and 6C). To identify potential targets responsible for these effects, we stimulated aortic SMC from miR-21 WT and KO mice with PDGF (n = 5) to elevate miR-21 levels (3.03 ± 0.23 -fold vs. controls; $p < 0.01$) (Figure 6D). The messenger RNA levels of known miR-21 targets with defined roles in SMC proliferation and migration were profiled. The expression of programmed cell death protein 4 (PDCD4) and signal transducer and activator of transcription 3 were significantly reduced in aortic SMC from WT mice after PDGF stimulation. These changes were not observed in miR-21 KO cells stimulated with PDGF (Figures 6E and 6F); however, further experiments are required to determine whether repression of these genes is direct or indirect via miR-21 regulation in this setting.

MiR-21 KO mice contained greater numbers of galactin-3+ (MAC-2) macrophages in the neointima compared with WT mice ($0.79 \pm 0.23\%$ vs. $2.54 \pm 0.75\%$; $p < 0.05$) (Figures 7A and 7B) and enhanced levels of YM-1-positive macrophages, a validated murine marker of the alternatively activated (M2) macrophage ($1.93 \pm 0.54\%$ vs. $0.50 \pm 0.21\%$; $p < 0.01$)



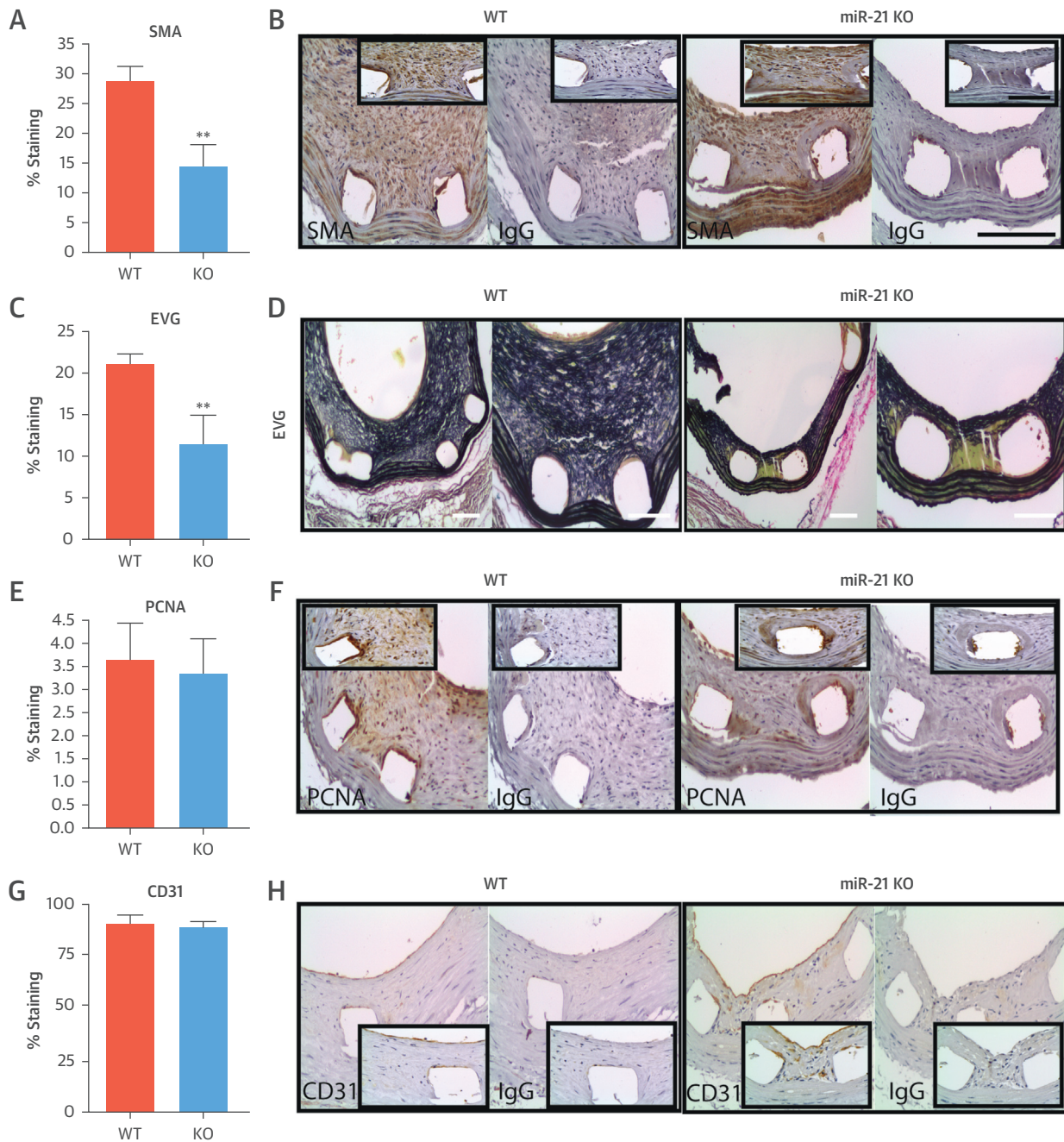
(Figures 7C and 7D). Thus, loss of miR-21 results in altered inflammatory cell phenotype within injured vessels. To investigate whether these effects were derived from any hematological defect, before cell recruitment to the vessel wall, the populations of immune cells in both bone marrow and blood of WT and miR-21 KO mice were examined (16). In bone marrow, the percentage of cluster of differentiation (CD) 3+ T cells was significantly reduced in miR-21 KO mice, but neutrophils, monocytes, B cells, CD4+, and CD8+ T cells did not differ (Online Figures 3A and 3B). In blood, miR-21 KO mice exhibited a significantly reduced percentage of circulating Ly6c+hi monocytes and CD3+ T cells (Figures 7E and 7F), potentially indicating a reduced capacity to develop proinflammatory responses.

To investigate whether the absence of miR-21 leads to altered macrophage differentiation, BMDMs from WT and miR-21 KO mice were generated and treated with either lipopolysaccharide (LPS) or interleukin (IL)-4 in vitro to induce M1 and M2 polarization, respectively. Both LPS and IL-4 significantly up-regulated the expression of miR-21-3p and miR-21-5p in WT macrophages (3.00 ± 0.23 -fold, 4.38 ± 0.91 -fold, 4.74 ± 0.13 -fold, and 4.88 ± 0.7 -fold, respectively; $p < 0.05$), indicating that inflammatory mediators can modulate the expression of miR-21 (Figure 8A). At baseline, unstimulated (M0, non-polarized) miR-21 KO macrophages had significantly higher levels of peroxisome proliferator-activated receptor (PPAR)- γ expression (M2 polarization marker) than WT cells ($p < 0.01$) (Figure 8B). After activation with LPS, expression of nitric oxide synthase (an M1 marker) was significantly reduced in miR-21 KO versus WT macrophages (Figure 8C). In addition, the ratio of messenger RNA expression of nitric oxide synthase, compared with arginase 1 (an M2 marker), was significantly higher in WT than miR-21 KO macrophages treated with LPS (20.6 ± 6.52 -fold vs. 2.7 ± 1.24 -fold; $p < 0.001$) (Figure 8D). Flow cytometric analysis demonstrated that after activation with LPS, CD69 was significantly reduced in miR-21 KO versus WT LPS-treated macrophages (1.8-fold; $p < 0.05$) (Figure 8E). However, all other markers examined by using flow cytometry (major histocompatibility complex-II, CD11c, CD86, CD206, and Toll-like receptor-2) were not significantly different in either LPS- or IL-4-treated WT or miR-21 KO BMDM (Online Figure 4). The levels of several proinflammatory mediators were significantly reduced from LPS-stimulated macrophages of miR-21 KO compared with WT mice: IL-1 α , IL-1 β , IL-6, IL-12, tumor necrosis factor- α , and macrophage inflammatory protein-1 α (Figure 8F). In addition, the IL-12/IL-10

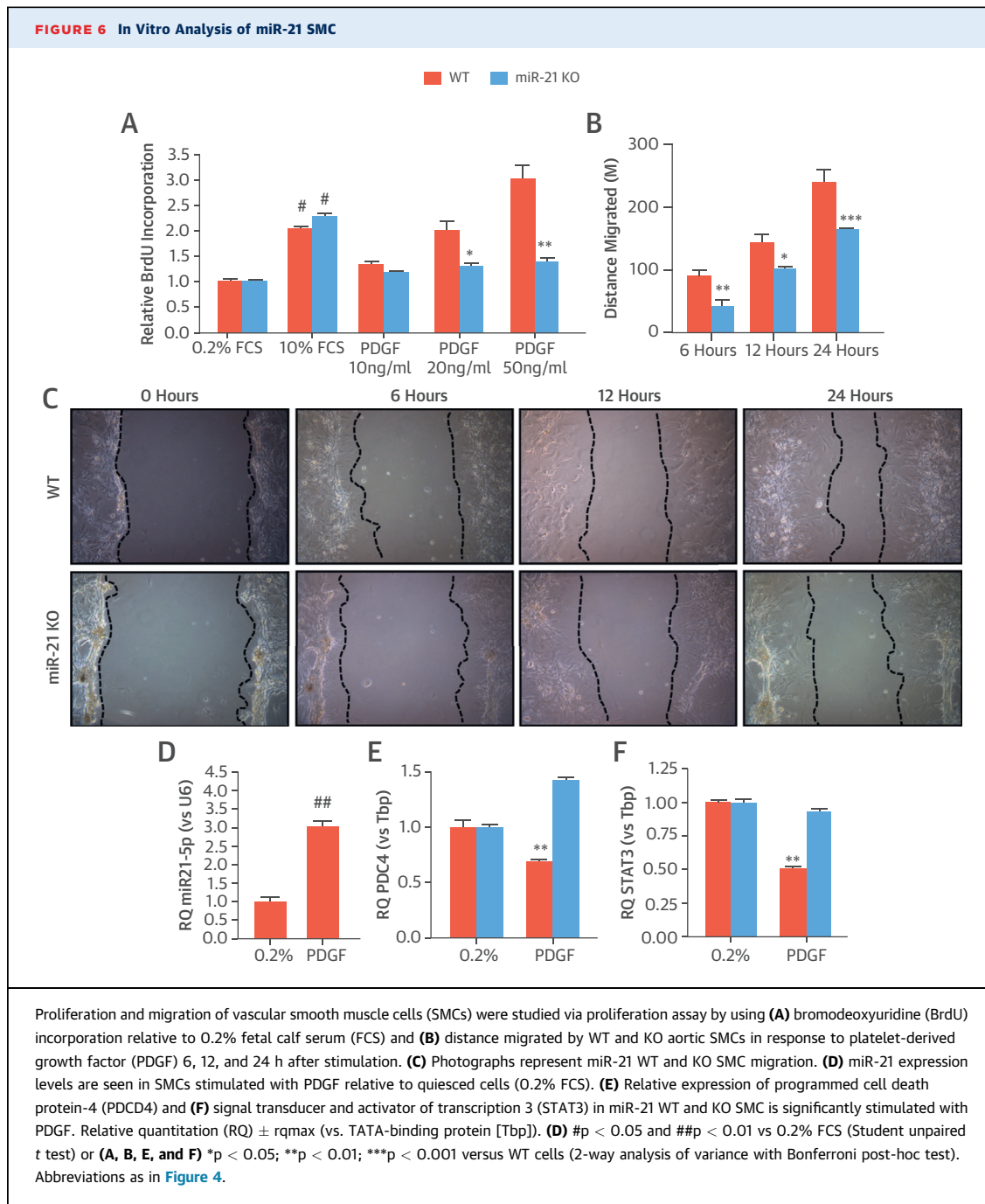


ratio for LPS-stimulated miR-21 macrophages was almost double that of KO macrophages (24 vs. 13).

To address whether miR-21 KO macrophages had a reduced capacity to infiltrate and migrate into vascular lesions after injury, we studied BMDM migration through Matrigel-coated transwell inserts containing 8- μ m pores (Sigma, United Kingdom). These experiments showed that both BMDM isolated from WT and miR-21 KO mice had the same capacity to migrate through a matrix membrane in response to monocyte chemoattractant protein-1 (Figure 8G).

FIGURE 5 Cellular Analysis of Murine Lesions

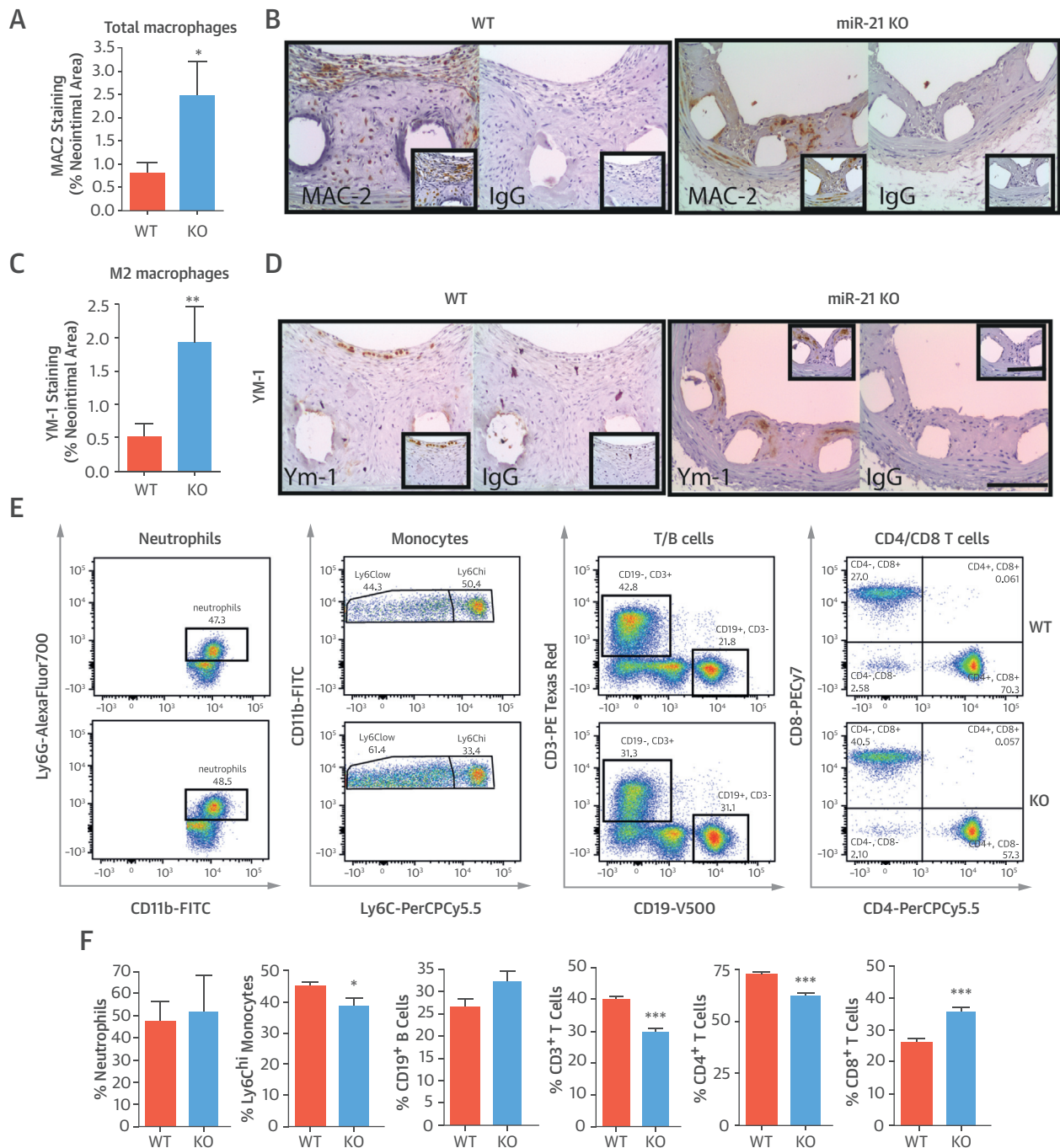
(A and B) The cellular composition of the neointimal lesions was quantified in WT and miR-21 KO mice at 28 days post-stenting, showing quantification of: the percentage of SMA-positive cells and representative image of the immunohistochemistry; **(C and D)** elastin Van Gieson (EVG) staining and representative images; **(E and F)** percentage of cells staining positive for proliferating cell nuclear antigen (PCNA); and **(G and H)** percentage of cell staining positive for CD31 within the circumference of the lumen and representative images. ** $p < 0.01$ versus WT mice (Student unpaired t test). Scale bar = 100 μ m. Abbreviations as in [Figures 2 and 4](#).



DISCUSSION

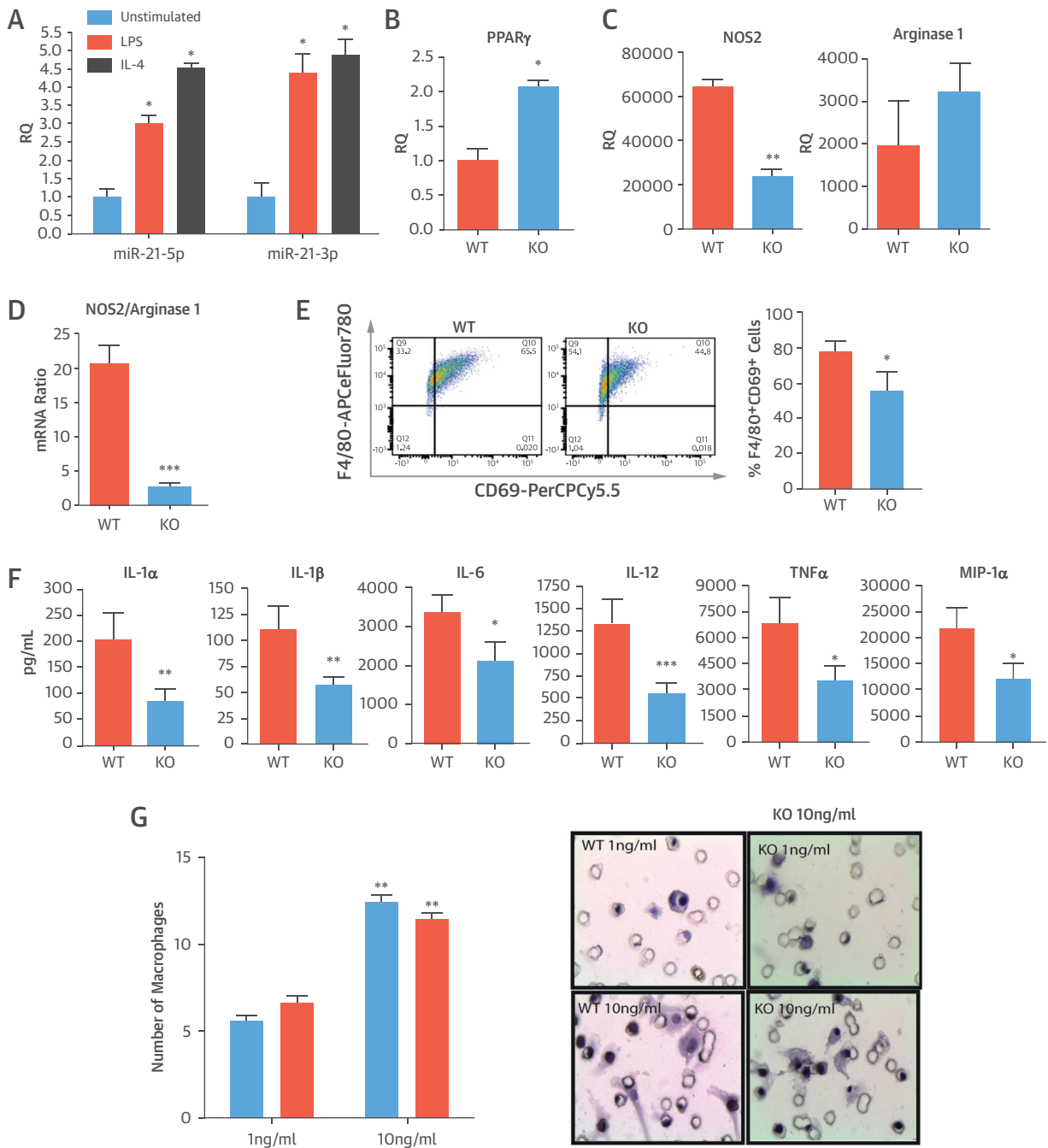
We report for the first time miRNA patterns associated with delayed arterial healing and neointima formation after stenting (Central Illustration). Aberrantly expressed miRNA lead and “passenger” strands associated with 7- and 28-day time points were identified.

Of particular interest, the stem loop of miR-21, including lead (miR-21-5p) and passenger (miR-21-3p) strands, was up-regulated in both the BMS and DES groups compared with controls. Further experiments highlighted that loss of the miR-21 stem loop in KO mice blocked neointimal formation through effects on SMC proliferation and migration,

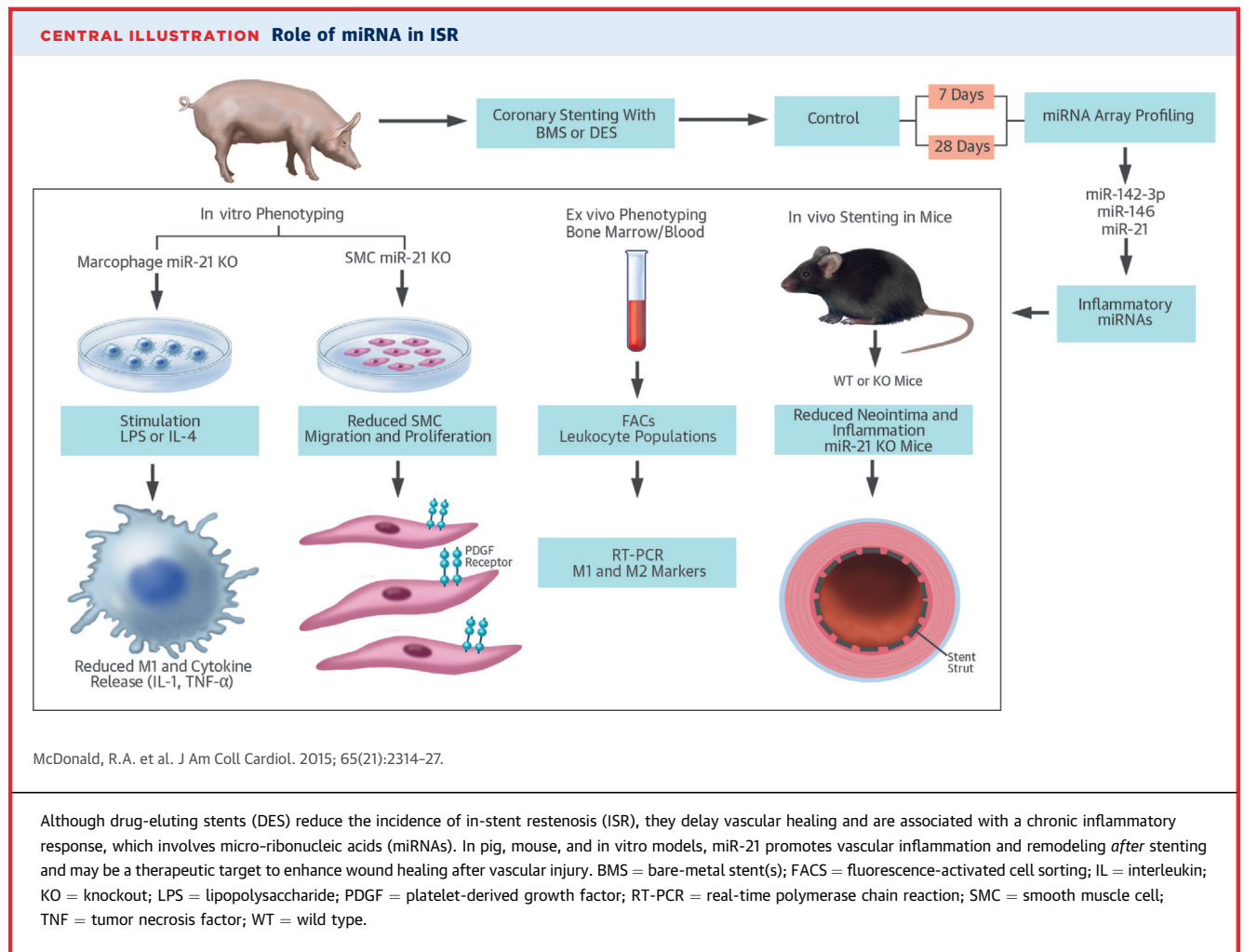
FIGURE 7 Inflammatory Cells in Neointimal Lesions and Blood of miR-21 KO Mice

(A) Quantification and (B) representative images of total galactose-specific lectin 3 (MAC2) staining (% neointimal area) are seen in sections of stented graft from WT and miR-21 KO mice 28 days post-stenting (scale bar = 100 μ M). (C) Quantification and (D) representative images of total chitinase 3-like 3 (YM-1) staining (marker for M2 macrophages) (% neointimal area) are seen in sections of stented graft from WT and miR-21 KO mice at day 28. Flow cytometric assessment of circulating cells in blood of WT and miR-21 KO mice. (E) Representative fluorescence-activated cell sorting plots and (F) bar charts showing percent quantification of cells in gate potentially indicate a reduced ability to develop proinflammatory responses. Gating markers used: neutrophils (CD45+Ly6G+CD11b+), monocytes (CD45+Ly6G-Ly6C+CD11b+), B cells (CD45+CD3-CD19+), and T cells (CD45+CD3+CD4+ or CD45+CD3+CD8+). * $p < 0.05$; ** $p < 0.01$; *** $p < 0.001$ versus WT mice (Student unpaired *t* test). Abbreviations as in Figures 2 and 4.

FIGURE 8 In Vitro Altered Inflammatory Response in miR-21-Deficient Macrophages



(A) RQ of expression of miR-21-5p and miR-21-3p in WT macrophages stimulated with either lipopolysaccharide (LPS) or interleukin (IL)-4 for 20 h; data normalized to U6. Expression of peroxisome proliferator-activated receptor (PPAR)- γ messenger ribonucleic acid (mRNA) by quantitative polymerase chain reaction in **(B)** unstimulated (baseline) macrophages and **(C)** nitric oxide synthase (NOS2) and arginase 1 mRNA in LPS-stimulated macrophages from WT and miR-21 KO mice. Data are normalized to Tbp. **(D)** Ratio of expression of NOS2/arginase mRNA by quantitative polymerase chain reaction in LPS-activated macrophages was significantly higher in WT mice than in miR-21 KO mice. **(E)** Flow cytometric assessments found that the cell surface marker CD69 was higher in WT versus miR-21 KO macrophages after stimulation with LPS for 20 h. Representative fluorescence-activated cell sorting plot and bar chart showing quantification of data (% of F4/80+ cells expressing the marker). **(F)** Inflammatory cytokine (IL-1 α , IL-1 β , IL-6, IL-12, and TNF- α) and chemokine (macrophage inflammatory protein [MIP]-1 α) production in LPS-activated macrophages was reduced in miR-21 KO compared with WT mice. **(G)** In a macrophage invasion and migration assay, the number of bone marrow-derived macrophages migrating through Matrigel-coated transwell inserts in response to monocyte chemoattractant protein (MCP)-1 was fixed at 6 h and quantified. Representative images of membranes are shown adjacent to graph. * $p < 0.05$; ** $p < 0.01$; *** $p < 0.001$ versus WT mice (Student unpaired *t* test). Abbreviations as in **Figures 2, 4, and 6**.



macrophage polarization, and inflammatory activation. A causal network analysis was performed of miR-21-3p and miR-21-5p targets to determine whether these miRNAs affect the inflammatory networks associated with vascular injury. Despite a relatively small overlap of predicted genes, pathways associated with tumor necrosis factor- α and IL-1 were 1 of the top-ranking regulatory networks (Online Figure 5); this finding may be relevant because both of these cytokines play prominent roles in neointima formation (17,18).

MiR-21 KO mice exhibited reduced SMC deposition, neointima formation, and an altered inflammatory phenotype, resulting in enhanced levels of anti-inflammatory M2 macrophages in response to vascular injury and stenting, with no effect on endothelial regeneration. Subsequent profiling of immune cell populations in the blood of miR-21 KO mice demonstrated reduced numbers of Ly6c+hi

cells, a cell type that can differentiate into M1 macrophages after tissue infiltration. This finding suggests that miR-21 KO mice have a reduced capacity to develop an M1 inflammatory phenotype in response to injury. We also found reduced total CD3+ T-cell counts in the bone marrow and blood of the miR-21 KO. Recently, it has been reported that miR-21 can modulate T-cell responses, including alterations in cytokine production and apoptosis rates (19-21). T cells are already known to contribute to the inflammatory response after coronary artery stenting (22); thus, the absence of miR-21 in T cells likely contributes to the altered inflammatory responses and reduced in-stent stenosis seen in miR-21 KO.

In support of the altered inflammatory responses in vivo, our BMDM experiments revealed that miR-21 KO macrophages contain enhanced baseline levels of PPAR- γ , a well-characterized M2 macrophage marker, and a reduced ratio of nitric oxide synthase/arginase

1 (M1/M2 markers). These findings are particularly relevant in the setting of inflammatory vascular disease because numerous studies suggest that PPAR- γ activation can curtail the inflammatory response. Activation of PPAR- γ in human macrophages reduces matrix metalloproteinase 9 activity and inhibits expression of IL-1 β , IL-6, and tumor necrosis factor- α (23-25). Furthermore, several groups have reported that PPAR- γ agonists inhibit atherosclerosis development and reduce inflammatory markers in apolipoprotein E KO mice (26,27). Furthermore, miR-21 KO macrophages exhibited a reduced capacity to secrete proinflammatory mediators such as IL-1, tumor necrosis factor- α , macrophage inflammatory protein-1, IL-6, and IL-12 in response to LPS, a substance known to stimulate the inflammatory M1 macrophage phenotype. However, a defective response to LPS does not necessarily mean altered polarization and may simply reflect, for example, defective CD14 expression. Further phenotyping of surface receptors from BMDM also showed reduced expression of CD69 in miR-21 KO mice. A CD69 deficiency may contribute to reduced inflammatory cytokine secretion, as previous studies have reported that CD69 activation mediates numerous inflammatory processes such as nitric oxide production and release of tumor necrosis factor- α from murine macrophages and T cells (28,29). Thus, loss of miR-21 may accelerate wound healing and resolution of the inflammatory response after vascular injury and stenting, events that could reduce the incidence of late stent thrombosis.

It is important to note that we used human arrays in the porcine samples to identify miRNAs that would extrapolate to the pathology in the clinical setting. It is possible that a proportion of miRNAs may be underrepresented due to the sequence variation or chromosomal locations between pig and human. We identified an almost 20-fold up-regulation of miR-21-3p after stenting with BMS and DES. Our subsequent experiments in BMDM demonstrated that both miR-21-3p and miR-21-5p were up-regulated in response to LPS, which induces classical macrophage polarization (M1). In combination with reduced inflammatory cytokine release from miR-21 KO macrophages, these results suggest that miR-21-3p and miR-21-5p may both play a pathological role in macrophage activation in response to inflammatory stimuli.

Currently available DES directly target SMC proliferation to prevent neointima formation. We observed that miR-21 plays a prominent role in SMC proliferation and migration in response to vascular injury, consistent with other studies (30,31). Aortic

SMC isolated from miR-21 KO mice had a reduced capacity to migrate and proliferate in response to PDGF, an important observation because novel DES must retain the antiproliferative effect on SMC accumulation to maintain their clinical efficacy. These findings are consistent with previous reports demonstrating that pharmacological or genetic knockdown of miR-21 reduces SMC proliferation and neointima formation after balloon injury or vein grafting (30-33). Several of these reports suggest that miR-21 mediates a beneficial effect on SMC proliferation and neointima, at least in part, via inhibition of phosphatase and tensin homolog.

We also found that the levels of PDCD4 were suppressed after PDGF exposure in WT mice. Importantly, the levels of PDCD4 were increased in miR-21 KO mice, suggesting that PDCD4 is modulated after exposure to PDGF and plays a role in SMC proliferation and migration, effects repressed in miR-21 KO SMCs. In concordance with these findings, previous studies suggest that PDCD4 is down-regulated after vascular injury, and overexpression of PDCD4 with adenoviral vectors increases apoptosis and reduces SMC proliferation (34).

STUDY LIMITATIONS. Although the present study demonstrates that miR-21 play a prominent role in the pathology of in-stent restenosis, it is important to note that these studies are based on data from pre-clinical animal models of restenosis. Although our results in miR-21 knockout mice demonstrate that loss of miR-21 reduces in-stent restenosis and inflammatory cell function, it is important to note that these defects are present before vascular injury, these deficiencies may alter the response to injury in these mice. In order to demonstrate that these findings have efficacy in the clinic, further studies are required to demonstrate that pharmacological knockdown of miR-21 or miR-21 targets can inhibit neointimal formation and vessel inflammation from current drug-eluting stent platforms. Furthermore, detailed pharmacokinetic profiling would be needed to demonstrate an effect elution profile of antimir-21 therapy, without any off-target effect.

CONCLUSIONS

The miR-21 stem loop plays an important role in SMC and macrophage activation after vascular injury. Our findings in the murine model of ISR revealed that loss of miR-21 attenuates neointima formation and macrophage activation, resulting in a less inflammatory phenotype. These findings suggest that miR-21 modulation could enhance wound

healing and resolve the inflammatory response, effects that could improve the clinical efficacy of currently available DES. The miR-21 axis warrants further investigation as a therapeutic target in the setting of stent-induced inflammatory vascular disease. Lineage-restricted knockouts maybe required to unravel the complex role of miR-21 in this setting.

ACKNOWLEDGMENTS The authors thank Ms. Nicola Britton and Mr. Gregor Aitchison for their excellent technical assistance. They also thank Ian McCurrach (Biosensors), for the supply of DES, and Eric Olson (University of Texas Southwestern Medical Center), for the miR-21 KO mice.

REPRINT REQUESTS AND CORRESPONDENCE: Dr. Andrew H. Baker, Institute of Cardiovascular and Medical Sciences, BHF Glasgow Cardiovascular Research Centre, University of Glasgow, 26 University Place, Glasgow, G12 8TA Scotland, United Kingdom. E-mail: andrew.h.baker@glasgow.ac.uk.

PERSPECTIVES

COMPETENCY IN PATIENT CARE: DES reduce in-stent restenosis after percutaneous coronary intervention but are associated with a greater risk of stent thrombosis due to delayed arterial healing that is characterized histologically by incomplete reendothelialization and persistent fibrin and inflammatory cell deposition. An array of microRNA molecules are involved in the inflammatory processes driving the cellular response to vascular injury, and genetic KO of the miR-21 stem loop attenuates neointimal formation after arterial stenting in mice.

TRANSLATIONAL OUTLOOK: Future investigations should seek to determine whether local anti-miR to knockdown miR-21 levels delivered directly from drug-eluting stents could reduce vessel inflammation and neointima formation and reduce the risk of both restenosis and stent thrombosis.

REFERENCES

- Serruys PW, de Jaegere P, Kiemeneij F, et al. A comparison of balloon-expandable-stent implantation with balloon angioplasty in patients with coronary artery disease. Benestent Study Group. *N Engl J Med* 1994;331:489-95.
- De Bruyne B, Pijls NH, Kalesan B, et al. Fractional flow reserve-guided PCI versus medical therapy in stable coronary disease. *N Engl J Med* 2012;367:991-1001.
- Andersen HR, Nielsen TT, Rasmussen K, et al. A comparison of coronary angioplasty with fibrinolytic therapy in acute myocardial infarction. *N Engl J Med* 2003;349:733-42.
- Serruys PW, Kutryk MJ, Ong AT. Coronary-artery stents. *N Engl J Med* 2006;354:483-95.
- Bavry AA, Bhatt DL. Appropriate use of drug-eluting stents: balancing the reduction in restenosis with the concern of late thrombosis. *Lancet* 2008;371:2134-43.
- McFadden EP, Stabile E, Regar E, et al. Late thrombosis in drug-eluting coronary stents after discontinuation of antiplatelet therapy. *Lancet* 2004;364:1519-21.
- Joner M, Finn AV, Farb A, et al. Pathology of drug-eluting stents in humans: delayed healing and late thrombotic risk. *J Am Coll Cardiol* 2006;48:193-202.
- Nishio S, Kosuga K, Igaki K, et al. Long-term (>10 years) clinical outcomes of first-in-man biodegradable poly-L-lactic acid coronary stents: Igaki-Tamai stents. *Circulation* 2012;125:2343-53.
- Mattesini A, Secco GG, Dall'Ara G, et al. ABSORB biodegradable stents versus second-generation metal stents: a comparison study of 100 complex lesions treated under OCT guidance. *J Am Coll Cardiol Intv* 2014;7:741-50.
- Zampetaki A, Mayr M. MicroRNAs in vascular and metabolic disease. *Circ Res* 2012;110:508-22.
- McDonald RA, Hata A, MacLean MR, Morrell NW, Baker AH. MicroRNA and vascular remodelling in acute vascular injury and pulmonary vascular remodelling. *Cardiovasc Res* 2012;93:594-604.
- Ambros V. The functions of animal microRNAs. *Nature* 2004;431:350-5.
- Friedman RC, Farh KK, Burge CB, Bartel DP. Most mammalian mRNAs are conserved targets of microRNAs. *Genome Res* 2009;19:92-105.
- Aurora AB, Mahmoud AI, Luo X, et al. MicroRNA-214 protects the mouse heart from ischemic injury by controlling Ca(2+)(+) overload and cell death. *J Clin Invest* 2012;122:1222-32.
- Bang C, Batkai S, Dangwal S, et al. Cardiac fibroblast-derived microRNA passenger strand-enriched exosomes mediate cardiomyocyte hypertrophy. *J Clin Invest* 2014;124:2136-46.
- Boehm M, Olive M, True AL, et al. Bone marrow-derived immune cells regulate vascular disease through a p27(Kip1)-dependent mechanism. *J Clin Invest* 2004;114:419-26.
- Rectenwald JE, Moldawer LL, Huber TS, Seeger JM, Ozaki CK. Direct evidence for cytokine involvement in neointimal hyperplasia. *Circulation* 2000;102:1697-702.
- Chamberlain J, Evans D, King A, et al. Interleukin-1beta and signaling of interleukin-1 in vascular wall and circulating cells modulates the extent of neointima formation in mice. *Am J Pathol* 2006;168:1396-403.
- Wang L, He LQ, Zhang R, et al. Regulation of T lymphocyte activation by microRNA-21. *Mol Immunol* 2014;59:163-71.
- Smigielska-Czepiel K, van den Berg A, Jellema P, et al. Dual role of miR-21 in CD4+ T-cells: activation-induced miR-21 supports survival of memory T-cells and regulates CCR7 expression in naive T-cells. *PLoS One* 2013;8:e76217.
- Ruan Q, Wang P, Wang T, et al. MicroRNA-21 regulates T-cell apoptosis by directly targeting the tumor suppressor gene Timp2. *Cell Death Dis* 2014;5:e1095.
- Virmani R, Farb A. Pathology of in-stent restenosis. *Curr Opin Lipidol* 1999;10:499-506.
- Jiang C, Ting AT, Seed B. PPAR-gamma agonists inhibit production of monocyte inflammatory cytokines. *Nature* 1998;391:82-6.
- Marx N, Schonbeck U, Lazar MA, Libby P, Plutzky J. Peroxisome proliferator-activated receptor gamma activators inhibit gene expression and migration in human vascular smooth muscle cells. *Circ Res* 1998;83:1097-103.
- Shu H, Wong B, Zhou G, et al. Activation of PPARalpha or gamma reduces secretion of matrix metalloproteinase 9 but not interleukin 8 from human monocytic THP-1 cells. *Biochem Biophys Res Commun* 2000;267:345-9.
- Collins AR, Meehan WP, Kintscher U, et al. Troglitazone inhibits formation of early atherosclerotic lesions in diabetic and nondiabetic low density lipoprotein receptor-deficient mice. *Arterioscler Thromb Vasc Biol* 2001;21:365-71.
- Li AC, Brown KK, Silvestre MJ, Willson TM, Palinski W, Glass CK. Peroxisome proliferator-activated receptor gamma ligands inhibit

development of atherosclerosis in LDL receptor-deficient mice. *J Clin Invest* 2000;106:523-31.

28. Marzio R, Jirillo E, Ransijn A, Mael J, Corradin SB. Expression and function of the early activation antigen CD69 in murine macrophages. *J Leukocyte Biol* 1997;62:349-55.

29. Santis AG, Campanero MR, Alonso JL, et al. Tumor necrosis factor- α production induced in T lymphocytes through the AIM/CD69 activation pathway. *Eur J Immunol* 1992;22:1253-9.

30. Ji R, Cheng Y, Yue J, et al. MicroRNA expression signature and antisense-mediated depletion reveal an essential role of MicroRNA in vascular

neointimal lesion formation. *Circ Res* 2007;100:1579-88.

31. Wang M, Li W, Chang GQ, et al. MicroRNA-21 regulates vascular smooth muscle cell function via targeting tropomyosin 1 in arteriosclerosis obliterans of lower extremities. *Arterioscler Thromb Vasc Biol* 2011;31:2044-53.

32. Maegdefessel L, Azuma J, Toh R, et al. MicroRNA-21 blocks abdominal aortic aneurysm development and nicotine-augmented expansion. *Sci Transl Med* 2012;4:122ra22.

33. McDonald RA, White KM, Wu J, et al. miRNA-21 is dysregulated in response to vein grafting in multiple models and genetic ablation in mice

attenuates neointima formation. *Eur Heart J* 2013;34:1636-43.

34. Liu X, Cheng Y, Yang J, Krall TJ, Huo Y, Zhang C. An essential role of PDCD4 in vascular smooth muscle cell apoptosis and proliferation: implications for vascular disease. *Am J Physiol Cell Physiol* 2010;298:C1481-8.

KEY WORDS late stent thrombosis, miRNA stem loop, neointima, smooth muscle cell

APPENDIX For an expanded Methods section and supplemental tables and figures, please see the online version of this article.